THÈSE

présentée en vue de l'obtention du
Doctorat de l'Université de Toulouse
délivré par l'Université Toulouse III Paul Sabatier
Spécialité: Mathématiques Appliquées

Sébastien MOTSCH

MODÉLISATION MATHÉMATIQUE DES DÉPLACEMENTS D'ANIMAUX ET DÉRIVATION DE MODÈLES MACROSCOPIQUES

(MATHEMATICAL MODELING OF ANIMAL DISPLACEMENTS AND DERIVATION OF MACROSCOPIC MODELS)

I. Gamba	University of Texas	*(Rapporteur)*
I. Giardina	University of Rome	*(Rapporteur)*
P. Degond	Université de Toulouse	*(Directeur de thèse)*
G. Theraulaz	Université de Toulouse	*(Directeur de thèse)*
P. Cattiaux	Université de Toulouse	*(Examinateur)*
F. Filbet	Université de Lyon	*(Examinateur)*

Laboratoire de Mathématiques appliquées à l'Industrie et la Physique
Institut de Mathématiques de Toulouse
Université Paul Sabatier UFR MIG
118 Route de Narbonne 31062 Toulouse cedex 9 France

À ma famille, passée, présente et future

Remerciements (Acknowledgements)

Je voudrais tout d'abord remercier Pierre Degond pour m'avoir donné l'opportunité de faire cette thèse et de m'avoir fait confiance sur un sujet original. Durant ces trois années, j'ai eu la chance de partager son enthousiasme permanent pour la recherche et j'ai aussi pu apprécier ses qualités humaines car il a su me soutenir quand j'en avais besoin. Je remercie également Guy Théraulaz pour m'avoir fait découvrir le vaste monde de la biologie. Son ouverture aux autres disciplines scientifiques et ses vastes connaissances m'ont été d'une grande aide pour réaliser ce travail pluridisciplinaire.

Je tiens ensuite à remercier toutes les personnes avec qui j'ai eu la chance de collaborer : tout d'abord Guillaume Ball, Josselin Garnier et Vincent Perrier avec qui j'ai pu m'initier aux processus stochastiques au Cemracs, Axel Klar et Michael Herty qui m'ont chaleureusement reçu à Kaiserslautern. Je voudrais dire un grand merci à Tamas Vicsek et son équipe pour m'avoir accueilli pendant deux mois à Budapest. Plus proche d'ici, je remercie également Christian Jost, Jacques Gautrais, Richard Fournier et Stéphane Blanco avec qui j'ai partagé un travail de recherche pluridisciplinaire très enrichissant. Et enfin, je remercie Djalil Chafaï et Patrick Cattiaux avec qui j'ai pu poursuivre ma formation sur ces fameux processus stochastiques.

Je remercie Irène Gamba et Irène Giardina pour avoir accepté de rapporter ce manuscrit ainsi que Francis Filbet et Patrick Cattiaux pour leur participation à mon jury de thèse.

Je voudrais aussi remercier Michel Ledoux pour ses passionnants cours de topologie en licence, il y a de ça 7 ans déjà, qui m'ont véritablement donnés envie de poursuivre dans la recherche en mathématique.

Je tiens à remercier les membres de l'institut de mathématique de Toulouse, je pense tout d'abord à Laurent pour ces longues discussions à chercher sans cesse, aux "petits nouveaux" Amic, Manu et Robin, puis à Domi et Laétitia (bon courage à vous deux). Un grand merci aussi aux "anciens" Samy, Thierry, Michael, Jean-Luc, Ali, Mounir et Raymond qui m'ont fait part de leur expérience.

Quant à ma seconde "famille scientifique" du CRCA, je voudrais remercier l'ensemble de l'équipe EMCC pour m'avoir fait découvrir l'univers de la biologie (ainsi que des discussions scientifiques "enflammées" auxquelles, en tant que mathématicien, je n'étais pas habitué...). Je pense à Abel, Arnold, Mehdi, Simon, Alex, mais aussi à Pablo, Marie-Hélène, Chaker, Carole, Niriaska... Sous peine de *représailles*, je me dois aussi de saluer Raphaël (sans qui les discussions seraient sans doute moins passionnées) et

j'en profite pour saluer Vincent, Richard et Audrey.

Je tiens enfin à remercier ma famille qui m'a soutenu dans cette entreprise, mon père, mon frère et Valérie (et ses filles) à qui je dis encore merci.

Et pour finir, comme on dit le meilleur pour la fin, un grand merci à ma petite déesse Hayet qui a su tenir bon et me soutenir dans les flots tumultueux d'un travail de thèse (en espérant qu'elle tienne encore bon jusqu'au 1er Août...).

Contents

Introduction générale (version française)

1 Motivations

On rencontre dans la nature de nombreuses sociétés animales ou groupes d'animaux qui sont le siège de phénomènes collectifs impliquant une coordination très précise des activités individuelles. Ainsi les déplacements collectifs en formation comme les vols d'oiseaux, les bancs de poissons et les migrations d'ongulés conduisent à la formation de structures spatio-temporelles parfois très complexes et donnent lieu à des spectacles saisissants [9, 16]. La question qui se pose est alors de comprendre comment se coordonne le groupe, qu'est-ce qui permet l'apparition de ces structures ? Or pour les vols d'oiseaux ou les bancs de poissons, l'organisation au sein du groupe ne se fait pas de manière centralisée, il n'y a pas de leader qui coordonne le groupe. C'est uniquement au travers d'interactions locales entre congénères que se fait la coordination de l'ensemble du groupe. Dès lors, il est naturel de se demander quelles sont les règles qui gouvernent les interactions entre individus et qui permettent la coordination de leurs comportements [25].

Devant la multitude des réponses possibles à cette question, certains biologistes ou physiciens ont parfois recours à la modélisation pour tester différentes hypothèses de règles d'interactions et étudier différents scénarios. La plupart des modèles utilisés sont des modèles individus centrés qui décrivent le comportement de chaque individu séparément. Pour faire une analogie avec la physique, on parle aussi de modèles microscopiques. Il est généralement difficile de prédire quelle va être le comportement collectif du groupe à partir d'un modèle individu centré. Pour répondre à cette question, on utilise des simulations numériques des modèles individus centrés afin d'observer le comportement du groupe.

L'approche qui est développée dans cette thèse est différente, nous essayons de comprendre les déplacements collectifs en introduisant des modèles macroscopiques. L'idée principale est de pouvoir dériver des modèles macroscopiques à partir des modèles microscopiques ce qui nous permet d'établir un lien analytique entre dynamique individuelle et dynamique collective.

2 Modèles de déplacements en biologie

Le comportement collectif des sociétés animaux reste bien souvent un phénomène mystérieux. Il est très difficile de déterminer quelles sont les mécanismes individuels qui permettent l'apparition de structures au niveau collectif. Cette difficulté provient d'une part que les individus peuvent avoir des comportements différents et d'autre part que la multitude des interactions provoquent des effets non-linéaires. L'apport des modèles pour étudier les déplacements collectifs réside alors dans le fait de pouvoir tester différentes hypothèses sur les mécanismes d'interactions entre individus. Un modèle pourra alors dans certains cas "valider" certaines hypothèses sur les interactions si la dynamique collective observée reproduit certaines caractéristiques de la dynamique collective. Dans d'autres cas, le modèle permettra d'infirmer certaines hypothèses si la dynamique collective obtenue est sensiblement différente de la dynamique collective observée. Néanmoins, il faut garder en mémoire que le but d'un modèle n'est pas de reproduire fidèlement la réalité mais plus modestement d'aider à la compréhension d'un phénomène observé[1].

2.1 Modèles et expériences

On peut distinguer deux types d'approches pour modéliser les déplacements en biologie. Une première approche consiste à se baser d'abord sur les phénomènes collectifs observés. On propose ensuite un modèle d'interactions pour reproduire la dynamique collective. Les hypothèses faites sur les règles d'interactions entre individus sont déterminées *a priori*. Beaucoup de modèles, en particulier pour les bancs de poissons, reposent sur cette approche. L'apparition des ordinateurs et l'utilisation de simulations numériques ont beaucoup contribué au développement de cette méthode.

L'intérêt principal de cette approche est de montrer qu'à partir de règles simples, on peut reproduire des phénomènes collectifs complexes. Néanmoins, le principal inconvénient est qu'il est difficile de montrer que le modèle proposé correspond bien aux lois d'interactions entre individus. Plusieurs modèles se basant sur des règles d'interactions différentes peuvent aboutir à des comportements collectifs similaires. Dès lors, comment déterminer quelles sont les véritables règles d'interactions ?

Une autre approche pour modéliser les phénomènes collectifs consiste à étudier et modéliser le comportement des individus à partir des expériences dédiées à cet effet. On cherche alors à construire un modèle pas à pas à partir des données expérimentales. C'est une approche plus ambitieuse que la méthode précédente mais aussi plus délicate. D'une part les résultats expérimentaux peuvent varier d'une expérience sur l'autre et par conséquent les mesures effectuées peuvent fluctuer sensiblement. D'autre part, on dispose d'un nombre limité d'expériences alors qu'un modèle nécessite de nombreux paramètres. Des exemples de ce type d'approche ont été utilisés pour modéliser le déplacement des blattes [13], des fourmis [23, 2] et des piétons [37].

[1] "*Essentially, all models are wrong, but some are useful.*" George E. P. Box

2.2 Des exemples de modèles pour les déplacements collectifs

Dans cette partie, on introduit des modèles standards utilisés pour modéliser le déplacement collectif de groupes d'animaux en séparant ces modèles en deux catégories. On distingue tout d'abord les modèles individus centrés, appelées aussi "modèles microscopiques". Ces derniers décrivent le déplacement de chaque individu séparément. Un autre type de modèle consiste à décrire le déplacement d'un groupe d'individus dans son ensemble. On regarde l'évolution d'une masse d'individus indiscernables. On parle alors de "modèles macroscopiques".

2.2.1 Modèles individus centrés

Dans les modèles individus centrés, on décrit le déplacement de chaque individu séparément. Un individu est représenté par certaines variables comme sa position, sa vitesse et son accélération. Le modèle décrit alors l'évolution de ces variables dans le temps, cette évolution pouvant être décrite de manière continue ou discrète. Le comportement d'un individu ne pouvant être décrit de façon déterministe, les modèles individus centrés possèdent pour la plupart une part d'aléatoire. Autrement dit, mathématiquement, l'évolution dans le temps des variables est décrite par des processus stochastiques.

Pour décrire les règles d'interactions entre individus, un modèle doit tout d'abord décrire le déplacement d'un individu isolé. Un modèle standard consiste à segmenter la trajectoire des individus par des droites. La vitesse des individus est alors décrite par des changements brusques de direction. Les différents paramètres de ce modèle peuvent être mesurés expérimentalement. Ce modèle est notamment utilisé pour décrire le déplacement des fourmis et des blattes [13, 23, 2]. Un autre modèle couramment utilisé décrit l'évolution de la vitesse non pas par des changements brusques mais par une succession de petites perturbations [8, 5]. On parle de marche aléatoire corrélée. Mathématiquement, on dira que le premier modèle est un processus de sauts sur la vitesse, alors que le deuxième modèle est un processus de diffusion. Un des travaux de cette thèse a été d'étendre la modélisation de déplacement individuel pour décrire des trajectoires courbes que ne permettent pas ces deux modèles.

De nombreux modèles individus centrés sont utilisés pour décrire les déplacements collectifs [42, 16]. On se propose ici simplement de donner un bref aperçu de modèles présents dans la littérature. Ces modèles ont comme avantage de reposer sur des règles d'interactions simples, mais ils ont comme inconvénient de ne pas être basés sur des données expérimentales.

Un premier modèle générique pour décrire les interactions entre individus est le modèle de Vicsek [53]. Dans ce modèle, les individus s'alignent à chaque pas de temps avec la vitesse moyenne de leurs voisins (voir figure 1). Á partir de cette dynamique, on observe l'apparition d'un déplacement collectif global dans lequel les individus se déplacent dans une même direction. Dans le modèle, une perturbation est aussi ajoutée sur la vitesse des individus à chaque pas de temps. Si la perturbation est importante, l'alignement global des individus sera très faible. Beaucoup de travaux ont été consacrées sur la dépendance de l'alignement global avec l'intensité de la perturbation

[53, 26, 39, 13]. D'autres travaux portent sur les conditions suffisantes pour que les vitesses de tous les individus convergent vers une même direction [18, 28]. D'un point de vue modélisation, le modèle de Vicsek est souvent vu comme un modèle sur les vols d'oiseaux mais il a été aussi utilisé récemment pour étudier le déplacement de crickets [7]. De part son aspect minimal, d'autres règles d'interactions peuvent aisément lui être rajoutées [27, 26]. Dans le cadre du projet Starflag [11, 12], une autre façon d'implémenter le modèle a été proposée. Pour calculer la vitesse moyenne, chaque individu prendra en compte ses 6 ou 7 plus proches voisins, quelque soit leur distance [2]. Cette nouvelle façon d'implémenter la règle d'alignement permet d'obtenir au niveau collectif des structures plus stables face à des perturbations.

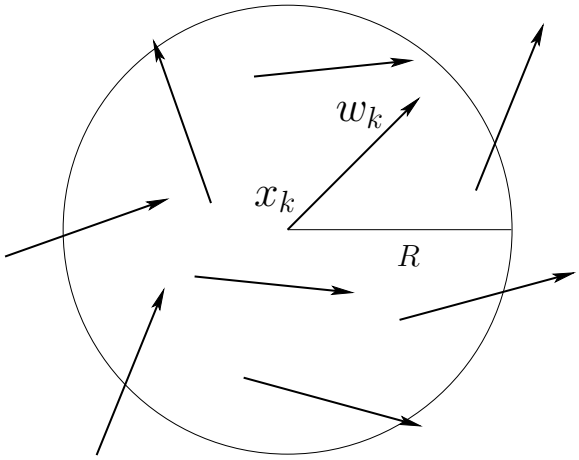

Figure 1: Le modèle de Vicsek : chaque particule renouvelle sa vitesse en s'alignant avec la vitesse moyenne des particules autour d'elle. Le disque de rayon R détermine quelles sont les particules prisent en compte pour évaluer cette moyenne.

Pour les déplacements de bancs de poissons, les modèles généralement utilisés reposent sur 3 règles d'interactions, à savoir l'attraction, l'alignement et la répulsion. Chacune de ces règles comportementales est représentée par une zone autour du poisson (voir figure 2). Suivant la position relative d'un voisin, le poisson aura comme réaction soit de se rapprocher de son congénère (zone d'attraction), soit de s'aligner (zone d'orientation), soit de s'éloigner (zone de répulsion). Le premier modèle utilisant cette description est le modèle d'Aoki [1]. Dans ce modèle, le poisson considère uniquement ces 4 plus proches voisins et pour renouveler sa vitesse l'algorithme consiste à faire une moyenne de l'influence des 4 plus proches voisins. Les simulations numériques de ce modèle permettent d'observer la formation d'un groupe compact avec un mouvement plus ou moins coordonné suivant les paramètres du modèle. Cette étude a permis de développer l'idée qu'il n'y avait pas besoin de leader pour avoir un groupe cohérent se déplaçant de façon homogène. Ce modèle a ensuite été repris par Huth & Wissel [31] en modifiant la sommation des influences (un poids supplémentaire est rajouté aux plus proches voisins). Dans cette étude, les auteurs observent que la moyenne des influences permet d'obtenir une cohérence du groupe plus grande que si l'on ne prend en compte que le plus proche voisin.

Plus récemment, un modèle simplifié des 3 zones a été introduit par Couzin et al [17]. Les vitesses des poissons sont supposées constantes en module (elles étaient distribuées selon une loi gamma dans les modèles précédents), pour renouveler les vitesses on effectue une moyenne de vecteurs (dans le modèle d'Aoki, on construit d'abord une certaine loi de probabilité pour ensuite générer un nombre aléatoire). En revanche, les simulations numériques sont réalisées avec un plus grand nombre d'individus (100 au lieu de 8 pour le modèle d'Aoki). Suivant les paramètres du modèles, on observe alors la formation de 3 types de configuration spatial pour le groupe. Les poissons peuvent soit rester groupés sans cohésion (formation essaim), soit tourner autour d'un axe virtuel (formation en vortex), ou bien encore se déplacer dans une même direction (formation alignée). Le modèle de Couzin et al. a été étendu par [30], les auteurs considèrent une zone d'interaction R qui va dépendre de la densité de poissons. Lorsque la densité d'individus autour du poisson est grande, le rayon d'interaction R diminue. Cette idée se rapproche du modèle proposé dans le projet Starflag on l'on ne prend en compte que les 6 ou 7 plus proches voisins.

L'étude des modèles à 3 zones est toujours un domaine de recherche actif. On trouvera par exemple des travaux sur des modèles où les zones d'interaction changent graduellement avec la distance du poisson [54, 34]. Pour avoir une vue d'ensemble des différents modèles sur la modélisation des déplacements de poissons, on pourra se référer aux articles [43, 44].

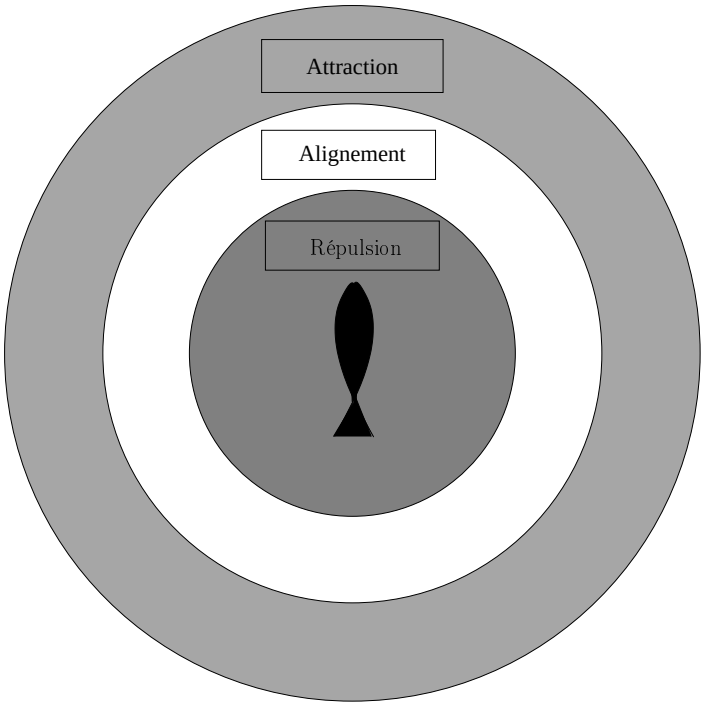

Figure 2: Le modèle des 3 zones décrivant l'interaction d'un poisson avec ces congénères. À courte distance, les poissons se repoussent, à une distance intermédiaire, les poissons s'alignent et à une distance plus éloignée, les poissons s'attirent.

Enfin, une autre approche très populaire pour les modèles individus centrés est

d'interpréter le déplacement des individus comme une particule soumise à des "champs de forces". On considère que chaque individu va agir comme une force qui va repousser ou attirer ces voisins [36]. Ce type d'approche a par exemple été utilisée pour modéliser les bancs de poissons [40] ou bien encore le déplacement de piétons [29]. Á la différence des modèles précédents (modèle de Vicsek ou modèle des 3 zones), les interactions entre individus sont des sommes linéaires ce qui permet d'obtenir des résultats analytiques sur le comportement du système de particules [19]. Il est d'ailleurs intéressant de constater qu'avec ce type de modèle d'attraction-répulsion, on peut observer dans certains cas l'apparition d'un alignement global des particules [15]. Ceci est à l'encontre des observations faites sur les modèles à 3 zones pour lesquels, si l'on enlève la zone d'alignement, on perd l'alignement global du groupe.

2.2.2 Modèles macroscopiques

Comme dans les déplacements collectifs, on peut compter plusieurs millions d'individus, il peut être intéressant de modéliser non pas les individus séparément mais la masse d'individus. Les modèles macroscopiques décrivent alors l'évolution de cette masse indiscernable d'individus [41, 38, 22]. Les modèles généralement utilisés sont des équations d'advection-diffusion. Le terme de diffusion traduit au niveau macroscopique le comportement aléatoire des individus, alors que le terme d'advection exprime dans quelle direction se dirige en moyenne les individus. Généralement le terme de diffusion est supposé constant (indépendant de la densité), la non-linéarité du modèle provient du terme d'advection. Différents modèles sont utilisés pour exprimer ce terme d'advection. Par exemple, le terme d'advection peut être définit par une convolution sur la densité [35, 21, 50, 51]. Cette convolution traduit au niveau macroscopique l'attraction et la répulsion entre les individus. Le terme d'advection peut aussi dépendre d'une quantité autre que la densité, comme la vitesse moyenne des individus qui devient à son tour une inconnue [52]. Pour les modèles de déplacements de bactéries, le terme d'advection va dépendre d'une quantité appelé chimioattractant. Ceci permet de modéliser l'attraction des bactéries vers une substance chimique. On a alors deux équations d'évolution couplées, une pour la masse de bactérie et l'autre pour le chimioattractant [38].

Les modèles macroscopiques ont l'avantage de pouvoir être analysés théoriquement. On dispose d'un cadre mathématique dans lequel on peut prédire et *démontrer* quel va être le comportement des solutions au modèle. Pour les modèles individus centrés, les résultats théoriques sont peu nombreux [15]. Une majorité des travaux sont empiriques, on observe le résultat des simulations numériques. Néanmoins dans la littérature sur les déplacements collectifs, les modèles individus centrés sont plus fréquemment étudiés que les modèles macroscopiques. La raison principale est que la démarche généralement employée pour comprendre les déplacements collectifs est de se baser sur le comportement individuel, comme le font les modèles individus centrés. C'est une approche *bottom-up*, on cherche à comprendre le comportement collectif à partir du comportement individuel. Or pour les modèles macroscopiques, on se place directement au niveau du groupe. La démarche de modélisation se rapproche plus d'une méthode *top-down*.

Une façon de remédier à cette faiblesse des modèles macroscopiques est de lier modèles individus centrés et modèles macroscopiques, c'est-à-dire que l'on cherche à *dériver* un modèle macroscopique à partir d'un modèle individus centrés. Le passage d'un modèle à un autre se fait par un changement d'échelle sur les variables de temps et d'espace. Autrement dit, pour passer d'un modèle individus centrés à un modèle macroscopique, on regarde la dynamique sur de grandes périodes de temps et sur de grandes distances. Si l'on arrive ainsi à dériver un modèle macroscopique, celui-ci aura l'avantage de pouvoir être relié à une dynamique individuelle pouvant être mesurée expérimentalement. De plus, le modèle macroscopique dispose d'un cadre mathématique adéquat dans lequel on peut prédire le comportement des solutions. On cumule ainsi l'avantage des modèles individus centrés et des modèles macroscopiques.

Pour dériver un modèle macroscopique à partir d'un modèle microscopique, on utilise généralement une description intermédiaire entre ces deux échelles appelée échelle mésoscopique (on parle alors d'*équation cinétique*). Cette démarche a été utilisée par exemple pour un modèle de chimiotaxie décrivant le déplacement de bactéries attirées par du chimioattractant [45, 23, 24]. À l'origine, cette approche a été développée dans le cadre de la dynamique des gaz, elle permet de passer d'un modèle de collision entre particules (échelle microscopique) à des modèles de dynamique des fluides (échelle macroscopique) [20].

Le présent mémoire s'inscrit dans cette démarche où l'on cherche à relier modèles individus centrés et modèles macroscopiques, les modèles individus centré étant si possible basés sur des données expérimentales (figure 3).

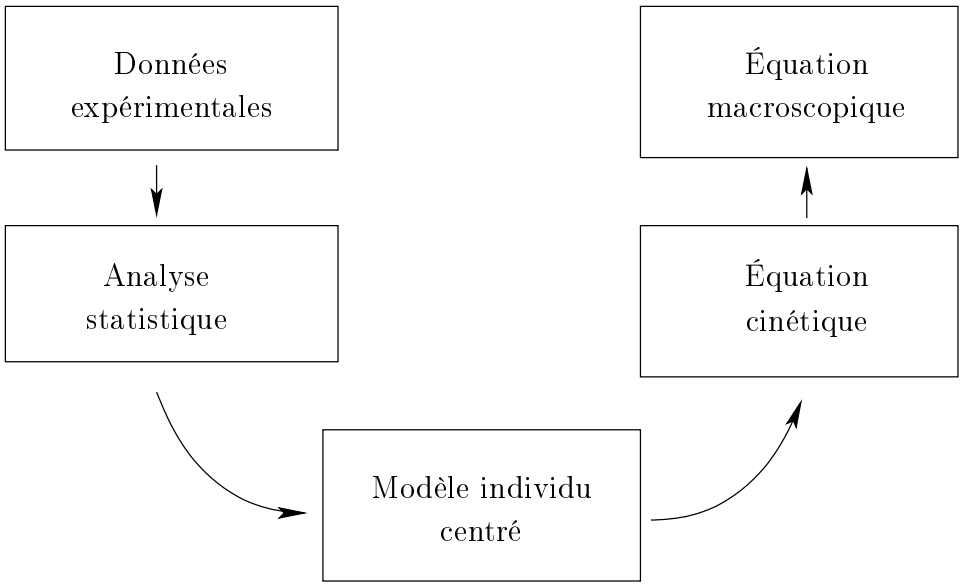

Figure 3: Un schéma idéalisé pour obtenir un modèle de déplacement macroscopique. En se basant sur une étude statistique de données expérimentales, un modèle de déplacement individus centrés est développé. À la suite de quoi, un modèle macroscopique est dérivé en utilisant l'équation cinétique associée au modèle individus centrés.

3 Apport des travaux réalisés

Afin de développer un modèle de déplacement de poissons basé sur des données expérimentales, des expériences ont été réalisées à la Réunion en 2002 sur une espèce de poisson pélagique le Kuhlia mugil. Ces expériences ont abouti à la construction d'un nouveau modèle intitulé "Persistent Turning Walker" (PTW). Une grande partie des travaux réalisés au cours de cette thèse sont associés à l'étude de ce modèle. Une des caractéristiques qui rend ce modèle intéressant est qu'il nécessite de prendre en compte la dérivée troisième de la position. Or jusqu'à présent, l'ensemble des modèles utilisés pour les déplacements individuels ne faisaient intervenir que la dérivée seconde, c'est-à-dire l'accélération par analogie avec la physique. Ainsi, nous avons disposé de nouvelles équations sur lesquelles travailler. De plus, les différents résultats obtenus sur le modèle PTW ont pu ensuite être confrontés avec les données expérimentales. Les travaux réalisés ont permis en particulier de déterminer quel était le modèle macroscopique associé au modèle PTW. Une des motivations de cette étude a été initiée par nos collaborateurs biologistes qui souhaitaient connaître l'équation de diffusion associée au modèle PTW. La dérivation du modèle macroscopique a permis de fournir une réponse à cette interrogation.

D'une manière générale, nos travaux se sont concentrés sur la dérivation de modèles macroscopiques à partir de modèles individus centrés. Cette démarche nous a également permis de dériver un modèle macroscopique à partir du modèle de Vicsek. Le

modèle que nous avons obtenu est original et la méthode utilisée pour la dérivation est non conventionnelle. En effet, à l'origine, les méthodes de dérivation de modèles macroscopiques sont issues de la dynamique des gaz. Elles reposent sur des lois de conservation. Or dans le modèle de Vicsek, et plus généralement dans les modèles individus centrés en biologie, nous n'avons pas de lois de conservation. Certes, les modèles préservent le nombre d'individus et donc nous avons à l'échelle macroscopique l'équation de conservation de la masse. Mais cela n'est pas suffisant pour déterminer un modèle macroscopique. C'est pour cela qu'il a fallu généraliser les méthodes utilisées pour dériver des modèles macroscopiques.

L'intérêt des modèles macroscopiques est tout d'abord qu'ils s'écrivent dans un cadre unifié, celui des équations aux dérivées partielles. Ceci facilite le développement d'une théorie et par conséquent permet de trouver des résultats analytiques. On peut de plus comparer les modèles macroscopiques entre eux grâce à ce formalisme. Une des faiblesses des modèles individus centrés est que bien souvent on ne peut pas les comparer si ce n'est de façon qualitative. De plus, des modèles individus centrés basés sur des règles d'interactions similaires peuvent aboutir à des conclusions contradictoires [44]. D'autre part les modèles macroscopiques s'écrivent avec des paramètres différents des modèles individus centrés (comme par exemple le coefficient de diffusion), ceci donne d'autres informations sur la dynamique du modèle. De plus, dans les modèles individus centrés, le temps de simulation numérique grandit fortement avec le nombre d'individus mise en jeu. Plus on a d'individus, plus la simulation numérique nécessitera du temps de calcul. Pour les modèles macroscopiques, ce n'est pas le cas. Le nombre d'individus est simplement représenté par une densité, le temps de calcul ne va pas dépendre de la valeur de cette densité.

Enfin, les modèles macroscopiques peuvent aider à comprendre la formation de structures particulières, comme par exemple les ondes de propagation ou les ondes de choc. Dans les modèles individus centrés, nous avons uniquement une description des trajectoires individuelles et par conséquent nous n'avons pas directement accès aux grandeurs qui permettent de décrire les structures macroscopiques.

3.1 Le modèle Persistent Turning Walker

Comme la plupart des modèles de déplacements, le modèle PTW utilisé pour modéliser le déplacement des poissons est un modèle stochastique, c'est-à-dire qu'il introduit une part d'aléatoire dans le comportement du poisson. Mais à la différence des modèles utilisés jusqu'à présent, l'aléa est ici porté par la courbure de la trajectoire du poisson et non pas par la vitesse. L'idée originale qui a aboutit à ce modèle est d'avoir considéré le déplacement des poissons non pas comme une succession de lignes droites mais comme une succession d'arcs de cercle. Par conséquent, la trajectoire est décrite par une série de courbures. Ceci explique pourquoi l'aléa dans le modèle PTW est porté sur la courbure et non pas sur la vitesse. Ce modèle permet en particulier d'obtenir des trajectoires qui sont davantage régulières. On retrouve ainsi une des caractéristiques des trajectoires expérimentales (figure 4).

La méthode utilisée pour dériver un modèle macroscopique à partir du modèle PTW repose sur un changement d'échelle. Ceci nous permet d'observer la dynamique

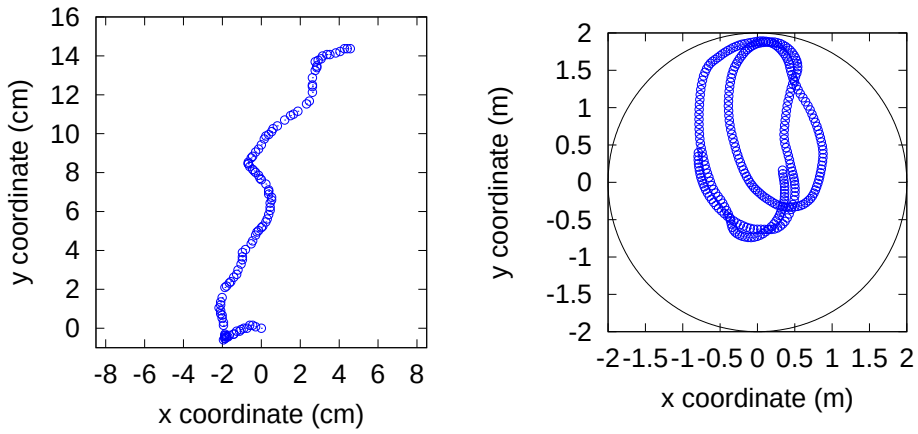

Figure 4: Deux exemples de trajectoires individuelles avec à gauche le déplacement d'une fourmi (genre messor) et à droite le déplacement d'un poisson (espèce Kuhlia mugil). La fourmi a dans cet exemple une trajectoire rectiligne ponctuée de brusques changements de direction alors que la trajectoire du poisson est beaucoup plus arrondie. Les cercles représentent la position de la fourmi (figure gauche) et du poisson (figure droite) au cours du temps. Nous disposons de 8 positions à la seconde pour la figure de gauche et de 12 images par secondes pour la figure de droite.

du modèle dans des variables macroscopiques. Dans le cas du modèle PTW, nous avons effectué un changement d'échelle diffusif. Il nous a permis de dériver une équation de diffusion pour laquelle nous avons pu trouver une expression explicite pour le coefficient de diffusion. Des simulations numériques du modèle PTW ont permis d'illustrer les résultats analytiques obtenus. En particulier, nous avons pu par les simulations numériques du modèle individus centrés estimer le coefficient de diffusion et les mesures effectuées s'accordent avec la valeur théorique du coefficient de diffusion du modèle macroscopique.

Pour étudier le modèle PTW, plusieurs points de vue sont possibles. Tout d'abord, nous pouvons regarder le modèle comme une équation aux dérivées partielles. L'objet de l'étude est alors la densité de distribution des poissons. L'autre point de vue consiste à regarder le modèle d'un point de vue probabiliste, on se place alors dans le cadre des équations différentielles stochastiques. De ce point de vue, une trajectoire d'un poisson représente la réalisation d'un processus stochastique. Les deux angles d'approche utilisent des outils différents, les cadres mathématiques ne sont pas les mêmes. Fort heureusement, les conclusions auxquelles nous avons abouti en utilisant les deux approches sont identiques. Dans les deux cas, nous avons, à partir du modèle PTW, dérivé une équation de diffusion avec le même coefficient de diffusion. Pour la version probabiliste, il s'agissait de montrer qu'à l'échelle macroscopique le modèle PTW devenait simplement un mouvement brownien.

La vision probabiliste a aussi permis de calculer de façon analytique le déplacement carré moyen des trajectoires du modèle PTW. Cette mesure statistique peut également

se calculer dans les expériences menées sur les poissons. Ainsi nous avons obtenu des résultats analytiques pouvant être comparés avec des données expérimentales.

Dans un tout autre contexte, le modèle PTW a aussi permis d'étendre un modèle utilisé dans le cadre d'un problème industriel pour la fabrication de fibres composites. Le modèle décrit le mouvement des fibres sous l'influence de turbulences. Ce modèle introduit de l'aléa sur la dérivée seconde des trajectoires. En s'inspirant du modèle PTW nous avons alors développé un nouveau modèle où l'aléa est introduit sur la dérivée troisième. En utilisant ce nouveau modèle nous obtenons des trajectoires qui ressemblent davantage aux trajectoires réelles des fibres. Un des défauts de l'ancien modèle utilisé était la non-régularité des trajectoires. Ce problème disparaît avec le nouveau modèle. Nous avons également montré que dans un certain régime de paramètres le nouveau modèle introduit se ramène au modèle initial.

3.2 Le modèle de Vicsek : dérivation d'un modèle macroscopique

La seconde partie des travaux a été consacrée à l'étude du modèle de Vicsek. Contrairement au modèle PTW, le modèle de Vicsek n'est pas basé sur des données expérimentales. Cependant de part sa simplicité, il est utilisé dans de nombreux domaines, c'est en quelque sorte un modèle universel.

Plusieurs problèmes restaient en suspens avec ce modèle. D'une part, il est écrit sous la forme d'un algorithme itératif, par conséquent ce n'est pas une dynamique continue dans le temps. Différentes tentatives ont été menées dans le but d'obtenir une version continue de ce modèle [48, 47, 33]. D'autre part, il n'existait pas de modèle macroscopique associé à la dynamique microscopique du modèle de Vicsek. Des travaux ont été initiés dans ce sens en se basant sur une version différente du modèle de Vicsek [4].

Le premier travail accompli a été de trouver une version continue du modèle de Vicsek. Lorsque nous discrétisons la version continue, nous retrouvons exactement le modèle original de Vicsek, à condition de respecter une hypothèse sur la discrétisation. Ensuite concernant la dérivation d'un modèle macroscopique, nous avons du faire face à un obstacle particulier. Le nombre de quantités indépendantes conservé par l'interaction est de dimension strictement inférieure à la dimension de la variété des équilibres thermodynamiques. Cela pose un problème pour la détermination du modèle macroscopique qui se trouve sous-déterminé. Ce problème a été résolu par l'introduction d'un nouveau concept d'invariants collisionnels qui possède une grande généralité et ouvre une voie nouvelle en théorie cinétique. Le modèle macroscopique obtenu est un système hyperbolique non-conservatif avec une contrainte sur la vitesse qui doit être de norme 1 en tout point.

Dans la littérature, il existe d'autres modèles hyperboliques avec contraintes mais ces modèles sont généralement conservatifs [14]. Pour le modèle macroscopique que nous avons obtenu, toute l'étude analytique reste ouverte. Pour le moment, nous nous sommes concentrés sur l'étude numérique du modèle macroscopique où de nouvelles

méthodes numériques doivent être développées. Les simulations numériques montrent que la structure des solutions est plus complexe que ce qui était attendu.

4 Présentation des résultats

Les travaux se sont essentiellement portés sur deux axes de recherche.

Tout d'abord, un premier axe de recherche s'est concentré sur un nouveau modèle appelé "Persistent Turning Walker" (PTW). Ce modèle est issu d'une étude statistique sur le déplacement du poisson Kuhlia mugil (chapitre 1). Nous nous sommes intéressés à la dynamique à grande échelle de ce modèle menant à une équation de diffusion. Cette étude s'est faite d'abord avec des outils issus des équations aux dérivées partielles (chapitre 2) puis avec des outils probabilistes (chapitre 3). Le modèle PTW a aussi permis une extension d'un modèle décrivant le dépôt de fibres utilisé dans le cadre d'un problème industriel pour la fabrication de fibres composites (chapitre 4). En vue d'étendre le modèle PTW pour inclure des interactions entre poissons, nous avons menés une première analyse des données expérimentales du poisson Kuhlia mugil en groupe (chapitre 5).

Dans la perspective d'étudier un modèle d'interactions entre poissons, nous nous sommes consacrés dans une deuxième partie sur l'étude d'un modèle minimal d'interactions introduit par Vicsek. Nous avons tout d'abord dériver un modèle macroscopique à partir de ce modèle en nous basant sur une formulation continue en temps (chapitre 6). Ensuite, nous avons étudié numériquement le modèle macroscopique obtenu en le comparant au modèle microscopique initial (chapitre 7).

Enfin, dans un cadre différent, nous avons étudié un problème d'homogénéisation stochastique provenant de l'étude des déformations de matériaux (chapitre 8). Le lien entre ce problème et la thématique abordée jusqu'alors provient des outils probabilistes utilisés dans cette méthode, l'approche probabiliste étant très répandue pour la modélisation de comportements animaux [6, 46]. De plus, ce problème ouvre de nouvelles perspectives dans la modélisation de déplacement collectif à savoir l'utilisation de modèles macroscopiques probabilistes. Dans la littérature, la plupart des modèles macroscopiques sont déterministes.

4.1 Le modèle PTW

4.1.1 Chap. 1 : Analyzing Fish Movement as a Persistent Turning Walker

Ce chapitre introduit l'analyse des trajectoires du poisson *Kuhlia mugil* se déplaçant dans un bassin. Les expériences montrent que contrairement aux modèles utilisés jusqu'à présent, le déplacement du Kuhlia mugil ne peut être vu comme une succession de segments de droites. En effet, nous observons que le déplacement s'effectue sur des trajectoires courbes. D'après ces observations, une nouvelle façon de modéliser le déplacement du Kuhlia mugil est introduite. Le modèle se base sur l'analyse de l'évolution de la vitesse angulaire du poisson dans les expériences. L'évolution de cette quantité est alors modélisée par une équation différentielle stochastique (équation

d'Ornstein-Uhlenbeck) :

$$dW(t) = -\frac{1}{\tau}W(t)dt + \sigma dB(t) \tag{4.1}$$

où W est la vitesse angulaire du poisson, $B(t)$ est le mouvement brownien, τ et σ sont deux paramètres du modèle. Comme le modèle suppose que la vitesse du poisson est constante en module, cette équation peut aussi s'écrire sur la courbure de la trajectoire du poisson. Ce modèle a été appelé "Persistent Turning Walker" (PTW). Par une analyse statistique des données expérimentales, les paramètres du modèle ont pu être estimés. Pour cela, il a fallu modéliser l'influence du bord du domaine sur la vitesse angulaire du poisson. Ceci a permis de comparer les trajectoires du modèle avec les trajectoires expérimentales. En particulier, une comparaison a été faites sur le calcul du déplacement carré moyen de la position du poisson (figure 5).

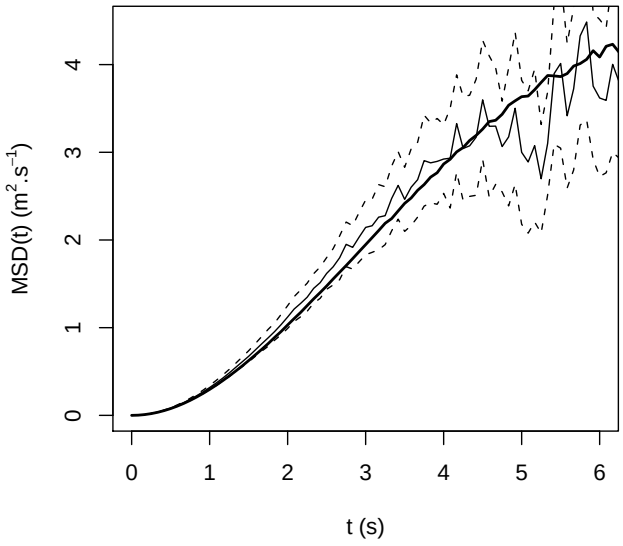

Figure 5: Déplacement carré moyen pour le modèle (trait plein continu) et les données expérimentales (trait pointillé). Pour le modèle, l'estimation a été faites par une méthode de Monte-Carlo. Pour les données expérimentales, nous avons représenté un intervalle de confiance à 95% ainsi qu'une moyenne sur les expériences.

4.1.2 Chap. 2 : Large scale dynamics of the Persistent Turning Walker model of fish behavior

Dans ce chapitre, nous avons étudié la dynamique à grande échelle du modèle PTW introduit pour décrire le déplacement de poissons. Ce modèle s'écrit sous la forme

d'une équation différentielle stochastique :

$$\begin{array}{rcl} \dfrac{d\vec{x}}{dt} & = & \vec{\tau}(\theta), \\ \dfrac{d\theta}{dt} & = & \kappa, \\ d\kappa & = & -\kappa\, dt + \alpha\, dB_t, \end{array} \tag{4.2}$$

où $\vec{x} = (x_1, x_2) \in \mathbb{R}^2$ est le vecteur position du poisson, $\vec{\tau}(\theta) = (\cos\theta\,, \sin\theta)$ est la direction de la vitesse du poisson avec l'angle $\theta \in \Pi = \mathbb{R}/2\pi\mathbb{Z}$ qui est mesuré à partir de la direction x_1, $\kappa \in \mathbb{R}$ est la courbure de la trajectoire du poisson et B_t est le mouvement brownien standard.

Pour étudier la dynamique à grande échelle, nous avons eu recours à deux méthodes différentes. Une première méthode consiste à étudier l'équation différentielle stochastique qui décrit le modèle. Nous nous sommes en particulier intéressés à la variance de la position, nous avons montré que celle-ci se comporte comme une fonction linéaire pour une grande échelle de temps. Le coefficient de diffusion associé au modèle PTW peut être assimilé à la pente de cette fonction linéaire. Ceci nous a permis de trouver une formule explicite pour ce coefficient de diffusion :

$$\mathrm{Var}\{\vec{x}(t)\} \overset{t\to+\infty}{\sim} 2\mathcal{D}\, t, \quad \text{avec} \quad \mathcal{D} = \int_0^\infty \exp\left(-\alpha^2(-1+s+\mathrm{e}^{-s})\right) ds, \tag{4.3}$$

où Var représente la variance.
La deuxième méthode se base sur l'équation de Kolmogorov *forward* associée au modèle PTW. C'est une équation aux dérivées partielles qui décrit l'évolution de la densité de distribution de poisson, notée f, au cours du temps. Elle est donnée par la formule suivante :

$$\partial_t f + \vec{\tau}\cdot\nabla_{\vec{x}} f + \kappa\partial_\theta f - \partial_\kappa(\kappa f) - \alpha^2\partial_{\kappa^2} f = 0. \tag{4.4}$$

Pour étudier la dynamique à grande échelle à partir de cette équation, nous avons utilisé un changement d'échelle diffusif dans les variables de temps et d'espace. Pour cela nous introduisons un petit paramètre ε et l'on définit de nouvelles variables de temps et d'espace :

$$t' = \varepsilon^2 t \quad ; \quad \vec{x}' = \varepsilon\vec{x}. \tag{4.5}$$

Le passage d'une échelle microscopique à une échelle macroscopique est obtenu lorsque ε tend vers zéro. En utilisant ce changement d'échelle, nous avons montré que l'équation (4.4) est ramenée à une équation de diffusion à l'échelle macroscopique. Nous montrons que la fonction de distribution f converge vers un certain état "d'équilibre thermodynamique", qui est une distribution gaussienne en courbure et une distribution uniforme pour la direction de la vitesse. L'équilibre dépend alors seulement de la densité, celle-ci vérifie une équation de diffusion.

Afin de lier les deux approches développées précédemment, nous avons montré que le tenseur de diffusion présent dans la deuxième méthode peut être représenté par une

formule qui introduit la solution de l'équation différentielle stochastique présent dans la première méthode. Ceci nous a permis de trouver la formule explicite du tenseur de diffusion, qui correspond exactement à ce qui a été démontré à partir de la première méthode (voir 4.3).

4.1.3 Chap. 3 : Long time fluctuation and diffusion limit for the Persistent Turning Walker Model

Dans ce chapitre, nous étudions la limite de diffusion du modèle PTW. À la différence du chapitre précédent, nous utilisons dans cette étude uniquement des outils probabilistes.

Pour obtenir une équation de diffusion à partir du modèle PTW, nous utilisons seulement l'équation différentielle stochastique donnée par le système (4.2). En utilisant le changement d'échelle diffusif (voir équation 4.5), le modèle PTW devient avec les notations probabilistes :

$$\begin{cases} d\vec{x}_t = \varepsilon \vec{\tau}(\theta_t)\, dt \\ d\theta_t = \kappa_t \dfrac{dt}{\varepsilon^2} \\ d\kappa_t = -\kappa_t \dfrac{dt}{\varepsilon^2} + \sqrt{2}\alpha \dfrac{dB_t}{\varepsilon}, \end{cases} \tag{4.6}$$

où l'on a repris les notations du chapitre 4.1.2 (voir équation 4.2). L'étude consiste à étudier la limite lorsque ε tend vers zéro de ce système.

Cette étude se fait en deux étapes. Tout d'abord, nous étudions la dynamique du processus (θ_t, κ_t). Pour cela, nous analysons le générateur infinitésimal L de ce processus. Nous montrons grâce à l'utilisation d'une fonction de Lyapunov que le générateur satisfait une inégalité de Poincaré. Ceci entraîne la convergence exponentielle du processus (θ_t, κ_t) vers une mesure stationnaire. En particulier, nous prouvons l'existence d'une solution à l'équation elliptique associée à l'opérateur L.

Dans une deuxième étape, nous étudions le vecteur position $\vec{x}_t$. Celui-ci est donnée simplement par l'intégrale du vecteur vitesse $\vec{\tau}(\theta_t)$. En utilisant, la solution de l'équation elliptique associé à l'opérateur L, nous obtenons une nouvelle formulation de l'intégrale satisfaite par $\vec{x}_t$. Il ne nous reste plus qu'à utiliser des outils standards en probabilité comme la formule d'Itô pour montrer que le processus $\vec{x}_t$ est dans la limite $\varepsilon \to 0$ un mouvement brownien.

4.1.4 Chap. 4 : A smooth model for fiber lay-down processes and its diffusion approximations

Dans ce chapitre, nous introduisons un nouveau modèle développé pour décrire le mouvement de fibres sous l'influence de turbulences. Ce modèle est utilisé dans le cadre d'un problème industriel pour la fabrication de matériaux composites.

Le modèle original pour modéliser les trajectoires de fibres possède une lacune à savoir la non-régularité des trajectoires. Pour palier à ce problème, nous avons introduit un nouveau modèle inspiré du modèle PTW. Ce modèle est donné par l'équation

différentielle stochastique suivante :

$$\begin{aligned} d\vec{x}_t &= \vec{\tau}(\theta_t)\, dt \\ d\theta_t &= \kappa_t\, dt \\ d\kappa_t &= \lambda(\kappa_0 - \kappa)\, dt + \mu dB_t, \end{aligned} \tag{4.7}$$

où l'on a repris les notations du chapitre 4.1.2 (voir équation 4.2), avec de plus un terme de rappel vers l'origine κ_0 donné par

$$\kappa_0 = b(|\vec{x}_t|)\sin(\theta_t - \phi), \tag{4.8}$$

avec $b(.)$ une fonction positive, ϕ la direction du vecteur position $\vec{x}_t$ c'est-à-dire $\vec{\tau}(\phi) = \frac{\vec{x}_t}{|\vec{x}_t|}$. Afin de faire le lien entre ce nouveau modèle et les modèles existants, nous nous sommes alors intéressés à étudier la limite de l'équation (4.7) dans différents régimes.

Dans un premier temps, nous avons étudié la limite de l'équation (4.7) lorsque les deux paramètres λ et μ vérifiaient :

$$\lambda' = \varepsilon^2\lambda \quad ; \quad \mu' = \varepsilon^2\mu \tag{4.9}$$

avec $\varepsilon << 1$. Dans la limite $\varepsilon \to 0$, nous obtenons le modèle original utilisé pour modéliser les trajectoires de fibres.

Ensuite, nous avons étudié un autre asymptotique à savoir :

$$\lambda' = \varepsilon\lambda \quad ; \quad \mu' = \varepsilon^{3/2}\mu. \tag{4.10}$$

Dans cette asymptotique, l'équation (4.7) devient à la limite $\varepsilon \to 0$ une équation d'advection-diffusion.

Cette étude nous permet d'avoir un schéma complet liant 3 types de modèle pour d'écrire les trajectoires de fibres. Des simulations numériques du nouveau modèle introduit dans les différents régimes (4.9-4.10) viennent illustrer la théorie développée.

4.1.5 Chap. 5 : Statistical analysis of the trajectories of Kuhlia Mugil fish

Ce chapitre a pour but d'étudier les données expérimentales sur le poisson Kuhlia mugil en groupe. Cette étude constitue une première étape dans la construction d'un modèle de poissons en interactions qui sera une extension du modèle PTW.

Nous disposons de données expérimentales pour les trajectoires de poissons pour différentes tailles de groupe. Des expériences ont été menées avec 2, 5, 10, 15 et 30 poissons. Pour étudier ces trajectoires, nous avons mené une étude statistique en nous basant sur 3 points de vue différents.

Tout d'abord, nous avons analysé les trajectoires prises individuellement en fonction de la taille du groupe. Nous remarquons en particulier que les trajectoires individuelles possèdent une caractéristique commune quelque soit la taille du groupe (voir figure 6). L'autre point de vue adopté est de regarder le déplacement du groupe de poissons dans son ensemble. Nous étudions pour cela la densité de poissons d'une part et la vitesse du groupe de poissons dans le bassin d'autre part. Nous observons en particulier que

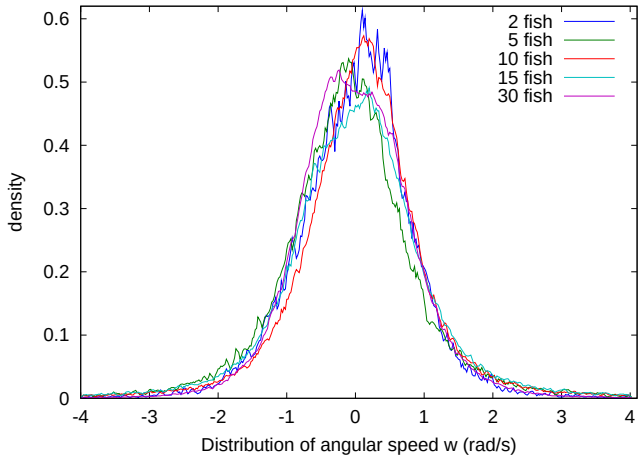

Figure 6: Les distributions de vitesse angulaires W des trajectoires individuelles des poissons pour différentes tailles de groupe. Les distributions ont une forme gaussienne centrée avec une variance voisine de .7 $(1/s^2)$.

pour certaines expériences une structure spécifique se dessine. Au niveau collectif, un phénomène inattendu se produit : plus la taille du groupe augmente, moins le groupe est aligné. Ce phénomène est à l'opposé de ce que prédit par exemple le modèle de Vicsek [53].

Enfin, nous avons regardé comment un individu se positionne au sein du groupe. Pour cela, nous analysons différentes caractéristiques d'un poisson (vitesse, accélération) en fonction de la position de ses voisins. Par exemple, nous avons regardé quelle était la position des voisins dans le référentiel d'un poisson. Nous observons alors dans les expériences à deux poissons que les poissons sont préférentiellement l'un devant l'autre. Nous pouvons aussi observer que l'alignement des poissons est maximal à une certaine distance caractéristique (correspondant à environ deux fois la taille du corps du poisson) quelle que soit la taille du groupe.

Cette étude nous apporte des mesures statistiques que nous pourrons par la suite utilisés pour valider un modèle d'interactions entre poisson.

4.2 Le modèle de Vicsek

4.2.1 Chap. 6 : Continuum limit of self-driven particles with orientation interaction

Ce chapitre est consacré à la dérivation d'un modèle macroscopique à partir du modèle de Vicsek.

Dans le modèle de Vicsek, nous considérons des particules se déplaçant à vitesse constante en module et qui interagissent de manière à augmenter leur alignement. En notant $\vec{x}_k^n$ la position de la particule k au temps $n\Delta t$ avec Δt un pas de temps et ω_k^n

la vitesse, cette dynamique est décrite par les équations suivantes :

$$\vec{x}_k^{n+1} = \vec{x}_k^n + c\,\omega_k^n \Delta t, \tag{4.11}$$
$$\omega_k^{n+1} = \bar{\omega}_k + \varepsilon^n, \tag{4.12}$$

où c est la vitesse des particules, ε^n est une variable aléatoire indépendante représentant le bruit dans le système et $\bar{\omega}_k$ est la moyenne des vitesses autour de la particule $\vec{x}_k$ défini par

$$\bar{\omega}_k = \frac{J_k^n}{|J_k^n|}, \quad J_k^n = \sum_{j,\,|\vec{x}_j^n - \vec{x}_k^n| \le R} \omega_j^n. \tag{4.13}$$

où R est le rayon de perception.

Dans ce travail, nous avons tout d'abord dérivé à partir de cette dynamique discrète une dynamique continue. Celle-ci s'écrit sous la forme d'une équation différentielle stochastique :

$$\frac{d\vec{x}_k}{dt} = c\,\omega_k, \tag{4.14}$$
$$d\omega_k = (\mathrm{Id} - \omega_k \otimes \omega_k)(\nu\,\bar{\omega}_k\,dt + \sqrt{2d}\,dB_t), \tag{4.15}$$

où B_t est le mouvement brownien, $\sqrt{2d}$ est l'intensité du bruit, ν est la fréquence d'interaction. L'opérateur de projection $(\mathrm{Id} - \omega_k \otimes \omega_k)$ permet de garantir que la vitesse reste de module 1 (voir figure 7).

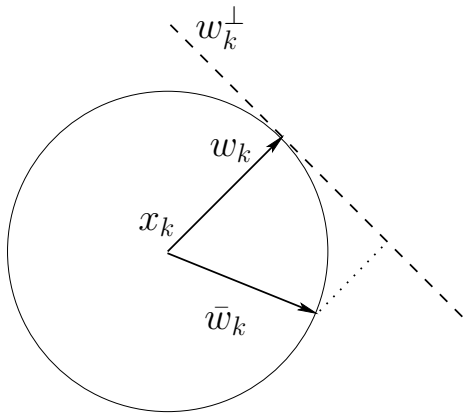

Figure 7: La projection du vecteur $\bar{\omega}_k$ sur l'orthogonal de ω_k permet de garantir que la vitesse des particules reste de module 1.

Pour dériver un modèle macroscopique à partir de la dynamique continue, nous nous sommes servi de l'équation cinétique associé à cette dynamique. Comme les particules sont en interaction, le passage de la dynamique particulaire à l'équation cinétique est uniquement formel. Pour être prouvé rigoureusement, ce passage nécessite l'hypothèse de propagation du chaos qui reste à démontrer. Une fois l'équation cinétique posée, pour dériver un modèle macroscopique, nous nous servons d'un changement d'échelle hydrodynamique :

$$t' = \varepsilon t \quad ; \quad \vec{x}' = \varepsilon \vec{x}. \tag{4.16}$$

Dans les variables (t', x'), la densité de distribution f^ε satisfait l'équation cinétique suivante :

$$\varepsilon(\partial_t f^\varepsilon + \omega \cdot \nabla_x f^\varepsilon) = Q(f^\varepsilon) + O(\varepsilon^2), \tag{4.17}$$

avec :

$$Q(f^\varepsilon) = -\nabla_\omega \cdot (F[f^\varepsilon] f^\varepsilon) + d\Delta_\omega f^\varepsilon \tag{4.18}$$

$$F[f^\varepsilon] = \nu\ (\mathrm{Id} - \omega \otimes \omega)\Omega[f^\varepsilon], \tag{4.19}$$

$$\Omega[f^\varepsilon] = \frac{j[f^\varepsilon]}{|j[f^\varepsilon]|}, \quad \text{et} \quad j[f^\varepsilon] = \int_{v \in \mathbb{S}^2} v\, f^\varepsilon(x, v, t)\, dv. \tag{4.20}$$

Pour obtenir la limite $\varepsilon \to 0$, nous déterminons l'ensemble des états d'équilibre de cette équation cinétique :

$$\mathcal{E} = \{\rho M_\Omega(\omega) \ \mid \ \rho \in \mathbb{R}_+, \quad \Omega \in \mathbb{S}^2\}, \tag{4.21}$$

avec $M_\Omega(\omega) = C \exp\left(\frac{\nu}{d}\, \omega \cdot \Omega\right)$ où Ω est la direction du flux et C est une constante tel que M_Ω soit une densité de distribution. Les états d'équilibre $\mathcal{E}$ forment ainsi une variété de dimension 3. Or les seuls invariants collisionnels pour l'opérateur Q sont les fonctions constantes qui sont de dimension 1. Le modèle macroscopique va donc être sous-déterminé. C'est pour cela que nous introduisons une nouvelle notion plus faible d'invariant collisionnel qui nous permet de récupérer d'autres invariant collisionnel que l'on dit "généralisé". Ceux-ci nous permet de déterminer la limite macroscopique de notre équation cinétique. À la limite $\varepsilon \to 0$, nous obtenons un système d'équation sur la densité ρ et le vecteur direction Ω du flux :

$$\partial_t \rho + \nabla_x \cdot (c_1 \rho \Omega) = 0, \tag{4.22}$$

$$\rho\ (\partial_t \Omega + c_2(\Omega \cdot \nabla)\Omega) + \lambda\, (\mathrm{Id} - \Omega \otimes \Omega)\nabla_x \rho = 0, \tag{4.23}$$

où c_1, c_2 sont les vitesses de convection distinctes et λ est une constante positive. Le modèle macroscopique obtenu est hyperbolique mais non-conservatif à cause de la contrainte sur le vecteur Ω qui doit être de norme 1 ($|\Omega| = 1$), ce qui en fait un modèle original non étudié jusqu'à présent dans la littérature.

4.2.2 Chap. 7 : Numerical studies of the CVA models

Le but de ce chapitre est de valider le modèle macroscopique développé dans le chapitre précédent en le comparant par des simulations numériques avec le modèle microscopique.

Pour réaliser cette analyse, nous devons mieux connaître le modèle macroscopique. Celui-ci est non-conservatif et possède une contrainte géométrique qui en font un modèle non standard ne relevant pas d'une théorie préalable. Nous proposons deux approches différentes pour étudier théoriquement et numériquement le modèle macroscopique. Tout d'abord, nous reformulons le modèle sous une forme conservative particulièrement simple qui semble être la formulation conservative naturelle pour ce problème. Ensuite, nous proposons une autre écriture du modèle macroscopique s'écrivant

comme limite de relaxation d'un modèle conservatif avec un terme source raide modélisant la contrainte de norme 1. Ces deux approches donnent alors deux méthodes numériques différentes, appelé respectivement méthode conservative et méthode splitting.

Or les simulations du modèle microscopique dans un régime dense de particules s'accordent avec les résultats de la méthode splitting alors la méthode conservative donnent des résultats différents. Ceci montre d'une part que nous avons un accord entre le modèle microscopique et le modèle macroscopique. D'autre part, la bonne formulation du modèle macroscopique est donnée par l'intermédiaire de la limite de relaxation.

4.3 Homogenization theory

4.3.1 Chap. 8 : Random integrals and correctors in homogenization

Le but de ce chapitre est d'étudier théoriquement et numériquement l'homogénéisation stochastique d'une équation elliptique. Cette étude n'est pas directement relié avec la modélisation en biologie puisqu'il s'agit d'étudier un modèle de déformation de matériaux. Néanmoins, les outils probabilistes utilisés dans cette étude (mouvement brownien, intégrale stochastique, processus d'Ornstein-Uhlenbeck) sont très largement repris dans les travaux précédents.

La déformation d'un matériaux lorsqu'il est mélangé avec d'autres composants est modélisé par l'équation elliptique suivante :

$$\begin{aligned} &-\frac{d}{dx}\Big(a\Big(\frac{x}{\varepsilon},\omega\Big)\frac{d}{dx}u^\varepsilon\Big) = f(x), \qquad 0 \le x \le 1, \\ &u^\varepsilon(0,\omega) = 0, \qquad u^\varepsilon(1,\omega) = q. \end{aligned} \tag{4.24}$$

où f est la force appliquée sur le matériaux, $a(x,\omega)$ est le coefficient d'élasticité modélisé par un processus stochastique stationnaire. Sous certaines hypothèses, nous pouvons démontrer que la solution $u^\varepsilon(x,\Omega)$ de cette équation elliptique converge lorsque ε tend vers zéro vers la solution déterministe $\bar{u}(x)$ de l'équation suivante :

$$\begin{aligned} &-\frac{d}{dx}\Big(a^*\frac{d}{dx}\bar{u}\Big) = f(x), \qquad 0 \le x \le 1, \\ &\bar{u}(0) = 0, \qquad \bar{u}(1) = q. \end{aligned} \tag{4.25}$$

où le coefficient d'élasticité a^* est donnée par $a^* = \Big(\mathbb{E}\{a^{-1}(0,\cdot)\}\Big)^{-1}$, avec $\mathbb{E}$ l'espérance mathématique selon ω. L'équation (4.25) est appelée équation homogénéisée. Nous nous intéressons alors à la différence entre la solution u^ε de l'équation (4.24) et la solution homogénéisée u^*. Nous distinguons deux cas suivant que la fonction d'autocorrélation du processus $a(x,\omega)$ soit intégrable ou pas. Dans le premier cas, la différence u^ε et u^* converge vers un processus stochastique s'écrivant à partir du mouvement brownien standard. Dans le cas non-intégrable, cette différence s'écrit avec un mouvement brownien fractionnaire. Nous prouvons alors rigoureusement ces deux convergences si le coefficient d'élasticité $a(x,\omega)$ est donnée par une certaine expression. Des simulations numériques viennent ensuite illustrer la théorie.

General Introduction (English version)

1 Motivations

In the nature, many animals societies or group of animals exhibit complex collective phenomena involving precise coordination of the individual activities. For example, the collective displacement of a flock of birds or a shoal of fish leads sometimes to complex spatiotemporal organization and gives spectacular shows [9, 16]. The main question is to understand how such groups manage to coordinate, how could a global structure emerge? In a fish school or in a flock of birds, there is no leader to coordinate the group. It is only through local interactions between individuals that the group manage to coordinate itself [25]. Therefore, it is natural to ask what are these interaction rules which govern their behavior.

Since there are many answers to this questions, some biologists and physicists use models to test different hypotheses for the interaction rules and explore different scenarios. Most of the models used are individual based models which describe how each individual behaves according to its neighbors. To make an analogy with physics, these models are called "microscopic models". It is generally difficult to predict the collective behavior of the group when we use an individual based model. A partial answer is given by numerical simulations. It allows to observe the global dynamics of the models with different parameters.

The approach developed in this manuscript is different, we try to understand the collective behavior using macroscopic models. The main challenge is to connect individual behavior and macroscopic models which enables to link analytically individual and global dynamics.

2 Models of displacement in biology

Collective behavior in animal societies remains a mystery phenomenon. It is very hard to identify what are the individual mechanisms which enables the emergence of collective behavior. One reason is the high degree of variability in the individual behavior. The other reason is the multitude of interactions involved which induce nonlinear effects. The interesting aspect of models is to be able to test different hypotheses on the individual mechanism. A model may in some cases "validate" some assumptions

on the interactions if the collective behavior within the model produces some features observed. On the contrary, a model could invalidate some hypothesis if the collective behavior obtained is very different from the experiments. Nevertheless, we have to keep in mind that the aim of a model is not to reproduce the reality, its purpose is to help the understanding of the observed phenomenon[2].

2.1 Models and experiments

We can distinguish two types of approaches to model collective displacement in biology. One approach is based on the observation of the global dynamics. The purpose is to find the rules of interactions which reproduce the global dynamics. The assumptions made about the rules between individuals are determined a priori. Many models, especially for fish, are based on this approach. The development of computers has popularized this approach.

The main interest of this approach is to show that from simple rules we can reproduce complex collective phenomena. However, the drawback of this approach is the difficulty to prove that the interaction rules within the model corresponds to real mechanisms of individuals. Several models based on different interaction rules may lead to similar collective behavior. Therefore, how could we determine what are the real interaction rules?

Another approach to model the collective displacement consists in measuring and modeling individual behavior from experiments. We try to build a model step by step using experimental data. It is a more ambitious approach than the previous method but also more delicate. First, the experimental results may vary from one experience to another and therefore measurements can fluctuate a lot. Secondly, we have a limited number of experiments while a model requires many parameters. Examples of this type of approach have been used to model the motion of cockroaches [13], ants [23, 2] and pedestrians [37].

2.2 Examples of models for collective displacement

In this part, we introduce standard models used for the collective displacements of animals. We distinguish between two types of model. A first class of models are the individual based models, also called "microscopic models". They describe how each individual moves according to its neighbors. The other type of model describes the displacement of the group of individual as a whole, we have an indistinguishable mass of individuals which evolves in time. We also call these type of models "macroscopic models".

2.2.1 Individual based models

In the individual based model, we describe the motion of each individual separately. An individual is represented by some variables such as its position, its velocity and its

[2] "*Essentially, all models are wrong, but some are useful.*" George E. P. Box

acceleration. The model describes how these variables evolve in time. The evolution could be discrete or continuous in time. The individual behavior could be described by deterministic models, therefore we generally have a stochastic component in individual based models. Mathematically, this means that the evolution of the variables is described by stochastic process.

To model collective displacements, an individual based model must first describe the motion of a single individual. A standard model consists in segmenting the trajectory of the displacement by lines. The velocity of the individual is described by sudden changes in the direction of the velocity. The various parameters of this model can be measured experimentally. This model is used to describe the movement of ants and cockroaches [13, 23, 2].

Another model commonly used is the correlated random walk. In this model, instead of jumps on the velocity, there is a succession of small perturbations [8, 5]. Mathematically, we would say that the first model is a jump process on the velocity, while the second model is a diffusion process. In this manuscript, we study an extension of the correlated random walk in order to model smooth trajectories.

There are many individual based models which describe collective displacements [42, 16]. Here, we simply give a short overview of some models in the literature. The interaction rules in these models are relatively simple but they are not based on experimental data.

A generic model to describe interactions between individuals is the Vicsek model [53]. In this model, individuals align with their neighbors at each time step. To do so, the velocity of each individual is update with the mean velocity of its neighbors (see figure 8). From this individual dynamics, we observe the emergence of a collective movement in which individuals move in the same direction. In the model, a noise is also added on the individual velocity at each time step. If the noise is important, the global alignment of individuals will be very low. Many studies have been done to understand the dependence of the group polarization with the intensity of the noise [53, 26, 39, 13]. Other type of works study the necessary conditions to have the convergence of all the individual velocities to a common direction [18, 28].

From a modeling perspective, the Vicsek model is usually seen as a model for flocks of birds but it has also been recently used to model the movement of locusts [7]. Due to its simplicity, other interaction rules can easily be added [27, 26]. In the Starflag project [11, 12], another way to implement the interaction rules has been proposed. To calculate the mean velocity, each individual takes into account its 6 or 7 nearest neighbors, whatever the distances they are [2]. This new way to implement the alignment rule makes the collective motion more stable.

The models commonly used to describe fish motion are based on 3 interaction rules, namely the attraction, the alignment and the repulsion. Each of these rules is represented by an area around the fish (see figure 9). Depending on the relative position of a neighbor, the fish will either tend to move closer to its congener (attraction area), or align (alignment area) or move away (repulsion area). The first model using this description is the model of Aoki [1]. In this model, a fish only takes into account its 4 nearest neighbors. To update the velocity, the algorithm consists in making a mean of

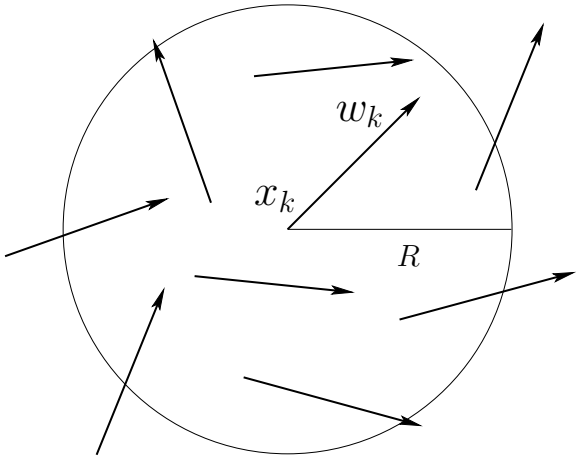

Figure 8: The Vicsek model: each particle updates its velocity with the mean velocity of the particles around it. The disc with radius R determines which are the particles taken into account in the estimation of the mean velocity.

the influence of the 4 nearest neighbors. In the numerical simulations of this model, we observe the formation of a compact group with a collective movement more or less coordinated according to the parameters of the model. This model enabled to develop the idea that it is not necessary to have a leader to generate a coordinated group motion. This model is studied again by Huth & Wissel [31] where they change the summation rule (an additional weight is added to nearest neighbors). In this study, authors observe that the group is more stable when fish take an average influence of their neighbors instead of taking into account only their nearest neighbor.

More recently, a simplified version of the 3 "zone-based" model was introduced by Couzin et al. [17]. The speeds of the fish are assumed to be constant (they were distributed according to a Gamma distribution in the previous models), to update the velocities, we simply take an average of vectors (in the model of Aoki, we first construct a certain law of probability and then we generate a random number according to its law). On the other hand, numerical simulations are performed with a larger number of fish (100 instead of 8 in the work of Aoki and Huth & Wissel). Depending on the parameters of the model, the spatial configuration of the group can be in three different formations. Fish can form a compact group without cohesion (swarm formation), or turn around a virtual axis (torus formation), or move in one direction (highly parallel group).

The study of "zone-based" is still an active research field. For example, the model of Couzin et al. has been recently extended in [30]. The authors consider a zone of interaction which depends on the density of fish. When the density around the fish is large, the radius of interaction R decreases. This idea is connected to the model proposed in the Starflag project where individual takes into account the 6 or 7 nearest neighbors. There are also others extensions of the "zone-based" where the interaction zones change gradually with the distance [54, 34]. For an overview of the different models for fish behavior, we refer to the articles [43, 44].

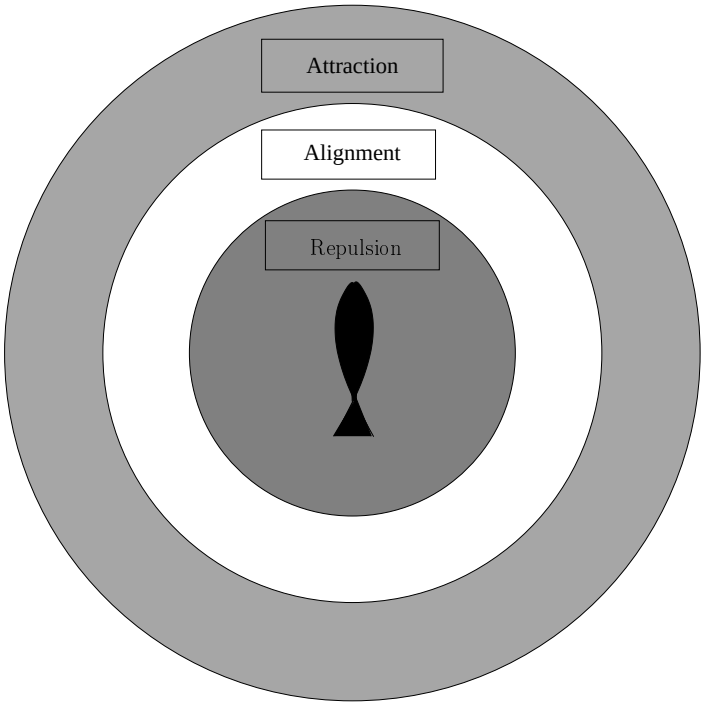

Figure 9: The 3 "zone-based" model describing the interaction of a fish with its congeners.

Another very popular approach to model individual behavior consists in interpreting the movement of individuals as a particle submitted to a "force field". In this type of models, each individual will act as a force that will push or attract the other neighbors [36]. This type of approach has for example been used to model fish schools [40] or pedestrians movement [29]. One the main difference between this approach and previous models (Vicsek model or "zone-based" models) is the summation of the interactions. In the models with forces, the interaction is a linear summation of pairwise interaction which is not the case in the previous models. That is why we could obtain analytical results more easily with these type of models [19]. It is interesting to notice that models of attraction-repulsion can produce a global alignment of particles [15]. We do not observe this phenomenon in the "zone-based" model, if we remove the alignment zone, there is no global alignment for the group.

2.2.2 Macroscopic models

For the modeling of large fish schools or flock of birds, it may be more efficient to use macroscopic models which describe the evolution of macroscopic variables such as mean density and mean velocity. In a macroscopic model, we do not describe the evolution of each individual displacement, we rather describe the evolution of a mass of indistinguishable individuals [41, 38, 22]. The models generally used are advection-diffusion equations. The diffusion term expresses at the macroscopic level the random behavior of the individuals, while the advection term expresses in which direction individual are

moving in average. Usually the diffusion term is assumed to be constant (independent of the density), the non-linearity of the model comes from the advection term. Different models are used to express this advection term. For example, the advection term can be defined by a convolution of the density [35, 21, 50, 51]. The convolution expresses at a macroscopic level the attraction and repulsion between individuals. The advection term may also depend on another quantity different from the density, as the average speed of individuals which becomes another unknown in the model [52]. In the models of bacteria displacement, the advection term depends on a quantity called chemo-attractant. This allows to model the attraction of bacteria to a chemical substance. The models are therefore given by two coupled evolution equations, one for the mass of bacteria and the other for the chemo-attractant [38].

One of the advantages of the macroscopic models is the possibility to analyze them theoretically. There is a well established mathematical framework in which we can predict and demonstrate what will be the solutions of our models. For individual based models, there are few theoretical results [15]. Most of the works are empirical studies, we observe and measure the results of numerical simulations. However in the literature on collective displacement, individual based models are more frequently used than the macroscopic models. In the individual based models, the collective dynamics is explained by individual dynamics. It is a bottom-up approach. In the macroscopic models, we look directly at the group level. The modeling approach is more similar to a top-down approach.

To overcome this weakness of the macroscopic models, a solution is to link individual based models with macroscopic model, which means that we would like to *derive* macroscopic equations from individual based models. The methodology used consists in changing the time and space scales in the individual based models. So the dynamics are studied over longer periods of time and larger distances. If we manage to derive a macroscopic model with this method, then the model obtained would be linked with the individual dynamics that can be measured experimentally. In addition, the macroscopic model would combine the advantages of individual based modes and has an adequate mathematical formulation for which we can predict the behavior of solutions.

To derive a macroscopic model from a microscopic model, we use an intermediate description between the micro and macro scale, called mesoscopic scale. Originally, this multi-scale approach has been developed in gas dynamics. The method enables to pass from a model of collision between particles (microscopic scale) to mathematical models of fluids dynamics (macroscopic scale) [20]. Nowadays this approach is widely used in many research fields. For example, the kinetic approach has been used in models of chemo-taxis describing the movement of bacteria attracted by chemio-attractant [45, 23, 24]. We refer to [3] for a overview of kinetic modeling in biology.

In this manuscript, we use this approach to link individual based models with macroscopic models. The individual based models are ideally based on experimental data (figure 10).

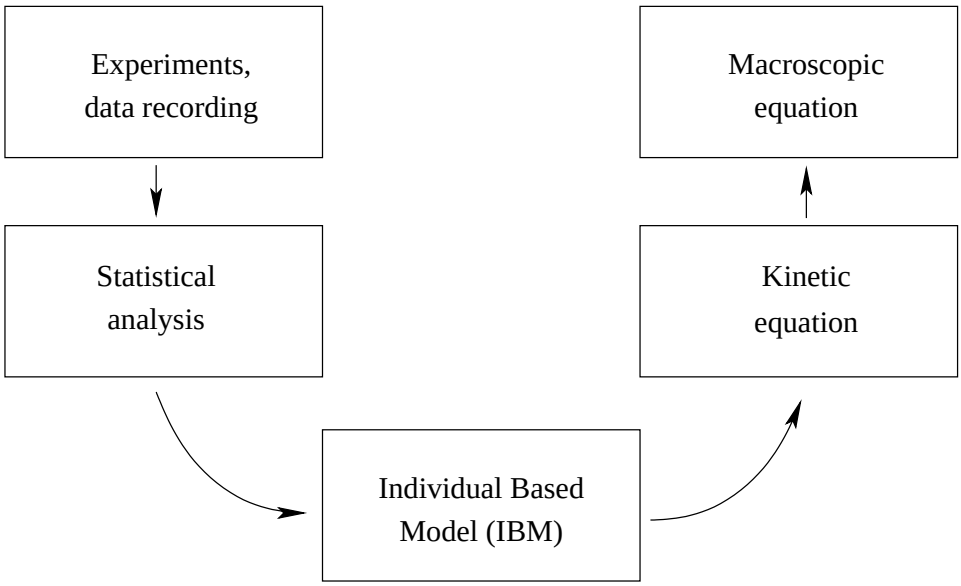

Figure 10: An idealized diagram for a model of macroscopic displacement. Based on a statistical analysis of experimental data, an individual based model is developed. After that, a macroscopic model is derived using the kinetic equation associated with the individual based model.

3 Main contributions

To build a model for fish displacement based on experimental data, experiments were conducted at the Reunion in 2002 on a species of fish named Kuhlia mugil. These experiments led to the construction of a new model called "Persistent Turning Walker" (PTW). Much of the work done during this thesis is related to the study of this model. One of the characteristics that makes this model interesting is the necessity to take into account the third derivative of the position with respect to time. So far, all the models only involve the second derivative, which is the acceleration of the fish. Therefore, we have new equations to work with. Moreover, the different results in the PTW model could be compared with experimental data.

In particular, the work done enabled to determine what is the macroscopic model associated with the PTW model. One of the motivations of this study was initiated by our biologist colleagues, they wanted to know what was the diffusion equation associated with the PTW model. The derivation of the macroscopic model has provided an answer to this question.

Broadly speaking, our work focused on the derivation of macroscopic models from individual based models. This approach also allowed us to derive a macroscopic model from the Vicsek model. The model we have obtained is original and the method used in the derivation is not conventional. Indeed, originally the method used to derive macroscopic models comes from gas dynamics. The method is based on conservation

laws. But in the Vicsek model and more generally in individual based models in biology, we do not have any conservation. At least, the models preserve the number of individual and therefore we have at the macroscopic level the equation of conservation of mass. But this is not sufficient to determine a macroscopic model. That is why we have to generalize the method used so far to derive macroscopic equations.

The interest of macroscopic methods is first to be written in a unified framework, the partial differential equations. This facilitates the development of a theory and it also allows to compare the macroscopic models between them. A weakness of individual based models is the difficulty to compare the models, we only compare the results of numerical simulations.

On the other hand, macroscopic models are written with different parameters than individual based models (e.g. diffusion coefficient), this gives different information on the dynamics. Moreover, in individual based models, the time of the numerical simulation grows significantly with the number of individuals involved in the simulation. The more there are individuals in the simulation, the more it takes time for the computer to make the numerical simulation. For macroscopic models, it is not the case. The number of individuals is simply the density and the computation time does not depend on the value of this density.

Finally, the macroscopic models can help to understand the formation of structures such as wave propagation and shock waves. In individual based models, we have only a description of individual trajectories and therefore we have no direct access to these quantities which describe the macroscopic structures.

3.1 The Persistent Turning Walker Model

Like many displacement models, the PTW model which describes the motion of fish has a stochastic component in its formulation, it introduces a random part in the behavior of the fish. But unlike the models used so far, randomness is introduced on the curvature of the fish and not on its velocity. Therefore, the trajectories obtained with this model are more regular, it is one of the properties of the real trajectories of fish (figure 11). The main idea behind this model is to consider the trajectories as a succession of arcs rather than a succession of straight lines.

The method used to derive a macroscopic model from PTW model is based on a rescaling approach. We study the dynamics in macroscopic variables. For the PTW model, we use a diffusive scaling for the macroscopic variables. With this approach, we derived a diffusive equation from the PTW model and moreover we found an explicit expression for the diffusion coefficient. Numerical simulations of the PTW model illustrate the analytical results obtained. In particular, we were able to estimate numerically the diffusion coefficient in the individual based model and the measurement agrees with the theoretical value.

To study the PTW model, several point of view are possible. First, we can consider the model as a partial differential equation. The purpose of the study is the density distribution of fish. The other point of view is to consider the individual trajectories. Each trajectory of fish is considered as a realization of a stochastic process. The two methods use different tools, the mathematical frameworks are not the same. Fortu-

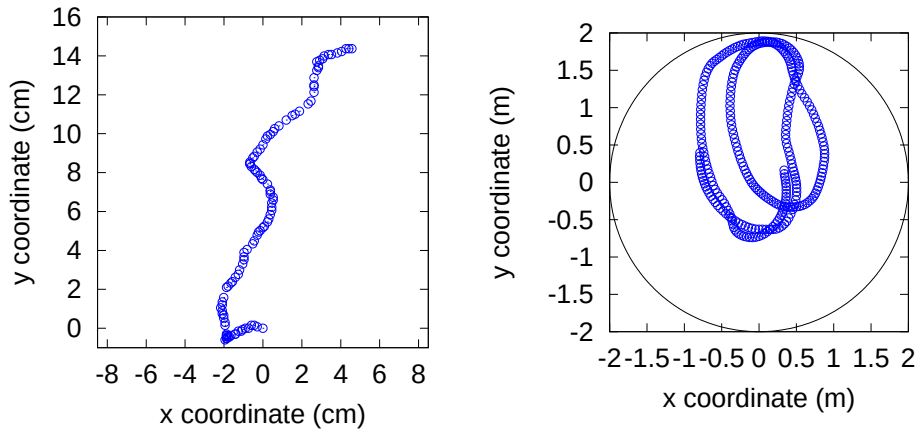

Figure 11: Two examples of individual trajectories with left displacement of an ant (genus Messor) and right-moving fish (Mugil species Kuhlia). The ant has in this instance a straight path punctuated by abrupt changes in direction while the trajectory of the fish is much more rounded. The circles represent the position of the ant (Figure left) and fish (picture right) over time. We have 8 positions per second for the left figure and 12 frames per second for the right figure.

nately, the conclusions we obtained using both approaches are identical. In both cases we obtained, from the PTW model, a diffusion equation with the same diffusion coefficient. From the probabilistic viewpoint, we prove that the PTW model converges in the diffusive scaling to a Brownian motion.

3.2 The Vicsek model: derivation of a macroscopic model

The second part of this manuscript is devoted to the study of the Vicsek model. Unlike the PTW model, the Vicsek model is not based on experimental data. However because of its simplicity, it is used in many fields, it is a kind of universal model.

Several outstanding issues remain with this model. First, the Vicsek model is a discrete model in time. It is an iterative algorithm, we do not have a continuous dynamics over time. Various attempts have been made to obtain a continuous version of this model [48, 47, 33]. On the other hand, there was no macroscopic model associated with the microscopic dynamics of the Vicsek model. Work has been initiated in this direction using a different version of the Vicsek model [4].

The first work done was to find a continuous version of the Vicsek model. When we discretize the continuous model, we recover exactly the original Vicsek model, provided that we respect an assumption on the discretization. To derive a macroscopic model, there is a main difficulty. The dimension of conserved quantities is strictly less than the dimension of the thermodynamic equilibrium. Therefore, the macroscopic model is under-determined. This problem was solved by introducing a new concept of collisional invariant that has great generality and opens new perspective in kinetic theory.

The macroscopic model obtained is a hyperbolic non-conservative equation with a geometric constraint. The norm of vector field is 1 at any points. In literature there are other models with hyperbolic constraints but these models are generally conservative. For the macroscopic model that we obtained, all the analytical studies remain open. For the moment, we focused on the numerical simulation of the macroscopic model where new numerical methods have been developed. The numerical simulations show that the structure of the solutions is more complex than we could expect.

4 Presentation of results

The works were based around two research areas. First,a line of research was based on a new model called "Persistent Turning Walker (PTW). This model is derived from a statistical study on the movement of the fish Mugil Kuhlia (chapter 1). We are interested in large-scale dynamics of this model leading to equation diffusion.This study was made primarily with tools from partial differential equations (chapter 2) and then with probabilistic tools (chapter 3). The PTW model also allowed an extension of a model describing the displacement of fiber used in an industrial problem in the manufacture of composite (chapter 4). In order to extend the PTW model to include interactions between fishes, we conducted a preliminary analysis of experimental data of the fish Mugil Kuhlia group (chapter 5) .

This study has not yet led to a model of interaction, we then concentrated in a second part on the study of a minimum of interaction model introduced by Vicsek. We first derive a macroscopic model from this model based on a formulation in continuous time (chapter 6). Then we study numerically the macroscopic model obtained by comparing the original microscopic model (chapter 7).

Finally, in a different context we consider a stochastic homogenization problem involving Brownian motion and fractional standard (chapter 8). These two processes stochastic are used for modeling in biology displacement.

4.1 The PTW model

4.1.1 Chap. 1 : Analyzing Fish Movement as a Persistent Turning Walker

This chapter introduces the data analysis of the trajectories of the *Kuhlia mugil* fish swimming in a circular tank. The experiments show that unlike the models used so far, the movement of the fish cannot be described as a succession of straight line. Indeed, we observe that the trajectories of the fish are curbed. From these observations, a new model for the fish displacement is introduced. The model is based on the analysis of the evolution of the angular velocity of the fish in the experiments. The evolution of the angular speed is then model by a stochastic differential equation (Ornstein-Uhlenbeck equation):

$$dW(t) = -\frac{1}{\tau}W(t)dt + \sigma dB(t) \tag{4.1}$$

where W is the angular velocity of the fish, $B(t)$ is the Brownian motion, τ and σ are two parameters of the model. Since we assume in the model that the speed of the fish

is constant, this equation can also be written for the curvature of the trajectory of the fish. We call this model "Persistent Turning Walker" (PTW). The statistical analysis of the experimental data enables to estimate the parameters of the model. Since the fish swim in a bounded domain, they are influenced by the wall, it is necessary to model also the effect of the wall on the angular velocity. This allowed to compare the trajectories of the PTW with experimental trajectories. In particular, we compare the mean square displacement within the experiments and in the PTW model (figure 12).

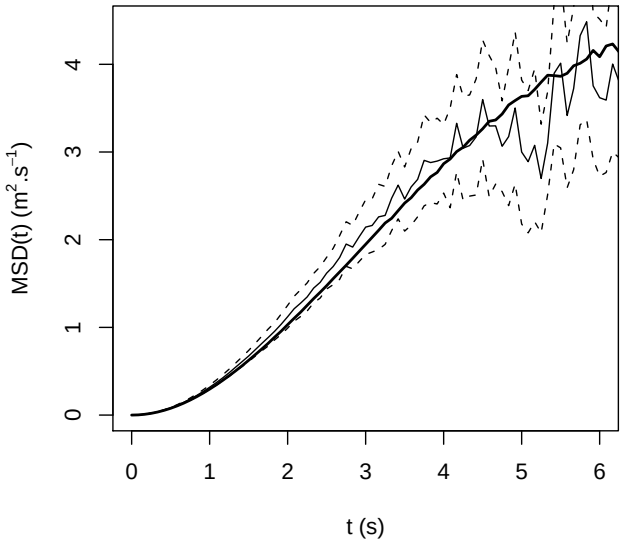

Figure 12: Average square displacement for the model (continuous solid line) and experimental data (dotted line). For the model,the estimation was made by a method of Monte-Carlo. For experimental data, we represented a confidence interval of 95% and an average over the experiments.

4.1.2 Chap. 2 : Large scale dynamics of the Persistent Turning Walker model of fish behavior

In this chapter we study the large-scale dynamic of the PTW model introduced to describe the fish movement. This model is described by the following systems of stochastic differential equations:

$$\begin{aligned} \frac{d\vec{x}}{dt} &= \vec{\tau}(\theta), \\ \frac{d\theta}{dt} &= \kappa, \\ d\kappa &= -\kappa\, dt + \alpha\, dB_t, \end{aligned} \tag{4.2}$$

where $\vec{x} = (x_1, x_2) \in \mathbb{R}^2$ is the (two-dimensional) position vector of fish, $\vec{\tau}(\theta) = (\cos\theta\,, \sin\theta)$ is the director of the velocity vector with the angle $\theta \in \Pi = \mathbb{R}/2\pi\mathbb{Z}$

measured from the x_1 direction, $\kappa \in \mathbb{R}$ is the curvature of the trajectory and B_t is the standard Brownian motion.

To study the dynamics on a large scale, we use two different methods. One approach is to study directly the stochastic differential equation. We manage to compute explicitly the variance of the position vector $\vec{x}$. We then prove that the variance of $\vec{x}$ growths linearly in time asymptotically. In particular, the slope of the linear growth can be view as the diffusion coefficient associated with the PTW model. Therefore we have an explicit formula for the diffusion coefficient :

$$\mathrm{Var}\{\vec{x}(t)\} \overset{t\to+\infty}{\sim} 2\mathcal{D}\,t, \quad \text{with} \quad \mathcal{D} = \int_0^\infty \exp\left(-\alpha^2(-1+s+\mathrm{e}^{-s})\right) ds, \tag{4.3}$$

The second method is based on the forward Kolmogorov equation associated with the PTW model. This is a partial differential equation which describes the evolution in time of the density distribution of fish, noted f. The equation is given by the following formula:

$$\partial_t f + \vec{\tau}\cdot\nabla_{\vec{x}} f + \kappa\partial_\theta f - \partial_\kappa(\kappa f) - \alpha^2\partial_{\kappa^2} f = 0. \tag{4.4}$$

To study this equation at large scale, we change the scale of the variables in time and space. To do so, we introduce a small parameter ε and we define macroscopic variables:

$$t' = \varepsilon^2 t \quad ; \quad \vec{x}' = \varepsilon\vec{x}. \tag{4.5}$$

The transition from a microscopic scale to a macroscopic scale is obtained when ε tends to zero. Using this change of scale, we prove that the equation (4.4) reduces to a diffusive equation at the macroscopic scale. For this, we prove that the density distribution function f converges to an "equilibrium state", where the distribution of curvature is given by a Gaussian distribution and an uniform distribution for the direction of speed. The equilibrium only depends on the density which satisfy a diffusive equation with a non-explicit diffusion tensor.

To link the two approaches above, we prove that the diffusion tensor involved in the second method can be represented as the mean expectation of a stochastic process. It allows us to find an explicit formulation for the diffusion tensor and moreover we recover the same expression for the diffusion coefficient as in the first method (see 4.3).

4.1.3 Chap. 3 : Long time fluctuation and diffusion limit for the Persistent Turning Walker Model

In this chapter, we study the asymptotic behavior of the PTW model. Unlike the previous chapter, we use in this work only probabilistic tools. To obtain a diffusion equation from the PTW model, we use only the stochastic differential equation given by the system (4.2). Using the diffusion rescaling (see equation 4.5), the PTW model becomes with probabilistic notations :

$$\begin{cases} d\vec{x}_t = \varepsilon\vec{\tau}(\theta_t)\,dt \\ d\theta_t = \kappa_t\,\dfrac{dt}{\varepsilon^2} \\ d\kappa_t = -\kappa_t\,\dfrac{dt}{\varepsilon^2} + \sqrt{2}\alpha\,\dfrac{dB_t}{\varepsilon}, \end{cases} \tag{4.6}$$

where we use the same notations as in chapter 4.1.2 (see equation 4.2). The study consists to determine the limit of this system when ε tends to zero.

This study is done in two steps.

First we study the dynamics of the process (θ_t, κ_t). To do, we analyze the infinitesimal generator L of this process. We prove using a Lyapunov function that the generator satisfies a Poincaré inequality. This leads to an exponential convergence of the process (θ_t, κ_t) to a stationary distribution. Moreover, we use this convergence to prove the existence of a solution to the elliptic equation associated with the operator L.

In a second step, we study the position vector $\vec{x}_t$. The vector is simply given by the integral of the velocity $\vec{\tau}(\theta_t)$ in time. Using the solution of the elliptic equation associated with the operator L, we obtain a new integral formula for $\vec{x}_t$. Then we only have to use standard tools in probability such as the Itô formula to prove that the process $\vec{x}_t$ converge in the limit $\varepsilon \to 0$ to Brownian motion.

4.1.4 Chap. 4 : A smooth model for fiber lay-down processes and its diffusion approximations

In this chapter we introduce a new model developed to describe the movement of fibers under the influence of turbulence. This model is used in an industrial problem in the manufacture of composite materials.

The original model used to describe the trajectories of fibers has a drawback since the paths are non-differentiable. The real physical process gives more regular trajectories. To overcome this problem, we introduce a new model for fiber which is an extension of the PTW model. The new model is given by the following stochastic differential equation:

$$\begin{aligned} d\vec{x}_t &= \vec{\tau}(\theta_t)\, dt \\ d\theta_t &= \kappa_t\, dt \\ d\kappa_t &= \lambda(\kappa_0 - \kappa)\, dt + \mu dB_t, \end{aligned} \tag{4.7}$$

where we use the same notations as in chapter 4.1.2 (see equation 4.2) with a second term κ_0 given by:

$$\kappa_0 = b(|\vec{x}_t|)\sin(\theta_t - \phi), \tag{4.8}$$

where $b(.)$ is a positive function, ϕ is the direction of the position vector $\vec{x}_t$ e.g. $\vec{\tau}(\phi) = \frac{\vec{x}_t}{|\vec{x}_t|}$. To make the connection between this new model and existing models, we study the limit of equation (4.7) in different regimes.

As a first step, we study the limit of equation (4.7) when the two parameters λ and μ satisfy:

$$\lambda' = \varepsilon^2\lambda \quad ; \quad \mu' = \varepsilon^2\mu \tag{4.9}$$

with $\varepsilon << 1$. In the limit $\varepsilon \to 0$, we obtain the original model used to model the trajectories of fiber.

Then we used another asymptotic namely:

$$\lambda' = \varepsilon\lambda \quad ; \quad \mu' = \varepsilon^{3/2}\mu. \tag{4.10}$$

In this asymptotic, the equation (4.7) becomes in the limit $\varepsilon \to 0$ a diffusion-advection equation.

This study allows to have a full schema between three types of model to describe the trajectories fibers (original model, generalized PTW model and advection-diffusion equation). Numerical simulations of the new model introduced at different regimes (4.9-4.10) illustrate the theory developed.

4.1.5 Chap. 5 : Statistical analysis of fish movements

This chapter is devoted to the statistical analysis of experimental data on the Kuhlia mugil fish in group. This study is a first step to build a relevant model for fish behavior in interaction.

We have experimental data for different group size of fish. Experiments were conducted with 2, 5, 10, 15 and 30 fish. To study the trajectories obtained, we start a statistical analysis of the data using two different view-point.

First, we measure several characteristics for the group of fish such as the density and the group polarization. In particular, we observe an unexpected phenomenon: the bigger the group is, the less the group is aligned. It is exactly the opposite that we observe in some individual based models such as the Vicsek model [53].

Then, we study the individual trajectories depending on the size of the group. We note in particular that the individual trajectories have some common feature regardless of the size of the group (see figure 13). To understand how individuals are positioned

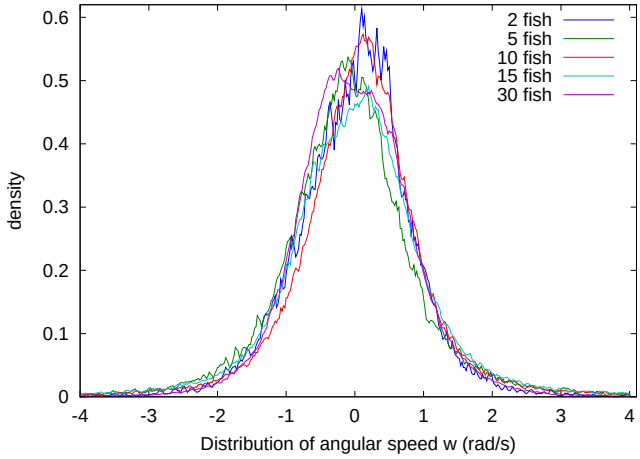

Figure 13: The distributions of angular velocity W of the individual trajectories of the fishes for different size of group. Distributions have a Gaussian shape with a variance .7 $(1/s^2)$.

within the group, we look at the correlation of different quantities (velocity, acceleration,...) between fish. For example, we observe that the fish tend to swim one in front of the other in the experiments with 2 fish, whereas in others experiments the position of the neighbors around a fish are isotropic. Others measures at the individual level explain why the group is less polarized when the number of fish increases.

This study provides statistical measures that we will thereafter use to validate a model of interaction between fish.

4.2 The Vicsek model

4.2.1 Chap. 6 : Continuum limit of self-driven particles with orientation interaction

This chapter is devoted to the derivation of a macroscopic model from the Vicsek model.

In the Vicsek model, we consider particles moving at constant speed which interact between each other in order to increase their alignment. Noting $\vec{x}_k^n$ the position of the k^{th} particle at time $n\Delta t$ with Δt a time step and ω_k^n the velocity, the dynamics are described by the following equations:

$$\vec{x}_k^{n+1} = \vec{x}_k^n + c\,\omega_k^n \Delta t, \tag{4.11}$$
$$\omega_k^{n+1} = \bar{\omega}_k + \varepsilon^n, \tag{4.12}$$

where c is the speed, ε^n is an independent random variable representing the noise in the system and $\bar{\omega}_k$ is the average velocity around the particle $\vec{x}_k$ defined by:

$$\bar{\omega}_k = \frac{J_k^n}{|J_k^n|}, \quad J_k^n = \sum_{j,\,|\vec{x}_j^n - \vec{x}_k^n| \le R} \omega_j^n. \tag{4.13}$$

where R is the radius of perception.

In this work, we first derive from this discrete dynamic a continuous dynamics. This dynamics is written as stochastic differential equation:

$$\frac{d\vec{x}_k}{dt} = c\,\omega_k, \tag{4.14}$$
$$d\omega_k = (\mathrm{Id} - \omega_k \otimes \omega_k)(\nu\,\bar{\omega}_k\,dt + \sqrt{2d}\,dB_t), \tag{4.15}$$

where B_t is the Brownian motion, $\sqrt{2d}$ is the intensity of noise, ν is the frequency of interaction. The projection operator $(\mathrm{Id} - \omega_k \otimes \omega_k)$ ensures that the speed remains of module 1 (see figure 14).

To derive a macroscopic model from this continuous equation, we use the kinetic equation associated with this particle dynamics. Since the particles are interacting, the transition between the particle dynamics to the kinetic equation is only formal. To prove rigorously the derivation of the kinetic equation, we need to prove the assumption of the propagation of chaos and it is still an open problem. Once we have the kinetic equation, we use an hydrodynamics scaling in order to derive a macroscopic model. More precisely, we introduce the new macroscopic variables:

$$t' = \varepsilon t \quad ; \quad \vec{x}' = \varepsilon \vec{x}. \tag{4.16}$$

In the variables (t', x'), the density distribution of f^ε satisfies the following kinetic equation:

$$\varepsilon(\partial_t f^\varepsilon + \omega \cdot \nabla_x f^\varepsilon) = Q(f^\varepsilon) + O(\varepsilon^2), \tag{4.17}$$

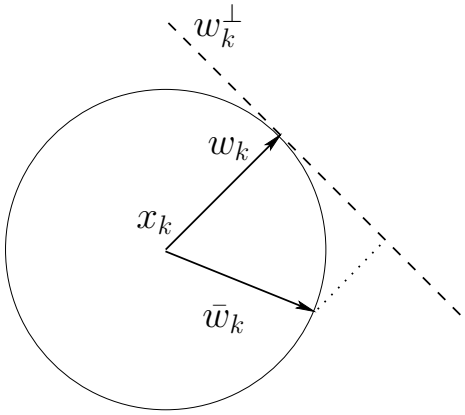

Figure 14: The projection of the vector $\bar{\omega}_k$ on the orthogonal of ω_k guarantees that the velocity of each particle remains constant.

with:

$$Q(f^\varepsilon) = -\nabla_\omega \cdot (F[f^\varepsilon] f^\varepsilon) + d\Delta_\omega f^\varepsilon \tag{4.18}$$

$$F[f^\varepsilon] = \nu\ (\mathrm{Id} - \omega \otimes \omega)\Omega[f^\varepsilon], \tag{4.19}$$

$$\Omega[f^\varepsilon] = \frac{j[f^\varepsilon]}{|j[f^\varepsilon]|}, \quad \text{and} \quad j[f^\varepsilon] = \int_{\upsilon \in \mathbb{S}^2} \upsilon\, f^\varepsilon(x, \upsilon, t)\, d\upsilon. \tag{4.20}$$

To find the limit when $\varepsilon \to 0$, we first prove that the equilibrium of this kinetic equation are given by:

$$\mathcal{E} = \{\rho M_\Omega(\omega) \ \mid \ \rho \in \mathbb{R}_+, \quad \Omega \in \mathbb{S}^2\}, \tag{4.21}$$

with $M_\Omega(\omega) = C \exp\left(\frac{\nu}{d}\, \omega \cdot \Omega\right)$ where Ω is the velocity director and C is a constant such that M_Ω is a density distribution. The equilibrium ensemble $\mathcal{E}$ is a three dimensional manifold. But the collision operator Q has only a one-dimensional set of collisional invariants (corresponding to constant function). Therefore we can not derive a macroscopic equation. This is why we introduce a new concept of generalized collisional invariant which enables to introduce collisional invariants. With this new concept, we manage to determine the macroscopic limit of our kinetic equation. At the limit $\varepsilon \to 0$, we obtain an equation for the density ρ and the velocity director Ω:

$$\partial_t \rho + \nabla_x \cdot (c_1 \rho \Omega) = 0, \tag{4.22}$$

$$\rho\ (\partial_t \Omega + c_2 (\Omega \cdot \nabla)\Omega) + \lambda\, (\mathrm{Id} - \Omega \otimes \Omega)\nabla_x \rho = 0, \tag{4.23}$$

where c_1, c_2 are the convection speed and λ is a positive constant. The macroscopic model obtained is hyperbolic but not conservative because of the constraint on the vector Ω who must have a constant norm ($|\Omega| = 1$). This properties makes the model original.

4.2.2 Chap. 7 : Numerical studies of the CVA models

The purpose of this chapter is to validate the macroscopic model developed in the previous chapter by comparing numerical simulations with the microscopic model. To

perform this analysis, we must better understand the macroscopic model. Since it is is non-conservative equation with a geometric constraint, we do not have theory that we could refer on. We propose two different approaches to study theoretically and numerically the macroscopic equation. First, we reformulate the model in a simple conservative form which appears to be the natural conservative formulation for this problem. Then, we propose an other formulation for the macroscopic equation where we replace the constraint on the vector field Ω by a relaxation operator.These two approaches give two different numerical methods, called conservative and splitting method. However, the numerical simulations of the microscopic model in a dense regime of particles are only in good agreement with the splitting method, the conservative method gives different results. This shows that first we have an agreement between the microscopic model and the macroscopic model and secondly that the correct formulation of the macroscopic model is given by the formulation with a stiff relaxation operator.

4.3 Homogenization theory

4.3.1 Chap. 8 : Random integrals and correctors in homogenization

The purpose of this chapter is to study theoretically and numerically stochastic homogenization of an elliptic equation. This study is not directly connected with biology, since the equation models a deformation of a material under some constraints. Nevertheless, the probabilistic tools used in this study (Brownian motion, stochastic integral, Ornstein-Uhlenbeck process) are widely used in previous work.

The deformation of a material when it is mixed with other components is modeled by the following elliptic equation:

$$\begin{aligned} &-\frac{d}{dx}\Big(a\Big(\frac{x}{\varepsilon},\omega\Big)\frac{d}{dx}u^\varepsilon\Big) = f(x), \qquad 0 \le x \le 1, \\ &u^\varepsilon(0,\omega) = 0, \qquad u^\varepsilon(1,\omega) = q. \end{aligned} \tag{4.24}$$

where f is the force applied to the materials, $a(x,\omega)$ is the coefficient of elasticity given by a stationary stochastic process. Under several assumptions, we can prove that the solution $u^\varepsilon(x,\Omega)$ of the elliptical equation converges when ε tends to zero to the deterministic solution $\bar{u}(x)$ of the following equation:

$$\begin{aligned} &-\frac{d}{dx}\Big(a^*\frac{d}{dx}\bar{u}\Big) = f(x), \qquad 0 \le x \le 1, \\ &\bar{u}(0) = 0, \qquad \bar{u}(1) = q. \end{aligned} \tag{4.25}$$

where the coefficient of elasticity a^* is given by $a^* = \Big(\mathbb{E}\{a^{-1}(0,\cdot)\}\Big)^{-1}$ with $\mathbb{E}$ the mathematical expectation. Equation (4.25) is called the homogenized equation. We are interested in the difference between the solution u^ε of the equation (4.24) and the homogenized solution u^*. We distinguish two cases depending on whether the autocorrelation function of the process $a(x,\omega)$ is integrable or not. In the first case, the difference between u^ε and u^* converges to a stochastic process which is written with the standard Brownian motion. In the non-integrable case, the difference involves

the fractional Brownian motion. We then prove rigorously these convergences when the elastic coefficient $a(x, \omega)$ is given by a certain expression. Numerical simulations illustrate the theory.

Bibliography

[1] I. Aoki. A simulation study on the schooling mechanism in fish. *Bulletin of the Japanese Society of Scientific Fisheries (Japan)*, 1982.

[2] M. Ballerini, N. Cabibbo, R. Candelier, A. Cavagna, E. Cisbani, I. Giardina, V. Lecomte, A. Orlandi, G. Parisi, A. Procaccini, et al. Interaction ruling animal collective behavior depends on topological rather than metric distance: Evidence from a field study. *Proceedings of the National Academy of Sciences*, 105(4):1232, 2008.

[3] N. Bellomo. Modeling complex living systems: a kinetic theory and stochastic game approach. 2007.

[4] E. Bertin, M. Droz, and G. Gregoire. Boltzmann and hydrodynamic description for self-propelled particles (4 pages). *PHYSICAL REVIEW-SERIES E-*, 74(2):22101, 2006.

[5] P. Bovet and S. Benhamou. Spatial analysis of animals' movements using a correlated random walk model. *Journal of theoretical biology*, 131(4):419–433, 1988.

[6] D.R. Brillinger, H.K. Preisler, A.A. Ager, J.G. Kie, and B.S. Stewart. Employing stochastic differential equations to model wildlife motion. *Bulletin of the Brazilian Mathematical Society*, 33(3):385–408, 2002.

[7] J. Buhl, DJT Sumpter, ID Couzin, JJ Hale, E. Despland, ER Miller, and SJ Simpson. From disorder to order in marching locusts, 2006.

[8] C. Calenge, S. Dray, and M. Royer-Carenzi. The concept of animals' trajectories from a data analysis perspective. *Ecological Informatics*, 2008.

[9] S. Camazine, JL Deneubourg, NR Franks, J. Sneyd, G. Theraulaz, and E. Bonabeau. Princeton University Press; Princeton, NJ: 2001. *Self-organization in biological systems*.

[10] E. Casellas, J. Gautrais, R. Fournier, S. Blanco, M. Combe, V. Fourcassie, G. Theraulaz, and C. Jost. From individual to collective displacements in heterogeneous environments. *Journal of Theoretical Biology*, 250(3):424–434, 2008.

[11] A. Cavagna, I. Giardina, A. Orlandi, G. Parisi, and A. Procaccini. The starflag handbook on collective animal behaviour: 2. three-dimensional analysis. *Arxiv preprint arXiv:0802.1674*, 2008.

[12] A. Cavagna, I. Giardina, A. Orlandi, G. Parisi, A. Procaccini, M. Viale, and V. Zdravkovic. The starflag handbook on collective animal behaviour: 1. empirical methods. *Animal Behaviour*, 76(1):217–236, 2008.

[13] H. Chaté, F. Ginelli, G. Grégoire, and F. Raynaud. Collective motion of self-propelled particles interacting without cohesion. *Physical Review E*, 77(4):46113, 2008.

[14] GQ Chen, CD Levermore, and TP Liu. Hyperbolic conservation laws with sti relaxation and entropy. *Comm. Pure Appl. Math*, 47:787, 1994.

[15] Y. Chuang, M.R. D'Orsogna, D. Marthaler, A.L. Bertozzi, and L.S. Chayes. State transitions and the continuum limit for a 2d interacting, self-propelled particle system. *Physica D: Nonlinear Phenomena*, 232(1):33–47, 2007.

[16] I.D. Couzin and J. Krause. Self-organization and collective behavior in vertebrates. *Advances in the Study of Behavior*, 32(1), 2003.

[17] I.D. Couzin, J. Krause, R. James, G.D. Ruxton, and N.R. Franks. Collective memory and spatial sorting in animal groups. *Journal of Theoretical Biology*, 218(1):1–11, 2002.

[18] F. Cucker and S. Smale. Emergent behavior in flocks. *IEEE TRANSACTIONS ON AUTOMATIC CONTROL*, 52(5):852, 2007.

[19] MR D Orsogna, YL Chuang, AL Bertozzi, and LS Chayes. Self-propelled particles with soft-core interactions: patterns, stability, and collapse. *Physical review letters*, 96(10):104302, 2006.

[20] P. Degond. Macroscopic limits of the Boltzmann equation: a review. *Modeling and computational methods for kinetic equations, P. Degond, G. Russo, L. Pareschi (eds), Birkhauser*, 2004.

[21] L. Edelstein-Keshet. Mathematical models of swarming and social aggregation. In *Proceedings of the 2001 International Symposium on Nonlinear Theory and Its Applications, Miyagi, Japan*, pages 1–7, 2001.

[22] L. Edelstein-Keshet. Mathematical models in biology. 2005.

[23] F. Filbet, P. Laurençot, and B. Perthame. Derivation of hyperbolic models for chemosensitive movement. *Journal of Mathematical Biology*, 50(2):189–207, 2005.

[24] F. Filbet and C. Shu. Approximation of hyperbolic models for chemosensitive movement. *SIAM JOURNAL ON SCIENTIFIC COMPUTING*, 27(3):850, 2006.

[25] S. Garnier, J. Gautrais, and G. Theraulaz. The biological principles of swarm intelligence. *Swarm Intelligence*, 1(1):3–31, 2007.

[26] G. Grégoire and H. Chaté. Onset of collective and cohesive motion. *Physical Review Letters*, 92(2):25702, 2004.

[27] G. Grégoire, H. Chaté, and Y. Tu. Moving and staying together without a leader. *Physica D: Nonlinear Phenomena*, 181(3-4):157–170, 2003.

[28] S.Y. Ha and E. Tadmor. From particle to kinetic and hydrodynamic descriptions of flocking. *Arxiv preprint arXiv:0806.2182*, 2008.

[29] Dirk Helbing and Péter Molnár. Social force model for pedestrian dynamics. *Phys. Rev. E*, 51(5):4282–4286, May 1995.

[30] C.K. Hemelrijk and H. Hildenbrandt. Self-Organized Shape and Frontal Density of Fish Schools. *Ethology*, 114(3):245–254, 2008.

[31] A. HUTH and C. WISSEL. The simulation of the movement of fish schools. *Journal of theoretical biology*, 156(3):365–385, 1992.

[32] R. Jeanson, S. Blanco, R. Fournier, J.L. Deneubourg, V. Fourcassié, and G. Theraulaz. A model of animal movements in a bounded space. *Journal of Theoretical Biology*, 225(4):443–451, 2003.

[33] VL Kulinskii, VI Ratushnaya, AV Zvelindovsky, and D. Bedeaux. Hydrodynamic model for a system of self-propelling particles with conservative kinematic constraints. *Europhysics Letters*, 71(2):207–213, 2005.

[34] V. Mirabet, P. Auger, and C. Lett. Spatial structures in simulations of animal grouping. *Ecological Modelling*, 201(3-4):468–476, 2007.

[35] A. Mogilner and L. Edelstein-Keshet. A non-local model for a swarm. *Journal of Mathematical Biology*, 38(6):534–570, 1999.

[36] A. Mogilner, L. Edelstein-Keshet, L. Bent, and A. Spiros. Mutual interactions, potentials, and individual distance in a social aggregation. *Journal of Mathematical Biology*, 47(4):353–389, 2003.

[37] M. Moussaid, S. Garnier, A. Johansson, D. Helbing, and G. Theraulaz. Experimental measurements of human interactions in space and time.

[38] J.D. Murray. Mathematical biology. 2003.

[39] M. Nagy, I. Daruka, and T. Vicsek. New aspects of the continuous phase transition in the scalar noise model (SNM) of collective motion. *Physica A: Statistical Mechanics and its Applications*, 373:445–454, 2007.

[40] H.S. Niwa. Newtonian dynamical approach to fish schooling. *Journal of Theoretical Biology*, 181(1):47–63, 1996.

[41] A. Okubo. Dynamical aspects of animal grouping: swarms, schools, flocks, and herds. *Adv Biophys*, 22:1–94, 1986.

[42] J.K. Parrish and W.M. Hamner. *Animal Groups in Three Dimensions*. Cambridge University Press, 1997.

[43] J.K. Parrish and S.V. Viscido. Traffic rules of fish schools: a review of agent-based approaches. *Self-organisation and Evolution of Social Systems*, 2005.

[44] J.K. Parrish, S.V. Viscido, and D. Grunbaum. Self-organized fish schools: an examination of emergent properties. *Biological Bulletin, Marine Biological Laboratory, Woods Hole*, 202(3):296–305, 2002.

[45] B. Perthame. Transport equations in biology. 2007.

[46] H.K. Preisler, D.R. Brillinger, A.A. Ager, J.G. Kie, and R.P. Akers. Stochastic differential equations: a tool for studying animal movement. *Proceedings of IUFRO4*, 11:25–29, 2001.

[47] VI Ratushnaya, D. Bedeaux, VL Kulinskii, and AV Zvelindovsky. Collective behavior of self-propelling particles with kinematic constraints: The relation between the discrete and the continuous description. *Physica A: Statistical Mechanics and its Applications*, 381:39–46, 2007.

[48] VI Ratushnaya, VL Kulinskii, AV Zvelindovsky, and D. Bedeaux. Hydrodynamic model for the system of self propelling particles with conservative kinematic constraints; two dimensional stationary solutions. *Physica A: Statistical Mechanics and its Applications*, 366:107–114, 2006.

[49] G. Theraulaz, E. Bonabeau, S.C. Nicolis, R.V. Sole, V. Fourcassie, S. Blanco, R. Fournier, J.L. Joly, P. Fernandez, A. Grimal, et al. Spatial patterns in ant colonies. *Proceedings of the National Academy of Sciences*, 99(15):9645, 2002.

[50] C.M. Topaz and A.L. Bertozzi. Swarming patterns in a two-dimensional kinematic model for biological groups. *SIAM Journal on Applied Mathematics*, 65(1):152–174, 2005.

[51] C.M. Topaz, A.L. Bertozzi, and M.A. Lewis. A nonlocal continuum model for biological aggregation. *Bulletin of Mathematical Biology*, 68(7):1601–1623, 2006.

[52] Y. Tyutyunov, I. Senina, and R. Arditi. Clustering due to acceleration in the response to population gradient: a simple self-organization model. *The American Naturalist*, 164(6):722–735, 2004.

[53] T. Vicsek, A. Czirók, E. Ben-Jacob, I. Cohen, and O. Shochet. Novel type of phase transition in a system of self-driven particles. *Physical Review Letters*, 75(6):1226–1229, 1995.

[54] S.V. Viscido, J.K. Parrish, and D. Grünbaum. Factors influencing the structure and maintenance of fish schools. *Ecological Modelling*, 206(1-2):153–165, 2007.

Part I
The Persistent Turning Walker model

Chapter 1

Analyzing Fish Movement as a Persistent Turning Walker

This chapter has given an article in the Journal of Mathematical Biology: J. Gautrais, C. Jost, M. Soria, A. Campo, S. Motsch, R. Fournier, S. Blanco and G. Theraulaz, *Analyzing fish movement as a persistent turning walker*, J. Math Biology, **58** (2009), no. 3, 429–445.

Abstract. The trajectories of *Kuhlia mugil* fish swimming freely in a tank are analyzed in order to develop a model of spontaneous fish movement. The data show that *Kuhlia mugil* displacement is best described by turning speed and its auto-correlation. The continuous-time process governing this new kind of displacement is modelled by a stochastic differential equation of Ornstein-Uhlenbeck family: the Persistent Turning Walker. The associated diffusive dynamics are compared to the standard persistent random walker model and we show that the resulting diffusion coefficient scales non-linearly with linear swimming speed. In order to illustrate how interactions with other fish or the environment can be added to this spontaneous movement model we quantify the effect of tank walls on the turning speed and adequately reproduce the characteristics of the observed fish trajectories.

Key words. Fish displacement model, Stochastic model, Ornstein-Uhlenbeck process.

1 Introduction

The highly coordinated displacement of hundreds or thousands of fishes in so-called fish schools has been the focus of many theoretical and some experimental studies. The spatial group cohesion, unless it is ensured by a confining environment, must be the result of interactions between the animals. As in any collective behaviour, these interactions should be considered as individual decision processes that synchronise the behavioural outputs [12].

Many authors have tried to understand these collective behaviours from a theoretical perspective. They propose biologically plausible (but nevertheless hypothetical) interactions that lead to a synchronization of the fish headings (moving directions), see [18, 61] and references therein. The interactions are implemented as a set of neighbour-dependent rules that modify a null-model of spontaneous and independent fish displacement. Such a null-model may gain particular importance in the case of fish groups with clearly identified leaders that swim rather independently ahead of the group, their null-model may therefore dominate the landscape of the collective patterns [60, 18, 19, 24].

In most of these studies this null-model is a random walk, that is the animal path is characterized by a series of straight moves separated by reorientation behaviour. In some cases, the new heading is simply uniformly distributed and the time series of headings obeys a Markov process of order 0 (pure random walk). More often, the new heading is a small deviation from the previous headings and the null-model corresponds to a correlated random walk or persistent random walker [34]. In this case, the time series of headings obeys a Markov process of order 1 (consecutive headings are autocorrelated) , and the time series of the turning angles obeys a Markov process of order 0 (consecutive turning angles are independent).

However, most of these studies are only loosely linked to biological data. In order to move towards a biological validation some experimental studies have attacked the quantitative description of the collective swimming behaviour [36, 49, 3] and its comparison to model predictions. Only very few studies have directly addressed the experimental identification and quantification of the underlying interactions between individuals [26, 46], and they all used the pure random walk as the null-model.

It is important to note that the estimation of interaction parameters depends crucially on the choice of the null-model. The prerequisite for such an estimation is the existence of a validated null-model of spontaneous displacement since interactions are detected as the departures from such a null-model. We therefore advocate that a prior step to interaction analysis is to quantify this spontaneous behavior experimentally and to check whether the random walk model indeed holds for an isolated fish. Otherwise a better grounded spontaneous model must be developped. To be applicable, this model should work as much as possible at the same space and time scale as the suspected interactions.

To address this question, we quantify in the present chapter the experimental trajectories of nine isolated fish that swim in a circular tank. The fish were Barred flagtail (*Kuhlia mugil*), a 20-25 cm pelagic fish that lives in schools along the coral reefs in La Réunion Island. In a data-driven approach we first develop a stochastic kinematic

model of their swimming behavior in the form of stochastic differential equations (sde): the persistent turning walker (PTW). This model is characterised by a constant swimming speed and an autocorrelation of the angular speed (turning angle per unit time) rather than autocorrelation of the heading as in the correlated random walk. The exploration of the model properties will help to identify the major differences to the random walk model, in particular the expected collective behaviour when many individuals move according to this null-model. In a second step we will also explore how to add interactions to this null-model by quantifying the interaction between the fish and the tank walls. This interaction takes the form of an additional term in the stochastic differential equation that bends the fish trajectory away from the wall. The extended model will be used to compare directly the net squared displacement between experimental and simulated trajectories.

2 Data collection

In the experiments described in [53], nine fish were filmed while swimming alone in a circular tank of radius $R = 2$ m, depth 1.2 m and filled with still clean sea water. The limited water depth ensured that the fish were swimming on a planar level, that is in two dimensions.

For each individual, two minutes were extracted from digital video recordings and the position of the individual's head was tracked every 1/12 second (1440 points per trajectory). Perspective errors were corrected, and oscillations of periods shorter or equal to 8/12 s that are due to the beating mode of swimming were removed using wavelet filtering with Daubechies bank of length 10 (Wave++ package [22]). This filtering procedure yielded the trajectory of the fish body and was never farther than 2 cm from the tracked head (for a fish of length 20 cm). These trajectories appeared rather winding (spiral course) with no well-defined points of directional changes as would be expected in standard correlated random walks (Fig. 1.1). Some fish exhibited some kind of thigmotactic behaviour (wall following / attraction, see fishes 1, 4 and 5) whereas the others displayed simple wall avoidance type patterns.

Cartesian 2D coordinates are arbitrary with respect to the origin and orientation of the axis, they are therefore badly suited to analyze movement. To adopt the fish point of view they were converted into the intrinsic coordinates along the trajectories. Starting from the initial point $P(0)$ at $t = 0$, intrinsic coordinates $(S(t), \varphi(t))$ denote respectively the curvilinear abcissa and the heading at time t when the fish is at position $P(t)$. The curvilinear abcissa $S(t)$ is the length of the trajectory since $t = 0$ when $S(0) = 0$. Correspondingly, the heading $\varphi(t)$ is computed relative to the initial heading $\varphi(0)$ at $t = 0$ (see Fig. 1.2). The time derivatives of these intrinsic coordinates are respectively the swimming (tangent) speed $V(t)$ ($m.s^{-1}$, which is the norm of the speed vector $\vec{V}(t)$) and the turning speed $W(t)$ ($rad.s^{-1}$).

To minimize the error due to time discretization, we estimated the intrinsic coordinates at each point $P_i = P(i\Delta t)$, $i = 1, .., 1338$, by fitting a circle to the three consecutive points P_{i-1}, P_i, P_{i+1}. We then recovered Δs_i and $\Delta\varphi_i$ (counter-clockwise

coded as positive) for each middle point P_i as shown in Fig. 1.2. The instantaneous swimming speed V_i and turning speed W_i were then estimated by:

$$\widehat{V_i} = \frac{\Delta s}{2\Delta t} \tag{2.1}$$

$$\widehat{W_i} = \frac{\Delta \varphi}{2\Delta t} \tag{2.2}$$

The curvilinear abcissa S_i and heading φ_i at point P_i were recovered by integrating the corresponding speeds over time, starting from the second point of the series ($P_1 = P(\Delta t)$), according to the equations

$$\widehat{S_i} = \int\limits_{\Delta t<t<i\Delta t} dS(t) \simeq \sum_{j=1}^{i-1} \widehat{V_j}\Delta t \tag{2.3}$$

$$\widehat{\varphi_i} = \int\limits_{\Delta t<t<i\Delta t} d\varphi(t) \simeq \sum_{j=1}^{i-1} \widehat{W_j}\Delta t \tag{2.4}$$

Note that this procedure yields a heading value φ_i which is relative to the heading at the starting point P_1 and can fluctuate away from the standard trigonometric limits $[-\pi.. + \pi]$ because φ_i is not taken modulo 2π (e.g. three complete counter-clockwise revolutions would yield a φ-shift of $3 * 2\pi$). Such a definition of heading is the most relevant one when dealing with rotational diffusion [9, 11, 47] because it is consistent with the continuous evolution of the heading (no artificial jumps at the transitions between $-\pi$ and π).

3 Kinematic model

3.1 Rationale for the model

The time evolution of $S(t)$ indicated that the swimming speeds could be considered as constant for each fish (Fig. 1.3a: constant slopes with some residual tracking noise) but different across fishes. As for the time evolution of the heading, we found that the autocorrelation of the turning speed $\langle W_i, W_{i+h}\rangle$ was significant over several seconds (Fig. 1.3b). Contrastingly, an essential property of random walks is that consecutive changes of heading are independent. Therefore, the autocorrelation of the turning speeds, defined as

$$\langle(\varphi_i - \varphi_{i-1})/\Delta t, (\varphi_{i+1} - \varphi_i)/\Delta t\rangle = \langle W_i, W_{i+1}\rangle, \tag{3.5}$$

would be negligible. This is obviously not the case in our data. Hence, the random walk model, whether correlated or not, could not account for the persistence of the turning speed in our fish and would be inadequate. Data rather suggest a process based on a correlated turning speed [1, 2] with constant swimming speed. Following the terminology of the persistent random walker (PRW) which denotes the random

walk with an autocorrelation of the heading, we shall hereafter call the persistent turning walker (PTW) this new kind of random walk with an autocorrelation of the turning speed. In its simplest form, this model states:

$$V_i = V \quad \text{(constant swimming speed)} \tag{3.6}$$

$$W_i = aW_{i-1} + b_i \tag{3.7}$$

where b_i is a random gaussian variable of mean 0 and variance s^2, and a the one-step correlation coefficient of W_i.

Equation 3.7 is an auto-regressive process of order 1 (AR(1) in the statistics literature). Its parameters a and s can be estimated from a time series (N points sampled every Δt) by the standard equations

$$\widehat{a} = \frac{\sum_i^{N-1} W_i W_{i+1}}{\sum_i^{N-1} W_i} \tag{3.8}$$

$$\widehat{s^2} = \frac{1}{N} \sum_i^{N-1} \left(W_{i+1} - \widehat{a} W_i\right)^2 . \tag{3.9}$$

For a continuous signal such as a moving fish, a and s depend on the discretization time step Δt, but this dependency can be resolved by computing their continuous-time equivalents α and σ:

$$\alpha = -\frac{\log(a)}{\Delta t} \tag{3.10}$$

$$\sigma^2 = s^2 \frac{2\alpha}{1 - e^{-2\alpha\Delta t}}. \tag{3.11}$$

α expresses the inverse of the autocorrelation time τ (that is $\tau = 1/\alpha$) and $a = e^{-\Delta t/\tau}$. Since $W(t)$ is a continuous-time process, (3.7) ought to be understood as the discretized solution over $[(i-1)\Delta t..i\Delta t]$ of the stochastic differential equation (sde):

$$dW(t) = -\frac{1}{\tau} W(t) dt + \sigma dB(t) \tag{3.12}$$

with $B(t)$ representing a Brownian process (white noise). This is known in statistical physics as the Ornstein-Uhlenbeck (OU) process [59] and as the Vasicek model in the financial economics literature [7]. In the stationary regime, this equation leads to a Gaussian random process of the turning speed with zero mean, variance $\tau\sigma^2/2$ and an exponentially decaying autocorrelation function with decay rate α.

3.2 Parameter estimation

In order to estimate the parameter values of this spontaneous moving behavior from the fish trajectories in Fig. 1.1 we had to take the confining effect of the wall into account. Taken a constant swimming speed for granted, this effect can only operate on the turning speed, acting as an external field which skews the turning speeds towards

repulsive moves (for further details see next section). This might have biased the estimates of the autocorrelation time lag. Hence, we restricted this estimation by using only positions farther than 1 m from the wall (Fig. 1.4) and censored, i.e. treated as unknown values, the trajectories when the fish was outside the innermost 1 m wide disk. Those estimates are reported for each fish on Fig. 1.5 (black dots, •). They were rather homogeneous across the fish, except for the individuals 1 and 4 that were identified above as exhibiting a strong attraction towards the wall with a rythmic pattern to and from the wall (Fig. 1.1). To estimate the confidence interval of the parameters, we produced repeated simulated series of W using (3.7) with a common set of parameters ($\tau^\star = 0.6$ s and $\sigma^\star = 1.5\,\mathrm{rad.s}^{-0.5}$, same time step Δt), and applied to each fish the same censoring filter as to the original data. We then computed the corresponding mean and confidence interval at the 95% level (percentile method, estimated from 100,000 simulations each). These confidence intervals show that all fish have a τ-value that is not significantly different from a common autocorrelation time around $\tau^\star$. As expected, the outlier fish 1 and 4 depart clearly from the others (and their confidence intervals are much larger because of a lack of data in the inner 1-m disk). The individual variances σ^2 seemed more contrasted and were significantly less homogeneous than the correlation times. However, it is unlikely that these slight deviations from $\sigma^\star$ would actually raise significant differences at the level of the trajectories.

4 Properties of the spontaneous model

4.1 Macroscopic prediction

Degond & Motsch [20] have analysed the large time scale behaviour of a similar model (with an autocorrelation of the curvature instead of the turning speed). They have shown by a space-time rescaling technique that their model leads to a diffusion process at the macroscopic scale. Since our fish swim at constant speed, an autocorrelation of the curvature is equivalent to an autocorrelation of the turning speed, so their conclusion holds also for the PTW model and the mean square displacement scales linearly with time at large scale:

$$Var\left[\overrightarrow{x(t)}\right] \xrightarrow{t\to+\infty} 2Dt \tag{4.13}$$

where $\overrightarrow{x(t)}$ denotes the vector from the starting point to the position at time t. The diffusion coefficient D indicates how fast the fish spreads out from its initial position across the 2D-space.

Figure 1.6 reports the dependence of the associated macroscopic diffusion coefficient D on the swimming speed V and the autocorrelation time of the turning speed τ. An analytical derivation of this dependance is under study. In contrast to the macroscopic version of the random walk, the diffusion coefficient in the PTW model is not proportional to the swimming speed, but rather increases non linearly as the swimming speed increases. For a given speed V, an increase of the autocorrelation time of the turning speed τ yields a lower diffusion coefficient. This happens because

the fish is more often trapped in a high value of turning speed and for a longer time, so it turns around more locally.

5 Inclusion of wall avoidance

The kinematic model presented above only applies to fish behavior in unconstrained open water. As an example of how additional components can be integrated into this model and quantified from data we added the wall avoidance behavior. Focusing on the fastest fish (Fish 9) we found that the wall had a salient effect only when the fish was close to and heading towards the wall. We consequently reconstructed the effect of wall repulsion as a function of the distance D_c before collision with the wall (if heading were not changed), i.e. the distance between the fish and the intersection of the heading line with the wall.

We assumed that the repulsive effect of the wall made the fish tend towards a turning speed $F(D_c)$ which bends its trajectory away from the wall. In order to keep the model independent of the time step, we adopted the sde formalism of equation (3.12) and introduced the new term $F(D_c(t))$ as:

$$dW(t) = -\frac{1}{\tau}\ (W(t) - F(D_c(t)))\, dt\ + \sigma dB(t) \tag{5.14}$$

If the wall effect were constant over time (e.g. $F(D_c(t)) = F^\star$) process (5.14) should be understood as a relaxation of $W(t)$ towards the equilibrium value $F^\star$. Of course, since the fish position and its heading change over time, so does $F(D_c(t))$.

Over a small time step Δt however, we can assume that $F(D_c(t)) \simeq F(D_i)$ (with $t = (i-1)\Delta t$) is constant, and the discrete version of (5.14) is given in [7] by

$$W_{i+1} = a\, W_i + c\, F(D_i) + b_i \tag{5.15}$$

where $c = (1 - e^{-\Delta t/\tau})$, and a and b_i are defined as in (3.7). Given a from the spontaneous model we reconstructed $F(D_c)$ based on

$$\widehat{F(D_i)} = \frac{W_{i+1} - a\, W_i}{c} \tag{5.16}$$

plotted against D_i.

Finally, since the repulsive effect of the wall has to induce a change of the turning speed in the correct direction, we corrected the sign of $\widehat{F(D_i)}$ such that positive values corresponded to a fish steering away from the wall (Fig. 1.7a). Following [9], we used a nonparametric locally weighted regression procedure (loess, [17]) to estimate the decay of this wall effect as the distance to collision increases. This decay could be adequately modeled by the parametric function $F(Dc) \simeq 3\, e^{-1.5 D_c}$ (Fig.1.7a).

We finally simulated the complete model, using the discrete version (5.15), and checked the simulated trajectories against the experimental one. A typical example is shown in Fig.1.7b. Note in particular that the wall avoidance results from the

time integration of the wall effect quantified above, with no ad-hoc correction in case of collisions (which do not happen with sufficiently small Δt). As a final test of the relevance of this model, we compared the experimental and the expected mean squared displacement (MSD). Both agreed perfectly well up to 6 seconds (i.e. 3.6 m, which is of the same order of magnitude as the tank width of 4 m) despite the fact that the statistical quantifications of the model were done on the turning speed fluctuations (third derivative of the position) whereas this test is performed directly with the integrated time series of the fish positions.

6 Discussion

6.1 Why a new kind of random walk model is needed

Random walks and the associated diffusion models were originally developed in biology to describe the movements of single cells [44, 45]. Later they were adopted by ecologists to model the displacement of animals [35, 56], and particular attention was paid to the underlying behavioral mechanisms and how they are modulated by environmental conditions. Inspired from the model of gas particles that travel straight ahead between collisions, random walk models break the path into a series of consecutive straight moves, separated by random reorientation behavior. The biological rules determine, for each move, a direction, a duration and a length that can depend on the preceeding move (in the case of the correlated random walk) but also on the animal's state and goals and the environmental conditions (including the presence of conspecifics). Most often, these discrete random walk models have equivalent continuous time formulations, either at the population level (macro-scale diffusion models) or at the individual level (stochastic differential equations and Langevin theory of Brownian motion [16]). They are especially useful when the focus is put on the interplay between the behavior and the environment at large time and space scales (e.g. how ovipositing butterflies respond to changes in the dispersion of their food plants [34]). More generally, simple random walks have proved to be appropriate to quantify the movement of animals or cells which exhibit clear bouts of straight moves separated by reorientation behaviour (e.g. in ants [14, 13], cockroaches [32] or E. coli [2]).

Our fish in the tank did not exhibit such clear bouts of straight moves nor clear reorientation behaviour. They are rather characterized by smooth variations of their heading. Of course, it would still have been possible to approximate their trajectory as a series of straight segments at some fine scale. This would have required a subtle choice where to break up the path, with a trade-off between inappropriate lumping of small displacements and excessive splitting of long ones. Excessive splitting yields series of headings that are still highly autocorrelated which complicates statistical factor analyses and the translation of individual movements into population dispersal models [34, 57]. To avoid this, Tourtellot advocates for instance to sub-sample trajectories of cockroaches in order to enhance the discrimination between "gait noise" (lateral, side-to-side wobble) and course changes [55]. Accordingly, Turchin suggests to resample the path at a lower rate until the autocorrelation structure disappears [56, 58, 6].

Such a procedure applied to our fish has led to an overly rough approximation of the true path, impeding accurate predictions of the fish trajectory at the short time scale. At finer scales, not only was the heading highly autocorrelated from one segment to the next (one-step correlation as in the correlated random walk model), but the heading change itself was autocorrelated, because the circular-shaped trajectories imply sustained changes of the heading towards the same clock-wise sign. Modelling such a moving behaviour with straight moves separated by an *ad hoc* tortuous reorientation behaviour (e.g. a Markov process of higher order as in [27]) would have been unduly complicated.

We adopted a more parsimonious approach in which the random fluctuations act directly on the turning speed (the derivative of the heading) rather than on the heading itself. This led us to the persistent turning walker (PTW) model. Using this model, there were still two alternatives to express the random process at the individual scale, either as a discrete process or as a continuous process. We followed the two approaches and quantified the associated model parameters from experimental data. In the discrete alternative, the trajectory is split into a series of circular segments of random length (constant turning speed over a random time length), separated by a renewal process of the turning speed drawn from a Gaussian distribution. The associated quantification procedure yielded convincing results, but it involved the prior validation of methodological prerequisites, in particular the detailed development of the proper algorithm of path segmentation. It will be the subject of a future report. In the continuous alternative that is reported in the present chapter, the fish path is considered as a curvilinear track whose parameters are continuously updated by the animal. The renewal process of the turning speed leads to a description by stochastic differential equations [48, 10] where the turning speed follows an Ornstein-Uhlenbeck (OU) process. We used the discrete-time sampling of the path to estimate its parameters. This formalism allows predictions at any time scale.

Beyond the formalism, the experimental data have clearly shown that the classical random walk models (adjustments of headings) are inappropriate for the spontaneous movement of the fish species under study in which the steering process is based on adjustments of the turning speed. Obviously, this result has to be confirmed for other fish species and arguably in other experimental set-ups (e.g. varying the tank diameter). It is however a highly plausible model for many fishes that travel at constant swimming speed [23, 54]. The model used to quantify this behaviour may also be considered to analyze movements in other animals that exhibit some circularity in their displacement (e.g. the desert isopod searching for its burrow [28, 29] or the carabid beetles [51]) and to derive their properties at the macroscopic scale. Schimansky-Geier et al. showed for instance that the intensity of research associated with a noisy constant turning speed is higher than possible with a piecewise linear random walk [37, 52].

6.2 Towards the quantification of fish interactions

The principal aim of this study was to establish a biologically grounded model of the spontaneous displacement of a fish against which the interactions with neighbors can be quantified. Since the null-model is directly based on the turning speed it is

reasonable to address interactions also from this point of view. The presence of a neighbor would simply make a fish turn more or less quickly, either to avoid, to align with or to approach it. In this case the interactions should not be modeled as attraction or repulsion forces (in the Newtonian sense, which would affect the swimming and the turning speeds), but rather as attraction or repulsion torques (which would affect the turning speed only).

To illustrate this idea and as a first step towards an ad-hoc methodology to quantify fish interactions we addressed the interaction of isolated fish with the tank wall. This takes the form of an additional term in the stochastic differential equation governing the turning speed process ($W(t)$). The repulsive effect of the wall has been formally described as an OU process relaxing $W(t)$ towards $F(D_c(t))$ (which represents a mean turning speed away from the wall, $D_c(t)$ being the distance before wall collision if the heading were not changed) rather than towards 0 (which represents a mean turning speed that is independent of the wall as in the open space case). For an animal interacting with its environment, steering away might be the most natural mean to avoid obstacles since it can work without altering swimming speed (accelerate and decelerate might be more costly than just steering away). The estimated intensity of $F(D_c(t))$ displayed an exponential decay as the distance to collision with the wall increased. The simulations of the model showed that its integration over time is sufficient to avoid collisions in the normal regime. Some fish (1,4,5) failed to be correctly modeled within this simple framework since their trajectory clearly showed a tendency to be not just repulsed but also attracted by the wall (which is sometimes labeled thigmotactism [32]). This attractive effect may be due to the stress induced by isolation or represent a natural behavior in the fishes' usual habitat in coral reefs. We did not further investigate this special case since we were not interested to model the effect of the wall *per se*, but simply used it to illustrate that interactions can actually be taken into account by a simple additional term in the $W(t)$ process.

The focus of the present chapter on changing rates of rotation evokes the use of gyroscopic forces in control theory that were recently applied in the context of bio-inspired swarm robotics [50, 5, 38, 25, 31, 41, 40, 33, 4]. Especially the theoretical studies of systems with constrained speed capabilities (nonholonomic mobiles) [8, 42, 39, 21] or the studies that explore the minimal design that allow such coordination [15, 43, 30] may prove interesting for further insights into the modeling of fish interactions.

7 Conclusion

We showed that the fish *Kuhlia mugil* follows in the experimental tank a particular kind of random walk: the persistent turning walker (PTW). Even if this result has to be confirmed for other species and biological contexts, our results suggest that the standard null-models (random walks) that are used in interaction studies and in models of collective fish movements might be less representative than suggested by their predominance in the literature.

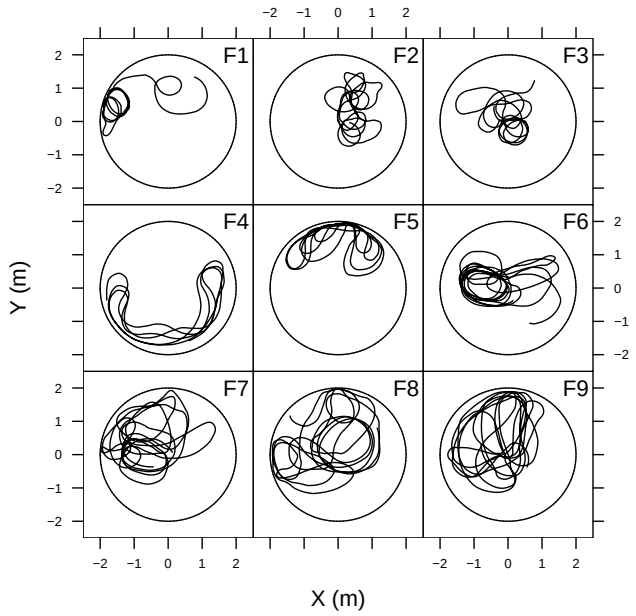

Figure 1.1: Nine fish trajectories in the water tank. The trajectories are displayed ranked by the fish speed, from the slowest (Fish 1, mean speed 0.16 m/s) to the fastest (Fish 9, mean speed 0.56 m/s). The outer circle indicates the tank wall and axis units are in m.

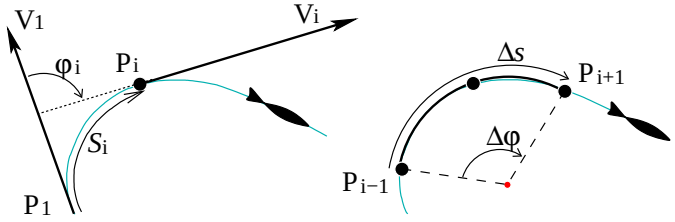

Figure 1.2: Symbols used in the path analysis. $P(t)$ is the fish position at time t, $V(t)$ its speed vector and $S(t)$ the path length since the beginning of the path $P(0)$. On the right side, the fitted circle arc (bold line) used for quantifying the intrinsic coordinates was superimposed on the actual fish trajectory . P_i denotes $P(t_i)$, that is the position of the fish at time step i.

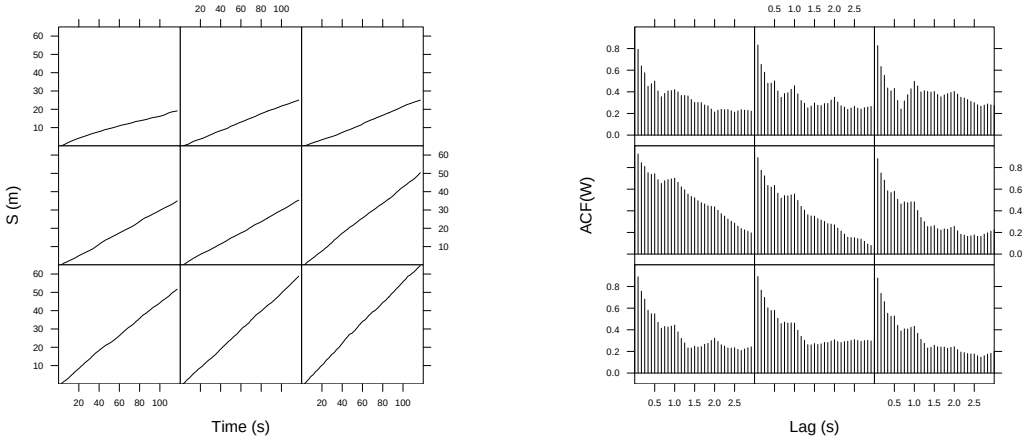

(a) Curvilinear distance S(t)

(b) Autocorrelation function of the turning speed $W(t)$

Figure 1.3: Evolution of the intrinsic coordinates $S(t)$ (top) and the autocorrelation function of the turning speeds W_i (bottom, both graphs in the same order as Fig. 1.1). The linear slopes of $S(t)$ indicate a constant swimming speed and the autocorrelation of the turning speed is significant over several seconds.

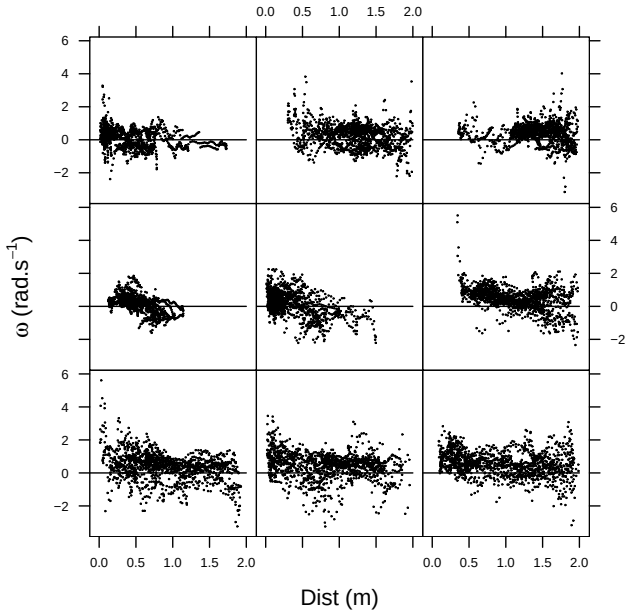

Figure 1.4: Effect of the wall on the turning speed $W(t)$ (same order as Fig. 1.1). The sign of $\widehat{W_i}$ was corrected so that positive values correspond to a fish steering away from the wall. The sign-corrected values $\widehat{\omega_i}$ are reported as a function of the shortest distance $Dist$ from the fish to the wall. Near the wall ($Dist < 1$ m), $\widehat{\omega}_i$ is skewed towards positive values, indicating an effect of the wall up to 1 m away from it.

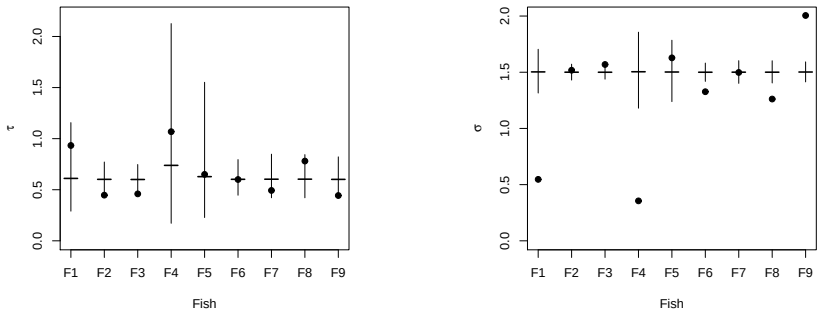

(a) Autocorrelation Time Constant, τ (s)

(b) Square root of variance, σ (rad.s$^{-1/2}$)

Figure 1.5: Parameter estimates for each fish of the AR process representing the angular speed W, mean time lag τ (a) and turning speed standard deviation σ (b). •: parameter estimate from the original data. Lines: numerical predictions of the means and 0.95 confidence intervals for the common set (see text for further details).

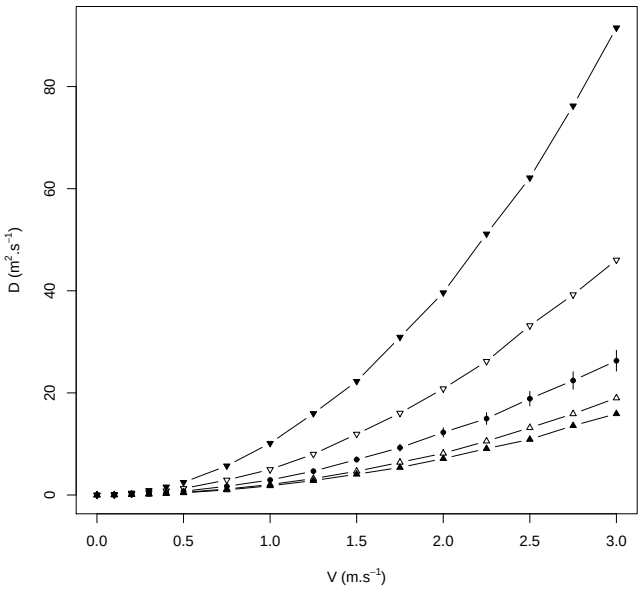

Figure 1.6: Diffusion coefficient D for the PTW model as a function of the swimming speed V, and for different values of the autocorrelation time τ, but keeping the variance $\frac{\tau\sigma^{\star 2}}{2}$ of W constant ($\blacktriangledown : \tau = \tau^\star/4$; $\triangledown : \tau = \tau^\star/2$; $\bullet : \tau = \tau^\star = 0.6$ s; $\triangle : \tau = 2\tau^\star$; $\blacktriangle : \tau = 4\tau^\star$). Each value was estimated by the Monte-Carlo method, with 10,000 replicates of individual trajectories simulated with $\Delta t = 0.01$ s over 1200 s and with random initial conditions (heading and turning speed). D was estimated by linear regression from the mean square displacement restricted to the time interval [600..1200] s in order to avoid the ballistic part of the curve. Bars denote the 0.95 confidence interval for the case $\bullet : \tau = \tau^\star$.

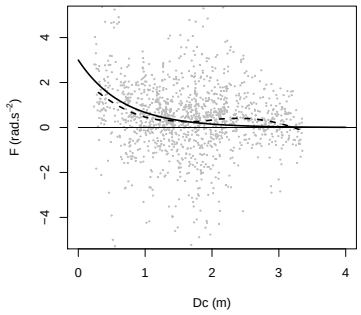

(a) Wall effect on the angular speed. D_c: distance to collision. A positive F denotes repulsion. Dotted line: *loess* estimate of $F(D_c)$. Thick line: parametric approximation $3\ \exp^{-1.5\,D_c}$

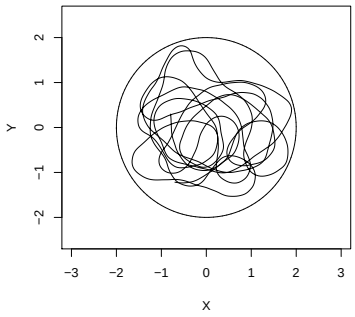

(b) Example of a typical simulated trajectory in the tank (equation 5.15, with $\tau = 0.6$ s, $\sigma = 1.5$ rad.s$^{-1/2}$, $\Delta t = 0.01$ s).

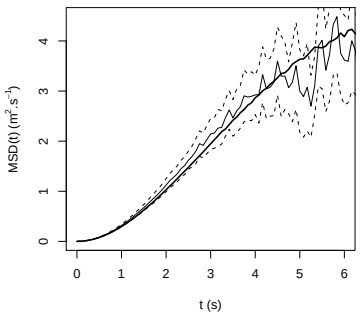

(c) Mean Squared Displacement of model and experimental data (fish 9). Thin line: experimental mean; dotted lines: experimental 95% confidence interval; thick line: model prediction estimated by Monte Carlo simulations (parameters as in b).

Figure 1.7: Integration of the wall repulsive effect in the model for fish 9

Bibliography

[1] Alt, W.: Modelling of motility in biological systems. In: McKenna, J., Temam, R. (eds.) ICIAM'87 Proceedings of the First International Conference on Industrial and Applied Mathematics, pp 15–30. Society for Industrial and Applied Mathematics, Philadelphia, PA (1988),

[2] Alt, W.: Correlation analysis of two-dimensional locomotion paths, In: Alt, W., Hoffmann, G. (eds), Biological motion, vol. 89 of Lecture Notes in Biomathematics. Springer-Verlag (1990)

[3] Aoki, I.: An analysis of the schooling behavior of fish: internal organization and communication process. Bull. Ocean Res. Inst. Univ. Tokyo 12,1–65 (1980)

[4] Bai, H.; Arcaka, M.; Wen, J.T.: Adaptive design for reference velocity recovery in motion coordination. Systems and Control Letters (in press) doi:10.1016/j.sysconle.2007.07.003

[5] Balch, T.; Arkin, R.: Behavior-based Formation Control for Multi-robot Teams. IEEE Transactions on Robotics and Automation 14, 926–939 (1998)

[6] Benhamou, S.: How to reliably estimate the tortuosity of an animal's path: straightness, sinuosity, or fractal dimension? J. Theor. Biol. 229, 209–220 (2004)

[7] Bianchi, C.; Cleur, E.M.: Indirect estimation of stochastic differential equation models: some computational experiments. Computational Economics 9, 257–274 (1996)

[8] Borenstein, J.; Koren, Y.: The vector field histogram - Fast obstacle avoidance for mobile robots. IEEE Transactions on Robotics and Automation 7, 278–288 (1991)

[9] Brillinger, D.R.: A particle migrating randomly on a sphere. J. Theor. Prob. 10, 429–443 (1997)

[10] Brillinger, D.R.; Preisler, H.K.; Ager, A.A.; Kie, J.G.; Stewart, B.S.: Employing stochastic differential equations to model wildlife motion. Bull. Braz. Math. Soc., New Series 33, 385–408 (2002)

[11] Caillol, J-M.: Random walks on hyperspheres of arbitrary dimensions. J. Phys. A Math. Gen. 37, 3077–3083 (2004)

[12] Camazine, S.; Deneubourg, J-L.; Franks, N.; Sneyd, J.; Theraulaz, G.; Bonabeau, E.: Self-Organization in Biological Systems. Princeton University Press (2001)

[13] Casellas, E.; Gautrais, J.; Fournier, R.; Blanco, S.; Combe, M.; Fourcassie, V.; Theraulaz, G.; Jost, C.: From individual to collective displacements in heterogeneous environments. J. of Theor. Biol. 250, 424–434 (2007).

[14] Challet, M.; Jost, C.; Grimal, A.; Lluc, J.; Theraulaz, G.: How temperature influences displacements and corpse aggregation behaviors in the ant Messor Sancta. Ins. Soc. 52, 309–315 (2005)

[15] Grégoire, G.; Chaté, H.; Tu, Y.: Moving and staying together without a leader. Physica D 181, 157–170 (2003)

[16] Chowdhury, D.: 100 years of Einstein's theory of Brownian motion: from pollen grains to protein trains. Resonance (Indian Academy of Sciences), 10, 63 (2005). arXiv:cond-mat/0504610.

[17] Cleveland, W.S.; Grosse, E.; Shyu, W.M.: Local regression models. In: Chambers, J.; Hastie, T.J. (eds) Statistical Models in S, pp. 309-376. Pacific Grove, Wadsworth (1992)

[18] Couzin, I. D.; Krause, J. K.; James, R.; Ruxton, G. D.; Franks, N. R.: Collective memory and spatial sorting in animal groups. J. Theor. Biol 218, 1–11 (2002)

[19] Couzin, I.D.; Krause, J.; Franks, N.R.; Levin, S.A.: Effective leadership and decision making in animal groups on the move. Nature 433, 513–516 (2005).

[20] Degond, P.; Motsch, S.: Large scale dynamics of the Persistent Turning Walker model of fish behavior. J. Stat. Phys 131, 989–1021(2008)

[21] Do, K.D.; Jiang, Z.P.; Pan, J.: Underactuated ship global tracking under relaxed conditions. IEEE Transactions on Automatic Control 47, 1529–1536 (2002)

[22] Ferrando, S. E.; Kolasa, L. A.; Kovacevic, N.: Wave++: a C++ library of signal analysis tools. http://www.scs.ryerson.ca/~lkolasa/CppWavelets.html (2007)

[23] Fish, F.E.: Performance constraints on the maneuverability of flexible and rigid biological systems. In: Proceedings of the Eleventh International Symposium on Unmanned Untethered Submersible Technology, pp 394-406. Autonomous Undersea Systems Institute, Durham New Hampshire. (1999)

[24] Gautrais, J.; Jost, C.; Theraulaz, G.: Key behavioural factors in a self-organised fish school model. Annales Zoologici Fennici, (in press), 2008

[25] Gazi V.; Passino K.M.: Stability analysis of swarms. IEEE Transactions on automatic control 48, 692–697 (2003)

[26] Grünbaum, D.; Viscido, S.; Parrish, J.K.: Extracting interactive control algorithms from group dynamics of schooling fish. In: Kumar, V.; Leonard, N.E. and Morse, A.S. (eds), Lecture Notes in Control and Information Sciences, Springer-Verlag, Berlin, 103–117 (2004)

[27] Hapca, S.; Crawford, J.W.; MacMillan, K.; Wilson, M.J.; Young, I.M.: Modelling nematode movement using time-fractional dynamics. J. Theor. Biol. 248, 212–224 (2007)

[28] Hoffman, G.: The random elements in the systematic search behavior of the desert isopod *Hemilepistus reaumuri*. Behav. Ecol. Sociobiol. 13, 81–92 (1983)

[29] Hoffman, G.: The search behavior of the desert isopod *Hemilepistus reaumuri* as compared with a systematic search. Behav. Ecol. Sociobiol. 13, 93–106 (1983)

[30] Huepe, C.; Aldana, M.: New tools for characterizing swarming systems: A comparison of minimal models. Physica A 387, 2809–2822 (2008)

[31] Jadbabaie, A.; Lin, J.; Morse A.S.: Coordination of groups of mobile autonomous agents using nearest neighbor rules. IEEE Transactions on Automatic Control, 988–1001 (2003)

[32] Jeanson, R.; Blanco, S.; Fournier, R.; Deneubourg, J-L.; Fourcassié, V.; Theraulaz, G.: A model of animal movements in a bounded space. J. Theor. Biol. 225, 443–451 (2003)

[33] Justh, E.W.; Krishnaprasad, P.S.: Equilibria and steering laws for planar formations. Systems & Control Letters 52, 25–38 (2004)

[34] Kareiva, P. M.; Shigesada, N.: Analyzing insect movement as a correlated random walk. Oecologia 56, 234–238 (1983)

[35] Kareiva, P.: Habitat fragmentation and the stability of predator-prey interactions. Nature 326, 388–390 (1987).

[36] Keenleyside, M.H.A.: Some aspects of the schooling behaviour of fish. Behaviour 8, 183-248 (1955)

[37] Komin, N.; Erdmann, U.; Schimansky-Geier, L.: Random walk theory applied to daphnia motion. Fluctuation and Noise Letters 4, 151–159 (2004)

[38] Latombe, J.C.: Motion Planning: A Journey of Robots, Molecules, Digital Actors, and Other Artifacts. Int. J. of Robotics Research 18, 1119–1128, (1999)

[39] Laumond, J.P.; Risler, J.J.: Nonholonomic systems: Controllability and complexity. Theoretical Computer Science 157, 101–114 (1996)

[40] Lin, Z.; Broucke, M.E.; Francis, B.A.: Local control strategies for groups of mobile autonomous agents. IEEE Transactions on Automatic Control 49, 622–629 (2004)

[41] Marshall, J.A.; Broucke, M.E.; Francis, B.A.: Formations of vehicles in cyclic pursuit. IEEE Transactions on Automatic Control 49, 1963–1974 (2004).

[42] Murray, R.M.; Sastry, S.S.: Nonholonomic motion planning: Steering using sinusoids. IEEE Transactions on Automatic Control 38, 700–716 (1993)

[43] Nagy, M.; Darukab, I.; Vicsek, T.: New aspects of the continuous phase transition in the scalar noise model (SNM) of collective motion. Physica A 373, 445–454 (2007)

[44] Patlak, C.S.: Random walk with persistence and external bias. Bull. Math. Biophys. 15, 311–338 (1953)

[45] Patlak, C.S.: A mathematical contribution to the study of orientation of organisms. Bull. Math. Biophys. 15, 431–476 (1953)

[46] Parrish, J.K.; Turchin, P.: Individual decisions, traffic rules, and emergent pattern in schooling fish. In: Parrish, J.K. and Hammer, W.M. (eds), Animal groups in three dimensions, pp. 126-142. Cambridge University Press (1997)

[47] Perrin, F.: Etude mathématique du mouvement brownien de rotation. Annales scientifiques de l'ENS 45, 1–51, (1928)

[48] Preisler, H. K.; Brillinger, D. R.; Ager, A. A.; Kie, J. G.; Akers, R. P.: Stochastic differential equations: a tool for studying animal movement. Proc. Internat. Union Forest Research Org. (2001)

[49] Radakov, D.: Schooling in the ecology of fish. New York, Wiley (1973)

[50] Reynolds, C.W.: Flocks, herds, and schools: A distributed behavioural model. Computer Graphics 21, 25–34 (1987)

[51] Scharstein, H.: Paths of carabid beetles walking in the absence of orienting stimuli and the time structure of their motor output. In: Alt, W and Hoffmann, G (eds) Biological motion, vol. 89 of Lecture Notes in Biomathematics. Springer-Verlag (1990)

[52] Schimansky-Geier, L.; Erdmann, U.; Komin, N.: Advantages of hopping on a zig-zag course. Physica A 351, 51–59 (2005)

[53] Soria, M.; Freon, P.; Chabanet, P.: Schooling properties of an obligate and a facultative fish species. Journal of Fish Biology 71, 1257–1269 (2007)

[54] Sfakiotakis, M.; Lane, D.M.; Davies, J.B.C.: Review of fish swimming modes for aquatic locomotion. IEEE Journal of oceanic engineering 24, 237–252 (1999)

[55] Tourtellot, M. K.; Collins, R. D.; Bell, W.J.: The problem of movelength and turn definition in analysis of orientation data. J. Theor. Biol 150, 287-297 (1991)

[56] Turchin, P.; Odendaal, F. J.;Rausher, M. D.: Quantifying Insect Movement in the Field. Environmental Entomology 20, 955–963 (1991)

[57] Turchin, P.: Translating foraging movements in heterogeneous environments into the spatial distribution of foragers. Ecology 72, 1253–1256 (1991)

[58] Turchin, P.: Quantitative Analysis of Movement: Measuring and Modeling Population Redistribution in Animals and Plants. Sinauer Associates, Sunderland, Massachusetts (1998)

[59] Uhlenbeck, G.E.; Ornstein, L.S.: On the theory of Brownian motion. Physical Review 36, 823–841 (1930)

[60] Umeda, T.; Inouye, K.: Possible role of contact following in the generation of coherent motion of *Dictyostelium* cells. J. Theor. Biol 291, 301–308 (2002)

[61] Viscido, S.V.; Parrish, J.K.; Grünbaum, D.: Factors influencing the structure and maintenance of fish schools. Ecological Modelling 206, 153–165 (2007)

Chapter 2

Large scale dynamics of the Persistent Turning Walker model of fish behavior

This chapter has given an article written in collaboration with P. Degond and published in Springer Journal of Statistical Physics: *Large Scale Dynamics of the Persistent Turning Walker Model of Fish Behavior*, J. Stat. Physics, **131**, no. 6, 989–1021.

Abstract. This chapter considers a new model of individual displacement, based on fish motion, the so-called Persistent Turning Walker (PTW) model, which involves an Ornstein-Uhlenbeck process on the curvature of the particle trajectory. The goal is to show that its large time and space scale dynamics is of diffusive type, and to provide an analytic expression of the diffusion coefficient. Two methods are investigated. In the first one, we compute the large time asymptotics of the variance of the individual stochastic trajectories. The second method is based on a diffusion approximation of the kinetic formulation of these stochastic trajectories. The kinetic model is a Fokker-Planck type equation posed in an extended phase-space involving the curvature among the kinetic variables. We show that both methods lead to the same value of the diffusion constant. We present some numerical simulations to illustrate the theoretical results.

Key words: Individual based model, Fish behavior, Persistent Turning Walker model, Ornstein-Uhlenbeck process, Kinetic Fokker-Planck equation, Asymptotic analysis, Diffusion approximation

1 Introduction

This chapter considers a new model of individual displacement, the so-called 'Persistent Turning Walker' (PTW) model, which has recently been introduced to describe fish behavior [27]. The fish evolves with a velocity of constant magnitude and its trajectory is subject to random turns (i.e. random changes of curvature) on the one hand and to curvature relaxation to zero on the other hand. The random changes of curvature can be interpreted as a way for the fish to explore its surroundings while relaxation to zero curvature just expresses that the fish cannot sustain too strongly curved trajectories and when the curvature becomes too large, it gets back to a straight line trajectory. The combination of these two antagonist behaviors gives rise to an Ornstein-Uhlenbeck process on the curvature. The curvature is the time derivative of the director of the velocity, while the velocity itself is the time derivative of position. The PTW process collects all these considerations into a system of stochastic differential equations.

This model is, to the knowledge of the authors, original, and has appeared for the first time in the works by Gautrais, Theraulaz, and coworkers [27]. The present paper considers the large time and space scale dynamics of a two-dimensional particle subject to this PTW process. It rigorously shows (in the mathematical sense) that, at large scales, the dynamics of the particle can be described by a diffusion process and it provides a formula for the diffusion coefficient. To prove this result, two methods are considered.

In the first method, the stochastic differential system itself is considered and the variance of the position is shown to behave, at large times, like a linear function of time. The diffusion coefficient is identified as the slope of this linear function. Because the curvature and the velocity angle can be explicitly computed, an explicit formula for the diffusion coefficient, involving some special functions, can be obtained.

The second method considers the forward Kolmogorov equation of the stochastic process. This equation gives the evolution of the probability distribution function of the particle in the extended phase space (position, velocity angle, curvature) as a function of time. It is a Fokker-Planck type equation. The passage from the microscopic to the macroscopic scales relies on a rescaling of the Kolmogorov equation. This rescaling depends on a small parameter $\varepsilon \ll 1$, which describes the ratio of the typical microscopic to macroscopic space units. After this rescaling, the problem has the typical form of the diffusion approximation of a kinetic problem (see references below). The goal is then to study the behaviour of the solution as $\varepsilon \to 0$. It is shown that the solution converges to some 'thermodynamical equilibrium' which is a Gaussian distribution of the curvature and a uniform distribution of the velocity angle. The equilibrium depends parametrically on the density which satisfies a spatial diffusion equation.

Finally, the connection between the two methods is made by showing that the diffusion tensor in the second approach can be represented by a formula involving the solution of the stochastic differential equation of the first approach. Additionally, this representation leads to explicit computations which show that the two formulas for the diffusion coefficient actually coincide. This seemingly innocuous result is actually quite powerful. Indeed, the diffusion approximation method leads to a non-explicit expression of the diffusion coefficient, involving the moments of a particular solution

of a stationary equation involving the leading order operator of the Fokker-Planck equation. That this non-explicit formula is equivalent to the explicit formula given by the stochastic trajectory method is by far not obvious. In this respect, the stochastic trajectory method is more powerful than the diffusion approximation approach, because it directly leads to the most simple expression of the diffusion constant.

A third route could have been taken and has been dismissed. This third method would actually use the stochastic differential equation itself to perform the diffusion approximation in the forward Kolmogorov equation. We have preferred to use partial differential equation techniques. One reason for this choice is that these techniques can be more easily extended to more complex situations. One typical example of these more complex situations are the nonlinear systems which are obtained when interactions between individual are included. The inclusion of interactions between individuals within the PTW model is actually work in progress.

From the biological viewpoint, one should not restrict the content of the paper to the sole expression of the diffusion coefficient. Indeed, once interactions between individuals will be included in the PTW model, it is not clear at all that the explicit computations which led to this expression will still be tractable. In the absence of an explicit solution of the stochastic differential system, there is little grasp to get information about the large scale behaviour of the system. By contrast, the diffusion approximation approach gives a systematic tool to study the large scale behavior of such systems, in all kinds of situations, be they linear or nonlinear. By its flexibility and its versatility, the diffusion approximation approach is the method of choice to study these problems.

One of the most popular models to describe fish behavior is the discrete Couzin-Vicsek algorithm (CVA) [1, 14, 30, 50] (see also [2, 10, 25, 38, 41, 42] for related models). For a large scale modeling of fish behavior, it is efficient to look at continuum models, which use macroscopic variables such as mean density, mean velocity and so on. Several such models based on phenomenological observations, exist (see e.g. [26, 37, 48, 49]). Several attempts to derive continuum models from the CVA model are also reported in the literature [35, 45, 46]. In [21, 22], a derivation of a continuum model from a kinetic version of the CVA model is proposed. However, few Individual Based Models for fish have been validated against experimental data with a comparable care as in [27] for the PTW process. As such, the continuum model derived in this paper has a firm experimental basis, although further work needs certainly to be done to fully validate its biological foundations. Additional references on swarm aggregation and fish schooling can be found in [11]. Among other types of animal societies, insects, and in particular ants [34, 47] or cockroaches [33] have been the subject of a vast literature (see references therein).

The derivation of macroscopic models from particle behavior has been initiated by the seminal works of Boltzmann, and later Hilbert, Chapman and Enskog. We refer to [13] for a mathematical perspective and to [16] for an introduction to the subject from a modeling perspective. More recently, the derivation of macroscopic models from microscopic behavior has been very productive in other context like traffic [4, 32] or supply-chains [3]. Diffusion approximation problems for kinetic equations have been

widely studied in the literature, in the context of neutron transport (see e.g. [6, 8]), semiconductors [7, 23, 28, 44], plasmas [17, 19, 20] or polymeric fluids [18].

The outline of the paper is as follows : in section 2, the PTW process is introduced and the main results are stated. In section 3 the diffusion coefficient is obtained by direct inspection of the trajectories of the stochastic differential system. In section 4, the diffusion approximation of the forward Kolmogorov equation of the stochastic process is performed. Section 5 is devoted to proving that the trajectory method and the diffusion approximation method give rise to the same value of the diffusion coefficient. In section 6, the theoretical results are illustrated by and complemented with some numerical simulations. A conclusion is drawn in section 7. Several proofs of auxiliary results, which are inessential for the main discussion are collected in three appendix (A, B and C).

2 The Persistent Turning Walker model: presentation and main results

The starting point of the present work is a new model of fish motion based on experimental data taken from experiments run in La Réunion islands during years 2001 and 2002 [27]. The studied species is a pelagic fish named Kuhlia Mugil. Its typical size ranges between 20 and 25 cm. The first experiments have been made with a single fish in a basin of 4 meters diameter during two minutes. A video records the positions of the fish every 12-th of a second (see figure 2.1). Then the data have been statistically analyzed and a model has been extracted [27].

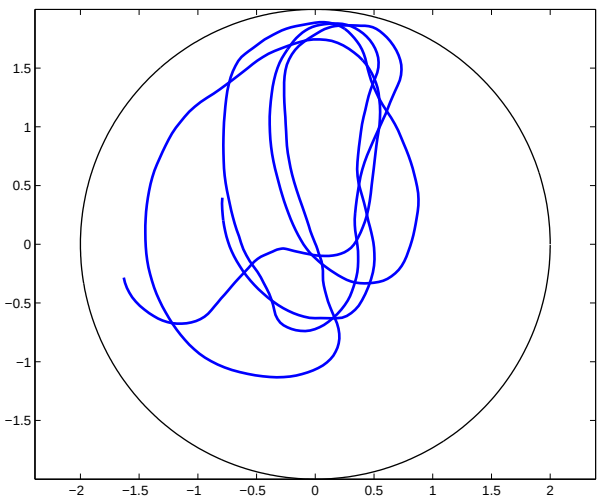

Figure 2.1: One trajectory of a Kuhlia Mugil fish

The conclusion of the statistical analysis is that the trajectories are well described

by the following systems of stochastic differential equations:

$$\frac{d\vec{x}}{dt} = c\vec{\tau}(\theta), \tag{2.1}$$
$$\frac{d\theta}{dt} = c\kappa, \tag{2.2}$$
$$d\kappa = -a\kappa\, dt + b\, dB_t, \tag{2.3}$$

where $\vec{x} = (x_1, x_2) \in \mathbb{R}^2$ is the (two-dimensional) position vector of the (centroid of the) fish, $\vec{\tau}(\theta) = (\cos\theta\,, \sin\theta)$ is the director of the velocity vector with the angle $\theta \in \Pi = \mathbb{R}/2\pi\mathbb{Z}$ measured from the x_1 direction, $\kappa \in \mathbb{R}$ is the curvature of the trajectory and dB_t is the standard Brownian motion. The magnitude of the velocity is constant and denoted by $c > 0$. The constant a is a relaxation frequency and b quantifies the intensity of the random curvature jumps. b has the dimension of $1/(L\sqrt{T})$ where L and T stand for the dimensions of length and time.

The κ-dynamics is a standard Ornstein-Uhlenbeck process. The term "$b\, dB_t$" models a diffusion process in curvature space while the term "$-a\, K\, dt$" expresses the tendency of the individual to return to a straight line trajectory. The curvature cannot increase endlessly as a consequence of the diffusion process, but rather, must relax to zero and the relaxation is stronger as the curvature gets larger. This model has been called the *Persistent Turning Walker* model (PTW) because it allows large excursions of the curvature towards positive or negative values, during which the spinning of the trajectory persists for a certain time.

We stress the difference with more standard diffusion processes (such as those suffered by photons in a diffusive medium), in which the Brownian motion acts on the velocity itself (or, in the case of a velocity of constant magnitude, on the angle θ). In this case, the diffusion process acts on the second derivative of the particle positions, and the associated kinetic equation is of Fokker-Planck type. This model of photon diffusion is also relevant for a certain number of animal species [40].

In the PTW model, the diffusion process acts on the curvature, i.e. on the third derivative of the position vector. An intuitive justification of the relevance of this model for animal behaviour is by considering the non-differentiability of the Brownian motion. Because of this feature, the photon diffusion process involves infinite second derivatives of the position, i.e. infinite forces. However, an animal body can only exert finite forces and the muscles act only in such a way that the velocity angle undergoes smooth variations. The PTW model precisely presents this feature of having smooth second order derivatives, i.e. smooth forces.

Our goal in the present work is to study the large-scale dynamics of the stochastic differential system (2.1)-(2.3). This is best done in scaled variables, where the dimensionless parameters of the model are highlighted. We use $t_0 = a^{-1}$ as time unit, $x_0 = ca^{-1}$ as space unit, and $\kappa_0 = x_0^{-1}$ as curvature unit, and we introduce the dimensionless time, space and curvature as $t' = t/t_0$, $x' = x/x_0$ and $\kappa' = \kappa/\kappa_0$. For

simplicity, we omit the primes. In scaled variables, the PTW model is written:

$$\frac{d\vec{x}}{dt} = \vec{\tau}(\theta), \tag{2.4}$$

$$\frac{d\theta}{dt} = \kappa, \tag{2.5}$$

$$d\kappa = -\kappa\, dt + \sqrt{2}\alpha dB_t, \tag{2.6}$$

where the only dimensionless parameter left is α such that

$$\alpha^2 = \frac{b^2c^2}{2a^3}, \tag{2.7}$$

The meaning of α^2 is the following: $b/\sqrt{a}$ is the amplitude of a curvature change during a relaxation time a^{-1}, while c/a is obviously the distance travelled by the particle during this time. The product of these two quantities is dimensionless and is equal to $\sqrt{2}\alpha$. It quantifies the strength of the curvature jumps relative to the other phenomena.

The individual dynamics can be translated in terms of a probability distribution $f(t, \vec{x}, \theta, \kappa)\, d\vec{x}\, d\theta\, d\kappa$ of finding particles at times t with position in small neighborhoods $d\vec{x}\, d\theta\, d\kappa$ of position $\vec{x}$, velocity angle θ and curvature κ. The link between the individual dynamics and the evolution of the probability distribution f is given by the forward Kolmogorov equation :

$$\partial_t f + \vec{\tau} \cdot \nabla_{\vec{x}} f + \kappa \partial_\theta f - \partial_\kappa(\kappa f) - \alpha^2 \partial_{\kappa^2} f = 0. \tag{2.8}$$

This equation is an exact transcription of the individual dynamics, where the initial value f_0 at time $t = 0$ is given by the probability distribution of the initial conditions of the stochastic differential system (2.4)-(2.6). For more detailed considerations about the forward Kolmogorov equation and its link with stochastic differential systems, we refer the reader to [39, 5].

In order to capture the macroscopic dynamics, two possible routes can be taken, using either the stochastic differential system (2.4)-(2.6) or the partial differential equation (2.8). In this work, we follow both routes and verify that they lead to the same large-scale behaviour. The advantage of working directly on the stochastic system is that it is simpler and it leads to explicit formulas. However, as soon as the system gets more complicated, and in particular nonlinear, explicit solutions can no longer be found and this methodology can hardly be pursued. On the other hand, the PDE approach, which, in the present case is more complicated, is also more systematic and more general. In particular, it is generally usable in the more complex nonlinear cases (see e.g. [21, 22]). A particular important complex situation is the case of many interacting fish. In future work, we plan to extend the PTW model to populations of interacting fish and to use the PDE approach to extract the large-scale dynamics of the system.

From the analysis of the individual trajectories, explicit exact expressions for κ and θ in terms of stochastic integrals can be found. Unfortunately, there is no such explicit result for the position $\vec{x}(t)$, but we can calculate the first two moments of the

probability distribution of $\vec{x}(t)$ explicitly, using the expressions of κ and θ. We show that the mean of the position vector stays at the origin: $\mathbb{E}\{\vec{x}(t)\} = (0,0)$ (where $\mathbb{E}$ denotes the expectation over all sources of randomness, in the initial data and in the stochastic process) and that the variance grows asymptotically linearly in time. More exactly, we prove:

Theorem 2.1 *Under assumptions on the initial conditions that will be specified later on (see (3.1)-(3.4)), the solution of system (2.4)-(2.6) satisfies:*

$$\mathrm{Var}\{\vec{x}(t)\} \overset{t\to+\infty}{\sim} 2\mathcal{D}\,t, \quad \textit{with} \quad \mathcal{D} = \int_0^\infty \exp\left(-\alpha^2(-1+s+\mathrm{e}^{-s})\right) ds. \tag{2.9}$$

The notation Var is for the variance over all sources of randomness. The asymptotic linear growth of the variance (2.9) suggests that the dynamics of the system is of diffusive type at large times with diffusion coefficient $\mathcal{D}$. We can find an expression of $\mathcal{D}$ in terms of special functions. Indeed, we have

Proposition 2.2 *The following expression holds true:*

$$\mathcal{D} = \left(\frac{\mathrm{e}}{\alpha^2}\right)^{\alpha^2} \gamma(\alpha^2, \alpha^2), \tag{2.10}$$

where $\gamma(z,u)$ is the incomplete gamma function:

$$\gamma(z,u) = \int_0^u \mathrm{e}^{-t}\, t^{z-1}\, dt. \tag{2.11}$$

$\mathcal{D}$ has the following series representation:

$$\mathcal{D} = \mathrm{e}^{\alpha^2} \sum_{n=0}^{\infty} \frac{(-1)^n \alpha^{2n}}{n!\,(n+\alpha^2)}. \tag{2.12}$$

It is a decreasing function of α which has the following asymptotic behavior:

$$\mathcal{D} \sim \frac{1}{\alpha^2} \ \textit{ as } \ \alpha \to 0, \qquad \mathcal{D} \sim \sqrt{\frac{\pi}{2}}\,\frac{1}{\alpha} \ \textit{ as } \ \alpha \to \infty. \tag{2.13}$$

To investigate the large scale dynamics of the solution of the kinetic equation (2.8) (the existence of which can be easily proved, see proposition 4.2), we need to rescale the variables to the macroscopic scale. Indeed, in eq. (2.8), all the coefficients are supposed to be of order unity. This means that the time and space scales of the experiment are of the same order as the typical time and length scales involved in the dynamics, such as, the relaxation time or the inverse of the typical random curvature excursions. Of course, in most experiments, this is not true, since the duration of the experiment and the size of the experimental region are large compared with the time and length scales involved in the dynamics.

To translate this observation, we change the space unit x_0 to a new space space unit $x_0' = x_0/\varepsilon$, where $\varepsilon \ll 1$ is a small parameter. This induces a change of variables

$x' = \varepsilon x$. We make a similar operation on the time unit $t'_0 = t_0/\eta$, $t' = \eta t$ with $\eta \ll 1$. Now, the question of linking η to ε is a subtle one and is largely determined by the nature of the asymptotic regime which is achieved by the system. In the present case, we expect that the asymptotic regime will be of diffusive nature, in view of theorem 2.1 and so, we will investigate the so-called 'diffusion approximation' which involves a quadratic relationship between η and ε: $\eta = \varepsilon^2$.

For this reason, we introduce the diffusive rescaling:

$$t' = \varepsilon^2 t \quad ; \quad \vec{x}' = \varepsilon \vec{x}, \tag{2.14}$$

and we make the following change of variable in the distribution f :

$$f^\varepsilon(t', \vec{x}', \theta, \kappa) = \frac{1}{\varepsilon^2} f\left(\frac{t'}{\varepsilon^2}, \frac{\vec{x}'}{\varepsilon}, \theta, \kappa\right).$$

The scaling of the magnitude of the distribution function is unnecessary, since the problem is linear. However, it is chosen in order to preserve the total number of particles. Introducing (2.14) into (2.8) leads to the following problem for f^ε:

$$\varepsilon \partial_t f^\varepsilon + \vec{\tau} \cdot \nabla_{\vec{x}} f^\varepsilon + \frac{1}{\varepsilon} \left[\kappa \partial_\theta f^\varepsilon - \partial_\kappa (\kappa f^\varepsilon) - \alpha^2 \partial_{\kappa^2} f^\varepsilon \right] = 0 \tag{2.15}$$

In order to analyze the large-scale dynamics of (2.15), we need to investigate the limit $\varepsilon \to 0$. We show that f^ε converges to an equilibrium distribution function (i.e. a function which cancels the $O(\varepsilon^{-1})$ term of (2.15)) f^0 which depends parametrically on the particle density $n^0(x,t)$ and n^0 evolves according to a diffusion equation. More precisely, we prove:

Theorem 2.3 *Under hypothesis 4.1 on the initial data to be precised below, the solution f^ε of (2.15) converge weakly in a Banach space also to be specified below, (see (4.21)) X:*

$$f^\varepsilon \overset{\varepsilon \to 0}{\rightharpoonup} n^0 \frac{M(\kappa)}{2\pi} \quad \text{in } X \text{ weak star}, \tag{2.16}$$

where M is a Gaussian distribution of the curvature with zero mean and variance α^2 (see 4.4) and $n^0 = n^0(x,t)$ is the solution of the system:

$$\partial_t n^0 + \nabla_{\vec{x}} \cdot J^0 = 0, \tag{2.17}$$

$$J^0 = -D \nabla_{\vec{x}} n^0, \tag{2.18}$$

where the initial datum n_0^0 and the diffusion tensor D will be defined later on (see (4.31) and (4.28) respectively).

The following theorem connects the two methods by showing that the tensor D is related to $\mathcal{D}$ given by (2.9):

Theorem 2.4 *The tensor D defined by (4.28) satisfies :*

$$D = \frac{\mathcal{D}}{2}\, Id, \tag{2.19}$$

where $\mathcal{D}$ is given by (2.9) and Id denotes the 2×2 identity tensor.

This theorem confirms that the trajectory method and the asymptotic PDE method are equivalent. The factor 2 between the two coefficients comes from the dimension of the problem. Indeed, $\mathcal{D}$ is the average of $|x|^2 = |x_1|^2 + |x_2|^2$ while D is the diffusion coefficient in a given direction.

The graphical representation of $\mathcal{D}$ is given in figure 2.2. The expression $\mathcal{D}_0$ of the diffusion coefficient in 'physical' variables is obtained by multiplying the dimensionless expression $\mathcal{D}$ by the appropriate scaling units. The scaling unit for a diffusion coefficient is the square of the space scale divided by the time scale. Therefore, in the present case, its value is c^2/a. Therefore, we find:

$$\mathcal{D}_0 = \frac{c^2}{a}\, \mathcal{D}\left(\frac{b^2 c^2}{2a^3}\right). \tag{2.20}$$

Expression (2.20) and the fact that $\mathcal{D}(\alpha)$ is a decreasing function of α shows that the diffusion coefficient is decreasing with respect to b for fixed a and c. This is explained by the fact that, with an increasing noise intensity, the trajectory has a larger probability to reach strong curvatures (in magnitude). Therefore, the trajectory spins more, and the distance travelled in straight line is shorter.

On the other hand, the monotonicity of $\mathcal{D}_0$ with respect to a and c is unclear. Still, we can investigate the asymptotic limits and find that for $c \to \infty$ or $b \to \infty$ or $a \to 0$, (each limit being taken with the other two parameters kept fixed), we have $\mathcal{D}_0 \sim \sqrt{\pi}\sqrt{a}\, c/b$. In particular, for large c or small a, the diffusion increases with respect to both c and a. Conversely, if $c \to 0$ or $b \to 0$ or $a \to \infty$, (again, each limit being taken with the other two parameters kept fixed), we have $\mathcal{D}_0 \sim 2a^2/b^2$. Here, the diffusion is increasing with a but is independent of c.

The increase of $\mathcal{D}_0$ with a is easily explained: with a stronger relaxation parameter a, the curvature is more likely to be small, and the trajectory resembles more a straight line.

On the other hand, the diffusion $\mathcal{D}_0$ is independent of the velocity c when c is small. This is somehow paradoxical since one would expect that, as the particle moves faster, it travels larger distances. However, as c increases, the spinning of the trajectory increases, because the particle moves along a circle before undergoing a random change of curvature or a relaxation. Therefore, the average linear distance from the origin does not increase so much when the velocity is increased, at least for small velocities. For large velocities, the intuitive feeling that the diffusion should increase with the velocity is actually true: the diffusion is asymptotically proportional c for large values of c.

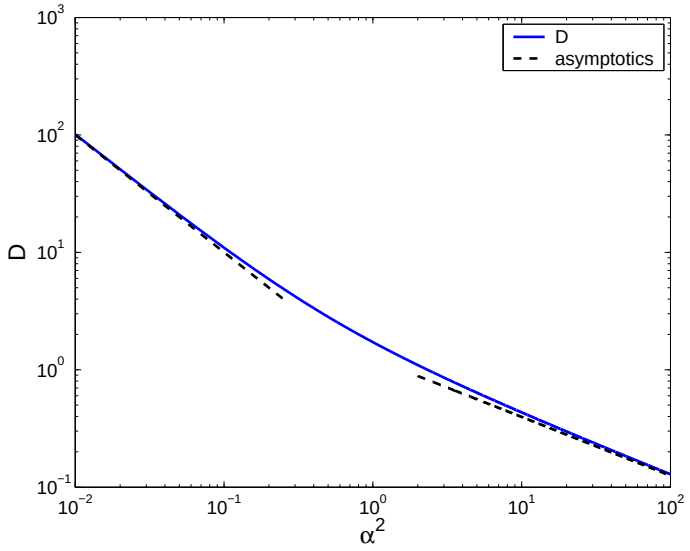

Figure 2.2: Scaled diffusion coefficient $\mathcal{D}$ as a function of α^2 in log-log scale (solid line). Asymptotic behavior of $\mathcal{D}$ as $\alpha \to 0$ or $\alpha \to \infty$ (dashed lines): $\mathcal{D} \sim \alpha^{-2}$ as $\alpha \to 0$ and $\mathcal{D} \sim \sqrt{\frac{\pi}{2}}\,\alpha^{-1}$ as $\alpha \to \infty$.

3 Large-scale dynamics of the PTW model by the trajectory method

In this section, we want to show theorem 2.1 and proposition 2.2. We first specify the initial conditions. First, we fix the starting point of the particle at the origin :

$$\vec{x}(t=0) = (0,0). \tag{3.1}$$

We suppose that the initial velocity angle is uniformly distributed on the one-dimensional sphere, i.e. :

$$dP\{\theta|_{t=0} = \theta\} = \frac{d\theta}{2\pi}. \tag{3.2}$$

For the curvature, we make the following observation: eq. (2.6) predicts that the process $\kappa(t)$ converges exponentially fast to its stationary state, which is a Gaussian distribution with zero mean and variance equal to α^2 [39]. We denote such a Gaussian distribution by $\mathcal{N}(0,\alpha^2)$. For this reason, we suppose:

$$dP\{\kappa|_{t=0} = \kappa\} = \mathcal{N}(0,\alpha^2)(\kappa). \tag{3.3}$$

The last hypothesis on the initial conditions is the following:

$$\text{The processes } \theta(t=0),\ \kappa(t=0) \text{ and } B_t \text{ are independents.} \tag{3.4}$$

We stress that this choice of initial conditions is for simplicity only. Completely arbitrary initial conditions would lead to the same large time behaviour, but the computation would be slightly more complicated. Since we are mainly interested in the

explicit expression of $\mathcal{D}$, a choice of initial conditions which simplifies the calculations is legitimate.

We begin by proving the following proposition:

Proposition 3.1 *The solution of the stochastic differential equation (2.4)-(2.6) with initial condition given by (3.1)-(3.4) satisfies :*

$$\mathbb{E}\{\vec{x}(t)\} = (0,0)\,, \qquad \forall\, t \geq 0, \tag{3.5}$$

$$\mathrm{Var}\{\vec{x}(t)\} = 2\int_{s=0}^{t}(t-s)\exp\left(-\alpha^2\left(-1+s+\mathrm{e}^{-s}\right)\right)\,ds. \tag{3.6}$$

To prove this proposition, we first establish explicit formulae for the solutions of (2.5) and (2.6). The proof is deferred to appendix A.

Lemma 3.2 *The solution of the stochastic differential system (2.5), (2.6) with initial conditions (3.2)-(3.4) is given by:*

$$\theta(t) = \theta_0 + \kappa_0 - \kappa(t) + \sqrt{2}\alpha B_t, \tag{3.7}$$

$$\kappa(t) = \mathrm{e}^{-t}\kappa_0 + \sqrt{2}\alpha\mathrm{e}^{-t}\int_0^t \mathrm{e}^s\,dB_s. \tag{3.8}$$

Additionally,

$$\theta(t) = \theta_0 + K_0^t, \tag{3.9}$$

where K_0^t is a Gaussian random variable independent of θ_0 with zero mean and variance β_t^2 given by :

$$\beta_t^2 = \mathrm{Var}\{K_0^t\} = 2\alpha^2(-1+t+\mathrm{e}^{-t}). \tag{3.10}$$

Proof of proposition 3.1: Using Lemma 3.2, we can compute the first two moments of $\vec{x}(t)$. Let us start with the computation of the mean. If we write $\vec{x}(t) = (x_1(t)\,,\,x_2(t))$, we have :

$$x_1(t) = \int_0^t \cos\theta(s)\,ds \quad , \quad x_2(t) = \int_0^t \sin\theta(s)\,ds,$$

and, computing the mean :

$$\mathbb{E}\{x_1(t)\} = \mathbb{E}\left\{\int_0^t \cos\theta(s)\,ds\right\} = \int_0^t \mathbb{E}\left\{\cos\theta(s)\right\}\,ds.$$

Now, we can develop $\theta(s)$ using (3.9):

$$\mathbb{E}\left\{\cos\theta(s)\right\} = \mathbb{E}\left\{\cos(\theta_0 + K_0^s)\right\} = \mathbb{E}\left\{\cos\theta_0\,\cos K_0^s - \sin\theta_0\,\sin K_0^s\right\}.$$

By the independence of θ_0 and K_0^s we finally have:

$$\mathbb{E}\left\{\cos\theta(s)\right\} = \mathbb{E}\{\cos\theta_0\}\mathbb{E}\{\cos K_0^s\} - \mathbb{E}\{\sin\theta_0\}\mathbb{E}\{\sin K_0^s\} = 0,$$

since the expectations of $\cos\theta_0$ and $\sin\theta_0$ over the uniform probability distribution on θ_0 are zero. Finally, we have $\mathbb{E}\{x_1(t)\} = 0$, and similarly for x_2. This proves (3.5).

Now for the variance of $\vec{x}(t)$, we write:

$$\mathrm{Var}\{\vec{x}(t)\} = \mathbb{E}\{x_1^2(t) + x_2^2(t)\} = 2\mathbb{E}\{x_1^2(t)\}. \tag{3.11}$$

by the isotropy of the problem. Then,

$$\begin{aligned}
\mathbb{E}\{x_1^2(t)\} &= \mathbb{E}\left\{\left(\int_0^t \cos\theta(s)\,ds\right)^2\right\} \\
&= \int_0^t\int_0^t \mathbb{E}\{\cos\theta(s)\,\cos\theta(u)\}\,dsdu \\
&= 2\int_0^t du\int_0^u ds\ \mathbb{E}\{\cos\theta(s)\cos\theta(u)\}.
\end{aligned}$$

Since $u \geq s$, we can write $\theta(u)$ as follows :

$$\theta(u) = \theta_0 + \int_0^s \kappa(z)\,dz + \int_s^u \kappa(z)\,dz = \theta_0 + K_0^s + K_s^u,$$

where K_0^s and K_s^u are Gaussian random variables independent of θ_0 with zero mean and variances β_s^2 and β_{u-s}^2 respectively, thanks to (3.10). Then, using standard identities for trigonometric functions, we get

$$\begin{aligned}
\mathbb{E}\{\cos\theta(s)\cos\theta(u)\} &= \mathbb{E}\{\cos(\theta_0 + K_0^s)\cos(\theta_0 + K_0^s + K_s^u)\} \\
&= \frac{1}{2}\left(\cos(2\theta_0 + 2K_0^s + K_s^u) + \cos(-K_s^u)\right).
\end{aligned}$$

But since θ_0 is independent of K_0^s and K_s^u we have $\mathbb{E}\{\cos(2\theta_0 + 2K_0^s + K_s^u)\} = 0$ since the mean of a $\cos(\theta_0 + C)$ over the uniform distribution of θ_0 is zero whatever the value of C. Then :

$$\begin{aligned}
\mathbb{E}\{\cos\theta(s)\cos\theta(u)\} &= \frac{1}{2}\,\mathbb{E}\{\cos\left(-K_s^u\right)\} \\
&= \frac{1}{2}\int_{\mathbb{R}} \cos(y)\frac{1}{\sqrt{2\pi}\beta_{u-s}}\,\mathrm{e}^{-\frac{y^2}{2\beta_{u-s}^2}}\,dy \\
&= \frac{1}{2}\,\mathrm{e}^{-\frac{1}{2}\beta_{u-s}^2}.
\end{aligned}$$

Indeed, an elementary computation shows that for any Gaussian random variable Z with zero mean and variance σ^2, one has

$$\mathbb{E}\{\cos(Z)\} = \exp(-\sigma^2/2). \tag{3.12}$$

Thus,

$$\mathbb{E}\{x_1(t)^2\} = \int_{u=0}^t\int_{s=0}^u \exp\left(-\alpha^2\left(-1 + |u-s| + \mathrm{e}^{-|u-s|}\right)\right)\,dsdu.$$

Using the change of unknowns $w = u - s$ and $y = u$ and inverting the order of integration we find :

$$\mathbb{E}\{x_1(t)^2\} = \int_{w=0}^{t} (t-w) \exp\left(-\alpha^2\left(-1+w+\mathrm{e}^{-w}\right)\right)\, dw.$$

Using (3.11), we finally find (3.6), which ends the proof of the proposition. ∎

In order to prove 2.1, we investigate the behavior of the variance $\mathrm{Var}\{\vec{x}(t)\}$ (given by (3.6)) when $t \to +\infty$.

End of proof of Theorem 2.1: We write, thanks to (3.6):

$$\mathrm{Var}\{\vec{x}(t)\} - 2\mathcal{D}t = -2\int_{s=0}^{t} s\mathrm{e}^{-\alpha^2(-1+s+\mathrm{e}^{-s})}\, ds - 2\int_{s=t}^{\infty} t\mathrm{e}^{-\alpha^2(-1+s+\mathrm{e}^{s})}\, ds.$$

We have to show that the difference is bounded independently of t. For the first term, we have:

$$\left|\int_{s=0}^{t} s\mathrm{e}^{-\alpha^2(-1+s+\mathrm{e}^{-s})}\, ds\right| \leq \int_{0}^{t} \mathrm{e}^{\alpha^2} s\mathrm{e}^{-\alpha^2 s}\, ds,$$

and integrating by parts, we find :

$$\left|\int_{s=0}^{t} s\mathrm{e}^{-\alpha^2(-1+s+\mathrm{e}^{s})}\, ds\right| \leq \frac{\mathrm{e}^{\alpha^2}}{\alpha^2}\left[-t\mathrm{e}^{-\alpha^2 t} - \frac{\mathrm{e}^{-\alpha^2 t}}{\alpha^2} + \frac{1}{\alpha^2}\right] \leq C_1.$$

For the second term, we have:

$$\left|\int_{s=t}^{\infty} t\mathrm{e}^{-\alpha^2(-1+s+\mathrm{e}^{s})}\, ds\right| \leq t\int_{t}^{\infty} \mathrm{e}^{\alpha^2}\mathrm{e}^{-\alpha^2 s}\, ds \leq t\mathrm{e}^{\alpha^2}\frac{\mathrm{e}^{-t\alpha^2}}{\alpha^2} \leq C_2.$$

This proves that the difference is $\mathrm{Var}\{\vec{x}(t)\} - 2\mathcal{D}t$ is bounded independently of t and completes the proof. ∎

We now prove Proposition 2.2 which gives an explicit approximation of the diffusion coefficient. This approximation is useful for practical simulations.

Proof of Proposition 2.2: The change of variables $t = \alpha^2\mathrm{e}^{-s}$ in the integral (2.9) leads to (2.10). The series representation (2.12) follows from a similar series representation of the incomplete gamma function (see e.g. formula (8.354) of [29]). The series representation can also be found by expanding the exponential in the integral (2.11) in power series (this point is left to the reader). That $\mathcal{D}$ is a decreasing function of α follows from (2.9) and the fact that the function $g(s) = -1 + s + \exp(-s)$ is non-negative for $s \geq 0$. The behavior of $\mathcal{D}$ for $\alpha \to 0$ (first formula (2.13)) is obtained by keeping only the zero-th order term in the series expansion (2.12). From (2.9), the behaviour of $\mathcal{D}$ for $\alpha \to \infty$ is controled by the behaviour of $g(s)$ near $s = 0$. Since $g(s) \sim s^2/2$, we find $\mathcal{D} \sim \int_0^\infty \exp(-\alpha^2 s^2/2)\, ds$, which leads to the second formula (2.13), and ends the proof. ∎

4 Large-scale dynamics of the PTW model through the diffusion approximation of the associated kinetic equation

4.1 Formal asymptotics

In this section, for the reader's convenience, we give a formal proof of theorem 2.3. We write (2.15) as follows:

$$\varepsilon\partial_t f^\varepsilon + \vec{\tau}\cdot\nabla_{\vec{x}} f^\varepsilon + \frac{1}{\varepsilon} A f^\varepsilon = 0 \tag{4.1}$$

where we define the operator A acting on functions $u(\theta,\kappa)$ as follows:

$$Au = \kappa\partial_\theta u - \partial_\kappa(\kappa u) - \alpha^2\partial_{\kappa^2} u. \tag{4.2}$$

The formal investigation of the limit $\varepsilon \to 0$ usually starts by considering the Hilbert expansion (see e.g. [16] for the general theory or [20] for an application in the context of Fokker-Planck equations):

$$f^\varepsilon = f^0 + \varepsilon f^1 + O(\varepsilon^2), \tag{4.3}$$

with f^k being independent of ε and inserting it into (4.1). Then, collecting all the the terms of comparable orders with respect to ε, we are led to a sequence of equations. The first one, corresponding to the leading $O(\varepsilon^{-1})$ term is $Af^0 = 0$, which means that f^0 lies in the kernel of A. In section 4.3, we show that the kernel of A is composed of functions of the form $f^0(t,\vec{x},\theta,\kappa) = n^0(t,\vec{x})M(\kappa)/(2\pi)$ where $M(\kappa)$ is a normalized Gaussian with zero mean and variance α^2:

$$M(\kappa) = \frac{1}{\sqrt{2\pi}\alpha^2}\,\mathrm{e}^{-\frac{\kappa^2}{2\alpha^2}}, \tag{4.4}$$

and $n^0(t,\vec{x})$ is a function still to be determined.

In order to determine n^0, we first integrate (4.1) with respect to $(\theta,\kappa) \in \Pi\times\mathbb{R}$ and use that $\int Au\,d\theta\,d\kappa = 0$. Defining the density $n^\varepsilon(t,\vec{x})$ and the flux $J^\varepsilon(t,\vec{x})$ by

$$n^\varepsilon(t,\vec{x}) = \int_{\theta,\kappa} f^\varepsilon\ d\kappa\,d\theta, \quad J^\varepsilon(t,\vec{x}) = \int_{\theta,\kappa} \frac{f^\varepsilon}{\varepsilon}\,\vec{\tau}(\theta)\,d\kappa d\theta, \tag{4.5}$$

we find:

$$\partial_t n^\varepsilon + \nabla_{\vec{x}}\cdot J^\varepsilon = 0. \tag{4.6}$$

We note that this continuity equation is valid for all values of ε. Then, letting $\varepsilon\to 0$, we formally have $n^\varepsilon \to n^0$. If we prove that J^0 given by (2.18) is the limit of J^ε, as $\varepsilon\to 0$, then, we can pass to the limit in (4.6) and find (2.17).

System (2.17) and (2.18) is a diffusion system, which completely determines $n^0(t,\vec{x})$, given its initial datum $n_0^0(\vec{x})$. Here, for simplicity, we assume that the initial datum for (4.1) is of the form $f^\varepsilon(0,\vec{x},\theta,\kappa) = n_0(\vec{x})M(\kappa)/(2\pi)$ and the resulting initial condition

for n^0 is therefore $n_0^0 = n_0$ (in this formal convergence proof, we admit the functions and the convergences are as smooth as required).

So, the only points left in the proof are the existence of a limit for J^ε and the validity of (2.18) for J^0. Note that the existence of a limit is not obvious because of the factor ε at the denominator of the integral (4.5) defining J^ε. To prove that the limit exists, we use the Hilbert expansion (4.3) again and compute f^1. Since A is linear, collecting the terms of order $O(\varepsilon^0)$ leads to:

$$-Af^1 = \frac{M(\kappa)}{2\pi}\ \vec{\tau}\cdot\nabla_{\vec{x}} n^0\,. \tag{4.7}$$

Again using the linearity of A and the fact that it operates only with respect to the (θ,κ) variables, we can write the solution of (4.7) as $f^1 = -\vec{\chi}\cdot\nabla_{\vec{x}} n^0$, where $\vec{\chi} = (\chi_1,\chi_2)$ is a solution of the problem

$$A\vec{\chi} = \frac{M(\kappa)}{2\pi}\ \vec{\tau}\,. \tag{4.8}$$

This equation must be understood componentwise (i.e χ_1 is associated with $\tau_1 = \cos\theta$ and χ_2 with $\tau_2 = \sin\theta$). Since the right-hand side of (4.8) has zero average with respect to (θ,κ), proposition 4.5 below shows that it has a unique solution, up to an element of the kernel of A. We can single out a unique solution by requesting that $\vec{\chi}$ has zero average with respect to (θ,κ) as well. Then, all solutions f^1 to (4.7) can be written as

$$f^1 = -\vec{\chi}\cdot\nabla_{\vec{x}} n^0 + n^1(t,\vec{x})\frac{M(\kappa)}{2\pi}\,, \tag{4.9}$$

where the second term of (4.9) is an arbitrary element of the kernel of A. We shall see that the determination of n^1 is unnecessary.

Now, inserting the Hilbert expansion (4.3) into the integral (4.5) defining J^ε, we find:

$$\begin{aligned} J^\varepsilon(t,\vec{x}) &= \frac{1}{\varepsilon}\int_{\theta,\kappa} f^0\,\vec{\tau}(\theta)\,d\kappa d\theta + \int_{\theta,\kappa} f^1\,\vec{\tau}(\theta)\,d\kappa d\theta + O(\varepsilon) \\ &= \qquad 0 \qquad\quad + \int_{\theta,\kappa} f^1\,\vec{\tau}(\theta)\,d\kappa d\theta + O(\varepsilon), \end{aligned} \tag{4.10}$$

because f^0 is independent of θ and $\int \vec{\tau}(\theta)\,d\theta = 0$. Therefore, J^ε has a limit when $\varepsilon\to 0$ and this limit is given by

$$J^0(t,\vec{x}) = \int_{\theta,\kappa} f^1\,\vec{\tau}(\theta)\,d\kappa d\theta. \tag{4.11}$$

To compute J^0 we insert expression (4.9) into (4.11) and find

$$J^0(t,\vec{x}) = \int_{\theta,\kappa} (-\vec{\chi}\cdot\nabla_{\vec{x}} n^0 + n^1\frac{M}{2\pi})\,\vec{\tau}(\theta)\,d\kappa d\theta. \tag{4.12}$$

The second term vanishes and the first one can be written

$$J^0(t,\vec{x}) = -\left(\int_{\theta,\kappa} \vec{\tau}\otimes\vec{\chi}\,d\theta\,d\kappa\right)\,\nabla_{\vec{x}} n^0, \tag{4.13}$$

which is nothing but formula (2.18) with the diffusivity tensor D given by (4.28).

This shows the formal convergence of the solution of the Fokker-Planck equation (2.15) to that of the diffusion system (2.17), (2.18).

Now, to make this proof rigorous, we need to justify all the formal convergences. In the framework of the Hilbert expansion, this requires to work out the regularity of the various terms of the expansion. This is doable and actually leads to stronger convergences than the one we are going to prove, but this is a bit technical (see e.g. [20]).

What we are going to do instead is proving a convergence result in a weaker topology without using the Hilbert expansion technique. The method is close to the so-called moment method, which consists in integrating the equation against suitable test functions. This convergence proof is developed in section 4.3, but before that, we state an existence result for the original Fokker-Planck equation (4.1).

4.2 Functional setting and existence result

We define the differential operator D acting on smooth functions $f(\kappa)$ by :

$$Df = \partial_\kappa(\kappa f) + \alpha^2 \partial_{\kappa^2} f. \tag{4.14}$$

We state some properties of D, the proofs of which are easy and left to the reader. We recall that $M(\kappa)$ denotes the normalized Gaussian with zero mean and variance α^2 (4.4).

Proposition 4.1 *Let f and g be smooth functions decreasing at infinity. The following identities hold true:*

$$Df = \alpha^2 \frac{\partial}{\partial\kappa}\left(M \frac{\partial}{\partial\kappa}\frac{f}{M}\right), \tag{4.15}$$

$$\int_{\mathbb{R}} Df\ g\,\frac{d\kappa}{M} = -\alpha^2 \int_{\mathbb{R}} M\,\partial_\kappa\left(\frac{f}{M}\right)\partial_\kappa\left(\frac{g}{M}\right)\,d\kappa = \int_{\mathbb{R}} f\,Dg\,\frac{d\kappa}{M}, \tag{4.16}$$

$$\int_{\mathbb{R}} Df\,f\,\frac{d\kappa}{M} = -\alpha^2 \int_{\mathbb{R}} M\left|\partial_\kappa\left(\frac{f}{M}\right)\right|^2\,d\kappa \le 0, \tag{4.17}$$

$$Df = 0 \Leftrightarrow \exists c \in \mathbb{R}, \quad f = cM. \tag{4.18}$$

The first identity translates the fact that M is the stationary measure of the Ornstein-Uhlenbeck process. The second one that D is formally self-adjoint with respect to the measure $d\kappa/M$. The third one shows that D is dissipative. The same inequality holds with any non-decreasing function $\eta(f)$, indeed, $\int D(f)\,\eta(f)\,M^{-1}\,d\kappa \le 0$. If η is the logarithm function, the corresponding quantity would be the relative entropy dissipation of f with respect to M. Entropy plays an important role in kinetic theory (see [13] for a review). Finally, the last quantity states that the kernel of D is one-dimensional and spanned by M.

Proposition 4.1 shows that the natural L^2 norm associated with this operator has a weight M^{-1} and that the natural H^1 semi-norm is given by the right-hand side of (4.17). This motivates the introduction of the following functional spaces, endowed with their naturally associated Hilbert structures and norms:

$$H = \{u : \Pi_\theta \times \mathbb{R}_\kappa \to \mathbb{R} \,/\, \int_{\theta,\kappa} |u(\theta,\kappa)|^2 \frac{d\theta d\kappa}{M} < +\infty\}, \tag{4.19}$$

$$V = \left\{u \in H \,/\, \int_{\Pi,\mathbb{R}} M \left|\partial_\kappa \left(\frac{u}{M}\right)\right|^2 d\kappa d\theta < +\infty\right\}, \tag{4.20}$$

$$L^2_M = L^2(\mathbb{R}^2_{\vec{x}}, H), \quad X = L^2([0,T] \times \mathbb{R}^2_{\vec{x}}, V). \tag{4.21}$$

Identifying H with its dual, with have a Hilbertian triple $V \subset H \subset V'$, where V' is the dual of V and all injections are continuous. They are not compact because V does not bring any regularity with respect to θ.

The existence proof follows closely the existence proof of [15] (see appendix A of this reference) and for this reason, is omitted (see also [20]). The proof relies on an existence theorem due to J. L. Lions [36].

Proposition 4.2 *Let $\varepsilon > 0$. We assume that f_0 belongs to L^2_M defined by (4.21). Then there exists a unique solution f^ε to (2.15) with initial datum f^0 in the class of functions Y defined by :*

$$Y = \left\{f \in X \,/\, \partial_t f + \varepsilon^{-1}\vec{\tau}\cdot\nabla_{\vec{x}} f + \varepsilon^{-2}\kappa\partial_\theta f \in X'\right\}.$$

Moreover, we have the inequality for any $T > 0$:

$$||f^\varepsilon(T)||^2_{L^2_M} + \frac{\alpha^2}{\varepsilon^2}\int_0^T \int_{\vec{x},\theta,\kappa} M \left|\partial_\kappa\left(\frac{f^\varepsilon}{M}\right)\right|^2 d\kappa\, d\theta\, d\vec{x}\, dt = ||f^\varepsilon(0)||^2_{L^2_M}. \tag{4.22}$$

Estimate (4.22) is obtained via a Green and a trace formula for functions belonging to Y which can be deduced from the one proved in [15].

4.3 Rigorous asymptotics

We first study operator A given by (4.2), i.e. $Af = \kappa\partial_\theta f - Df$ and state some properties which will be proved in appendix B. We view A as an unbounded operator on the Hilbert space H with domain $D(A)$ given by:

$$D(A) = \{u(\theta,\kappa) \in V \,/\, Au \in H\}.$$

Lemma 4.3 *Operator A is maximal monotone. Moreover its kernel (or Null-space) is given by:*

$$\mathrm{Ker}(A) = \{cM\,,\ c \in \mathbb{R}\}, \tag{4.23}$$

with M defined by (4.4).

Lemma 4.4 *The adjoint A^* of A in H is given by $A^*f = -\kappa\partial_\theta f - Df$. It is a Maximal monotone operator with domain $D(A^*) = D(A)$ and $Ker(A^*) = Ker(A)$.*

Proposition 4.5 *Let $g \in H$. Then, there exists $u \in D(A)$ such that*

$$Au = g, \tag{4.24}$$

if and only if g satisfies the following solvability condition:

$$\int_{\theta,\kappa} g(\theta,\kappa)\, d\theta d\kappa = 0. \tag{4.25}$$

Moreover, the solution u is unique up to a constant times M. A unique solution can be singled out by prescribing the condition

$$\int_{\theta,\kappa} u(\theta,\kappa)\, d\theta d\kappa = 0. \tag{4.26}$$

The same lemma applies to the equation $A^*u = g$.

As an application of this lemma, let $\vec{\chi}$ be the solution of :

$$A\vec{\chi} = \vec{\tau}(\theta)\,\frac{M}{2\pi}, \tag{4.27}$$

with $\vec{\tau}(\theta) = (\cos\theta\,, \sin\theta)$. Since τ has zero average over θ and κ, $\vec{\chi}$ is well-defined and unique thanks to Proposition 4.5. Then, we define the tensor D by:

$$D = \int_{\theta,\kappa} \vec{\tau}(\theta) \otimes \vec{\chi}\, d\theta d\kappa. \tag{4.28}$$

Note that, since $\int_{\theta,\kappa} \vec{\tau}(\theta) M(\kappa)\, d\theta d\kappa = 0$, it would not change the value of D to add any element of $\mathrm{Ker}(A)$ to $\vec{\chi}$.

Lemma 4.6 *Let R denote the reflection operator $u(\theta,\kappa) \to Ru(\theta,\kappa) = u(\theta,-\kappa)$. Then, $\vec{\chi}^* = R\vec{\chi}$ is the unique solution (satisfying (4.26)) of*

$$A^*\vec{\chi}^* = \vec{\tau}(\theta)\,\frac{M}{2\pi}, \tag{4.29}$$

and we have

$$D = \int_{\theta,\kappa} \vec{\tau}(\theta) \otimes \vec{\chi}^*\, d\theta d\kappa. \tag{4.30}$$

Proof: Obviously, D commutes with R: $DR = RD$ while $\kappa\partial_\theta$ anticommutes with R: $\kappa\partial_\theta(Ru) = -R(\kappa\partial_\theta u)$. Therefore, $RA = A^*R$. Since the right-hand side of (4.27) is invariant by R, applying R to both sides of (4.27) leads to (4.29). Then, the change of variables $\kappa' = -\kappa$ in the integral at the right-hand side of (4.30) shows that it is equal to D. ∎

To study the limit $\varepsilon \to 0$, we make the following hypothesis on the initial conditions.

Hypothesis 4.1 *We suppose that the initial condition f_0^ε is uniformly bounded in L^2_M and converges weakly in L^2_M to f_0^0 as $\varepsilon \to 0$.*

We can now prove theorem 2.3. The initial datum for the diffusion system (2.17, (2.18) will be shown to be:

$$n^0_{t=0} = n^0_0 = \int_{\theta,\kappa} f^0_0(\vec{x},\theta,\kappa)\, d\kappa d\theta. \tag{4.31}$$

Proof of theorem 2.3: By hypothesis 4.1 inequality (4.22) implies :

$$||f^\varepsilon(T)||^2_{L^2_M} + \frac{\alpha^2}{\varepsilon^2}\int_0^T \int_{\vec{x},\theta,\kappa} M \left|\partial_\kappa\left(\frac{f^\varepsilon}{M}\right)\right|^2 d\kappa\, d\theta\, d\vec{x}\, dt \le C\,, \tag{4.32}$$

with C independent of ε. So $(f^\varepsilon)_\varepsilon$ is a bounded sequence in $L^\infty(0,T,L^2_M)$ and satisfies

$$\int_0^T \int_{\vec{x},\theta,\kappa} M \left|\partial_\kappa\left(\frac{f^\varepsilon}{M}\right)\right|^2 d\kappa\, d\theta\, d\vec{x}\, dt \le C\varepsilon^2\,, \tag{4.33}$$

for any time interval T (by the diagonal process, we will eventually be able to take an increasing sequence of times T tending to infinity, so that the result will be valid on the whole interval $t \in (0,\infty)$). Therefore, there exists $f^0 \in L^\infty(0,T,L^2_M)$ and a subsequence, still denoted by f^ε, satisfying :

$$f^\varepsilon \overset{\varepsilon\to 0}{\rightharpoonup} f^0 \quad \text{ in } L^\infty(0,T,L^2_M) \text{ weak star }.$$

Furthermore, with (4.33), we deduce that $f^0 = C(\vec{x},\theta,t)M(\kappa)$. Then, letting $\varepsilon \to 0$ in (2.15), we get that $Af^0 = 0$ in the distributional sense. This implies that $C(\vec{x},\theta,t)$ is independent of θ and we can write

$$f^0(t,\vec{x},\theta,\kappa) = n^0(t,\vec{x})\frac{M(\kappa)}{2\pi}, \tag{4.34}$$

the quantity $n^0(t,\vec{x}) = \int f^0(t,\vec{x},\theta,\kappa)\, d\theta\, d\kappa$ being the density associated with f^0.

Our next task is to show that n^0 satisfies the diffusion model (2.17), (2.18) with initial condition (4.31). We first note that f^ε is a week solution of (2.15) with initial condition f_0^ε in the following sense: f^ε satisfies:

$$\int_0^T \int_{\vec{x},\theta,\kappa} f^\varepsilon\left(-\varepsilon\partial_t\varphi - \vec{\tau}\cdot\nabla_{\vec{x}}\varphi + \frac{1}{\varepsilon}A^*(\varphi)\right)\frac{d\kappa d\theta d\vec{x}}{M}dt = \varepsilon\int_{\vec{x},\theta,\kappa} f^\varepsilon_0\varphi_{t=0}\,\frac{d\kappa d\theta d\vec{x}}{M}, \tag{4.35}$$

for all test functions φ in the space $C^2_c([0,T)\times\mathbb{R}^2_{\vec{x}}\times\Pi_\theta\times\mathbb{R}_\kappa)$ of twice continuously differentiable functions with compact support in $[0,T)\times\mathbb{R}^2_{\vec{x}}\times\Pi_\theta\times\mathbb{R}_\kappa$. Again, the trace at $t=0$ has a meaning, thanks to a trace formula for functions in Y which is proven in [15].

We recall the definition of the flux (4.5). We prove that J^ε has a weak limit as $\varepsilon \to 0$. To this aim, in the weak formulation (4.35), we take as a test function $\varphi = \vec{\phi}(t,\vec{x})\cdot\vec{\chi}^*(\theta,\kappa)$ with $\vec{\chi}^*$ the auxiliary function defined as the solution to (4.29)

and $\vec{\phi}$ is a smooth compactly supported vector test function of $(\vec{x},t)$. Although φ does not have a compact support, a standard truncation argument (which is omitted here) can be used to bypass this restriction. This allows us to write:

$$\int_0^T \int_{\vec{x},\theta,\kappa} [f^\varepsilon(-\varepsilon\partial_t - (\vec{\tau}\cdot\nabla_{\vec{x}}))(\vec{\phi}\cdot\vec{\chi^*}) + \frac{1}{\varepsilon} f^\varepsilon \vec{\tau}\frac{M}{2\pi}\cdot\vec{\phi}]\,\frac{d\kappa d\theta d\vec{x}}{M} dt = \varepsilon \int_{\vec{x},\theta,\kappa} f_0^\varepsilon \vec{\phi}_{t=0}\cdot\vec{\chi}\,\frac{d\kappa d\theta d\vec{x}}{M}.$$

Taking the limit $\varepsilon \to 0$, we find :

$$\begin{aligned}\lim_{\varepsilon\to 0}\int_0^T \int_{\vec{x}} J^\varepsilon\cdot\vec{\phi}\,d\vec{x}dt &= 2\pi\int_0^T\int_{\vec{x},\theta,\kappa} f^0(\vec{\tau}\cdot\nabla_{\vec{x}})(\vec{\phi}\cdot\vec{\chi^*})\,\frac{d\kappa d\theta d\vec{x}}{M}dt \\ &= \int_0^T\int_{\vec{x}} n^0\,\nabla_{\vec{x}}\cdot\left(\left(\int_{\theta,\kappa}\vec{\chi^*}\otimes\vec{\tau}\,d\kappa d\theta\right)^T\vec{\phi}\right)\,d\vec{x}dt,\end{aligned}$$

where the exponent T denotes the transpose of a matrix. Using (4.30) and taking the limit $\varepsilon \to 0$ shows that J^ε converges weakly (in the distributional sense) towards J^0 satisfying

$$\int_0^T\int_{\vec{x}} J^0\cdot\vec{\phi}\,d\vec{x}dt = \int_0^T\int_{\vec{x}} n^0\,\nabla_{\vec{x}}\cdot\left((D)^T\vec{\phi}\right)\,d\vec{x}dt.$$

This last equation is the weak form of eq. (2.18).

Finally, to prove (2.17), we apply the weak formulation (4.35) to a test function of the form $\varphi = \phi(t,\vec{x})M(\kappa)$, where again, $\phi(x,t)$ is a scalar, smooth and compactly supported test function of $(\vec{x},t)$ in $\mathbb{R}^2\times[0,T)$. This gives :

$$-\int_0^T\int_{\vec{x},\theta,\kappa} f^\varepsilon\,((\varepsilon\partial_t + (\vec{\tau}\cdot\nabla_{\vec{x}}))\varphi)\,d\kappa d\theta d\vec{x}dt = \varepsilon\int_{\vec{x},\theta,\kappa} f_0^\varepsilon\phi_{t=0}\,d\kappa d\theta d\vec{x}.$$

Dividing by ε and taking the limit $\varepsilon\to 0$, we get :

$$-\int_0^T\int_{\vec{x}}(n^0\partial_t\varphi + J^0\cdot\nabla_{\vec{x}}\phi)\,d\vec{x}dt = \int_{\vec{x}} n_0^0\phi_{t=0}\,d\vec{x},$$

where n_0^0 is defined by (4.31). This last equation is exactly the weak formulation of equation (2.17), with initial datum n_0^0. This concludes the proof. ∎

5 Equivalence of the two methods

In this section, we show that both methods lead to the same value of the diffusion coefficient (theorem 2.4).

The first step is to show that we can approximate the solution of equation (4.24) by the solution of the associated evolution equation. More precisely, in appendix C, we prove the following lemma :

Lemma 5.1 *Let g in H satisfying (4.25) and u_∞ in $D(A)$ be the solution of (4.24) satisfying (4.26). Let $u_0\in D(A)$ satisfying (4.26). Then, the solution $u(t)$ of the evolution problem:*

$$\partial_t u = -Au + g\,,\quad u_{t=0} = u_0, \tag{5.1}$$

weakly converges to u_∞ in H as t tends to ∞.

With this lemma we can explicitly calculate the tensor D and prove the theorem 2.4 :

Proof of theorem 2.4: Let $\vec{\chi}(t)$ be the solution of

$$\partial_t \vec{\chi} = -A\vec{\chi} + \vec{\tau}(\theta)\frac{M(\kappa)}{2\pi}, \quad \vec{\chi}(t=0) = 0. \tag{5.2}$$

Thanks to Lemma 5.1, $\vec{\chi}(t)$ weakly converges to $\vec{\chi}$ in H when $t \to \infty$. It follows that :

$$\int_{\kappa,\theta} \vec{\chi}(t) \otimes \vec{\tau}\, d\kappa d\theta \overset{t\to+\infty}{\longrightarrow} \int_{\kappa,\theta} \vec{\chi} \otimes \vec{\tau}\, d\kappa d\theta. \tag{5.3}$$

Let us consider the first component of $\vec{\chi}(t)$, which we denote by $u(t)$ and the integrals
$\int_{\kappa,\theta} u(t)\cos\theta\, d\kappa d\theta$ and $\int_{\kappa,\theta} u(t)\sin\theta\, d\kappa d\theta$. Because u satisfies (5.2), it admits the following representation (see the proof of lemma 5.1):

$$u(t) = \int_0^t T_s\left(\cos\theta\frac{M(\kappa)}{2\pi}\right) ds,$$

where T_t is the semi-group generated by $-A$ (see [43]). With this expression, we evaluate the integral of $u(t)$ against $\cos\theta$:

$$\begin{aligned}\int_{\kappa,\theta} u(t)\cos\theta\, d\kappa d\theta &= \int_{\kappa,\theta}\int_0^t T_s\left(\cos\theta\frac{M(\kappa)}{2\pi}\right) ds\, \cos\theta\, d\kappa\, d\theta \\ &= \int_0^t \int_{\kappa,\theta} \cos\theta\frac{M(\kappa)}{2\pi} T_s^*(\cos\theta)\, d\kappa\, d\theta\, ds,\end{aligned}$$

where T^* is the adjoint operator of T in $L^2(\theta,\kappa)$ generated by $-\mathcal{A}^*$, where

$$\mathcal{A}^*(f) = -\kappa\partial_\theta f + \kappa\partial_\kappa f - \alpha^2\partial_{\kappa^2} f.$$

Note that we are referring here to the adjoint in the standard L^2 sense and not in the weighted space H. This is why $\mathcal{A}^*$ does not coincide with A^* defined in Lemma 4.4. The semi-group T_t^* admits a probabilistic representation: for all regular functions $f(\theta,\kappa)$

$$T_t^*(f)(\theta,\kappa) = \mathbb{E}\{f(\theta(t),\kappa(t))|\theta_0 = \theta, \kappa_0 = \kappa\},$$

where $(\kappa(t),\theta(t))$ is the solution of the stochastic differential equation (2.5), (2.6). Using this representation, we have :

$$\begin{aligned}\int_\kappa M(\kappa)\, T_s^*(\cos\theta)\, d\kappa &= \int_\kappa M(\kappa)\, \mathbb{E}\{\cos\theta_s|\theta_0 = \theta, \kappa_0 = \kappa\}\, d\kappa \\ &= \mathbb{E}\{\cos\theta_s|\theta_0 = \theta, \kappa_0 = Z\},\end{aligned}$$

where Z is a random variable independent of B_t with density M. Using lemma 3.2, we have :

$$\mathbb{E}\{\cos\theta_s|\theta_0 = \theta, \kappa_0 = Z\} = \mathbb{E}\{\cos(\theta + Y_s)\},$$

with Y_s a Gaussian random variable with zero mean and variance β_s^2 given by (3.10). Then:

$$\mathbb{E}\{\cos(\theta + Y_s)\} = \mathbb{E}\{\cos\theta\ \cos Y_s - \sin\theta\ \sin Y_s\} = \cos\theta\ \mathbb{E}\{\cos Y_s\},$$

because the density of Y_s is even and implies that $\mathbb{E}\{\sin Y_s\} = 0$. Finally using (3.12), we have:

$$\int_\kappa M(\kappa)\, T_s^*(\cos\theta)\, d\kappa = \cos\theta\ \mathrm{e}^{-\frac{\beta_s^2}{2}}.$$

Then, the first integral is given by:

$$\int_{\kappa,\theta} u(t)\cos\theta\, d\kappa\, d\theta = \int_0^t \int_\theta \frac{\cos\theta}{2\pi}\cos\theta\, \mathrm{e}^{-\frac{\beta_s^2}{2}}\, d\theta\, ds = \int_0^t \frac{1}{2}\,\mathrm{e}^{-\frac{\beta_s^2}{2}}\, ds.$$

We can proceed similarly to evaluate the integral of $u(t)$ against $\sin(t)$. This gives:

$$\int_{\kappa,\theta} u(t)\sin\theta\, d\kappa d\theta = \int_0^t \int_\theta \frac{\cos\theta\sin\theta}{2\pi}\mathbb{E}\{\cos Y_s\}\, d\theta ds = 0.$$

It remains to evaluate the integrals involving the second component of vector $\vec{\chi}(t)$ which we denote by $v(t)$. By the same method as for $u(t)$, we get :

$$\int_{\kappa,\theta} v(t)\cos\theta\, d\kappa\, d\theta = 0 \quad \text{and} \quad \int_{\kappa,\theta} v(t)\sin\theta\, d\kappa\, d\theta = \int_0^t \frac{1}{2}\,\mathrm{e}^{-\frac{\beta_s^2}{2}}\, dt.$$

Collecting these formulae, we can write:

$$\int_{\kappa,\theta} \vec{\chi}(t)\otimes\vec{\tau}\, d\kappa d\theta = \frac{\mathcal{D}(t)}{2}\, Id,$$

with $\mathcal{D}(t) = \int_0^t \mathrm{e}^{-\alpha^2(-1+u+\mathrm{e}^{-u})}\, du$. Taking the limit $t \to +\infty$ and using equation (5.3), shows that (2.19) holds true and completes the proof of the theorem. ∎

6 Numerical simulation

We simulate individual trajectories satisfying equation (2.4)-(2.6) with initial conditions given by (3.1)-(3.4). If we fix a time step Δt, using (3.7), (3.8), we have :

$$\begin{cases} \kappa_{(n+1)\Delta t} &= \gamma\kappa_{n\Delta t} + G_{(n+1)} \\ \theta_{(n+1)\Delta t} &= \theta_0 \ + \ \kappa_0 - \kappa_{(n+1)\Delta t} + \sqrt{2}\alpha B_{(n+1)\Delta t} \end{cases}$$

with $\gamma = \mathrm{e}^{-\Delta t}$ and $G_{(n+1)}$ a Gaussian random variable with zero mean and variance $2\alpha^2\left(1-\mathrm{e}^{-2\Delta t}\right)$ independent of $\kappa_{n\Delta t}$. With this formula, we can simulate recursively the process $(\kappa_{n\Delta t}, \theta_{n\Delta t})_n$ exactly (in the sense that it has the same law as the exact solution). To generate the Brownian motion, we just compute the increments $B_{(n+1)\Delta t} - B_{n\Delta t}$ since they are Gaussian and independent of $B_{n\Delta t}$. On the other hand, these

increments are not independent of $G_{(n+1)}$. Fortunately, we can compute the covariance matrix of the Gaussian vector $(G_{(n+1)}, B_{(n+1)\Delta t} - B_{n\Delta t})$:

$$\begin{pmatrix} G_{(n+1)} \\ B_{(n+1)\Delta t} - B_{n\Delta t} \end{pmatrix} \sim \mathcal{N}(0, C)$$

where $\mathcal{N}(0, C)$ is a two-dimensional Gaussian vector with zero mean and covariance matrix C given by:

$$C = \begin{bmatrix} 2\alpha^2 \left(1 - \mathrm{e}^{-2\Delta t}\right) & \sqrt{2}\alpha(1 - \mathrm{e}^{-\Delta t}) \\ \sqrt{2}\alpha(1 - \mathrm{e}^{-\Delta t}) & \Delta t \end{bmatrix}.$$

Knowing this covariance matrix, we can simulate the Gaussian vector $(G_{(n+1)}, B_{(n+1)\Delta t} - B_{n\Delta t})$ using the Cholesky method : we generate (X_1, X_2) a vector of two independent normal law, and take $\sqrt{C}(X_1, X_2)^T$ as realization of the Gaussian vector.

Now for the position $\vec{x}$, since we do not have any explicit expression, we use a discrete approximation scheme of order $O((\Delta t)^2)$. For example, the first component x_1 of $\vec{x}$ is approximated by:

$$\begin{aligned} x_1((n+1)\Delta t) &= x_1(n\Delta t) + \int_{n\Delta t}^{(n+1)\Delta t} \cos\theta(s)\, ds \\ &\approx x_1(n\Delta t) + \frac{\Delta t}{2}(\cos\theta(n\Delta t) + \cos\theta((n+1)\Delta t)). \end{aligned}$$

We present four trajectories obtained with different values of the parameter α in figure 2.3. As the parameter α increases, the excursions towards large positive or negative curvatures become larger. As a consequence, the spinning of the trajectory around itself increases and, from almost a straight line when $\alpha = 0.1$, the trajectory shrinks and looks closer and closer to a wool ball. In this way, we can visualize the decay of $\mathcal{D}$ with respect to α.

To illustrate theorem 2.1, we use a Monte-Carlo method to simulate the variance of the process $\vec{x}$. We simulate N independent trajectories and we compute the variance of the sample at each time step. In figure (2.4), we compare the result obtained with $N = 2000$ and the theoretical prediction given by the (3.6). The figure shows an excellent agreement between the computation and the theoretical prediction. Additionally, after an initial transient, the growth of the variance is linear, in accordance with the theoretical result (2.9).

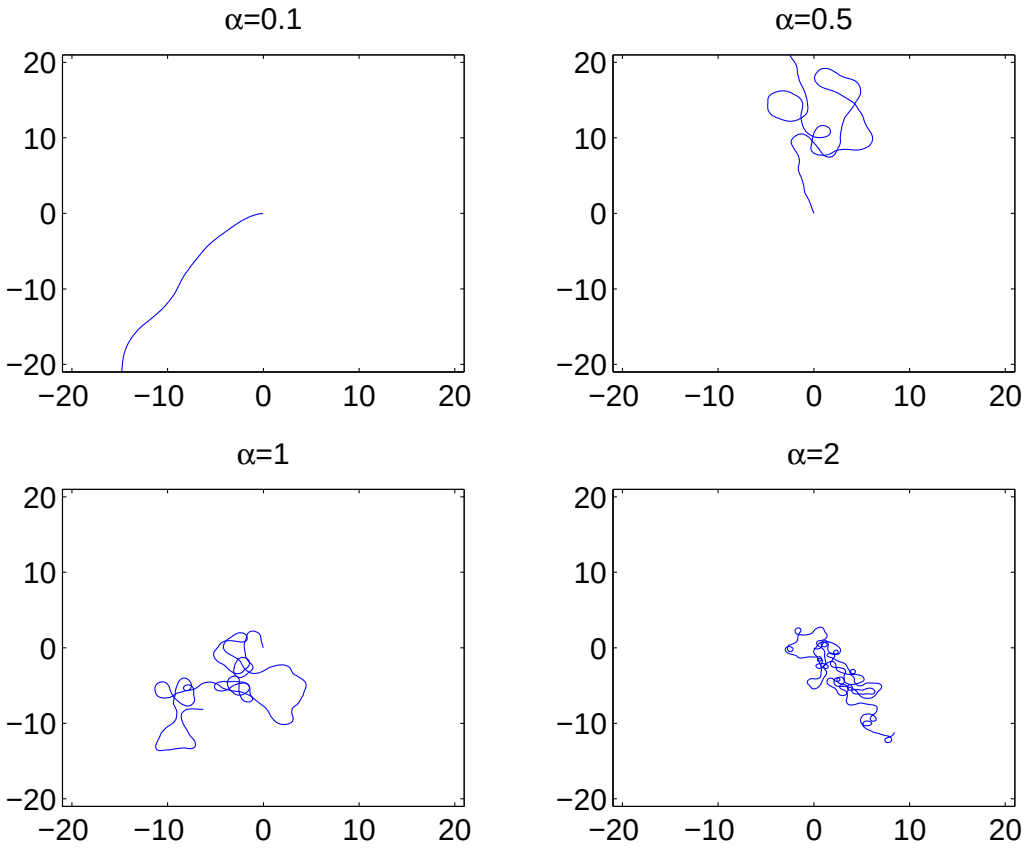

Figure 2.3: Four trajectories simulated with different value of α: $\alpha = 0.1$ (top left), $\alpha = 0.5$ (top right), $\alpha = 1.$ (bottom left) and $\alpha = 2.$ (bottom right). The simulation is run during 120 time units with a time step $dt = 0.05$ time unit

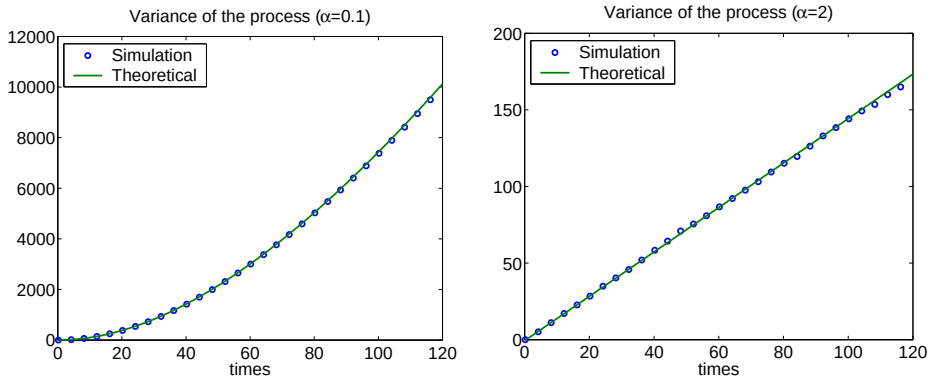

Figure 2.4: Variance of the process $\vec{x}(t)$: comparison between the numerical simulation (points) and the theoretical prediction (solid line) for two values of α : $\alpha = 0.1$ (left) and $\alpha = 2$ (right).

We can use the slope of the asymptotically linear part of the curve to give a numerical estimate of the diffusion coefficient $\mathcal{D}$. Fro this purpose, we fit a straight line (in the mean-square sense) between times $T/2$ and T. We remove the data between 0 and $T/2$ because the initial transient is not linear and including them would deteriorate the accuracy of the measurement. We compare the slope of the fitted line with the theoretical value (2.9). We report the result of this comparison for two values of α ($\alpha = 0.1$ and $\alpha = 2.$, with $T = 1200$ time units in Table 2.1). The approximation is quite good, with an error comprised between 2 and 3%, which can be attributed to numerical noise and to an unsufficient approximation of the asymptotic state.

	D simulation	D theoretical	relative error
$\alpha = 0.1$	98.5	101	2.5 %
$\alpha = 2$	0.708	0.725	2.4 %

Table 2.1: Diffusion coefficient: comparison of the numerical estimate obtained by fitting the numerical values with a straight line over the time interval $[T/2, T]$ with the theoretical prediction (2.9). $T = 1200$ units of time.

To illustrate the influence of the initial transient, we take $T = 120$ time units in the case $\alpha = 0.1$ and report the result in Table 2.2. There, the approximation is quite poor, because the asymptotic state has not yet been reached.

	D simulation	D theoretical	relative error
$\alpha = 0.1$	58.8	101	72 %

Table 2.2: Same as Table 2.1 but with $T = 120$ units of time. The agreement is poor because the asymptotic state is not reached.

In order to illustrate theorem 2.3, we plot the spatial density $n(t, \vec{x})$ of the distribution $f(t, \vec{x}, \theta, \kappa)$ using a Monte-Carlo algorithm for $\alpha = 2$ and $T = 30$ time units on figure 2.5. We see that the density has the Gaussian shape of the solution of a diffusion equation, in accordance with the prediction of the theorem.

To make a more quantitative comparison, we compare it with the asymptotic prediction, i.e. the solution of the diffusion equation (2.17), (2.18), by computing the difference in L^1 norm. The results are reported in figure 2.6. We plot the L^1 norm of the difference for $\alpha = 1.$ and for four values of the parameter ε : 1, $\frac{1}{2}$ $\frac{1}{5}$ and $\frac{1}{10}$. As expected, the agreement is better as ε is smaller. However, at large times, all solutions are eventually close to the solution of the diffusion equation. Roughly speaking, the time at which the solution of the diffusion equation starts to be a good approximation of the solution of the kinetic equation scales like ε. This means that, after an initial transient the duration of which may depend on ε, the solution is close to that of the diffusion equation, no matter the value of ε.

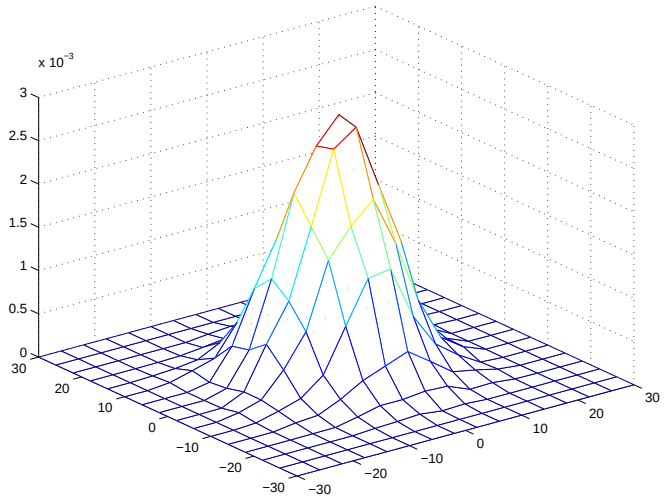

Figure 2.5: The spatial distribution n for $\alpha = 2$ at time $T = 30$ time units.

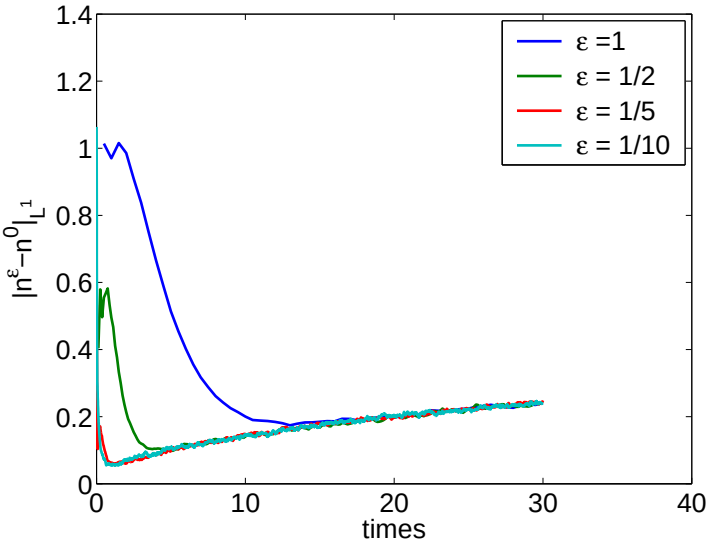

Figure 2.6: L^1 norm of the difference between $n^\varepsilon(t,) = \int f^\varepsilon(t,\cdot,\theta,\kappa)\,d\theta\,d\kappa$ and its asymptotic limit $n^0(t)$ as a function of time t, with $\alpha = 1$ and $N = 10^4$ simulation particles.

7 Conclusion

In this paper, the large-scale dynamics of the 'Persistent Turning Walker' (PTW) model of fish behavior has been analyzed. It has been shown, by two different methods, that the large scale limit of this model is of diffusion type, and an explicit formula for the diffusion coefficient has been provided. While the direct analysis of the stochastic trajectories provides a direct route to the value of the diffusion constant, the diffusion approximation of the associated forward Kolmogorov equation, which is of Fokker-Planck type, gives a more systematic way to extend the theory to more complex nonlinear cases. Such a nonlinear situation will be encountered when, in the near future, the nonlinear interactions between the individuals will be introduced within the PTW model. We expect that, in this context, the diffusion approximation methodology will have to be exploited thoroughly to allow access to the large scale behaviour of the system.

Appendix A : Proofs of section 3.

Proof of Lemma 3.2: Formula (3.8) is standard in the theory of Ornstein-Uhlenbeck processes [39]. To obtain (3.7), we integrate $\kappa(t)$ with respect to time:

$$\int_0^t \kappa(s)\,ds = (1-\mathrm{e}^{-t})\kappa_0 + \sqrt{2}\alpha \int_0^t \int_0^s \mathrm{e}^{-s}\mathrm{e}^{u}\,dB_u ds.$$

Interchanging the order of integrations and integrating with respect to s, we deduce:

$$\int_0^t \kappa(s)\,ds = (1-\mathrm{e}^{-t})\kappa_0 + \sqrt{2}\alpha \int_0^t (1-\mathrm{e}^{-(t-u)})\,dB_u.$$

Then we develop the integral :

$$\int_0^t \kappa(s)\,ds = (1-\mathrm{e}^{-t})\kappa_0 + \sqrt{2}\alpha B_t - (\kappa(t) - \mathrm{e}^{-t}\kappa_0).$$

This formula can be rewritten:

$$\int_0^t \kappa(s)\,ds = \kappa_0 - \kappa(t) + \sqrt{2}\alpha B_t,$$

which easily leads to (3.7).

We now calculate the mean and the variance of $K_0^t = \int_0^t \kappa(s)\,ds$. Since $\kappa(s)$ is of zero mean, its integral K_0^t is also of zero mean: $\mathbb{E}\{K_0^t\} = 0$. Now for the variance of K_0^t, we can write :

$$\mathrm{Var}\{K_0^t\} = \mathbb{E}\left\{\left((1-\mathrm{e}^{-t})\kappa_0 - \sqrt{2}\alpha\mathrm{e}^{-t}\int_0^t \mathrm{e}^{s}\,dB_s + \sqrt{2}\alpha B_t\right)^2\right\}.$$

Using that κ_0 and B_s are independent, we can develop the square and get:

$$\mathrm{Var}\{K_0^t\} = (1-\mathrm{e}^{-t})^2\mathbb{E}\{\kappa_0^2\} + 2\alpha^2\mathbb{E}\left\{\left(-\mathrm{e}^{-t}\int_0^t \mathrm{e}^{s}\,dB_s + B_t\right)^2\right\}.$$

Let us consider the second term. By Ito's formula, we have

$$\begin{aligned}\mathbb{E}\left\{\left(-\mathrm{e}^{-t}\int_0^t \mathrm{e}^{s}\,dB_s + B_t\right)^2\right\} &= \mathrm{e}^{-2t}\mathbb{E}\left\{\left(\int_0^t \mathrm{e}^{s}\,dB_s\right)^2\right\} - 2\mathrm{e}^{-t}\mathbb{E}\left\{B_t\int_0^t \mathrm{e}^{s}\,dB_s\right\} + \mathbb{E}\left\{B_t^2\right\} \\ &= \mathrm{e}^{-2t}\int_0^t \mathrm{e}^{2s}\,ds - 2\mathrm{e}^{-t}\mathbb{E}\left\{B_t(\mathrm{e}^{t}B_t - \int_0^t \mathrm{e}^{s}B_s\,ds)\right\} + t,\end{aligned}$$

where the Ito correction term is zero due to the fact that $\exp s$ is a deterministic process. We can simplify this expression again since $\mathbb{E}\{B_tB_s\} = \min(t,s)$ and get:

$$\begin{aligned}\mathbb{E}\left\{\left(-\mathrm{e}^{-t}\int_0^t \mathrm{e}^{s}\,dB_s + B_t\right)^2\right\} &= \frac{1-\mathrm{e}^{-2t}}{2} - 2\mathrm{e}^{-t}\left(\mathrm{e}^{t}t - \int_0^t \mathrm{e}^{s}s\,ds\right) + t \\ &= \frac{1-\mathrm{e}^{-2t}}{2} - 2\left(1-\mathrm{e}^{-t}\right) + t.\end{aligned}$$

Using also that $\mathbb{E}\{\kappa_0^2\} = \alpha^2$, the variance of K_0^t is written:

$$\mathrm{Var}\{K_0^t\} = (1-\mathrm{e}^{-t})^2\alpha^2 + 2\alpha^2\left(\frac{1-\mathrm{e}^{-2t}}{2} - 2\left(1-\mathrm{e}^{-t}\right) + t\right).$$

Developing and simplifying the expression, we find (3.10), which ends the proof. ∎

Appendix B : Proofs of section 4.

Proof of Lemma 4.3: Let $u \in D(A)$. Then, $\kappa\partial_\theta u \in V'$ and Lemma A1 of [15] shows that the Green formula for functions $u \in V$ such that $\kappa\partial_\theta u \in V'$ is legitimate. Therefore, taking the inner product of $A(u)$ against u, we find:

$$< A(u), u >_H = \int_{\theta,\kappa} \alpha^2 M \left|\partial_\kappa \left(\frac{u}{M}\right)\right|^2 d\theta d\kappa \geq 0. \tag{7.1}$$

So, A is a monotone operator in H. To show that A is maximal monotone, we prove that for any $g \in H$, there exists $u \in D(A)$ such that :

$$u + Au = g. \tag{7.2}$$

Taking the inner product of (7.2) against a test function φ in the space $\mathcal{D}(\Pi_\theta \times \mathbb{R}_\kappa)$ of infinitely differentiable and compactly supported functions on $\Pi_\theta \times \mathbb{R}_\kappa$ leads to the variational problem :

$$\int_{\kappa,\theta} [u\,(\varphi - \kappa\partial_\theta\varphi)\,\frac{1}{M} \,+\, M\partial_k \left(\frac{u}{M}\right) \partial_k \left(\frac{\varphi}{M}\right)]\, d\theta d\kappa = \int_{\theta,\kappa} g\varphi\, \frac{d\kappa d\theta}{M}. \tag{7.3}$$

Again, the same theory as in the appendix A of [15] (based the result by J. L. Lions in [36]) applies to prove the existence of a solution to (7.3) with u in V such that $\kappa\partial_\theta u \in V'$. From there, it immediately follows that $u \in D(A)$.

It is immediate to see that any function of the form $u(\theta,\kappa) = CM(\kappa)$ for any constant C belongs to the kernel of A. Conversely, suppose that $u \in \operatorname{Ker} A$. Then, by (7.1), there exists a function $C(\theta) \in L^2(\Pi)$ such that $u(\theta,\kappa) = C(\theta)M(\kappa)$. But again, $A(u) = 0$ implies that $\kappa\,\partial_\theta C(\theta)\,M = 0$. So $C(\theta)$ is a constant, which proves (4.23). ∎

Proof of Proposition 4.5: The 'only if' part of the theorem is obvious since, using Green's formula (again, obtained by adapting that of appendix B of [15], we have $\int Au\, d\theta\, d\kappa = 0$).

To prove the 'if' part, we borrow a method from (for instance) [12]. To find a solution to (4.24), we look at a perturbed equation :

$$\lambda u + Au = g, \tag{7.4}$$

with $\lambda > 0$. Since A is maximal monotone in H (Lemma 4.3), eq. (7.4) admits a solution u_λ for all positive λ ([9]). To prove the existence of a solution to (4.24), we want to extract a subsequence, still denoted by (u_λ) which converges weakly in H. For this purpose, it is enough to show that there exists a bounded subsequence.

We proceed by contradiction, supposing that the (full) sequence $N_\lambda = \|u_\lambda\|_H \overset{\lambda\to 0}{\to} +\infty$. We define $U_\lambda = \frac{u_\lambda}{N_\lambda}$. U_λ satisfies $\|U_\lambda\|_H = 1$ for all λ and

$$\lambda U_\lambda + AU_\lambda = \frac{g}{N_\lambda}. \tag{7.5}$$

Since $(U_\lambda)_\lambda$ is a bounded sequence in H, we can extract a subsequence (still denoted by U_λ) such that $U_\lambda \rightharpoonup U$ in H weak as $\lambda \to 0$. Taking the limit $\lambda \to 0$ in (7.5), gives $A(U) = 0$. If we take the inner product of (7.5) with U_λ and then pass to the limit $\lambda \to 0$, we also find that U belongs to V. So Lemma 4.3 applies and gives $U = cM$ with a constant $c \in \mathbb{R}$. Using (4.25), we also have :

$$< \lambda U_\lambda + AU_\lambda, M >_H = < \frac{g}{N_\lambda}, M >_H = 0.$$

So $\int_{\kappa,\theta} U_\lambda \, d\theta d\kappa = 0$ for all λ. Taking the limit $\lambda \to 0$ leads to $\int_{\kappa,\theta} U \, d\theta d\kappa = \int_{\kappa,\theta} CM(\kappa) \, d\theta d\kappa = 2\pi C = 0$, which implies $U = 0$. This proves:

$$U_\lambda \rightharpoonup 0 \qquad \text{in } H \text{ weak} . \tag{7.6}$$

To get a contradiction, we now prove that the convergence is strong.

To this aim, we introduce a decomposition of the space H into two orthogonal subspaces. Let L be the closed subspace of H defined by :

$$L = \{c(\theta)M \,/\, c(\theta) \in L^2(\Pi_\theta)\},$$

with M defined by (4.4). So $H = L \overset{\perp}{\oplus} L^\perp$. We also define the orthogonal projector P of H onto L such that $Pf = (\int_\kappa f(\kappa,\theta) \, d\kappa) \, M$. Using this projection, we decompose the sequence $(U_\lambda)_\lambda$ as follows:

$$U_\lambda = c_\lambda(\theta)M + v_\lambda, \tag{7.7}$$

with $v_\lambda \in L^\perp$, i.e. $\int_\kappa v_\lambda \, d\kappa = 0$. To demonstrate that $U_\lambda \overset{\lambda\to 0}{\longrightarrow} 0$ in H strongly, we first demonstrate that $v_\lambda \overset{\lambda\to 0}{\longrightarrow} 0$ in H strongly.

Taking the inner product of the equation satisfied by U_λ (7.5) with U_λ gives :

$$\lambda \|U_\lambda\|_H^2 + \int_{\theta,\kappa} M \left|\partial_\kappa \frac{U_\lambda}{M}\right|^2 d\theta d\kappa = \frac{1}{N_\lambda} \, < g, U_\lambda >_H .$$

Since $\partial_\kappa \frac{U_\lambda}{M} = \partial_\kappa \frac{v_\lambda}{M}$ and $\|U_\lambda\|_H = 1$, we get by taking the limit $\lambda \to 0$:

$$\int_{\theta,\kappa} M \left|\partial_\kappa \frac{v_\lambda}{M}\right|^2 d\theta d\kappa \overset{\lambda\to 0}{\longrightarrow} 0. \tag{7.8}$$

Now Gross inequality [31] gives, for any $v \in V$:

$$\alpha^2 \int_{\mathbb{R}} \left|\partial_\kappa \left(\frac{f}{M}\right)\right|^2 M \, d\kappa \geq \int_{\mathbb{R}} |f|^2 \frac{d\kappa}{M} - \left(\int_{\mathbb{R}} f \, d\kappa\right)^2 . \tag{7.9}$$

Then, since $\int_\kappa v_\lambda \, d\kappa = 0$, we deduce:

$$\alpha^2 \int_{\mathbb{R}} \left|\partial_\kappa \frac{v_\lambda}{M}\right|^2 M \, d\kappa \geq \int_{\mathbb{R}} \frac{|v_\lambda|^2}{M} \, d\kappa.$$

Integrating this inequality with respect to θ and using (7.8), we find:

$$\|v_\lambda\|_H \xrightarrow{\lambda\to 0} 0, \quad \text{in } H \text{ strong.} \tag{7.10}$$

To prove the convergence of c_λ, we define the bounded operator T: $H \to L^2(\Pi_\theta)$ such that $Tf = \int_\kappa \kappa f \, d\kappa$. Having T acting on (7.5) and taking the limit $\lambda \to 0$, leads to:

$$T\,A\,U_\lambda \xrightarrow{\lambda\to 0} 0 \quad \text{in } L^2(\Pi_\theta) \text{ strong.} \tag{7.11}$$

If we develop the left-hand side, we find:

$$\begin{aligned} T\,A\,U_\lambda &= \int_\kappa \kappa^2 \partial_\theta U_\lambda \, d\kappa - \int_\kappa \left[\kappa \partial_\kappa(\kappa U_\lambda) - \alpha^2 \kappa \partial_{\kappa^2} U_\lambda\right] d\kappa \\ &= \int_\kappa \kappa^2 \partial_\theta U_\lambda \, d\kappa + \int_\kappa \kappa U_\lambda \, d\kappa. \end{aligned}$$

But using the decomposition $U_\lambda = c_\lambda M + v_\lambda$ (7.7), we have:

$$\left\| \int_\kappa \kappa U_\lambda \, d\kappa \right\|_{L^2(\theta)} = \left\| \int_\kappa \kappa v_\lambda \, d\kappa \right\|_{L^2(\theta)} \xrightarrow{\lambda\to 0} 0.$$

So, (7.11) leads to :

$$\int_\kappa \kappa^2 \partial_\theta U_\lambda \, d\kappa \xrightarrow{\lambda\to 0} 0 \quad \text{in } L^2(\Pi_\theta) \text{ strong.} \tag{7.12}$$

If we define $h_\lambda(\theta) = \int_\kappa \kappa^2 U_\lambda \, d\kappa$, (7.12) is equivalent to saying that $\|\partial_\theta h_\lambda\|_{L^2(\theta)} \xrightarrow{\lambda\to 0} 0$. Using the Poincare-Wirtinger inequality [9], there exists a constant C_0 such that:

$$\|h_\lambda - \bar{h}_\lambda\|_{L^2(\theta)} \leq C_0 \|\partial_\theta h_\lambda\|_{L^2(\theta)}, \tag{7.13}$$

with $\bar{h}_\lambda = \frac{1}{2\pi} \int_0^{2\pi} h_\lambda(\theta) \, d\theta$. Then, we develop $\bar{h}_\lambda$. We get:

$$\bar{h}_\lambda = \frac{1}{2\pi} \int_0^{2\pi} \int_\kappa \kappa^2 U_\lambda \, d\kappa d\theta = < U_\lambda, M\kappa^2 >_H \xrightarrow{\lambda\to 0} 0 \quad \text{in } \mathbb{R},$$

since U_λ converges weakly to zero (see (7.6)). So, (7.13) leads to $h_\lambda \xrightarrow{\lambda\to 0} 0$ in $L^2(\Pi_\theta)$ strong. If we develop h_λ we find:

$$h_\lambda(\theta) = \int_\kappa \kappa^2 (c_\lambda(\theta) M + v_\lambda) \, d\kappa = \alpha^2 c_\lambda(\theta) + \int_\kappa \kappa^2 v_\lambda \, d\kappa.$$

Now, $\int_\kappa \kappa^2 v_\lambda \, d\kappa$ converges to zero in $L^2(\theta)$ strong because of (7.10) and we finally have :

$$c_\lambda(\theta) \xrightarrow{\lambda\to 0} 0 \ \text{ in } L^2(\theta) \text{ strong.}$$

Using the convergence of c_λ and v_λ, we can now prove the strong convergence of U_λ to 0 in H:

$$\|U_\lambda\|_H^2 = \|c_\lambda M\|_H^2 + \|v_\lambda\|_H^2 = \|c_\lambda\|_{L^2(\theta)}^2 + \|v_\lambda\|_H^2 \xrightarrow{\lambda\to 0} 0,$$

which contradicts the fact that U_λ has unit norm in H. This shows that there exists a bounded subsequence in the sequence u_λ. In fact, since the same proof can be applied to any subsequence, this shows that the whole sequence u_λ is bounded, but this is useless for our purpose.

We conclude the proof of Proposition 4.5 as follows: there exists a subsequence u_λ and a function u in H such that $u_\lambda \rightharpoonup u$ in H weak. Taking the limit of (7.4) as $\lambda \to 0$, we deduce that $Au = g$ in the sense of distributions. However, since $g \in H$, eq. $Au = g$ also holds in H. Moreover if we take the inner product of (7.4) with u_λ and pass to the limit $\lambda \to 0$, we find that u belongs to V. So u belongs to $D(A)$, which ends the proof of the 'if' part of the statement.

Finally, to prove uniqueness, we just remark that, two solutions of (4.24) differ from an element of the kernel of A and we apply (4.23). This ends the proof. ∎

Appendix C : Proofs of section 5.

Proof of Lemma 5.1: The proof borrows some ideas from [24], but is simpler, due to the linear character of the problem. The difficulty is getting some compactness in time. Here, instead of considering time translates of the solution as in [24], we will consider time integrals over a fixed interval length Δt.

Since operator A is maximal monotone on H (see Lemma 4.3), operator $-A$ generates a semi-group of contractions T_t on H. Moreover the solution of (5.1) is given by:

$$u(t) = T_t(u_0) + \int_0^t T_s(g)\, ds.$$

We define $f(t) = u(t) - u_\infty$ which satisfies :

$$\partial_t f = -Af, \quad f_{t=0} = f_0, \tag{7.14}$$

with $f_0 = u_0 - u_\infty$ and $\int_\kappa f_0(\kappa)\, d\kappa = 0$. To prove the weak convergence of $u(t)$ to u_∞, we have to prove that $f(t)$ converges to zero weakly in H.

To this aim, we make an orthogonal decomposition of $f(t)$ as in the proof of Proposition 4.5: $f(t) = c(t)M + v(t)$, with $c(t) \in L^2(\Pi_\theta)$, $v(t) \in H$ and $\int_\kappa v(t)\, d\kappa = 0$. Taking the inner product of (7.14) with f, we get :

$$\frac{1}{2}\,\partial_t \|f\|_H^2 = -\int_{\kappa,\theta} \alpha^2 M \left[\partial_\kappa\left(\frac{f}{M}\right)\right]^2 d\kappa d\theta.$$

Using the decomposition of $f(t)$ and noticing that $\partial_\kappa\left(\frac{f}{M}\right) = \partial_\kappa\left(\frac{v}{M}\right)$, this equality becomes:

$$\frac{1}{2}\,\partial_t \left(\|c(t)\|_{L^2}^2 + \|v(t)\|_H^2\right) = -\int_{\kappa,\theta} \alpha^2 M \left[\partial_\kappa\left(\frac{v(t)}{M}\right)\right]^2 d\kappa d\theta. \tag{7.15}$$

If we apply the Gross inequality (7.9), we get:

$$\frac{1}{2}\,\partial_t \left(\|c(t)\|_{L^2}^2 + \|v(t)\|_H^2\right) \leq -\|v(t)\|_H^2.$$

Since $c(t)$ is bounded by $\|f_0\|_H^2$, by integrating with respect to time, we have :

$$\frac{1}{2}\|v(t)\|_H^2 \leq -\int_0^t \|v(s)\|_H^2\, ds + C.$$

Using the Gronwall lemma, we deduce that $v(t)$ decays exponentially fast to zero strongly in H:

$$v(t) \overset{t\to+\infty}{\longrightarrow} 0 \text{ in } H \text{ strong.}$$

It remains to prove the convergence of $c(t)$ to zero. We integrate (7.14) with respect to κ. This gives, using that $\int_\kappa M(\kappa)\, d\kappa = 1$ and $\int_\kappa v(t)\, d\kappa = 0$:

$$\partial_t c(t) = \partial_\theta \int_\kappa \kappa v(t)\, d\kappa. \tag{7.16}$$

Now if we pre-multiply by κ before integrating with respect to κ, we obtain :

$$\partial_t \int_\kappa \kappa v(t)\, d\kappa = \alpha^2 \partial_\theta c(t) + \partial_\theta \int_\kappa \kappa^2 v(t)\, d\kappa - \int_\kappa \kappa v(t)\, d\kappa. \tag{7.17}$$

We fix a time interval Δt and integrate (7.17) over this time interval. This leads to:

$$\begin{aligned}\int_\kappa \kappa(v(t+\Delta t) - v(t))\, d\kappa &= \alpha^2 \partial_\theta \int_t^{t+\Delta t} c(s)\, ds + \partial_\theta \int_\kappa \kappa^2 \int_t^{t+\Delta t} v(s)\, ds\, d\kappa \\ &\quad - \int_\kappa \kappa \int_t^{t+\Delta t} v(s)\, ds\, d\kappa.\end{aligned}$$

Since $v(t)$ converges to zero in H, we have, in the sense of distributions:

$$\alpha^2 \partial_\theta \int_t^{t+\Delta t} c(s)\, ds \overset{t\to+\infty}{\rightharpoonup} 0. \tag{7.18}$$

Since c belongs to $L^\infty((0,\infty)_t, L^2(\Pi_\theta))$ (see (7.15)), we have $\int_t^{t+\Delta t} c(s)\, ds$ which belongs to
$L^\infty((0,\infty)_t, L^2(\Pi_\theta))$. So there exists a subsequence such that $\int_t^{t+\Delta t} c(s)\, ds$ is weakly convergent in $L^2(\Pi_\theta)$. Actually, (7.18) implies that there exists a constant function with respect to θ, depending on Δt and denoted by $L(\Delta t)$ such that

$$\int_t^{t+\Delta t} c(s)\, ds \overset{t\to+\infty}{\rightharpoonup} L(\Delta t).$$

To deduce the convergence of $c(t)$, we have to control the derivative of $c(t)$ in time. For this purpose, we rewrite :

$$\begin{aligned}\int_t^{t+\Delta t} c(s)\, ds &= \int_0^{\Delta t} \left(c(t) + \int_0^s \partial_t c(t+z)\, dz \right) ds \\ &= \Delta t\, c(t) + \int_0^{\Delta t} \int_0^s \partial_\theta \int_\kappa \kappa v(t+z)\, d\kappa\, dz ds.\end{aligned}$$

Using again the convergence of $v(t)$ to zero, we find :

$$\Delta t\, c(t) \overset{t\to+\infty}{\rightharpoonup} L(\Delta t),$$

or defining the constant $C = \frac{L(\Delta t)}{\Delta t}$, we have $c(t) \overset{t\to+\infty}{\rightharpoonup} C$ in $L^2(\Pi_\theta)$ weak.

To complete the proof, it remains to prove that C is equal to zero. Now, since eq. (7.14) is mass preserving i.e.:

$$\partial_t \int_{\kappa,\theta} f(t)\, d\kappa d\theta = -\int_{\kappa,\theta} Af(t)\, d\kappa d\theta = 0,$$

we have $\int_{\kappa,\theta} f(t)\, d\kappa d\theta = \int_{\kappa,\theta} f(0)\, d\kappa d\theta = 0$. Also :

$$\int_{\kappa,\theta} f(t)\, d\kappa d\theta = \int_{\kappa,\theta} (c(t)M + v(t))\, d\kappa d\theta \overset{t\to+\infty}{\rightharpoonup} \int_\theta C\, d\theta = 2\pi C.$$

So $C = 0$. This proves $f(t) \overset{t\to+\infty}{\rightharpoonup} 0$ in H weak and completes the proof. ∎

Bibliography

[1] M. Aldana and C. Huepe, Phase transitions in self-driven many-particle systems and related non-equilibrium models: a network approach, J. Stat. Phys., 112, no 1/2 (2003), pp. 135–153.

[2] I. Aoki, A simulation study on the schooling mechanism in fish, Bulletin of the Japan Society of Scientific Fisheries, 48 (1982), pp. 1081–1088.

[3] D. Armbruster, P. Degond and C. Ringhofer, A model for the dynamics of large queuing networks and supply chains, SIAM J. Appl. Math., 66 (2006), pp. 896–920.

[4] A. Aw, A. Klar, M. Rascle and T. Materne, Derivation of continuum traffic flow models from microscopic follow-the-leader models, SIAM J. Appl. Math., 63 (2002), pp. 259–278.

[5] R. Bass, Diffusions and elliptic operators, Springer-Verlag, 1997.

[6] C. Bardos, R. Santos and R. Sentis, Diffusion approximation and computation of the critical size, Trans. A. M. S., **284** (1984), pp. 617–649.

[7] N. Ben Abdallah, P. Degond, A. Mellet and F. Poupaud, Electron transport in semiconductor superlattices, Quarterly Appl. Math. **61** (2003), pp. 161–192.

[8] A. Bensoussan, J. L. Lions and G. C. Papanicolaou, Boundary layers and homogenization of transport processes, J. Publ. RIMS Kyoto Univ. **15** (1979), pp. 53–157.

[9] H. Brézis, Analyse fonctionnelle, Dunod, 1983.

[10] D. R. Brillinger, H. K. Preisler, A. A. Ager, J. G. Kie and B. S. Stewart, Employing stochastic differential equations to model wildlife motion, Bull Braz Math Soc, 33 (2002), pp. 385–408.

[11] S. Camazine, J-L. Deneubourg, N. R. Franks, J. Sneyd, G. Theraulaz and E. Bonabeau, Self-Organization in Biological Systems, Princeton University Press, 2002.

[12] F. Castella, P. Degond and T. Goudon, Diffusion dynamics of classical systems driven by an oscillatory force, J. Stat. Phys., 124 (2006), pp. 913–950.

[13] C. Cercignani, R. Illner, M. Pulvirenti, The mathematical theory of dilute gases, Springer-Verlag, New-York, 1991.

[14] I. D. Couzin, J. Krause, R. James, G. D. Ruxton and N. R. Franks, Collective Memory and Spatial Sorting in Animal Groups, J. theor. Biol., 218 (2002), pp. 1–11.

[15] P. Degond, Global Existence of Solutions for the Vlasov-Fokker-Planck Equation in 1 and 2 Space Dimensions, An. Scient. Ec. Norm. Sup., 19 (1986) pp. 519-542.

[16] P. Degond, Macroscopic limits of the Boltzmann equation: a review, in Modeling and computational methods for kinetic equations, P. Degond, L. Pareschi, G. Russo (eds), Modeling and Simulation in Science, Engineering and Technology Series, Birkhauser, 2003, pp. 3–57.

[17] P. Degond, V. Latocha, S. Mancini, A. Mellet, Diffusion dynamics of an electron gas confined between two plates, Methods and Applications of Analysis. **9** (2002), pp. 127–150.

[18] P. Degond, M. Lemou, M. Picasso, Viscoelastic fluid models derived from kinetic equations for polymers, SIAM J. Appl. Math. **62** (2002), pp. 1501–1519.

[19] P. Degond et S. Mancini, Diffusion driven by collisions with the boundary, Asymptotic Analysis **27** (2001), pp. 47–73.

[20] P. Degond, S. Mas-Gallic,m Existence of Solutions and Diffusion Approximation for a Model Fokker-Planck Equation, Transp. Theory Stat. Phys., 16 (1987) pp. 589-636.

[21] P. Degond and S. Motsch, Continuum limit of self-driven particles with orientation interaction, preprint

[22] P. Degond and S. Motsch, Macroscopic limit of self-driven particles with orientation interaction, note, to be published.

[23] P. Degond et K. Zhang, Diffusion approximation of a scattering matrix model of a semiconductor superlattice, SIAM J. Appl. Math. **63** (2002), pp. 279–298.

[24] L. Desvillettes and J. Dolbeault,m On Long Time Asymptotics of the Vlasov-Poisson-Boltzmann Equation, Comm. PDE, 16 (1991), pp. 451–489.

[25] M. R. D'Orsogna, Y. L. Chuang, A. L. Bertozzi and L. Chayes, Self-propelled particles with soft-core interactions: patterns, stability and collapse, Phys. Rev. Lett., 2006.

[26] L. Edelstein-Keshet, Mathematical models of swarming and social aggregation, invited lecture, The 2001 International Symposium on Nonlinear Theory and its Applications, (NOLTA 2001) Miyagi, Japan (Oct 28-Nov 1, 2001).

[27] J. Gautrais, C. Jost, M. Soria, A. Campo, S. Motsch, R. Fournier, S. Blanco and G. Theraulaz, Analyzing Fish Movement as a Persistent Turning Walker, J Math Biol, 2008.

[28] F. Golse and F. Poupaud, Limite fluide des équations de Boltzmann des semiconducteurs pour une statistique de Fermi-Dirac, Asymptotic Analysis **6** (1992), pp. 135–160.

[29] I. S. Gradshteyn, I. M. Ryzhik, Tables of integrals, series and products, 6th edition, Academic Press, New-York, 2000

[30] G. Grégoire, and H. Chaté, Onset of collective and cohesive motion, Phys. Rev. Lett., 92 (2004) 025702.

[31] L. Gross, Logarithmic Sobolev inequalities and contractivity properties of semigroups, Lectures Notes in Mathematics, Vol. 1563, pp. 54–88, Springer, Berlin, 1992.

[32] D. Helbing, Traffic and related self-driven many-particle systems, Reviews of modern physics, 73 (2001), pp. 1067–1141.

[33] R. Jeanson, S. Blanco, R., Fournier, J. L. Deneubourg, V. Fourcassié & G. Theraulaz, A model of animal movements in a bounded space, Journal of Theoretical Biology, 225 (2003), pp. 443-451

[34] C. Jost et al., From individual to collective ant displacements in heterogenous environments, preprint, 2007.

[35] V. L. Kulinskii, V. I. Ratushnaya, A. V. Zvelindovsky, D. Bedeaux, Hydrodynamic model for a system of self-propelling particles with conservative kinematic constraints, Europhys. Lett., 71 (2005), pp. 207–213.

[36] J.L. Lions, Equations diffé, Springer-Verlag, 1961.

[37] A. Mogilner and L. Edelstein-Keshet, A non-local model for a swarm, J. Math. Biol., 38 (1999), pp. 534–570.

[38] A. Mogilner, L. Edelstein-Keshet, L. Bent and A. Spiros, Mutual interactions, potentials, and individual distance in a social aggregation, J. Math. Biol., 47 (2003), pp. 353–389.

[39] B. Oksendal, Stochastic differential equations, Springer-Verlag, 1992.

[40] H. G. Othmer and Thomas Hillen, The Diffusion Limit of Transport Equations II: Chemotaxis Equations, SIAM J. Appl. Math., 62 (2002), pp. 1222-1250.

[41] J. K. Parrish and S. V. Viscido, Traffic rules of fish schools: a review of agent-based approaches, in 'Self-Organization and Complexity', CK Hemelrijk (ed.), Cambridge University Press, 2003.

[42] J. K. Parrish, S. V. Viscido and D. Grünbaum, Self-organized fish schools: an examination of emergent properties, The biological bulletin, 202 (2002), pp. 296–305.

[43] A. Pazy, Semigroups of linear operators and applications to partial differential equations, Springer-Verlag, 1983.

[44] F. Poupaud, Diffusion approximation of the linear semiconductor equation: analysis of boundary layers, Asymptotic Analysis **4** (1991), pp. 293–317.

[45] V. I. Ratushnaya, D. Bedeaux, V. L. Kulinskii and A. V. Zvelindovsky, Collective behaviour of self propelling particles with kinematic constraints ; the relations between the discrete and the continuous description, Physica A, to appear.

[46] V. I. Ratushnaya, V. L. Kulinskii, A. V. Zvelindovsky, D. Bedeaux, Hydrodynamic model for the system of self propelling particles with conservative kinematic constraints; two dimensional stationary solutions Physica A, 366, (2006), pp. 107–114.

[47] Theraulaz et al., Spatial patterns in ant colonies, Proceedings of the National Academy of Sciences, 99 (2002), pp. 9645–9649.

[48] C. M. Topaz and A. L. Bertozzi, Swarming patterns in a two-dimensional kinematic model for biological groups, SIAM J. Appl. Math, 65 (2004), pp. 152–174.

[49] C. M. Topaz, A. L. Bertozzi, M. A. Lewis, A nonlocal continuum model for biological aggregation, Bull. Math. Biol., 68 (2006), pp. 1601–1623.

[50] T. Vicsek, A. Czirók, E. Ben-Jacob, I. Cohen and O. Shochet, Novel type of phase transition in a system of self-driven particles, Phys. Rev. Lett., 75 (1995), pp. 1226–1229.

Chapter 3

Long time fluctuation and diffusion limit for the Persistent Turning Walker Model

This chapter has been written in collaboration with P. Cattiaux and D. Chafaï, it has been submitted to the journal Asymptotic Analysis.

Abstract. The Persistent Turning Walker Model (PTWM) was introduced by Gautrais et al in Mathematical Biology for the modelling of fish motion. It involves a nonlinear pathwise functional of a non-elliptic hypo-elliptic diffusion. This diffusion solves a kinetic Fokker-Planck equation based on an Ornstein-Uhlenbeck Gaussian process. The long time "diffusive" behavior of this model was recently studied by Degond & Motsch using partial differential equations techniques. This model is however intrinsically probabilistic. In the present paper, we show how the long time diffusive behavior of this model can be essentially recovered and extended by using appropriate tools from stochastic analysis. The approach can be adapted to many other kinetic "probabilistic" models. Beyond the mathematical results, the aim of this short paper is also to contribute to the diffusion of stochastic techniques in the domain of partial differential equations.

Key words: Mathematical biology, animal behavior, hypo-elliptic diffusions, kinetic Fokker-Planck equations, Poisson equation, invariance principles, central limit theorems, Gaussian and Markov processes.

1 Introduction

Different types of models are used in Biology to describe individual displacement. For instance, correlated/reinforced random walks are used for the modelling of ant, see e.g. [2, 23], and cockroaches, see e.g. [13] and [4] for a review. On the other hand, a lot of natural phenomena can be described by kinetic equations and their stochastic counterpart, stochastic differential equations. The long time behavior of such models is particularly relevant since it captures some "stationary" evolution. Recently, a new model, called the Persistent Turning Walker model (PTWM for short), involving a kinetic equation, has been introduced to describe the motion of fish [9, 5]. The natural long time behavior of this model is "diffusive" and leads asymptotically to a Brownian Motion.

The diffusive behavior of the PTWM has been obtained in [5] using partial differential equations techniques. In the present work, we show how to recover this result by using appropriate tools from stochastic processes theory. First, we indicate how the diffusive behavior arises naturally as a consequence of the Central Limit Theorem (in fact an Invariance Principle). As expected, the asymptotic process is a Brownian Motion in space. As a corollary, we recover the result of [5] which appears as a special case where the variance of the Brownian Motion can be explicitly computed. We finally extend our main result to more general initial conditions. We emphasize that the method used in the present paper is not restricted to the original PTWM. In particular, the hypotheses for the convergence enables to use more general kinetic models than the original PTWM.

The present paper is organized as follows: in Section 2, we recall the PTWM and its main properties, and we give the main results. Section 3 is dedicated to the proofs.

2 Main results

In the PTWM, the motion is described using three variables: *position* $x \in \mathbb{R}^2$, *velocity angle* $\theta \in \mathbb{R}$, and *curvature* $\kappa \in \mathbb{R}$. For some fixed real constant α, the probability distribution $p(t, x, \theta, \kappa)$ of finding particles at time t in a small neighborhood of (x, θ, κ) is given by a forward Chapman-Kolmogorov equation

$$\partial_t p + \tau.\nabla_x p + \kappa \partial_\theta p - \partial_\kappa(\kappa p) - \alpha^2\, \partial^2_{\kappa^2} p \;=\; 0 \tag{2.1}$$

with initial value p_0, where

$$\tau(\theta) = (\cos\theta, \sin\theta) = e^{\sqrt{-1}\,\theta}.$$

The stochastic transcription of (2.1) is given by the stochastic differential system ($t \geq 0$)

$$\begin{cases} dx_t = \tau(\theta_t)\, dt \\ d\theta_t = \kappa_t\, dt \\ d\kappa_t = -\kappa_t\, dt \;+\; \sqrt{2}\alpha\, dB_t \end{cases} \tag{2.2}$$

where $(B_t)_{t\geq 0}$ is a standard Brownian Motion on $\mathbb{R}^2$. The probability density function $p(t,x,\theta,\kappa)$ of (x_t,θ_t,κ_t) with a given initial law $p_0\,dx\,d\theta\,d\kappa$ is then solution of (2.1). Also, (2.1) is in fact a kinetic Fokker-Planck equation. Note that $(\kappa_t)_{t\geq 0}$ is an Ornstein-Uhlenbeck Gaussian process. The formula

$$\theta_t = \theta_0 + \int_0^t \kappa_s\,ds$$

expresses $(\theta_t)_{t\geq 0}$ as a pathwise linear functional of $(\kappa_t)_{t\geq 0}$. In particular the process $(\theta_t)_{t\geq 0}$ is Gaussian and is thus fully characterized by its initial value, together with its time covariance and mean which can be easily computed from the ones of $(\kappa_t)_{t\geq 0}$ conditional on θ_0 and κ_0. The process $(\theta_t)_{t\geq 0}$ is not Markov. However, the pair $(\theta_t,\kappa_t)_{t\geq 0}$ is a Markov Gaussian diffusion process and can be considered as the solution of a degenerate stochastic differential equation, namely the last two equations of the system (2.2). Additionally, the process $(x_t)_{t\geq 0}$ is an "additive functional" of $(\theta_t,\kappa_t)_{t\geq 0}$ since

$$x_t \;=\; x_0 + \int_0^t \tau(\theta_s)\,ds \;=\; x_0 + \int_0^t \tau\Big(\theta_0 + \int_0^s \kappa_u\,du\Big)\,ds. \tag{2.3}$$

Note that x_t is a nonlinear function of $(\theta_s)_{0\leq s\leq t}$ due to the nonlinear nature of τ, and thus $(x_t)_{t\geq 0}$ is not Gaussian. The invariant measures of the process $(\theta_t,\kappa_t)_{t\geq 0}$ are multiples of the tensor product of the Lebesgue measure on $\mathbb{R}$ with the the Gaussian law of mean zero and variance α^2. These measures cannot be normalized into probability laws. Since τ is 2π-periodic, the process $(\theta_t)_{t\geq 0}$ acts in the definition of x_t only modulo 2π, and one may replace θ by $\underline{\theta}\in S^1 := \mathbb{R}/2\pi\mathbb{Z}$. The Markov diffusion process

$$(y_t)_{t\geq 0} = (\underline{\theta}_t,\kappa_t)_{t\geq 0}$$

has state space $S^1\times\mathbb{R}$ and admits a unique invariant law μ which is the tensor product of the uniform law on S^1 with the Gaussian law of mean zero and variance α^2, namely

$$d\mu(\underline{\theta},\kappa) = \frac{1}{\sqrt{2\pi\alpha^2}}\mathbb{1}_{S^1}(\underline{\theta})\exp\left(-\frac{\kappa^2}{2\alpha^2}\right)d\underline{\theta}d\kappa.$$

Note that $(y_t)_{t\geq 0}$ is ergodic but is not reversible (this is simply due to the fact that the dynamics on observables depending only on $\underline{\theta}$ is not reversible). The famous Birkhoff-von Neumann Ergodic Theorem [15, 21, 12, 16, 6] states that for every μ-integrable function $f: S^1\times\mathbb{R}\to\mathbb{R}$ and any initial law ν (i.e. the law of y_0), we have,

$$\mathbb{P}\Big(\lim_{t\to\infty}\Big(\frac{1}{t}\int_0^t f(y_s)\,ds - \int_{S^1\times\mathbb{R}} f\,d\mu\Big) = 0\Big) = 1. \tag{2.4}$$

Beyond this Law of Large Numbers describing for instance the limit of the functional (2.3), one can ask for the asymptotic fluctuations, namely the long time behavior as $t\to\infty$ of

$$\sigma_t\Big(\frac{1}{t}\int_0^t f(y_s)\,ds - \int_{S^1\times\mathbb{R}} f\,d\mu\Big) \tag{2.5}$$

where σ_t is some renormalizing constant such that $\sigma_t\to\infty$ as $t\to\infty$. By analogy with the Central Limit Theorem (CLT for short) for reversible diffusion processes (see e.g.

[8, 16]), we may expect, when f is "good enough" and when $\sigma_t = \sqrt{t}$, a convergence in distribution of (2.5) as $t \to \infty$ to some Gaussian distribution with variance depending on f and on the infinitesimal dynamics of $(y_t)_{t\geq 0}$. This is the aim of Theorem 2.1 below, which goes actually further by stating a so called *Invariance Principle*, in other words a CLT for the whole process and not only for a fixed single time.

Theorem 2.1 (Invariance Principle at equilibrium) *Assume that $y_0 = (\underline{\theta}_0, \kappa_0)$ is distributed according to the equilibrium law μ. Then for any C^∞ bounded $f : S^1 \times \mathbb{R} \to \mathbb{R}$ with zero μ-mean, the law of the process*

$$(z_t^\varepsilon)_{t\geq 0} := \left(\varepsilon \int_0^{t/\varepsilon^2} f(y_s)\, ds,\, y_{t/\varepsilon^2}\right)_{t\geq 0}$$

converges as $\varepsilon \to 0$ to $\mathcal{W}^f \otimes \mu^{\otimes\infty}$ where $\mathcal{W}^f$ is the law of a Brownian Motion with variance

$$V_f = -\int gLg\, d\mu = 2\alpha^2 \int |\partial_\kappa g|^2\, d\mu$$

where $L = \alpha^2\partial_\kappa^2 - \kappa\partial_\kappa + \kappa\,\partial_\theta$ acts on 2π-periodic functions in θ, and $g : S^1 \times \mathbb{R} \to \mathbb{R}$ is

$$g(y) = -\mathbb{E}\left(\int_0^\infty f(y_s)\, ds \,\middle|\, y_0 = y\right).$$

In other words, for any fixed integer $k \geq 1$, any fixed times $0 \leq t_1 < \cdots < t_k$, and any bounded continuous function $F : (\mathbb{R} \times S^1 \times \mathbb{R})^k \to \mathbb{R}$, we have

$$\lim_{\varepsilon\to 0} \mathbb{E}\Big[F(z_{t_1}^\varepsilon, \ldots, z_{t_k}^\varepsilon)\Big] = \mathbb{E}\Big[F((W_{t_1}^f, Y_1), \ldots, (W_{t_k}^f, Y_k))\Big]$$

where $Y_1, \ldots, Y_k$ are independent and equally distributed random variables of law μ and where $(W_t^f)_{t\geq 0}$ is a Brownian Motion with law $\mathcal{W}^f$, independent of $Y_1, \ldots, Y_k$.

Theorem 2.1 encloses some decorrelation information as ε goes to 0 since the limiting law is a tensor product (just take for F a tensor product function). Such a convergence in law at the level of the processes expresses a so called Invariance Principle. Here the Invariant Principle is *at equilibrium* since y_0 follows the law μ. The proof of Theorem 2.1 is probabilistic, and relies on the fact that g solves the Poisson[1] equation $Lg = f$. Note that neither the reversible nor the sectorial assumptions of [8] are satisfied here.

Theorem 2.1 remains valid when f is complex valued (this needs the computation of the asymptotic covariance of the real and the imaginary part of f). The hypothesis on f enables to go beyond the original framework of [5]. For instance, we could add the following rule in the model: *the speed of the fish decreases as the curvature increases.* Mathematically, this is roughly translated as:

$$f(y) = f(\theta, \kappa) = c(|\kappa|)(\cos\theta,\, \sin\theta) \tag{2.6}$$

where $s \mapsto c(s)$ is a regular enough decreasing function, see Figure 3.1 for a simulation.

[1] It is amusing to remark that "poisson" means "fish" in French....

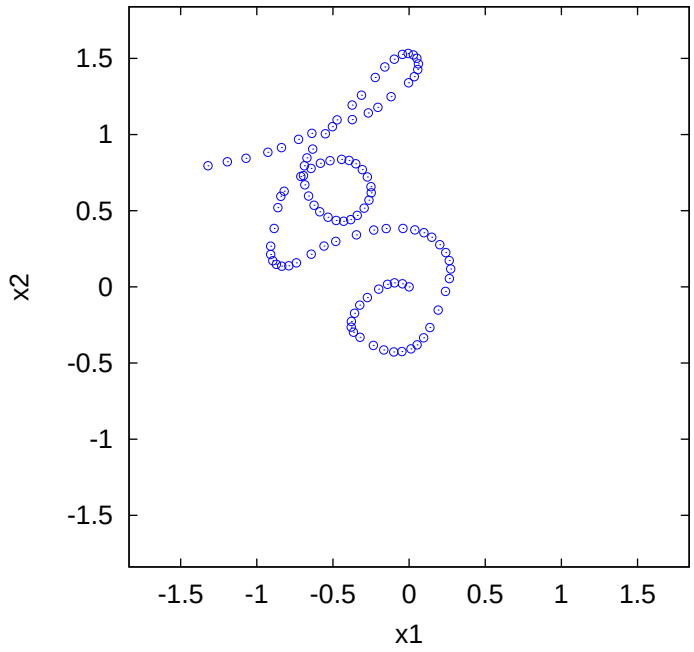

Figure 3.1: An example of the trajectory $t \mapsto x_t = (x_t^1, x_t^2)$ of the PTWM where the speed of the fish decreases with higher curvature (eq. 2.6). Here $\alpha = 1$ and $c(|\kappa|) = 1/(1+2|\kappa|)$. The simulation is run during 10 time units, we plot a point each .1 time unit.

The following corollary is obtained from Theorem 2.1 by taking roughly $f = \tau$ and by computing V_τ explicitly. In contrast with the function f in Theorem 2.1, the function τ is complex valued. Also, an additional argument is in fact used in the proof of Corollary 2.2 to compute the asymptotic covariance of the real and imaginary parts of the additive functional based on τ (note that this seems to be missing in [5]).

Corollary 2.2 (Invariance Principle for PTWM at equilibrium) *Assume that the initial value $y_0 = (\underline{\theta}_0, \kappa_0)$ is distributed according to the equilibrium μ. Then the law of the process*

$$\left(\varepsilon \int_0^{t/\varepsilon^2} \tau(\theta_s)\, ds,\, y_{t/\varepsilon^2} \right)_{t \geq 0} \tag{2.7}$$

converges as $\varepsilon \to 0$ to $\mathcal{W}^\tau \otimes \mu^{\otimes \infty}$ where $\mathcal{W}^\tau$ is the law of a 2-dimensional Brownian Motion with covariance matrix $\mathbb{D} I_2$ where

$$\mathbb{D} = \int_0^\infty e^{-\alpha^2(s-1+e^{-s})}\, ds.$$

It can be shown that the constant $\mathbb{D}$ which appears in Corollary 2.2 satisfies to

$$\mathbb{D} = \lim_{t\to\infty} \frac{1}{t} \mathrm{Var}(x_t^1) = \lim_{t\to\infty} \frac{1}{t} \mathrm{Var}(x_t^2) \quad \text{where} \quad (x_t^1, x_t^2) = x_t = \int_0^t \tau(\theta_s)\, ds$$

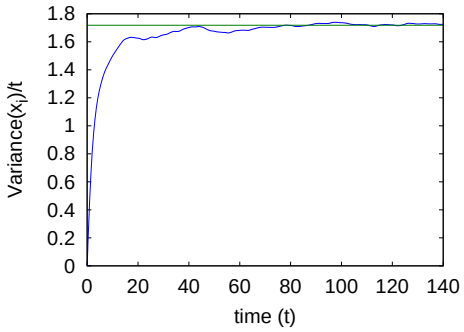

Figure 3.2: Convergence of $t^{-1}\mathrm{Var}(x_t)$ to the constant $\mathbb{D}$. Here $\alpha = 1$.

see e.g. Figure 3.2. Corollary 2.2 complements a result of Degond & Motsch [5, Theorem 2.2] which states – in their notations – that the probability density function

$$p^\varepsilon(t, x, \underline{\theta}, \kappa) = \frac{1}{\varepsilon^2}\, p\left(\frac{t}{\varepsilon^2}, \frac{x}{\varepsilon}, \underline{\theta}, \kappa\right)$$

converges as $\varepsilon \to 0$ to the probability density

$$\frac{1}{\sqrt{2\pi}}\, n^0(t, x)\, M(\kappa)$$

where M is the Gaussian law with zero mean and variance α^2, and n^0 solves the equation

$$\partial_t n^0 - \frac{1}{2}\mathbb{D}\Delta_x n^0 = 0$$

where $\mathbb{D}$ is as in Corollary 2.2. Convergence holds in a weak sense in some well chosen Banach space, depending on the initial distribution. The meaning of p^ε is clear from the stochastic point of view: it is the probability density function of the distribution of the rescaled process (recall that x is two-dimensional)

$$\left(\varepsilon x_{t/\varepsilon^2},\, y_{t/\varepsilon^2}\right)_{t\geq 0} = \left(\varepsilon x_{t/\varepsilon^2},\, \underline{\theta}_{t/\varepsilon^2},\, \kappa_{t/\varepsilon^2}\right)_{t\geq 0}.$$

In other words, the main result of [5] captures the asymptotic behavior at fixed time of the process (2.7) by stating that for any t, and as $\varepsilon \to 0$, the law of this process at time t tends to the law of $(\sqrt{\mathbb{D}}W_t, \underline{\theta}, M)$ where $(W_t)_{t\geq 0}$, and $(\underline{\theta}, M)$ are independent, $(W_t)_{t\geq 0}$ being a standard Brownian Motion, and $(\underline{\theta}, M)$ a random variable following the law μ. This result encompasses what is expected by biologists i.e. a "diffusive limiting behavior".

Starting from the equilibrium, Corollary 2.2 is on one hand stronger and on the other hand weaker than the result of [5] mentioned above. Stronger because it is relative to the full law of the process, not only to each marginal law at fixed time t. In particular it encompasses covariance type estimates at two different times. Weaker because it is concerned with the law and not with the density. For the density at time t we recover a weak convergence, while the one obtained in [5] using partial differential

equations techniques is of strong nature. We should of course go further using what is called "local CLTs", dealing with densities instead of laws, but this will require some estimates which are basically the key of the analytic approach used in [5].

Our last result concerns the behavior when the initial law is not the invariant law μ.

Theorem 2.3 (Invariance Principle out of equilibrium) *The conclusion of Corollary 2.2 still holds true when $y_0 = (\underline{\theta}_0, \kappa_0)$ is distributed according to some law ν such that $d\nu_{s_0}/d\mu$ belongs to $\mathbb{L}^q(\mu)$ for some $s_0 \geq 0$ and $q > 1$, where ν_{s_0} is the law of y_{s_0}. This condition is fulfilled for instance if $d\nu/d\mu$ belongs to $\mathbb{L}^q(\mu)$ or if ν is compactly supported.*

3 Proofs

The story of CLTs and Invariant Principles for Markov processes is quite intricate and it is out of reach to give a short account of the literature. The reader may find however a survey on some aspects in e.g. [8, 14, 25, 16]. Instead we shall exhibit some peculiarities of our model that make the long time study an (almost) original problem. First of all, as mentioned in Section 2, the underlying diffusion process $(\theta_t, \kappa_t)_{t\geq 0}$ with state space $\mathbb{R}^2$ is not ergodic: its invariant measures are multiples of the Lebesgue measure times a Gaussian law. This process is also degenerate in the sense that its infinitesimal generator

$$L = \alpha^2\, \partial^2_{\kappa^2} \,-\, \kappa\, \partial_\kappa \,+\, \kappa\, \partial_\theta \tag{3.8}$$

is not elliptic. Fortunately, the operator $\partial_t + L$ is Hörmander hypo-elliptic since the "diffusion" vector field $X = (0, \alpha^2)$ and the Lie bracket $[X, Y] = XY - YX$ of X with the "drift" vector field $Y = (\kappa, -\kappa)$ generate the full tangent space at each $(\theta, \kappa) \in \mathbb{R}^2$. The drift vector field Y is always required, so that the generator is "fully degenerate". This degeneracy of L has two annoying consequences:

1. any invariant measure ν of L is not symmetric, i.e. $\int fLg\, d\nu \neq \int gLf\, d\nu$ for some nice functions f and g in $\mathbb{L}^2(\nu)$, for instance only depending on θ.

2. the *carré du champ* of L given here by $\Gamma f = \frac{1}{2}L(f^2) - fLf = 2\alpha^2|\partial_\kappa f|^2$ is degenerate, so that one cannot expect to use any usual functional inequality such as the Poincaré inequality (spectral gap) in order to study the long time behavior of the process.

This situation is typical for kinetic models. In the more general framework of homogenization, a slightly more general version of this model has been studied in [10], see also the trilogy [18, 19, 20] for similar results from which one can derive the result in [5]. The main ingredient of the proof of Theorem 2.1 is the control of the "rate of convergence" to equilibrium in the Ergodic Theorem (2.4), for the process $(\underline{\theta}_t, \kappa_t)_{t\geq 0}$ instead of $(\theta_t, \kappa_t)_{t\geq 0}$. We begin with a simple lemma which expresses the propagation of chaos as ε goes to 0.

Lemma 3.1 (Propagation of chaos) *Assume that $y_0 = (\underline{\theta}_0, \kappa_0)$ is distributed according to the equilibrium law μ. Then the law of the process $(y^\varepsilon)_{t\geq 0} = \left(y_{t/\varepsilon^2}\right)_{t\geq 0}$ converges as $\varepsilon \to 0$ to $\mu^{\otimes\infty}$. In other words, for any fixed integer $k \geq 1$, any fixed times $0 \leq t_1 < \cdots < t_k$, and any bounded continuous function $F : (S^1 \times \mathbb{R})^k \to \mathbb{R}$, we have*

$$\lim_{\varepsilon\to\infty} \mathbb{E}\Big[F(y^\varepsilon_{t_1}, \ldots, y^\varepsilon_{t_k})\Big] = \mathbb{E}[F(Y_1, \ldots, Y_k)]$$

where $Y_1, \ldots, Y_k$ are independent and equally distributed random variables of law μ.

Proof of Lemma 3.1: Let us denote by L the operator (3.8) acting this time on 2π-periodic functions in θ, i.e. on functions $S^1 \times \mathbb{R} \to \mathbb{R}$. This operator L generates a non-negative contraction semi-group $(P_t)_{t\geq 0} = (e^{tL})_{t\geq 0}$ in $\mathbb{L}^2(\mu)$ with the stochastic representation $P_t f(y) = \mathbb{E}[f(y_s)|y_0 = y]$ for all bounded f. We denote by L^* the adjoint of L in $\mathbb{L}^2(\mu)$ generating the adjoint semi-group P_t^*, i.e.

$$L^* = \alpha^2\partial^2_\kappa - \kappa\partial_\kappa - \kappa\partial_\theta$$

acting again on the same functions. The function $H(y) = H(\underline{\theta}, \kappa) = 1 + \kappa^2$ satisfies

$$L^*H = -2H + 2(\alpha^2 + 1) \leq -H + 2(\alpha^2 + 1)\, \mathbb{1}_{|\kappa|\leq\sqrt{2\alpha^2+1}} \tag{3.9}$$

so H is a Lyapunov function in the sense of [1, Def. 1.1]. Since $C = S^1 \times \{|\kappa| \leq \sqrt{2\alpha^2 + 1}\}$ is compact and the process $(y_t)_{t\geq 0}$ is regular enough, C is a "petite set" in the terminology [1, Def. 1.1] of Meyn & Tweedie. Accordingly we may apply [1, Th. 2.1] and conclude that there exists a constant $K_2 > 0$ such that for all bounded f satisfying $\int f d\mu = 0$,

$$\|P_t f\|_{\mathbb{L}^2(\mu)} \leq K_2 \|f\|_\infty e^{-t}. \tag{3.10}$$

We shall give a proof of the Lemma for $k = 2$, the general case $k \geq 2$ being heavier but entirely similar. We set $s = t_1 < t_2 = t$. It is enough to show that for every bounded continuous functions $F, G : S^1 \times \mathbb{R} \to \mathbb{R}$, we have the convergence

$$\lim_{\varepsilon\to 0} \mathbb{E}[F(y^\varepsilon_s)G(y^\varepsilon_t)] = \mathbb{E}[F(Y)]\mathbb{E}[G(Y)]$$

where Y is a random variable of law μ. Since y_0 follows the law μ, we can safely assume that the functions F and G have zero μ-mean, and reduce the problem to show that

$$\mathbb{E}[F(y^\varepsilon_s)G(y^\varepsilon_t)] = \int P_{s/\varepsilon^2}(FP_{(t-s)/\varepsilon^2}G)\, d\mu = \int FP_{(t-s)/\varepsilon^2}G\, d\mu \underset{\varepsilon\to 0}{\longrightarrow} 0.$$

Now since μ is a probability measure, we have $\mathbb{L}^2(\mu) \subset \mathbb{L}^1(\mu)$ and thus

$$\left|\int FP_{(t-s)/\varepsilon^2}G\, d\mu\right| \leq \left\|FP_{(t-s)/\varepsilon^2}G\right\|_1 \leq \left\|FP_{(t-s)/\varepsilon^2}G\right\|_2 \leq \|F\|_\infty \left\|P_{(t-s)/\varepsilon^2}G\right\|_2.$$

The desired result follows then from the $\mathbb{L}^2 - \mathbb{L}^\infty$ bound (3.10) since

$$\left\|P_{(t-s)/\varepsilon^2}G\right\|_2 \leq K_2\|G\|_\infty e^{-(t-s)/\varepsilon^2} \underset{\varepsilon\to 0}{\longrightarrow} 0.$$

■

Proof of Theorem 2.1: The strategy is the usual one based on Itô's formula, Poisson equation, and a martingale CLT. However, each step involves some peculiar properties of the stochastic process. For convenience we split the proof into small parts with titles.

Poisson equation

Let L, L^*, and $(P_t)_{t\geq 0}$ be as in the proof of Lemma 3.1. Since f is bounded and satisfies $\int f d\mu = 0$ (i.e. f has zero μ-mean), the bound (3.10) ensures that

$$g = -\int_0^\infty P_s f \, ds \quad \in \mathbb{L}^2(\mu).$$

Furthermore, the formula $P_t g - g = \int_0^t P_s f \, ds$ ensures that

$$\lim_{t\to 0} \frac{1}{t}(P_t g - g) = f \quad \text{strongly in } \mathbb{L}^2(\mu).$$

It follows that g belongs to the $\mathbb{L}^2(\mu)$-domain of L and satisfies to the Poisson equation:

$$Lg = f \quad \text{in } \mathbb{L}^2(\mu).$$

Since μ has an everywhere positive density with respect to the Lebesgue measure on $S^1 \times \mathbb{R}$, we immediately deduce that g belongs to the set of Schwartz distributions $\mathcal{D}'$ and satisfies $Lg = f$ in this set. Since L is hypo-elliptic (it satisfies the Hörmander brackets condition) and f is C^∞, it follows that g belongs to C^∞. Hence we have solved the Poisson equation $Lg = f$ in a strong sense. Remark that since $g \in \mathbb{L}^2(\mu)$ and f is bounded, we get

$$\mathbb{E}_\mu[2\alpha^2 \, |\partial_\kappa \, g|^2] = -\mathbb{E}_\mu[gLg] = -\mathbb{E}_\mu[gf] < \infty.$$

Itô's formula

Since g is smooth, we may use Itô's formula to get

$$g(y_t) - g(y_0) = \int_0^t \alpha\sqrt{2}\, \partial_\kappa g(y_s) \, dB_s + \int_0^t Lg(y_s) \, ds \quad \text{almost surely}$$

which can be rewritten thanks to the Poisson equation $Lg = f$ as

$$\int_0^t f(y_s) \, ds = g(y_t) - g(y_0) - \alpha\sqrt{2} \int_0^t \partial_\kappa g(y_s) \, dB_s \quad \text{almost surely.} \tag{3.11}$$

This last equation (3.11) reduces the CLT for the process

$$\left(\varepsilon \int_0^{t/\varepsilon^2} f(y_s) \, ds\right)_{t\geq 0}$$

to showing that $(\varepsilon(g(y_{t/\varepsilon^2}) - g(y_0)))_{t\geq 0}$ goes to zero as $\varepsilon \to 0$ and to a CLT for the process

$$\left(\alpha\varepsilon\sqrt{2} \int_0^{t/\varepsilon^2} \partial_\kappa g(y_s) \, dB_s\right)_{t\geq 0}.$$

For such, we shall use the initial conditions and a martingale argument respectively.

Initial condition

Since the law μ of y_0 is stationary, Markov's inequality gives for any constant $K > 0$,

$$\mathbb{P}(|g(y_{t/\varepsilon^2})| \geq K/\varepsilon) = \mathbb{P}(|g(y_0)| \geq K/\varepsilon) \leq \frac{\mathrm{Var}_\mu(g)\,\varepsilon^2}{K^2} \underset{\varepsilon\to 0}{\longrightarrow} 0.$$

It follows that any n-uple of increments

$$\varepsilon\,(g(y_{t_1}) - g(y_{t_0}), \ldots, g(y_{t_n}) - g(y_{t_{n-1}}))$$

converges to 0 in probability as $\varepsilon \to 0$. Thanks to (3.11), this reduces the CLT for

$$\left(\varepsilon \int_0^{t/\varepsilon^2} f(y_s)\, ds\right)_{t\geq 0}$$

to the CLT for

$$(M_t^\varepsilon)_{t\geq 0} := \left(\varepsilon\alpha\sqrt{2} \int_0^{t/\varepsilon^2} \partial_\kappa g(y_s)\, dB_s\right)_{t\geq 0}.$$

Martingale argument

It turns out that $((M_t^\varepsilon)_{t\geq 0})_{\varepsilon>0}$ is a family of local martingales. These local martingales are actually $\mathbb{L}^2$ martingales whose brackets (increasing processes)

$$\langle M^\varepsilon\rangle_t = \varepsilon^2 2\alpha^2 \int_0^{t/\varepsilon^2} |\partial_\kappa g|^2(y_s)\, ds$$

converge almost surely to

$$2\alpha^2 t\mathbb{E}_\mu[|\partial_\kappa\, g|^2] = t\, V_f \quad \text{as } \varepsilon \to 0$$

thanks to the Ergodic Theorem (2.4). According to the CLT for $\mathbb{L}^2$-martingales due to Rebolledo, see e.g. [11] for an elementary proof, it follows that the family $(M_t^\varepsilon)_{t\geq 0}$ converges weakly (for the Skorohod topology) to $V_f\,(B_t^\tau)_{t\geq 0}$ where $(B_t^\tau)_{t\geq 0}$ is a standard Brownian Motion. Consequently, we obtain the desired CLT for the process

$$\left(\varepsilon \int_0^{t/\varepsilon^2} f(y_s)\, ds\right)_{t\geq 0}.$$

Namely, its increments are converging in distribution as $\varepsilon \to 0$ to the law of a Brownian Motion with variance V_τ. It remains to obtain the desired CLT for the process $(z_t^\varepsilon)_{t\geq 0}$.

Coupling with propagation of chaos and asymptotic independence

By the result above and Lemma 3.1, the CLT for $(z_t^\varepsilon)_{t\geq 0}$ will follow if we show that

$$\left(\varepsilon \int_0^{t/\varepsilon^2} f(y_s)\, ds\right)_{t\geq 0} \quad \text{and} \quad (y_{t/\varepsilon^2})_{t\geq 0} = (\underline{\theta}_{t/\varepsilon^2}, \kappa_{t/\varepsilon^2})_{t\geq 0}$$

are independent processes as $\varepsilon \to 0$. It suffices to establish the independence as $\varepsilon \to 0$ for an arbitrary k-uple of times $0 = t_0 < t_1 < \cdots < t_k = t$. To this end, let us introduce a bounded continuous function h and the smooth bounded functions

$$h_j(u) = e^{\sqrt{-1}b_j u}$$

where $1 \leq j \leq k$ for given real numbers $b_1, \ldots, b_k$. Let us define

$$A^\varepsilon = \mathbb{E}_\mu \left[h(y_{t/\varepsilon^2}) \prod_{j=1}^{k} h_j \left(\varepsilon \int_{t_{j-1}/\varepsilon^2}^{t_j/\varepsilon^2} f(y_s)\, ds \right) \right]$$

Introduce $t_\varepsilon = (t/\varepsilon^2) - (t/\sqrt{\varepsilon})$ and $s_\varepsilon = t/\sqrt{\varepsilon}$. For ε small enough, $t_\varepsilon > (t_{k-1}\varepsilon^2)$, so that using the Markov property at time t_ε we get

$$A^\varepsilon = \mathbb{E}_\mu \left[\prod_{j=1}^{k-1} h_j \left(\varepsilon \int_{t_{j-1}/\varepsilon^2}^{t_j/\varepsilon^2} f(y_s)\, ds \right) \mathbb{E}_\mu \left[h(y_{t/\varepsilon^2}) h_k \left(\varepsilon \int_{t_{k-1}/\varepsilon^2}^{t_k/\varepsilon^2} f(y_s)\, ds \right) \,\middle|\, \mathcal{F}_{t_\varepsilon} \right] \right]$$

The conditional expectation in the right hand side is equal to

$$h_k \left(\varepsilon \int_{t_{k-1}/\varepsilon^2}^{t_\varepsilon} f(y_s)\, ds \right) \mathbb{E} \left[h(y_{s_\varepsilon}) h_k \left(\varepsilon \int_0^{s_\varepsilon} f(y_s)\, ds \,\middle|\, y_0 = y_{t_\varepsilon} \right) \right]$$

and the second term can be replaced by

$$\mathbb{E} \left[h(y_{s_\varepsilon}) \,\middle|\, y_0 = y_{t_\varepsilon} \right]$$

up to an error less than

$$\varepsilon \|h\|_\infty \|f\|_\infty s_\varepsilon$$

going to 0 as $\varepsilon \to 0$. It thus remains to study

$$\mathbb{E}_\mu \left[\prod_{j=1}^{k-1} h_j \left(\varepsilon \int_{t_{j-1}/\varepsilon^2}^{t_j/\varepsilon^2} f(y_s)\, ds \right) h_k \left(\varepsilon \int_{t_{k-1}/\varepsilon^2}^{t_\varepsilon} f(y_s)\, ds \right) \mathbb{E} \left[h(y_{s_\varepsilon}) \,\middle|\, y_0 = y_{t_\varepsilon} \right] \right].$$

Conditioning by y_{t_ε}, this can be written in the form

$$\int H(\varepsilon, y)\, P_{s_\varepsilon} h(y)\, \mu(dy)$$

with a bounded H, so that using the convergence of the semi-group, we may again replace $P_{s_\varepsilon} h$ by $\int h d\mu$ up to an error term going to 0. It remains to apply the previously obtained CLT in order to conclude to the convergence and asymptotic independence.

■

Remark 3.1 (More general models) The proof of Theorem 2.1 immediately extends to more general cases. The main point is to prove that g solves the Poisson equation in $\mathbb{L}^2(\mu)$. In particular it is enough to have an estimate of the form

$$\|P_t f\|_{\mathbb{L}^2(\mu)} \leq \alpha(t)\, \|f\|_\infty$$

for every $t \geq 0$ with a function α satisfying

$$\int_0^\infty \alpha(s)\, ds < \infty.$$

According to [1], a sufficient condition for this to hold is to find a smooth increasing positive concave function φ such that the function α defined by

$$\alpha(t) = \frac{1}{(\varphi \circ G_\varphi^{-1})(t)} \quad \text{where} \quad G_\varphi(u) = \int_1^u \frac{1}{\varphi(s)}\, ds$$

satisfies the integrability condition above, and a Lyapunov function $H \geq 1$ such that

$$\int H\, d\mu < \infty \quad \text{and} \quad L^* H \leq -\varphi(H) + O(\mathbb{1}_C)$$

for some compact subset C. In particular we may replace the Ornstein-Uhlenbeck dynamics for κ by a more general Kolmogorov diffusion dynamics of the form

$$d\kappa_t = -\nabla V(\kappa_t) dt + \sqrt{2}\, dB_t.$$

The invariant measure of $(\kappa_t, \theta_t)_{t\geq 0}$ is then $e^{-V(\kappa)} d\kappa d\theta$. We refer for instance to [7, 1] for the construction of Lyapunov functions in this very general situation. For example, in one dimension, one can take $V'(x) = |x|^p$ for large $|x|$ and $0 < p \leq 1$. Choosing $H(y) = |\kappa|^q$ for large κ furnishes a polynomial decay of any order by taking q as large as necessary. Actually, in this last situation, the decay rate is sub–exponential, see e.g. [7, 1].

Remark 3.2 (Asymptotic covariance) It is worth noticing that if the asymptotic variance

$$(AV)_f = \lim_{t\to\infty} \frac{1}{t}\, \mathbb{E}_\mu \left[\left(\int_0^t f(y_s)\, ds \right)^2 \right]$$

exists, then $V_f = (AV)_f$. Similarly we may consider complex valued functions f and replace the asymptotic variance by the asymptotic covariance matrix which takes into account the variances and the covariance of the real and imaginary parts of f.

Proof of Corollary 2.2: We may now apply the previous theorem and the previous remark to the 2-dimensional smooth and μ-centered function τ. The only thing we have to do is to compute the asymptotic covariance matrix. To this end, first remark that elementary Gaussian computations furnishes the following explicit expressions

$$\kappa_t = e^{-t}\, \kappa_0 + \sqrt{2}\, \alpha \int_0^t e^{s-t}\, dB_s\,, \tag{3.12}$$

$$\theta_t = \theta_0 + (1 - e^{-t})\, \kappa_0 + \sqrt{2}\, \alpha \int_0^t (1 - e^{s-t})\, dB_s\,. \tag{3.13}$$

Since $x_t^1 = \int_0^t \cos\theta_s\, ds$ and $x_t^2 = \int_0^t \sin\theta_s\, ds$, Markov's property and stationarity yield

$$\begin{aligned}\mathbb{E}_\mu[x_t^1\, x_t^2] &= \mathbb{E}_\mu\left[\int_0^t (x_s^1 \sin\theta_s + x_s^2\cos\theta_s)\, ds\right] \\ &= \mathbb{E}_\mu\left[\int_0^t\int_0^s (\cos\theta_u \sin\theta_s + \sin\theta_u\cos\theta_s)\, du\, ds\right] \\ &= \int_0^t\int_0^s \mathbb{E}_\mu[\sin(\theta_u+\theta_s)]\, du\, ds \\ &= \int_0^t\int_0^s \mathbb{E}_\mu\left[\sin\left(2\theta_0 + 2(1-e^{u-s})\kappa_0 + \sqrt{2}\alpha\int_0^{s-u}(1-e^{v-(s-u)})\, dB'_v\right)\right] du\, ds\end{aligned} \tag{3.14}$$

where $(B'_t)_{t\geq 0}$ is a Brownian Motion independent of $(\kappa_0, \underline{\theta}_0)$. Since κ_0 and $\underline{\theta}_0$ are also independent (recall that μ is a product law), we may first integrate with respect to $\underline{\theta}_0$ (fixing the other variables), i.e. we have to calculate $\mathbb{E}_\mu(\sin(2\underline{\theta}_0 + C))$ which is equal to 0 since the law μ of $\underline{\theta}_0$ is uniform on $[0, 2\pi[$. Hence the μ-covariance of (x_t^1, x_t^2) is equal to 0 (since this is a Gaussian process, both variables are actually independent), and similar computations show that the asymptotic covariance matrix is thus $\mathbb{D}I_2$ where

$$\mathbb{D} = \int_0^\infty e^{-\alpha^2(s-1+e^{-s})}\, ds.$$

■

Proof of Theorem 2.3: We assume now that $y_0 \sim \nu$ instead of $y_0 \sim \mu$. We may mimic the proof of Theorem 2.1, provided we are able to control $\mathbb{E}_\nu(g^2(y_s))$. Indeed the invariance principle for the local martingales $(M_t^\varepsilon)_{t\geq 0}$ is still true for the finite-dimensional convergence in law, according for instance to [12, Th. 3.6 p. 470]. The Ergodic Theorem ensures the convergence of the brackets. The first remark is that these controls are required only for $s \geq s_0 \geq 0$ where s_0 is fixed but arbitrary. Indeed since τ is bounded, the quantity

$$\varepsilon\int_0^{s_0} \tau(\theta_s)\, ds$$

goes to 0 almost surely, so that we only have to deal with $\int_{s_0}^{t/\varepsilon^2}$ so that we may replace 0 by s_0 in all the previous derivation. Thanks to the Markov property we thus have to control $\mathbb{E}_{\nu_{s_0}}(g^2(y_s))$ for all $s > 0$, where ν_{s_0} denote the law of y_{s_0}. This remark allows us to reduce the problem to initial laws which are absolutely continuous with respect to μ. Indeed thanks to the hypo-ellipticity of $\frac{\partial}{\partial t} + L$ we know that for each $s_0 > 0$, ν_{s_0} is absolutely continuous with respect to μ. Hence we have to control terms of the form

$$\mathbb{E}_\mu\left[\frac{d\nu_{s_0}}{d\mu}(y_0)\, g^2(y_s)\right].$$

The next remark is that [1, Theorem 2.1] immediately extends to the $\mathbb{L}^p$ framework for $2 \leq p < \infty$, i.e. there exists a constant K_p such that for all bounded f satisfying $\int f d\mu = 0$,

$$\|P_t f\|_{\mathbb{L}^p(\mu)} \leq K_p \|f\|_\infty e^{-t}. \tag{3.15}$$

Since the function f is bounded and satisfies $\int f d\mu = 0$, the previous bound ensures that g belongs to $\mathbb{L}^p(\mu)$, for all $p < \infty$. In particular, as soon as $d\nu_{s_0}/d\mu$ belongs to $\mathbb{L}^q(\mu)$ for some $1 < q$, $g(y_s)$ belongs to $\mathbb{L}^2(\mathbb{P}_\nu)$ for all $s \geq s_0$. Additionally, these bounds allow to show without much efforts that the "propagation of chaos" of Lemma 3.1 still holds when the initial law is such a ν. To conclude we thus only have to find sufficient condition for $d\nu_{s_0}/d\mu$ to belong to one $\mathbb{L}^q(\mu)$ $(q > 1)$ for some $s_0 \geq 0$. Of course, a first situation is when this holds for $s_0 = 0$. But there are many other situations.

Indeed recall that for non-degenerate Gaussian laws η_1 and η_2 the density $d\eta_2/d\eta_1$ is bounded as soon as the covariance matrix of η_1 dominates (in the sense of quadratic forms) the one of η_2 at infinity, i.e. the associated quadratic forms satisfy $q_1(y) > q_2(y)$ for $|y|$ large enough. According to (3.12) and (3.13) the joint law of (κ_t, θ_t) starting from a point (κ, θ) is a 2-dimensional Gaussian law with mean

$$m_t = (e^{-t}\kappa, \theta + (1 - e^{-t})\kappa)$$

and covariance matrix $D_t = \alpha^2 A_t$ with

$$A_t = \begin{pmatrix} 1 - e^{-2t} & (1 - e^{-t})^2 \\ (1 - e^{-t})^2 & 2t - 3 + 4e^{-t} - e^{-2t} \end{pmatrix}.$$

Note that if the asymptotic covariance of (κ_t, θ_t) is not 0, the asymptotic correlation vanishes, explaining the asymptotic "decorrelation" of both variables. It is then not difficult to see that if $\nu = \delta_y$ is a Dirac mass, then $d\nu_s/d\mu$ is bounded for every $s > 0$. Indeed for t small enough, A_t is close to the null matrix, hence dominated by the identity matrix. It follows that $d\nu_t/d\eta$ is bounded, where η is a Gaussian variable with covariance matrix $\alpha^2 I_2$. The result follows by taking the projection of θ onto the unit circle. A simple continuity argument shows that the same hold if ν is a compactly supported measure. ∎

Remark 3.3 Once obtained such a convergence theorem we may ask about explicit bounds (concentration bounds) in the spirit of [3] (some bounds are actually contained in this paper). One can also ask about Edgeworth expansions etc. However, our aim was just to give an idea of the stochastic methods than can be used for models like the PTWM.

Remark 3.4 The most difficult point was to obtain $\mathbb{L}^p(\mu)$ estimates for $\partial_\kappa g$. Specialists of hypo-elliptic partial differential equations will certainly obtain the result by proving quantitative versions of Hörmander's estimates (holding on compact subsets U):

$$\|\partial_\kappa g\|_p \leq C(U)\,(\|g\|_p + \|Lg\|_p).$$

We end up the present paper by mentioning an interesting and probably difficult direction of research, which consists in the study of the long time behavior of interacting copies of PTWM–like processes, leading to some kind of kinetic hypo-elliptic mean-field/exchangeable Mac Kean-Vlasov equations (see e.g. [22, 17] and references therein

for some aspects). At the Biological level, the study of the collective behavior at equilibrium of a group of interacting individuals is particularly interesting, see for instance [24].

Bibliography

[1] D. Bakry, P. Cattiaux, and A. Guillin. Rate of convergence for ergodic continuous Markov processes : Lyapunov versus Poincaré. *J. Func. Anal.*, 254:727–759, 2008.

[2] E. Casellas, J. Gautrais, R. Fournier, S. Blanco, M. Combe, V. Fourcassié, G. Theraulaz, and C. Jost. From individual to collective displacements in heterogeneous environments. *Journal of Theoretical Biology*, 250(3):424–434, 2008.

[3] P. Cattiaux and A. Guillin. Deviation bounds for additive functionals of Markov processes. *ESAIM Probability and Statistics*, 12:12–29, 2008.

[4] E. A. Codling, M. J. Plank, and S. Benhamou. Random walk models in biology. *Journal of The Royal Society Interface*, 2008.

[5] P. Degond and S. Motsch. Large scale dynamics of the Persistent Turning Walker Model of fish behavior. *Journal of Statistical Physics*, 131(6):989–1021, 2008.

[6] J.-D. Deuschel and D. W. Stroock. *Large deviations*, volume 137 of *Pure and Applied Mathematics*. Academic Press Inc., Boston, MA, 1989.

[7] R. Douc, G. Fort, and A. Guillin. Subgeometric rates of convergence of f-ergodic strong Markov processes. Preprint. Available on Mathematics ArXiv.math.ST/0605791, 2006.

[8] N. Gantert, J. Garnier, S. Olla, Zh. Shi, and A.-S. Sznitman. *Milieux aléatoires*, volume 12 of *Panoramas et Synthèses [Panoramas and Syntheses]*. Société Mathématique de France, Paris, 2001. Edited by F. Comets and É. Pardoux.

[9] J. Gautrais, C. Jost, M. Soria, A. Campo, S. Motsch, R. Fournier, S. Blanco, and G. Theraulaz. Analyzing fish movement as a persistent turning walker. *J Math Biol*, 2008.

[10] M. Hairer and A. G. Pavliotis. Periodic homogenization for hypoelliptic diffusions. *J. Stat. Phys.*, 117(1):261–279, 2004.

[11] I. S. Helland. Central limit theorem for martingales with discrete or continuous time. *Scand. J. Statist.*, 9:79–94, 1982.

[12] J. Jacod and A. N. Shiryaev. *Limit theorems for stochastic processes*, volume 288 of *Grundlehren der Mathematischen Wissenschaften*. Springer-Verlag., Berlin, 2003.

[13] R. Jeanson, S. Blanco, R. Fournier, J.L. Deneubourg, V. Fourcassié, and G. Theraulaz. A model of animal movements in a bounded space. *Journal of Theoretical Biology*, 225(4):443–451, 2003.

[14] G. L. Jones. On the Markov chain central limit theorem. *Probab. Surv.*, 1:299–320 (electronic), 2004.

[15] U. Krengel. *Ergodic theorems*, volume 6 of *de Gruyter Studies in Mathematics*. Walter de Gruyter & Co., Berlin, 1985. With a supplement by Antoine Brunel.

[16] Y. A. Kutoyants. *Statistical inference for ergodic diffusion processes*. Springer Series in Statistics. Springer-Verlag London Ltd., London, 2004.

[17] S. Méléard. Asymptotic behaviour of some interacting particle systems; McKean-Vlasov and Boltzmann models. In *Probabilistic models for nonlinear partial differential equations (Montecatini Terme, 1995)*, volume 1627 of *Lecture Notes in Math.*, pages 42–95. Springer, Berlin, 1996.

[18] E. Pardoux and A. Y. Veretennikov. On the Poisson equation and diffusion approximation. I. *Ann. Prob.*, 29(3):1061–1085, 2001.

[19] E. Pardoux and A. Y. Veretennikov. On the Poisson equation and diffusion approximation. II. *Ann. Prob.*, 31(3):1116–1192, 2003.

[20] E. Pardoux and A. Y. Veretennikov. On the Poisson equation and diffusion approximation. III. *Ann. Prob.*, 33(3):1111–1133, 2005.

[21] D. Revuz and M. Yor. *Continuous martingales and Brownian motion*, volume 293 of *Grundlehren der Mathematischen Wissenschaften [Fundamental Principles of Mathematical Sciences]*. Springer-Verlag, Berlin, third edition, 1999.

[22] A.-S. Sznitman. Topics in propagation of chaos. In *École d'Été de Probabilités de Saint-Flour XIX—1989*, volume 1464 of *Lecture Notes in Math.*, pages 165–251. Springer, Berlin, 1991.

[23] G. Theraulaz, E. Bonabeau, S. C. Nicolis, R. V. Sole, V. Fourcassié, S. Blanco, R. Fournier, J. L. Joly, P. Fernandez, A. Grimal, et al. Spatial patterns in ant colonies. *Proceedings of the National Academy of Sciences*, 99(15):9645, 2002.

[24] T. Vicsek. A question of scale. *Nature*, 411(421), 2001. DOI: doi:10.1038/35078161.

[25] L.-S. Young. Statistical properties of dynamical systems with some hyperbolicity. *Ann. of Math. (2)*, 147(3):585–650, 1998.

Chapter 4

A smooth model for fiber lay-down processes and its diffusion approximations

This chapter has been written in collaboration with M. Herty, A. Klar and F. Olawsky, it has been submitted to the journal Kinetic and Related Models (KRM).

Abstract. In this chapter we improve and investigate a stochastic model and its associated Fokker-Planck equation for the lay-down of fibers on a conveyor belt in the production process of nonwoven materials which has been developed in [2]. The model is based on a stochastic differential equation taking into account the motion of the fiber under the influence of turbulence. In the present chapter we remove an obvious drawback of the model, namely the non-differentiability of the paths of the process. We develop a model with smoother trajectories and investigate the relations between the different models looking at different scalings and diffusion approximations. Moreover, we compare the numerical results to simulations of the full physical process.

Keywords. Fiber dynamics, Stochastic diffential equation, Fokker-Planck equations, diffusion approximation

1 Introduction

Nonwoven materials / fleece are webs of long flexible fibers that are used for composite materials (filters) as well as in the hygiene and textile industries. They are produced in melt-spinning operations: hundreds of individual endless fibers are obtained by the continuous extrusion of a molten polymer through narrow nozzles that are densely and equidistantly placed in a row at a spinning beam. The viscous / viscoelastic fibers are stretched and spun until they solidify due to cooling air streams. Before the elastic fibers lay down on a moving conveyor belt to form a web, they become entangled and form loops due to the highly turbulent air flows. The homogeneity and load capacity of the fiber web are the most important textile properties for quality assessment of industrial nonwoven fabrics. The optimization and control of the fleece quality require modeling and simulation of fiber dynamics and lay-down; in addition, it is necessary to determine the distribution of fiber mass and directional arrangement in the web.

The software FIDYST, developed at the Fraunhofer ITWM, Kaiserslautern, enables numerical simulation of the spinning and deposition regime in the nonwoven production processes. The interaction of the fiber with the turbulent air flows is described by a combination of deterministic and stochastic forces in the momentum equation, which is derived, analyzed and experimentally validated in [8]. Due to the huge amount of physical details incorporated in FIDYST, the simulations of the fiber spinning and lay-down usually require an extremely large computational effort. Hence the optimization and control of the full process with several hundreds of fibres, and of the quality of the fleece, are difficult. Thus, a simplified stochastic model for the fiber lay-down process has been presented in [1, 2]. The model describes the position of the fiber on the transport belt by a stochastic differential system containing parameters that characterize the process. The reduced model can be used to calculate fast and efficiently the performance of hundreds of long fibers for fleece production. The case of large turbulence noise has been investigated in the above papers. In this case the probability density of the fiber becomes rapidly independent of the angle between the fiber and the direction of the conveyor's motion and the angle between the fiber and the position vector of its tip, respectively. In particular, the limit processes turn out to be Ornstein–Uhlenbeck type stochastic processes. Further analytical and numerical investigations can be found in [6, 7].

Although this model describes already several features of the full physical process correctly, it has an obvious drawback, namely the non-differentiability of the paths of the process. This is not true for the physical process and can also be seen, comparing simulation results of the full physical model and of the simplified model explained above, see Section 3.2. Thus, the purpose of the present chapter is to develop a model with smoother trajectories, compare the results with the full process and investigate the relations of this new model with the model described above and its simplifications.

The outline of this chapter is as follows: In Section 2, we introduce the new model and we investigate different scalings leading to the original model and to the reduce model. In section 3, we explore numerical simulation of the smooth model with different scales which illustrate the results of Section 2. We also compare the numerical simulation with the full physical model.

2 The new model with smooth trajectories

In the following we describe the original model in more detail. Consider a slender, elastic, non-extensible and endless fiber in a lay-down regime. The motion of the fiber on the belt is parameterized by its position $\vec{x}(t)$ and its velocity $c\vec{\tau}(\theta)$, where c is the magnitude of the velocity:

$$\vec{\tau}(\theta) = \begin{pmatrix} \cos\theta \\ \sin\theta \end{pmatrix}$$

and θ is the angle between the x-axis and the vector speed (see figure 4.1). Choosing arc-length parameterization, the non-extensibility condition gives $c = 1$. With $\vec{\tau}^{\perp}(\theta) = (-\sin\theta, \cos\theta)^T$ the original model [1, 2] for the process is given by

$$\begin{aligned} d\vec{x}_t &= \vec{\tau}(\theta_t)\, dt, \\ d\theta_t &= -b(|\vec{x}_t|)\frac{\vec{x}_t}{|\vec{x}_t|} \cdot \vec{\tau}^{\perp}(\theta_t)\, dt + A dB_t. \end{aligned} \tag{2.1}$$

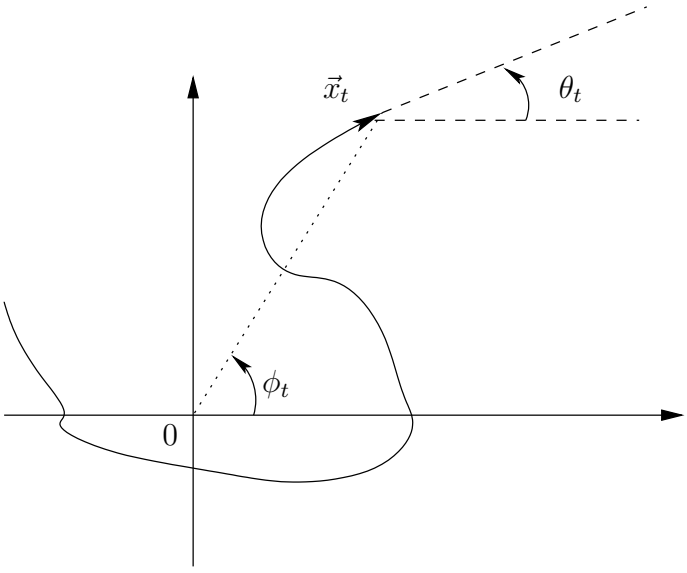

Figure 4.1: The description of the fiber process.

The function b denotes the effect of an external force which makes the fiber goes back to the origin, AdB_t express the stochasticity of the system due to the airflow. Another way to see the effect of the force is to look at the system in polar coordinates. Let's define $\vec{x} = r\vec{\tau}(\phi)$ then the force can be expressed as :

$$\begin{aligned} -b(|\vec{x}|)\frac{\vec{x}}{|\vec{x}|} \cdot \vec{\tau}^{\perp}(\theta) &= -b(r)\vec{\tau}(\phi) \cdot \vec{\tau}^{\perp}(\theta) \\ &= -b(r)\left(-\cos\phi\, \sin\theta + \sin\phi\, \cos\theta\right) \\ &= -b(r)\sin(\phi - \theta) \end{aligned}$$

I.e. another form of the model is :

$$\begin{aligned} d\vec{x}_t &= \vec{\tau}(\theta_t)\, dt, \\ d\theta_t &= b(r_t)\sin(\pi + \phi_t - \theta_t)\, dt + A dB_t. \end{aligned} \tag{2.2}$$

The equation on θ express the fact that θ is going to relax to $\pi+\phi$ which is the direction of the origin at the position $\vec{x}$.

For large value of noise A, we will see that the dynamic of equation (2.2) could be reduced to the simple equation

$$d\vec{x}_t = -\frac{1}{A^2}\frac{b(|\vec{x}_t|)}{|\vec{x}_t|}\vec{x}_t dt + \frac{\sqrt{2}}{A} dB_t. \tag{2.3}$$

(see Section 2.2). We call equation (2.2) the reduced model.

In order to get smoother fiber trajectories, we change the original model (2.1). To this aim, we add the white noise term in the differential equation not on the level of the velocity equation but on the second derivative, the curvature. We propose the following model:

$$\begin{aligned} d\vec{x}_t &= \vec{\tau}(\theta_t)\, dt \\ d\theta_t &= \kappa_t\, dt \\ d\kappa_t &= \lambda(\kappa_0 - \kappa)\, dt + \mu dB_t, \end{aligned} \tag{2.4}$$

where $\kappa_0(\vec{x}_t, \theta_t) = b(r_t)\sin(\theta_t - \phi)$. Here, the new parameter λ describes the inverse stiffness of the fiber and is related to the inverse elasticity module. The smaller λ the stiffer is the fiber. μ or better $\frac{\mu}{\lambda}$ describes the influence of the turbulent airflow on the curvature.

In the next subsection (Section 2.1), we are going to prove that the smooth model given by equation (2.4) leads to the original model (2.1) in a certain asymptotic scaling. Combining this with the large noise asymptotic (Section 2.2), one can jump from the smooth model to the original model and then to the reduced model (2.2). In the last subsection (Section 2.3), we will directly derive the reduced model (2.3) from the smooth model (2.4) with another asymptotic.

2.1 White noise limit: connection to the original model

In this part, we are going to prove that the smooth model leads under the appropriate scaling to the original model.

Proposition 2.1 *The following rescaling for equation (2.4):*

$$\lambda' = \varepsilon^2\lambda \quad ; \quad \mu' = \varepsilon^2\mu \tag{2.5}$$

together with a rescaling of the curvature

$$\kappa' = \varepsilon\kappa \tag{2.6}$$

leads to the original model (2.1) with the diffusion coefficient $A = \frac{\mu}{\lambda}$.

Proof. If we insert the rescaling given by (2.5) into the smooth model for the fiber, we obtain :

$$\begin{aligned} d\vec{x}_t &= \vec{\tau}(\theta_t)\,dt \\ d\theta_t &= \kappa_t\,dt \\ d\kappa_t &= \frac{\lambda'}{\varepsilon^2}(\kappa_0-\kappa)\,dt + \frac{\mu'}{\varepsilon^2}dB_t \end{aligned}$$

To facilitate the reading, we drop off the tilde. If we want to look at the limit when ε goes to zero, we have to make a change of variable for the κ-variable:

$$\kappa' = \varepsilon\kappa.$$

The dynamics for the fiber are then described by

$$\begin{aligned} d\vec{x}_t &= \vec{\tau}(\theta_t)\,dt \\ d\theta_t &= \frac{1}{\varepsilon}\kappa_t\,dt \\ d\kappa_t &= \frac{\lambda}{\varepsilon^2}(\varepsilon\kappa_0\,dt-\kappa)\,dt + \frac{\mu}{\varepsilon}dB_t \end{aligned}$$

The equations for θ and κ describe a process of Ornstein–Uhlenbeck type, the above scaling is the so called White-noise scaling of the Ornstein–Uhlenbeck process, see e.g. [4]. In terms of the Fokker-Planck equation, this gives after multiplication with ε

$$\partial_t f^\varepsilon + \vec{\tau}(\theta)\cdot\nabla_{\vec{x}} f^\varepsilon + \frac{1}{\varepsilon}\left(\kappa\partial_\theta f^\varepsilon + \lambda\kappa_0\partial_\kappa f^\varepsilon\right) = \frac{1}{\varepsilon^2}\left(\lambda\partial_\kappa(\kappa f^\varepsilon) + \frac{\mu^2}{2}\partial_{\kappa^2} f^\varepsilon\right) \tag{2.7}$$

We use an Hilbert expansion for f^ε ($f^\varepsilon = f^0 + \varepsilon f^1 + \dots$) in order to find the limit equation as ε goes to zero. At order ε^{-1}, we have :

$$\varepsilon^{-1} \quad : \quad \lambda\partial_\kappa(\kappa f^0) + \frac{\mu^2}{2}\partial_{\kappa^2} f^0 = 0.$$

This equation implies that f^0 is Gaussian in κ-variable. More exactly, if we define $p^\varepsilon = \int_\kappa f^\varepsilon\,d\kappa$, we then could write :

$$f^0 = p^0(\vec{x},\theta)\frac{1}{\sqrt{\pi\mu^2/\lambda}}\mathrm{e}^{-\frac{\kappa^2}{\mu^2/\lambda}}.$$

At the order ε^0 in equation (2.7), we have :

$$\varepsilon^0 \quad : \quad \kappa\partial_\theta f^0 + \lambda\kappa_0\partial_\kappa f^0 = \lambda\partial_\kappa(\kappa f^1) + \frac{\mu^2}{2}\partial_{\kappa^2} f^1.$$

Although an explicit expression for f^1 is not available, we can integrate this equation against κ. This gives :

$$\frac{\mu^2}{2\lambda}\partial_\theta p_0 - \lambda\kappa_0\,p_0 = -\lambda\int_\kappa \kappa f^1\,d\kappa.$$

Now we go back to the original equation on f^ε and we integrate in κ :

$$\varepsilon(\partial_t p^\varepsilon + \vec{\tau}(\theta)\cdot\nabla_{\vec{x}} p^\varepsilon) + \partial_\theta \int_\kappa \kappa f^\varepsilon \, d\kappa + 0 = 0,$$

But now we can compute the integral at order 1 :

$$\begin{aligned}\int_\kappa \kappa f^\varepsilon \, d\kappa &= \int_\kappa \kappa(f^0 + \varepsilon f^1)\, d\kappa + O(\varepsilon^2) \\ &= 0 + \varepsilon \int_\kappa \kappa f^1 \, d\kappa + O(\varepsilon^2) \\ &= \varepsilon\left(\kappa_0\, p_0 - \frac{\mu^2}{2\lambda^2}\partial_\theta p_0\right) + O(\varepsilon^2).\end{aligned}$$

So finally we have at the limit $\varepsilon \to 0$:

$$\partial_t p^0 + \vec{\tau}(\theta)\cdot\nabla_{\vec{x}} p^0 + \partial_\theta(\kappa_0 p_0) = \frac{\mu^2}{2\lambda^2}\partial_{\theta^2} p_0.$$

We recover our initial Fokker-Planck equation for the fiber-process with $A = \frac{\mu}{\lambda}$. □

2.2 Large diffusion for the original model

Now we connect the original model with the reduced model looking at the large noise regime in the equation:

$$\begin{aligned} d\vec{x}_t &= \vec{\tau}(\theta_t)\, dt, \\ d\theta_t &= b(r_t)\sin(\theta_t - \phi_t)\, dt + A dB_t. \end{aligned}$$

Since the proof is very similar to the previous one (proposition 2.1), we defer the proof in the appendix. See also [2] for another proof.

Proposition 2.2 *Considering the dynamics given by equation (2.1) and the rescaling*

$$t' = \varepsilon t \quad , \quad A' = \sqrt{\varepsilon} A \tag{2.8}$$

leads to the reduced equations

$$d\vec{x}_t = -\frac{1}{A^2} b(r_t)\vec{\tau}(\phi_t) dt + \frac{\sqrt{2}}{A} dB_t,$$

or

$$d\vec{x}_t = -\frac{1}{A^2}\frac{b(|\vec{x}_t|)}{|\vec{x}_t|}\vec{x}_t dt + \frac{\sqrt{2}}{A} dB_t. \tag{2.9}$$

In terms of the density distribution $n(t,\vec{x})$ the Fokker-Planck equation reads:

$$\partial_t n - \frac{1}{A^2}\nabla_{\vec{x}}\cdot(b(r)\vec{\tau}(\phi)\, n) = \frac{1}{A^2}\Delta_{\vec{x}} n \tag{2.10}$$

2.3 Large diffusion limit of the smooth model

In this Section, we derive the reduced model (2.3) directly from the smooth model (2.4).

Proposition 2.3 *The following rescaling for the dynamic given by equation (2.4) :*

$$\lambda' = \varepsilon\lambda \quad ; \quad \mu' = \varepsilon^{3/2}\mu \tag{2.11}$$

together with a rescaling of time and curvature

$$t' = \varepsilon t \quad ; \quad \kappa' = \varepsilon\kappa \tag{2.12}$$

lead to a reduced model of the form

$$\partial_t n^0 - \frac{\lambda^2}{\mu^2}\nabla_{\vec{x}} \cdot \left(\vec{\tau}(\phi) b(r) n^0\right) = \frac{1}{2\lambda} D(\frac{\mu^2}{2\lambda^3})\Delta_{\vec{x}} n^0, \tag{2.13}$$

Proof. As for the proof of proposition 2.1, we have to rescale κ if we want to find a limit when ε goes to zero. Once again, we use :

$$\kappa' = \varepsilon\kappa.$$

Therefore, using (2.11) the equation for the fiber is :

$$\begin{aligned} d\vec{x}_t &= \vec{\tau}(\theta_t)\, dt \\ d\theta_t &= \frac{1}{\varepsilon}\kappa_t\, dt \\ d\kappa_t &= \frac{\lambda'}{\varepsilon}(\varepsilon\kappa_0 - \kappa)\, dt + \frac{\mu'}{\sqrt{\varepsilon}} dB_t. \end{aligned}$$

The associated Fokker-Planck equation is after the time rescale:

$$\varepsilon\partial_t f^\varepsilon + \vec{\tau}(\theta)\cdot\nabla_{\vec{x}} f^\varepsilon + \lambda\kappa_0\partial_\kappa f^\varepsilon = \frac{1}{\varepsilon}\left(-\kappa\partial_\theta f^\varepsilon + \lambda\partial_\kappa(\kappa f^\varepsilon) + \frac{\mu^2}{2}\partial_{\kappa^2} f^\varepsilon\right). \tag{2.14}$$

Let's denote by Q the operator on the right-hand side :

$$Q(f) = -\kappa\partial_\theta f + \lambda\partial_\kappa(\kappa f) + \frac{\mu^2}{2}\partial_{\kappa^2} f.$$

Making an Hilbert expansion for f^ε, we have at order ε^{-1} :

$$\varepsilon^{-1} \quad : \quad Q(f) = 0.$$

This equation is solved by :

$$f^0 = n^0(t,\vec{x})\,\frac{M(\kappa)}{2\pi},$$

where $M(\kappa)$ is a Gaussian with mean zero and variance $\frac{\mu^2}{2\lambda}$.
At order ε^0, we have :

$$\varepsilon^0 \quad : \quad \vec{\tau}(\theta)\cdot\nabla_{\vec{x}} f^0 + \lambda\kappa_0\partial_\kappa f^0 = Q(f^1).$$

This equation could not be solved explicitly for f^1. But since the equation is linear and only involved (θ,κ) variable which is decoupled in f^0, we can express f^1 as :

$$f^1 = \vec{\chi}_1\cdot\nabla_{\vec{x}} n^0 \; + \; b(r)n^0\vec{\chi}_2\cdot\begin{pmatrix} -\sin\phi \\ \cos\phi \end{pmatrix}$$

where $\vec{\chi}_1(\theta,\kappa)$ and $\vec{\chi}_2(\theta,\kappa)$ satisfy :

$$\vec{\tau}(\theta)\frac{M}{2\pi} \;=\; Q(\vec{\chi}_1) \tag{2.15}$$

$$\lambda\vec{\tau}(\theta)\partial_\kappa\left(\frac{M}{2\pi}\right) \;=\; Q(\vec{\chi}_2). \tag{2.16}$$

Now we can look at the order ε^1. We first integrate equation (2.14) over (θ,κ), this gives :

$$\partial_t n^\varepsilon + \nabla_{\vec{x}}\cdot J^\varepsilon = 0, \tag{2.17}$$

with :

$$J^\varepsilon = \frac{1}{\varepsilon}\int_{\theta,\kappa}\vec{\tau}(\theta)f^\varepsilon\,d\theta d\kappa.$$

The smaller λ the stiffer is the fiber.

Using the Hilbert expansion on f^ε, we then have :

$$\begin{aligned} J^\varepsilon &= 0 + \int_{\theta,\kappa}\vec{\tau}(\theta)f^1\,d\theta d\kappa + O(\varepsilon) \\ &= \int_{\theta,\kappa}\vec{\tau}(\theta)\left(\vec{\chi}_1\cdot\nabla_{\vec{x}} n^0 \; + \; b(r)n^0\,\vec{\chi}_2\cdot\begin{pmatrix} -\sin\phi \\ \cos\phi \end{pmatrix}\right)d\theta d\kappa \\ &= -A_1\nabla_{\vec{x}} n^0 \; - \; A_2\begin{pmatrix} -\sin\phi \\ \cos\phi \end{pmatrix}b(r)n^0 \; + \; O(\varepsilon), \end{aligned}$$

with :

$$A_1 \;=\; -\int_{\theta,\kappa}\vec{\tau}(\theta)\otimes\vec{\chi}_1\,d\theta d\kappa \tag{2.18}$$

$$A_2 \;=\; -\int_{\theta,\kappa}\vec{\tau}(\theta)\otimes\vec{\chi}_2\,d\theta d\kappa. \tag{2.19}$$

Finally, we replace J^ε by this last expression in equation (2.17) :

$$\partial_t n^\varepsilon + \nabla_{\vec{x}}\cdot\left(-A_1\nabla_{\vec{x}} n^0 \; - \; A_2\begin{pmatrix} -\sin\phi \\ \cos\phi \end{pmatrix}b(r)n^0\right) = O(\varepsilon).$$

At the limit ε goes to zero, we have :

$$\partial_t n^0 - \nabla_{\vec{x}} \cdot \left(A_2 \begin{pmatrix} -\sin\phi \\ \cos\phi \end{pmatrix} b(r) n^0 \right) = \nabla_{\vec{x}} \cdot \left(A_1 \nabla_{\vec{x}} n^0 \right). \tag{2.20}$$

To end the proof, we have to calculate the two tensors A_1, A_2. We give the result as a lemma :

Lemma 2.4 *The two tensors A_1 and A_2 given by equation (2.18) and equation (2.19) respectively are equal to :*

$$A_1 = \frac{1}{2\lambda}\mathcal{D}(\frac{\mu^2}{2\lambda^3}) Id_2 \qquad , \qquad A_2 = \frac{\lambda^2}{\mu^2} \begin{bmatrix} 0 & -1 \\ 1 & 0 \end{bmatrix},$$

where : $\mathcal{D}(\theta^2) = \int_0^\infty \exp\left(-\theta^2(-1+s+\mathrm{e}^{-s})\right) ds$ and Id_2 is the identity tensor in $\mathbb{R}^2$.

Using this lemma, we have :

$$\partial_t n^0 - \frac{\lambda^2}{\mu^2}\nabla_{\vec{x}} \cdot \left(\vec{\tau}(\phi) b(r) n^0 \right) = \frac{1}{2\lambda}\mathcal{D}(\frac{\mu^2}{2\lambda^3})\Delta_{\vec{x}} n^0, \tag{2.21}$$

which ends the proof. □

Proof Lemma 2.4. To compute the tensor A_1, we use the result established in [3] which we summarize here : let $\widetilde{\chi}$ be the solution of

$$\vec{\tau}(\theta)\frac{M_\sigma}{2\pi} = \kappa\partial_\theta\widetilde{\chi} + \partial_\kappa(\kappa\widetilde{\chi}) + \sigma^2\partial_{\kappa^2}\widetilde{\chi}, \tag{2.22}$$

with M_σ the Gaussian with mean zero and variance σ^2. Then we have :

$$-\int_{\theta,\kappa} \vec{\tau}(\theta) \otimes \widetilde{\chi}\, d\theta d\kappa = \frac{\mathcal{D}(\sigma^2)}{2}\,\mathrm{Id}_2, \tag{2.23}$$

where $\mathcal{D}(\sigma^2) = \int_0^\infty \exp\left(-\sigma^2(-1+s+\mathrm{e}^{-s})\right) ds$.

We want to express $\vec{\chi}_1$ (solution of equation (2.15)) with $\widetilde{\chi}$. In this aim, we make the change of unknowns $\lambda\kappa' = \kappa$ in (2.18). The Gaussian M is then transformed as

$$M(\kappa') = \frac{1}{\sqrt{2\pi\mu^2/2\lambda}}\,\mathrm{e}^{-\frac{\kappa^2/\lambda^2}{2\mu^2/2\lambda}} = \frac{1}{\lambda}M'(\kappa'),$$

where M' is a Gaussian with mean zero and variance $\mu^2/2\lambda^3$. With the notation $\vec{\chi'}_1 = \vec{\chi}_1(\theta, \lambda\kappa)$, the full equation (2.18) is written

$$\vec{\tau}(\theta)\frac{1}{\lambda}\frac{M'}{2\pi} = \lambda\kappa'\partial_\theta\vec{\chi'}_1 + \lambda\partial_{\kappa'}(\kappa'\vec{\chi'}_1) + \frac{\mu^2}{2\lambda^2}\,\partial_{\kappa^2}\vec{\chi'}_1$$

or again

$$\vec{\tau}(\theta)\frac{1}{\lambda^2}\frac{M'}{2\pi} = \kappa'\partial_\theta\vec{\chi'}_1 + \partial_{\kappa'}(\kappa'\vec{\chi'}_1) + \frac{\mu^2}{2\lambda^3}\,\partial_{\kappa^2}\vec{\chi'}_1.$$

Therefore, we have $\vec{\chi'}_1 = \frac{1}{\lambda^2}\,\widetilde{\chi}$, with $\widetilde{\chi}$ the solution of (2.22) with $\sigma^2 = \frac{\mu^2}{2\lambda^3}$. Now we can compute the tensor A_1 using the change of unknowns $\lambda\kappa' = \kappa$:

$$\begin{aligned} A_1 &= -\int_{\theta,\kappa} \vec{\tau}(\theta)\otimes\vec{\chi}_1\, d\theta d\kappa = -\int_{\theta,\kappa'} \vec{\tau}(\theta)\otimes\vec{\chi'}_1\,\lambda\, d\theta d\kappa' \\ &= -\int_{\theta,\kappa'} \vec{\tau}(\theta)\otimes\frac{1}{\lambda^2}\,\widetilde{\chi}\,\lambda\, d\theta d\kappa' = \frac{1}{\lambda}\,\frac{\mathcal{D}(\frac{\mu^2}{2\lambda^3})}{2}\,\mathrm{Id}_2, \end{aligned}$$

using the result of equation (2.23).

The calculus of the tensor A_2 is simpler since we can find explicitly a solution to equation (2.16) :

$$\vec{\chi}_2 = -\frac{2\lambda^2}{\mu^2}\begin{pmatrix} \sin\theta \\ -\cos\theta \end{pmatrix}\frac{M}{2\pi}$$

as we have :

$$\begin{aligned} Q(\vec{\chi}_2) &= \kappa\partial_\theta\vec{\chi}_2 + 0 = -\frac{2\lambda^2}{\mu^2}\kappa\begin{pmatrix} \cos\theta \\ \sin\theta \end{pmatrix}\frac{M}{2\pi} \\ &= \lambda\vec{\tau}(\phi)\partial_\kappa\left(\frac{M}{2\pi}\right). \end{aligned}$$

Therefore the computation of A_2 is straightforward :

$$\begin{aligned} A_2 &= -\int_{\theta,\kappa}\vec{\tau}(\theta)\otimes\left(-\frac{2\lambda^2}{\mu^2}\begin{pmatrix} \sin\theta \\ -\cos\theta \end{pmatrix}\frac{M}{2\pi}\right) d\theta d\kappa. \\ &= \frac{2\lambda^2}{\mu^2}\int_{\theta,\kappa}\begin{bmatrix} \cos\theta\,\sin\theta & -\cos^2\theta \\ \sin^2\theta & -\sin\theta\,\cos\theta \end{bmatrix}\frac{M}{2\pi}\,d\theta d\kappa \\ &= \frac{\lambda^2}{\mu^2}\begin{bmatrix} 0 & -1 \\ 1 & 0 \end{bmatrix}. \end{aligned}$$

□

Remark 2.1 Obviously the limit equations obtained in Lemma 2.3 are not exactly the reduced model (2.3) obtained in Section 2.1. However, also the scaling used in this section is still not equivalent to the combination of the scalings used in Sections 2.1. Compared to a combination of these scalings we have to rescale the coefficients λ and μ in this section once more using

$$\lambda' = \varepsilon\lambda, \quad \mu' = \varepsilon\mu$$

This leads to a constant value of $\frac{\lambda^2}{\mu^2}$ and a scaled value

$$\frac{\varepsilon}{2\lambda}\mathcal{D}(\frac{\mu^2\varepsilon}{2\lambda^3})$$

for the diffusion coefficient. According to [3] we have the following asymptotic for $\mathcal{D}$:

$$\mathcal{D}(\sigma^2) \overset{\sigma^2 \to 0}{\sim} \frac{1}{\sigma^2}.$$

Therefore since $\frac{\mu^2 \varepsilon}{2\lambda^3}$ goes to 0 as ε goes to 0, the diffusive coefficient behaves like :

$$\frac{\varepsilon}{2\lambda} D(\frac{\mu^2 \varepsilon}{2\lambda^3}) \sim \frac{1}{2\lambda} \frac{2\lambda^3}{\mu^2} = \frac{\lambda^2}{\mu^2},$$

which is exactly the diffusive coefficient we have obtained by making the big noise limit in two steps from the smooth model to the original one and then from the original model to the reduced model.

Remark 2.2 (Overview over models and scalings)
The three models discussed in this chapter are

Smooth	Original	Reduced
$d\vec{x}_t = \vec{\tau}(\theta_t)\, dt$	$d\vec{x}_t = \vec{\tau}(\theta_t)\, dt$	$d\vec{x}_t = -a_1 b(r)\vec{\tau}(\phi)dt + a_2 dB_t$
$d\theta_t = \kappa_t\, dt$	$d\theta_t = \kappa_0\, dt + A dB_t$	
$d\kappa_t = \lambda(\kappa_0 - \kappa)\, dt + \mu dB_t$		

where

$$\kappa_0 = b(r)\sin(\pi + \phi - \theta_t), \vec{x} = r\vec{\tau}(\phi). \tag{2.24}$$

The links between them are shown in Figure (4.2).

3 Numerical simulation of the model

3.1 The smooth model for different parameters

In this section we investigate the smooth model numerically. In particular, small and large values of the two parameters, λ related to the inverse elasticity module and turbulence amplitude $A = \frac{\mu}{\lambda}$ are investigated.

We first have to developp a numerical scheme to approximate the solution of the smooth model (eq. 2.4). All we have to to is to find an accurate scheme for the evolution of the curvature κ. After that we simply have to integrate in order to have the speed $\vec{\tau}(\theta)$ and the position $\vec{x}$ of the fiber.

A method to solve the equation on the curvature is simply to use an Euler scheme (see [5]). But since this equation is an Ornstein–Uhlenbeck process, we can use a more accurate method. Integrating the quantity $d(\mathrm{e}^{\lambda t}\kappa_t)$, we have the explicit expression:

$$\kappa_t = \mathrm{e}^{-\lambda t}\kappa_0 + \lambda \mathrm{e}^{\lambda t} \int_0^t \kappa_0(s)\mathrm{e}^{\lambda s}\, ds + \mu \mathrm{e}^{-\lambda t} \int_0^t \mathrm{e}^{\lambda s}\, dB_s$$

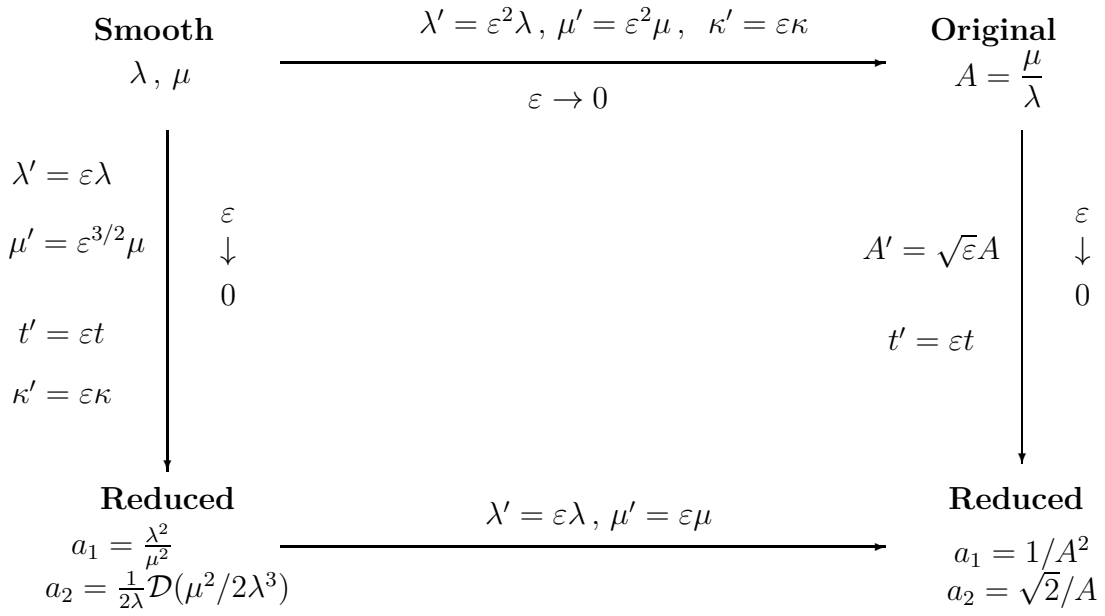

Figure 4.2: Diagram of the different scaling limits

Denoting by Δt the time step of our numerical scheme, this formulation lead at first order to the algorithm:

$$\kappa_{t_{n+1}} = \mathrm{e}^{-\lambda\Delta t}\kappa_{t_n} + (1 - \mathrm{e}^{-\lambda\Delta t})\kappa_0(t_n) + G_{t_n}$$

where κ_{t_n} is the curvature at time t_n, κ_0 is the effect of the external force (eq. 2.24), G_n is a Gaussian random variable independant of κ_{t_n} with mean 0 and variance $\frac{\mu^2}{\lambda}(1 - \mathrm{e}^{-2\lambda\Delta t})$.

After computing the new value of the curvature κ_{t_n}, we simply integrate to update the angle speed and the position using the trapezoidal rule:

$$\begin{aligned} \theta_{t_{n+1}} &= \theta_{t_n} + \Delta t\, \frac{\kappa_{t_n} + \kappa_{t_{n+1}}}{2} \\ \vec{x}_{t_{n+1}} &= \vec{x}_{t_n} + \Delta t\, \frac{\vec{\tau}(\theta_{t_n}) + \vec{\tau}(\theta_{t_{n+1}})}{2} \end{aligned}$$

where $\vec{\tau}(\theta) = (\cos\theta, \sin\theta)^T$.

In a first series of figures (4.3) the paths of the fibers for small stiffness ($\lambda = 100$) and different values of A are plotted. These plots are qualitatively the same as those for the original model. In all simulations we have chosen $b(r) = r$.

In a second series of figures (4.4) the case of moderate values of λ ($\lambda = 1$) is considered for different A. One clearly observes the smoother nature of the trajectories.

3.2 Comparison with numerical experiments

In this section the above results are qualitatively compared to the results of a numerical simulation of the full physical process developed in the software package FIDYST, see, for example [8, 9]. A more detailed quantitative comparison is planned for future work.

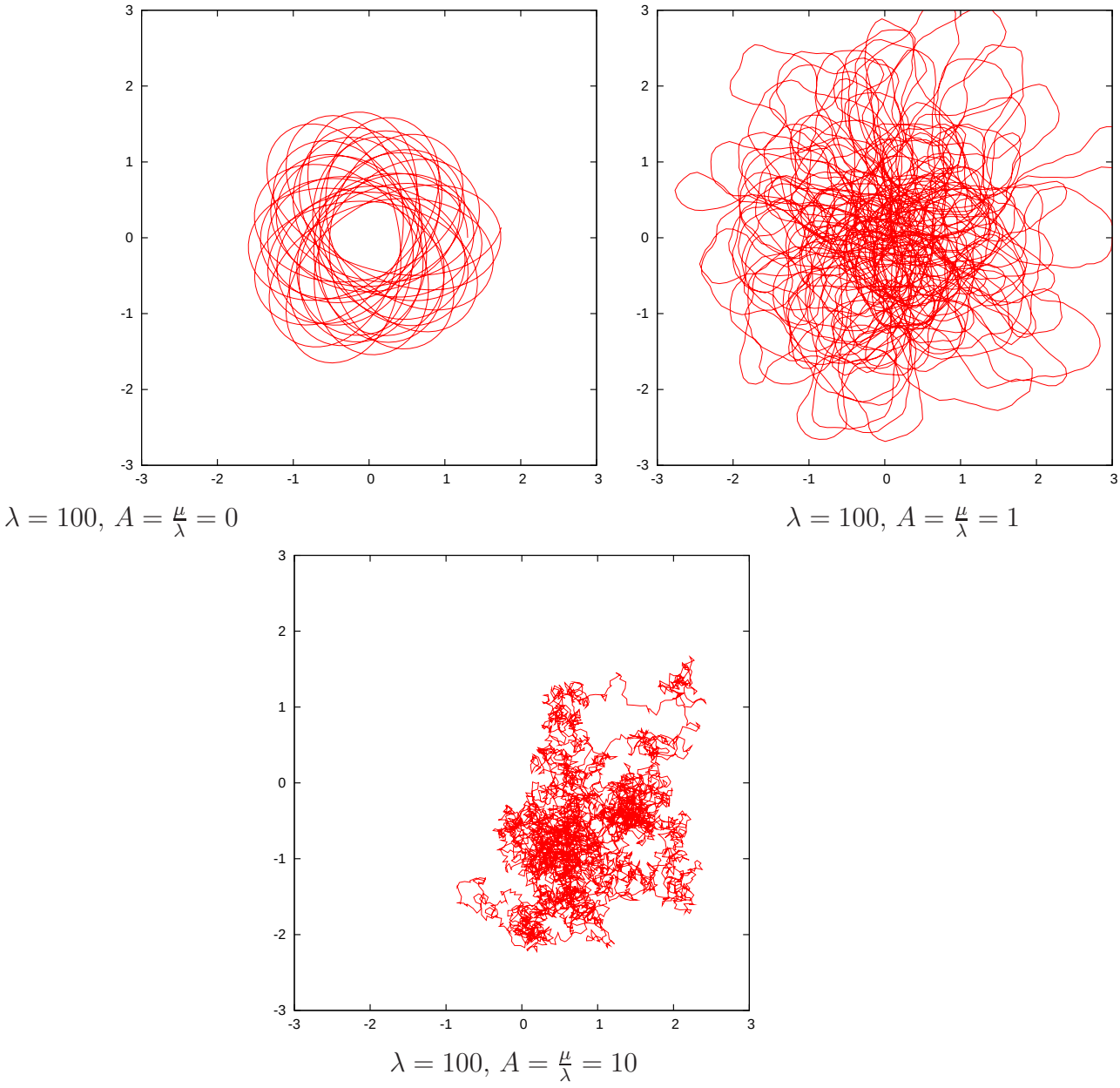

$\lambda = 100,\ A = \frac{\mu}{\lambda} = 0$

$\lambda = 100,\ A = \frac{\mu}{\lambda} = 1$

$\lambda = 100,\ A = \frac{\mu}{\lambda} = 10$

Figure 4.3: The smooth model near to the original model ($\lambda = 100$) for different values of A.

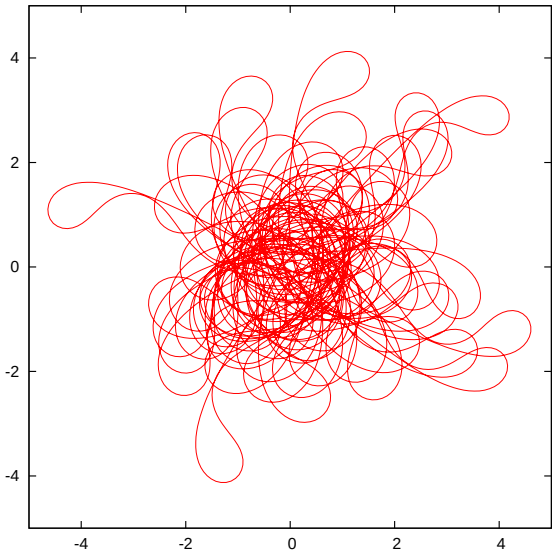

$\lambda = 1,\ A = \frac{\mu}{\lambda} = 0$

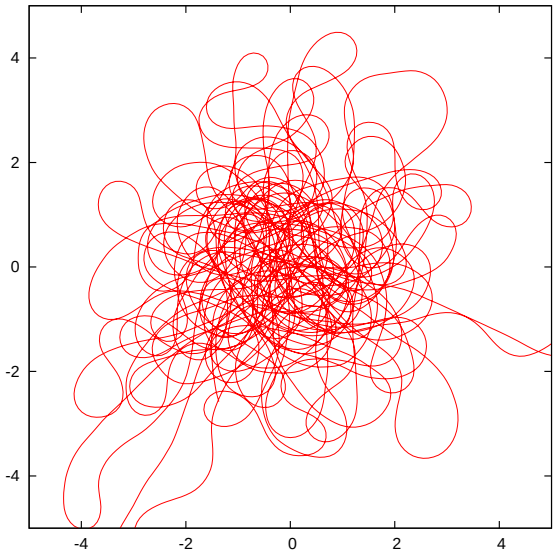

$\lambda = 1,\ A = \frac{\mu}{\lambda} = 1$

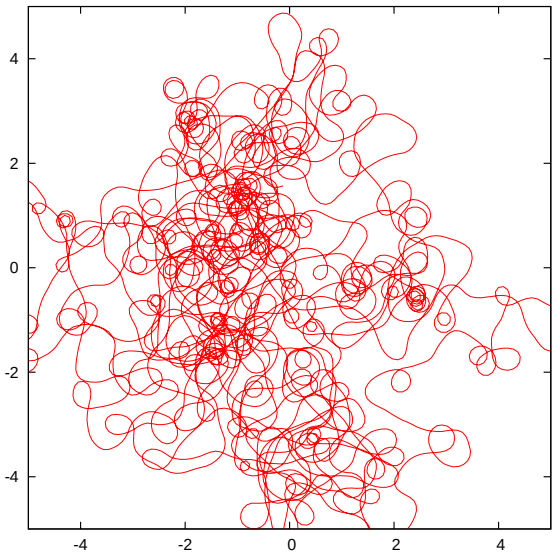

$\lambda = 1,\ A = \frac{\mu}{\lambda} = 5$

Figure 4.4: The smooth model with $\lambda = 1$ and different value of A

With FIDYST a single fiber in a spunbond process for nonwoven production is simulated. The fluid dynamic computations required for FIDYST are performed using the CFD tool FLUENT. For the simulation of the fiber dynamics the deterministic aerodynamic forces due to the mean stream and the stochastic forces due to turbulence are computed by means of the fluid dynamic results. The fiber is simulated for the full physical process between the exit nozzle and the conveyor belt including the lay-down process on the belt using a typical configuration of parameters. The fiber dynamics is given by a Newtonian equation of motion

$$\sigma\ddot{\vec{x}} = \partial_s(T(\partial_s\vec{x}) - EI\partial_{ssss}\vec{x} + f^{grav} + f^{air}$$

$$\|\partial_s\vec{x}\| = 1,$$

where the vector $\vec{x}(s,t)$ denotes the central line of the fibre.

Here, σ denotes the line density, T is a Lagrange parameter, I is the geometrical moment of inertia and E is the elasticity module. f^{grav} describes the influence of gravity and $f^{air} = f^{air}_{det} + Df^{air}_{stoch}$ give the deterministic and stochastic aerodynamic forces. In the present simulations the conveyor belt velocity is zero and a fixed distance between the nozzle and the conveyor belt is assumed. The inlet velocity of the fiber at the nozzle and the fiber length are also fixed. Only the fiber on the conveyor belt is shown. In the follwoing simulations we change the paramter E abd D.

In Figure 4.5 (upper left) a reference simulation is shown using an elasticity module $E = E_{ref}$ and a stochastic force with the parameter $D = D_{ref}$.

In Figure 4.5 (upper right) the stochastic forces are reduced by the factor 0.6, i.e. $D = 0.6D_{ref}$, leading to a more compact fiber lay-down.

Figure 4.5 (lower left) shows simulations with the original stochastic force and an increased elasticity module $E = 100E_{ref}$. This modification leads to larger loops of the fiber.

Figure 4.5 (lower right) finally shows results for reduced stochastic forces and increased elasticity module.

The paths in the upper two figures in Figure 4.5 showing a physical situation with moderate elasticity module E are qualitatively well approximated by simulations of the above stochastic model with values of A of size 3 and 2 and values of λ of size 5.

The paths in the lower two figures in Figure 4.5 showing situations with large elasticity module E. are qualitatively well approximated by simulations of the above model with values of A as above and values of λ of size 1.

4 Summary and Conclusions

In the present chapter we did remove a drawback of the model developed in [2], i.e. the non-differentiability of the paths of the process. A model with smoother trajectories is developed by introducing a relaxation approximation. This is equivalent to an approximation of the White-noise process involved in the original model by an Ohrnstein-Uhlenbeck process. The relations of the different models are investigated analytically looking at different scalings and using diffusion approximations. We also

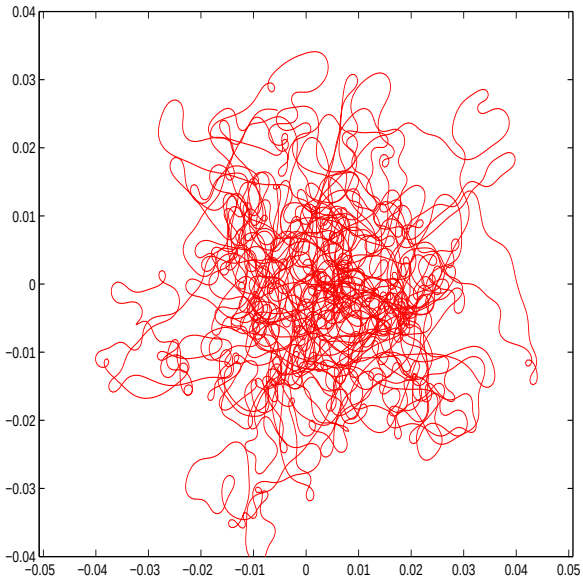

$D = D_{ref},\ E = E_{ref}$

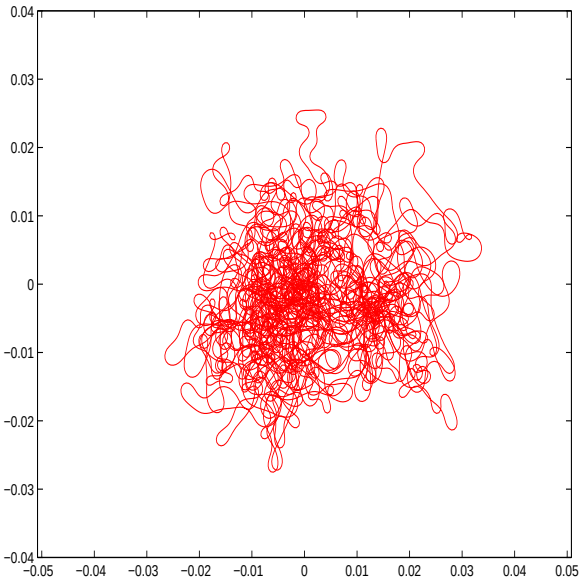

$D = 0.6D_{ref},\ E = E_{ref}$

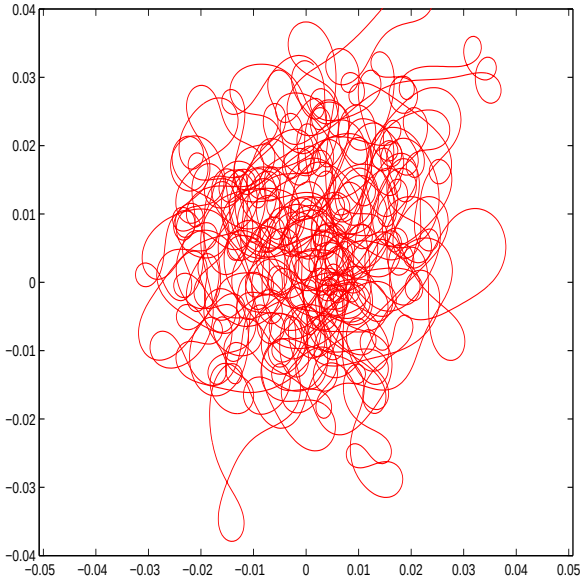

$D = D_{ref},\ E = 100E_{ref}$

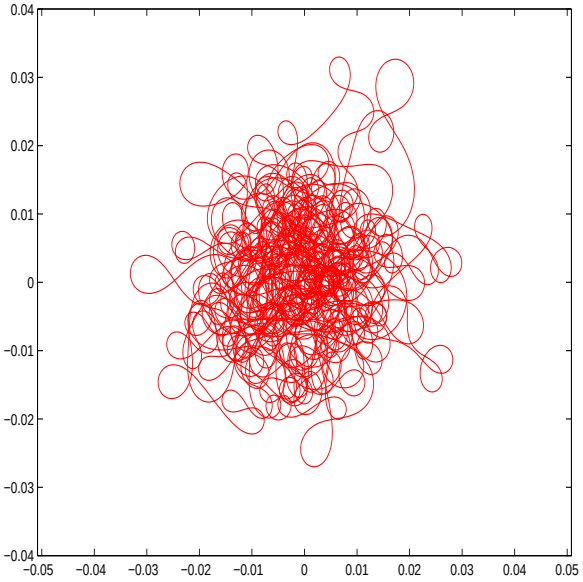

$D = 0.6D_{ref},\ E = 100E_{ref}$

Figure 4.5: Experimental results with small stochastic force (upper right), large elasticity module (lower left) and small stochastic force and large elasticity module (lower right).

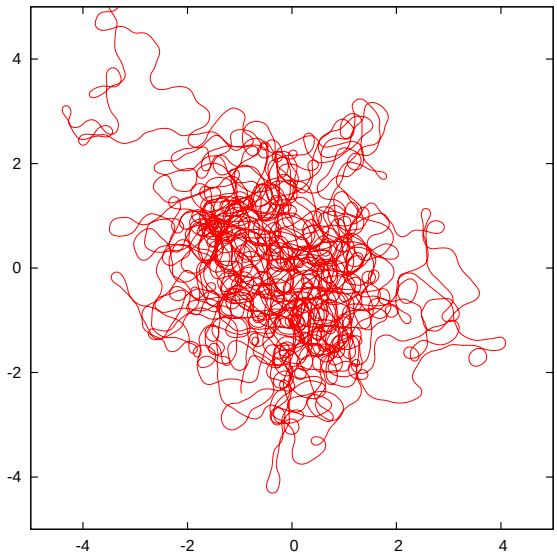

$\lambda = 5,\ A = \dfrac{\mu}{\lambda} = 3$

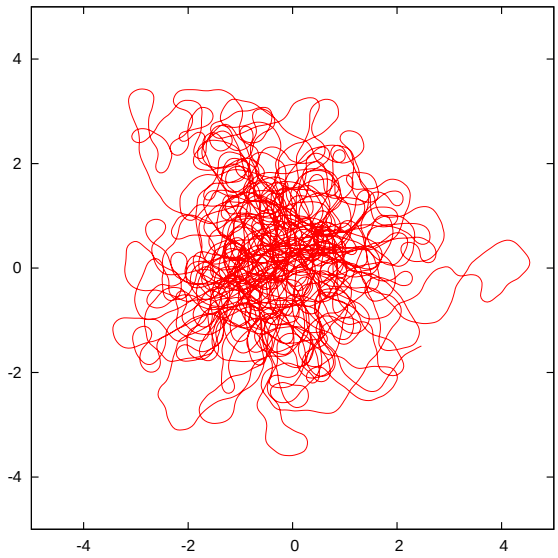

$\lambda = 5,\ A = 2$

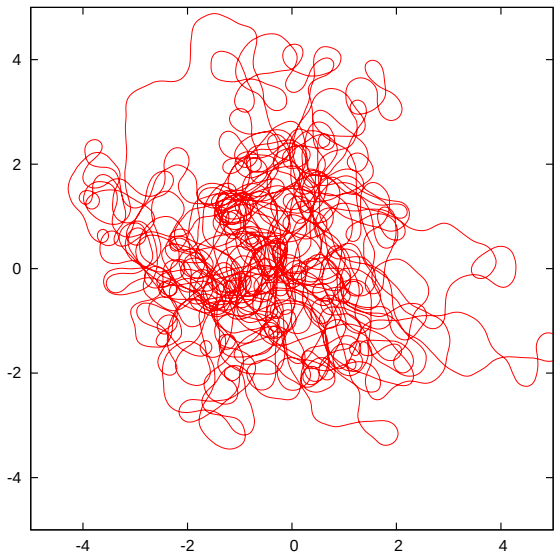

$\lambda = 2,\ A = 3$

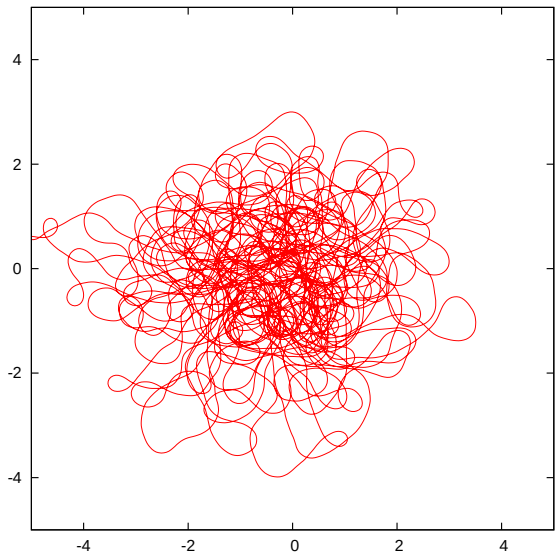

$\lambda = 2,\ A = 2$

Figure 4.6: The approximation of the experimental result using the smooth model.

included a qualitative numerical comparison of the paths of the models for different parameters. The results show the improvement of the approximation of the paths compared to the original model.

Future work will be, in particular, devoted to the identification of the parameters μ and λ in the smooth model using data generated by the simulation of the full fibre spinning process.

Appendix

Proof of Proposition 2.2. Let's take the Fokker-Planck equation associated with the equation (2.1) using the rescaling given by (2.8) :

$$\varepsilon\partial_t f^\varepsilon + \vec{\tau}(\theta)\cdot\nabla_{\vec{x}} f^\varepsilon + \partial_\theta\left(b(r)\sin(\theta-\phi)f^\varepsilon\right) = \frac{A^2}{2\varepsilon}\partial_{\theta^2} f^\varepsilon. \tag{4.25}$$

Using a Hilbert expansion for f^ε ($f^\varepsilon = f^0 + \varepsilon f^1 + \dots$), we find :

$$\varepsilon^{-1} \quad : \quad \partial_{\theta^2} f^0 = 0,$$

that means $f^0(t,\vec{x},\theta) = n^0(t,\vec{x})\,\frac{1}{2\pi}$. For the term in ε^0 we have:

$$\varepsilon^0 \quad : \quad \vec{\tau}(\theta)\cdot\nabla_{\vec{x}} f^0 + \partial_\theta\left(b(r)\sin(\theta-\phi)f^0\right) = \frac{A^2}{2}\partial_{\theta^2} f^1.$$

This equation can be explicitly solved since f^0 doesn't depend on θ. Integrating twice in θ, we have :

$$f^1 = \frac{2}{A^2}\frac{1}{2\pi}\left[-\vec{\tau}(\theta)\cdot\nabla_{\vec{x}} n^0 - b(r)\cos(\theta-\phi)\,n^0\right].$$

Finally, integrating the original equation for f^ε in θ, we have :

$$\varepsilon^{-1} \quad : \quad \varepsilon\partial_t n^\varepsilon + \nabla_{\vec{x}}\cdot\left(\int_0^{2\pi}\vec{\tau}(\theta)\,f^\varepsilon\,d\theta\right) = 0.$$

Replacing f^ε by its Hilbert expansion, we have :

$$\partial_t n^0 + \nabla_{\vec{x}}\cdot\left(\int_0^{2\pi}\vec{\tau}(\theta)\,f^1\,d\theta\right) = O(\varepsilon). \tag{4.26}$$

Then by some easy computations, we can evaluate the integral :

$$\begin{aligned}\int_0^{2\pi}\vec{\tau}(\theta)\,f^1\,d\theta &= \frac{1}{2\pi}\frac{2}{A^2}\int_0^{2\pi}\left[\nabla_{\vec{x}} n^0\,\vec{\tau}(\theta)\otimes\vec{\tau}(\theta) - b(r)\cos(\theta-\phi)\vec{\tau}(\theta)\,n^0\right]d\theta \\ &= -\frac{1}{\pi A^2}\left[\nabla_{\vec{x}} n^0\,\pi \;-\; b(r)n^0\int_0^{2\pi}\cos(\theta-\phi)\vec{\tau}(\theta)\,d\theta\right].\end{aligned}$$

Or we can develop the cosines of $(\theta-\phi)$, this gives :

$$\begin{aligned}\int_0^{2\pi}\cos(\theta-\phi)\vec{\tau}(\theta)\,d\theta &= \int_0^{2\pi}(\cos\theta\cos\phi+\sin\theta\sin\phi)\vec{\tau}(\theta)\,d\theta \\ &= \pi\begin{pmatrix}\cos\phi\\ \sin\phi\end{pmatrix}.\end{aligned}$$

Therefore, we have :

$$\int_0^{2\pi} \vec{\tau}(\theta)\, f^1\, d\theta = -\frac{1}{A^2}\,[\nabla_{\vec{x}} n^0 \;-\; b(r) n^0 \vec{\tau}(\phi)].$$

Now if we go back to equation (4.26), we have at the limit ε goes to zero :

$$\partial_t n^0 - \frac{1}{A^2}\nabla_{\vec{x}} \cdot \Big(b(r)\vec{\tau}(\phi)\, n^0\Big) = \frac{1}{A^2}\,\Delta_{\vec{x}} n^0.$$

□

Acknowledgments : Grateful acknowledgement is due to Egide for its financial support.

Bibliography

[1] T. Goetz, A. Klar, N. Marheineke, and R. Wegener, *A stochastic model for the fiber lay-down process in the nonwoven production*, SIAM J. Appl. Math., (2007). In press

[2] L. L. Bonilla, T. Goetz, A. Klar, N. Marheineke, R. Wegener *Hydrodynamic limit of a Fokker Planck equation describing fiber lay down processes*, SIAM J. Appl. Math., (2007). In press

[3] P. Degond, S. Motsch, *Large-scale dynamics of the Persistent Turning Walker model of fish behaviour*, J. Stat. Phys., 131(6):989–1021, 2008

[4] L. Arnold, *Stochastic Differential equations*, Springer, 1978.

[5] B. Oksendal, *Stochastic differential equations*, Springer-Verlag, 1992.

[6] M. Grothaus and A. Klar, *Ergodicity and rate of convergence for a non-sectorial fiber lay-down process*, preprint

[7] A. Klar, P. Reuterswärd, M. Seaïd *A semi-Lagrangian method for a Fokker-Planck equation describing fiber dynamics*, preprint

[8] N. Marheineke, R. Wegener, *Fiber dynamics in turbulent flows: General modeling framework*, SIAM J. Appl. Math. 66(5), 1703-1726, 2006.

[9] N. Marheineke, R. Wegener, *Fiber dynamics in turbulent flows: Specific Taylor drag*, SIAM J. Appl. Math., to appear

Chapter 5

The effect of group sizes on the displacement of the Kuhlia mugil fish

This chapter is a work in progress in collaboration with J. Gautrais, C. Jost and G. Theraulaz.

Abstract. In the experiments realized on the Kuhlia mugil fish, we observe a loss of cohesion of the group when the density of fish increases. In this work in progress, we develop different tools to measure this effect.

The different characteristics obtained would be used in the future to compare the experiments with an effective model for interacting fish.

---

1 Introduction

The formation of fish school is a very impressive phenomenon which is hard to understand. The main question is to link the individual behavior of fish with the global dynamic of the group. What is the key element of the fish to enable the group to self-organized?
There is a lot of literature about individual based model where authors manage to produce global alignment with simples between fish. Nevertheless, models do not give answer about the mechanics underlying animal groups. Different models could give the same pattern for the group. This is why it is necessary to measure how fish behave in real experiments.

Here, we are interested in the density effect on the fish behavior at the individual and global level. In the experiments realized on the Kuhlia mugil fish, we observe a loss of cohesion when the density of fish increases. Simple model like the Vicsek model [20] have a different behavior: when we increase the density of particles, the cohesion of the group grows. How could we measure and explain this loss at cohesion at the global and individual level in the experiments?

To answer this question, we group together experiments with the same number of fish. To observe the difference and the common points of the fish dynamics depending on the group size, we analyze the data collected at two different levels. First at the group level, we observe the main phenomena. As the group size increases, the cohesion of the group decreases. But other differences are also observed, the spatial distribution of fish are different depending on the group size.

Then, we would like to understand how the global behavior of the group emerge from the individual behavior. Therefore, we have to observe how the individual fish behave. We first look at the individual behavior looking at fish separately. We do observe common and different statistics. To connect the individual behavior with the global dynamics, we finally look at an intermediate level, we measure the pair-wise proximities/cohesion between fish. We observe similarities in the position of neighbors for different group size. But as the group size increase, the pairwise cohesion decreases.

2 Data collection

The fish species studied is the Kuhlia mugil, a pelagic fish living in the Indian and Pacific ocean. The size of this fish is around 22-25 centimeters. The experiments realized consist in letting the fish swim in a circular tank and recording their position. The diameter of the tank used is 4 meters and the depth of the water is 1.2 meter. A camera is placed above the basin to record the planar coordinate of the fish. Once we have the trajectories, a wavelet filtering is used to remove the beating mode of swimming (see [11] for more details about the wavelet filtering and [18] for the device used).

We finally have 2 minutes of recording for several experiments with 12 frames per second. There are 9 experiments with isolated fish, 6 experiments with 2 and 5 fish and 5 experiments with 10, 15, 30 fish.

The experiments with isolated fish [11] led to a new model (the Persistent Turning Walker model) where fish are supposed to move with a constant speed and their angular speeds satisfy a stochastic differential equation. In the following, we focus our analysis on the experiments with several fish.

3 Global behavior

One of the main characteristic of fish school is that the group is highly polarized, fish tend to swim in the same direction. To analyze this collective behavior, a common measure is the group polarization. This quantity denoted by φ is defined as the average of all the (normalized) velocity of fish:

$$\varphi(t) = \left| \frac{1}{N} \sum_{i=1}^{N} \frac{\vec{v}(t)}{|\vec{v}(t)|} \right|, \tag{3.1}$$

where N is the number of fish, $\vec{v}_i$ the velocity of the i$^{\text{th}}$ fish. The group is highly polarized when φ is around 1 and unpolarized when φ is around zero. To observe how the group polarization depends on the number of fish, we group together experiments with the same number of fish. Then we compute the distribution of the parameter φ during these experiments (figure 5.3). As we can see, the group polarization decreases as the number of fish increases. We can also observe this decreasing when we compute the average value of the group polarization (table 5.1). We cannot deduce from this

	2 fish	5 fish	10 fish	15 fish	30 fish
$\mathbb{E}[\varphi]$	0.884	0.612	0.387	0.304	0.225

Table 5.1: The mean value of the parameter order φ (eq. 3.1) for different group sizes.

decrease of the group polarization that the group is more disorganized. Fish could also be in "torus formation" which means they turn around a virtual center. In this formation, the group polarization is very low. To infirm or confirm this hypothesis, we compute the angular momentum of the group. If $\vec{x}_c$ is the center of the group ($\vec{x}_c = \frac{1}{N}\sum_{i=1}^{N} \vec{x}_i$ with N the number of fish and $\vec{x}_i$ their position), the angular momentum is defined as:.

$$L_c = \frac{1}{N} \sum_{i=1}^{N} (\vec{x}_i - \vec{x}_c) \wedge \frac{\vec{v}_i}{|\vec{v}_i|}, \tag{3.2}$$

where $\wedge$ is the cross product. If fish are in a vortex formation, the absolute value of the angular momentum $|L_c|$ would have an higher value. But as we see in the figure 5.4 and table 5.2, the angular momentum decreases as the group size increases. Therefore, there is no vortex formation in the experiments. According to the mean velocity φ and the angular momentum, the fish are less coordinated when the density increases.

Remark 3.1 We have to take care that φ is not independent of the number of individuals N. If individuals are independent ($\vec{v}_i$ are independent), φ is zero when N is large. But for small value of N, φ has an higher value (figure 5.5).

	2 fish	5 fish	10 fish	15 fish	30 fish
$\mathbb{E}[\|L_c\|]$	0.141	0.0556	0.0239	0.0116	0.00568

Table 5.2: The mean value of absolute angular momentum $|L_c|$ (eq. 3.2) for different group sizes.

Group polarity and angular momentum are only two indications about the group formation. The spatial distribution of fish and the flux give more precise information about the dynamics of the group. More precisely, we introduce:

- $\rho(t, \vec{x})$ the density distribution of finding fish at time t with position in a small neighborhood of $\vec{x}$,
- $J(t, \vec{x})$ the flux of fish at time t with position in a small neighborhood of $\vec{x}$.

In the experiments, since the number of fish is low, we have to take a mean in time of the density distribution, otherwise, the granular effect on the distribution would be too strong. For example, with the spatial distribution of fish, we introduce:

$$\bar{\rho}(\vec{x}) = \frac{1}{T} \int_0^T \rho(t, \vec{x})\, dt. \tag{3.3}$$

Numerically, we use Particle-In-Cell method to estimate the distribution [10, 13]. In figure 5.6, we plot the spatial distribution $\bar{\rho}$ for different group sizes. All the distributions have a maximum value at the center of the domain (see figure 5.6) and decreases near the boundary. This observation confirms the repulsive effect of the wall on fish measured for isolated fish [11]. Ants and cockroaches have another behavior, they tend to follow the wall (thigmotactism) [3, 15]. We also observe that the density is more spread out for the experiments with 2 and 30 fish.

For the flux J, the average in time is more problematic. Usually, the mean value obtained is around zero, since there is no reason for the fish to move at a certain point in a certain direction. Nevertheless, for some experiments where the cohesion of the group is important, we do observe a pattern for the flux 5.7. The persistence of this pattern over time is due to the group dynamics. For isolated fish, we could not observe this phenomenon.

4 Individual behavior

4.1 Individual characteristics

To quantify the individual behavior of fish, we analyze three different variables, the position $\vec{x}$ of the fish, its velocity $\vec{v}$ and its acceleration $\vec{a}$. In this part we introduce different tools to analyze them. In order to detect the effect of the group size, in the following we group together the experiments with the same number of fish.

In the experiments with isolated fish, the speed of each fish is approximately constant [11]. But the speed differs between experiments. Therefore it is not surprising

that in the experiments with several fish, the distribution of speed is not concentrated around one single value (figure 5.8). Moreover, we can observe that each speed distribution has two main values. These two peaks coincide with two different behaviors for fish, they can be at rest or "active". Another information contained in the distribution is that fish in the experiments with 2 and 30 fish are faster, the proportion of active fish is higher.

The distributions of angular speed are much more homogeneous (figure 5.9). All the distributions have a Gaussian shape with zero mean and a variance around $0.8\,s^{-2}$. This characteristic is important since it does not depend on the group size.

The distributions of speed and angular speed give information about the average behavior of the fish. To observe the evolution in time of velocity and angular speed, we compute the autocorrelation function. The autocorrelation is defined as

$$R(t) = \mathrm{Cor}[X(.+t)\,,\, X(.)] \tag{4.4}$$

where X is a random variable and $\mathrm{Cor}(X, Y)$ is the correlation coefficient between two random variables. The autocorrelation gives information on how long a variable is correlated in time. The faster R decreases, the faster the variable decorrelates. In figure 5.10, we compute the autocorrelation of θ (the angle of the velocity vector $\vec{v}$) and the autocorrelation of W the angular speed. We first observe that the decorrelation of θ and W is faster in the experiments with 2 and 30 fish. Since fish are faster in these experiments, we deduce from these graphics that the speed increases the variation in the fish behavior. But the autocorrelation of W is very noisy because we have to compute the second derivative of the position $\vec{x}$ to have W. Nevertheless, we can see that R_W has a strong decrease during 1 second and a slower decrease after that.

A common measure to analyze the vector position $\vec{x}$ is the Mean Square Displacement (MSD). This measure expresses how far a fish is from its original position at a certain time t. The MSD is defined by the following formula:

$$MSD(t) = \mathbb{E}[|\vec{x}(.+t) - \vec{x}(.)|^2] =< |\vec{x}(.+t) - \vec{x}(.)|^2 > . \tag{4.5}$$

where $|.|$ is the Euclidean norm. The MSD has been used in [11] for isolated fish to compare the PTW model with experiments. Typically, the MSD has an asymptotically linear growth when individuals are isolated:

$$MSD(t) \overset{t\to\infty}{\longrightarrow} \mathcal{D}t \tag{4.6}$$

where $\mathcal{D}$ is the so-called diffusion coefficient. When fish are interacting, the asymptotic behavior of the MSD could be different, we could have a power law growth different from 1/2 (see for example [12], where authors obtained different power law growth for the mean square displacement with models of self-propelled particles). In the experiments with the Kuhlia mugil fish, the domain is bounded, the fish could cover the basin in less than 8 seconds. Therefore, it is hard to detect the asymptotic behavior of the MSD. Nevertheless, as we can see in figure 5.11, we have a linear growth at the beginning of the MSD. The slope has a higher value within the experiments with 2 and 30 fish. This could be explained by the difference of speed between groups (figure 5.8).

	2 fish	5 fish	10 fish	15 fish	30 fish
Diffusion coefficient	0.374	0.153	0.143	0.201	0.405

Table 5.3: Diffusion coefficient (m^2/s) estimated for different group sizes.

For a large period of time, the MSD oscillates with a certain frequency. This behavior can be explained in this way: fish have a tendency to turn inside the basin (figure 5.7), therefore after a certain period of time τ, it is more likely that fish get back to their original position. During the period of time τ, the MSD would have a large value at time $\tau/2$ and a smaller one at time τ.

The long time behavior of the MSD gives another information. The maximum value of the MSD is higher in the experiments with 2 and 30 fish. But we have already seen that the spatial distribution of fish is more spread out in these experiments (figure 5.6). Therefore, it is not surprising that the MSD reaches higher values with 2 and 30 fish. In the experiments with 5, 10 and 15 fish since fish stay in the middle of the domain, the distance between two different positions $|\vec{x}(.+t) - \vec{x}(.)|$ can not be large.

4.2 Individual and its neighbors

To connect the individual and collective behaviors of fish, we need to understand how fish interact with its neighbors. Usually, fish models assert three different behaviors for fish (repulsion-alignment-attraction) depending on the relative position of theirs neighbors. In this part, we would like to measure in the experiments how fish are influence by theirs congeners depending on their relative position.

As a first step, we first measure how the inter-individual distance is distributed, then we observe how this distance influenced the coherence between fish.

4.2.1 Distribution of inter-individual distance

The distance is an important characteristic of the group. The distribution of inter-individual distance, also called Radial Distribution Function (RDF), can measure what is the comfort distance between fish.

Mathematically, the RDF is the probability to find two fish at a certain distance r. In figure 5.12, we estimate the RDF for the different group sizes. We observe that the maximum value of all the distribution is at a distance around 0.3 meter which corresponds to approximately with one body length. This information is interesting because it does not depend on the group size. This measure could be used to determine zone of interaction, in particular the zone where fish reach their comfort position.

When we estimate the RDF, we compute the distance between fish (i.e. $|\vec{x}_j - \vec{x}_i|$). Therefore, we loose information on the relative position of fish. For example, we do not take into account if the fish P_j is at the left side or the right side of P_i. To incorporate this information, we compute the relative position of P_j in the frame of reference of P_i. This means that we calculate the position of P_j from the point of view of the fish P_i (figure 5.1).

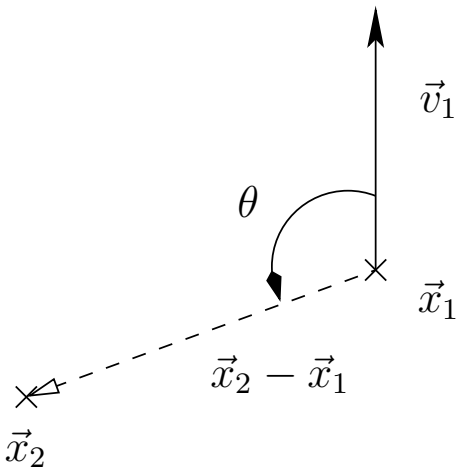

Figure 5.1: The relative position of a neighbor P_j in the frame of reference of P_i.

Mathematically, this vector is defined as :

$$R_{-\theta_i}(\vec{x}_j - \vec{x}_i) \tag{4.7}$$

where θ_i is the direction of the velocity of the fish P_i. In figure 5.13, we estimate the probability to find a neighbor at different position around a fish. In the experiments with two fish, we observe that fish have a tendency to be in front of the other one. For the other experiments, the distributions become isotropic as the group size increases. Nevertheless, we observe a small region around the fish where the density is low. The maximum value of the distribution is obtained at a distance around 0.3 meter as the radial distribution function suggests (figure 5.12).

4.2.2 Distance and alignment

In a shoal of fish, individual are aligned with their closed neighbors. The question is how far fish remain aligned. In this part, we want to measure how the alignment between fish depends on their relative distance.

To measure alignment between two fish, we take the scalar product of their normalized vector velocity (figure 5.2). Fish are polarized when the scalar product is around 1 and unpolarized when the scalar product is around 0. After that, we take all the pairs of fish that have a relative distance r (i.e. $|\vec{x}_j - \vec{x}_i| = r$) and we estimate the mean value of the scalar product of their velocity. We call the quantity obtained the velocity correlation function (VCF). As expected, the VCF has higher value for small distance r (fish are aligned) and decrease to zero for long distance (figure 5.14). Moreover the VCF is not simply a decreasing function: for short distance, the function increases. This means that fish need a certain distance to be aligned. But the main information contains in the figure 5.14 is that the VCF decreases drastically as the number of fish increases. This means that single fish becomes less coordinate with its neighbors. We already have seen that the group is less coordinated as the number of fish increases, the new information is that there is also a loss of coordination between fish *locally*.

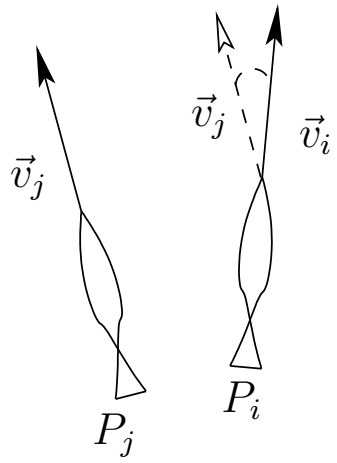

Figure 5.2: To measure the alignment between two fish, we compute the scalar product of their normalized velocity.

When we take the distance between fish, we loose information on the relative position of the neighbors. To include this element, we use as in figure .. the relative position of neighbors in the frame of reference of a fish. In more details, for a given pair of fish P_1 and P_2, we compute the mean velocity of P_2 in the frame of reference of P_1. In figure 5.15, we plot the vector field obtained for the experiments with 2, 5, 15 and 30 fish. We observe a region around the fish where the vectors are aligned.

4.2.3 Distance and acceleration

In the basin, fish have a tendency to turn around in the same direction. As the consequence, the angular speed of fish are correlated. We can measure this tendency as we have done for the alignment. We simply take the scalar product of the accelerations for each pair fish and we express the mean value of this quantity depending on the distance between fish. The distribution obtained is called acceleration correlation function.

But the estimation of the acceleration is very noisy as we have already seen for the angular speed (figure 5.9). Therefore, the acceleration correlation function will fluctuate a lot. To reduce this effect, we use a large step size to estimate it ($\Delta r = 20$ cm). In figure 5.16, we plot the angular speed correlation for different group size. For short distance, we observe a positive correlation for the angular speed in the experiments with 2 and 5 fish.

For example, in the experiments with 2 fish, we plot the acceleration of one fish, noted P_2, in the frame of reference of its neighbor, noted P_1. At short distance, we do not detect any clear correlation between the relative position of P_2 around P_1 and the acceleration of P_2 (figure 5.17). Then we distinguish between two situations whether P_1 turns to the left or to the right. We clearly see that the acceleration of P_2 is mainly determine by the acceleration of P_1 at short distance (figure 5.18). These graphics confirm that the acceleration of fish are correlated when the fish are closed (figure 5.16).

4.2.4 Nearest neighbors

As we have seen in the previous part, the distance has a strong influence on the alignment between fish. But it has been observed for flocks of birds [2] that the influence of a congener does not depend only on the distance, it also depends if a congener is the nearest neighbors or the second nearest neighbors and so on. In this part, we compute once again the previous index (distance, alignment, angular speed correlation) but this time with respect to nearest neighbors. In term of probability, we would say that we *conditionate* by the position order (nearest neighbor, second nearest neighbor,...) instead of conditioning by the distance r.

We first measure the mean distance of the nearest neighbor. To do so, we proceed as follows: for each fish, we compute the distance of every neighbors and we order the distance obtained. Then, we take the mean of the distance for the nearest one, the second nearest one, etc. As we observe in figure 5.19, the mean distances decrease as the number of fish increases. But there is no clear relationship between the density of fish in the basin and the mean distance of nearest neighbors. For example, it is surprising that the mean distance for the four nearest neighbors are the same within experiments with 15 and 30 fish. One explanation could be that fish in the experiments with 30 fish are more spread out in the domain which increase the distance between fish. This could compensate the increase of the density which has the opposite effect to reduce the distance between fish.

Concerning the relative position of the nearest neighbors, we have to compute the angle direction of the neighbors, denoted by α (see figure 5.1). Then, we can take the density distribution of the angle α. As it could be expect, in the experiments with two fish, the density distribution of α has a strong anisotropy (see figure 5.20). There is an higher probability to have a fish in front or behind the other one. The anisotropy on the distribution of α completely disappears for the other group sizes (figure 5.20). The distribution of α is uniform for every group size whatever the nearest neighbors we take. To be exact, there is anisotropy for the distribution of the farthest neighbors within experiments with 30 fish (figure 5.21). This is due to the shape of the basin. When fish are near the boundary, they are usually aligned with the wall, therefore it is more likely that the farthest neighbors would be sidelong (figure 5.21).

The computation of the density distribution of α (the angle direction of the nearest neighbors) is motivated by the work [2] on birds where they observe a strong anisotropy of the 6th or 7th nearest neighbors. We do not have this phenomenon in our experiments with fish, except in the experiments with 2 fish.

To measure the alignment between a fish and its nearest neighbor, we take once again the scalar product of their normalized velocity vector. We plot the mean value of this scalar product in figure 5.22. As we could expect, the alignment decreases as we take into account farther neighbors. We also observe that the alignment with the first and second nearest neighbors decreases as the group size increases. The experiments with 10 and 15 unable to go further the second nearest neighbors. As we have seen in figure 5.19, the mean distance with the 4 nearest neighbors are similar, therefore it is surprising that the alignment is different (alignment is weaker in the experiments with 30 fish). Two characteristics could explain this phenomena. In the experiments with

30 fish, the fish are more likely near the boundary of the domain, therefore they are more influenced by the boundary. But we also have seen that fish are also faster at thirty. If fish anticipate their future positions, the avoidance effect should be stronger.

Our last graphic (figure 5.23) represents the product of the angular speed between a fish and its nearest neighbors ($W_i W_j$). For the experiments with 2 and 5 fish, we have positive values and the curves decrease as we look at farther neighbors. But the interpretation of the curves is difficult for the others experiments.

5 Graphics

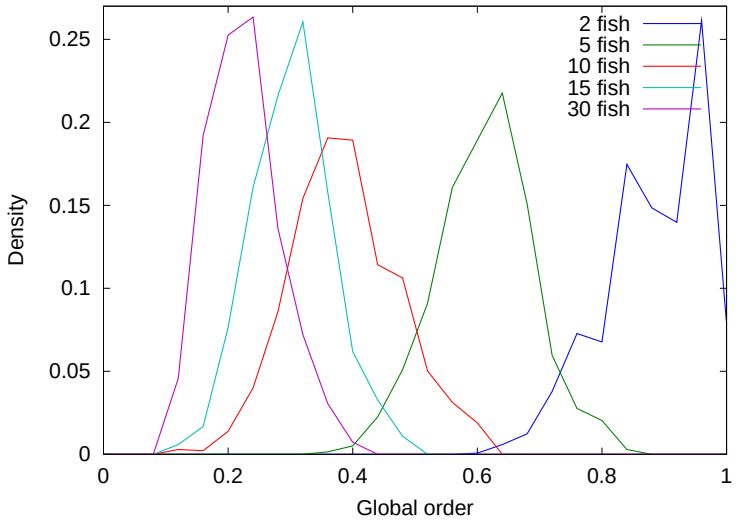

Figure 5.3: The distribution of the global order φ for different group sizes. Surprisingly, when we increase the number of fish, the group becomes less polarized.

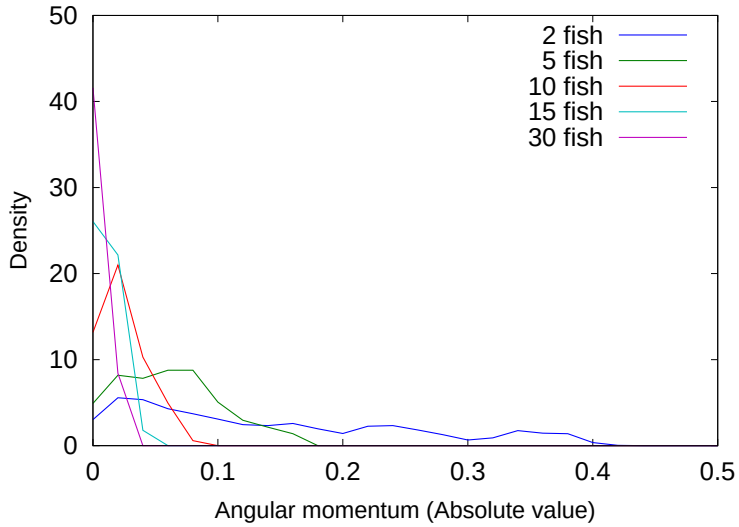

Figure 5.4: The distribution of the absolute value of the angular momentum $|L_c|$ for different group sizes. As the group size increases, the angular momentum decreases.

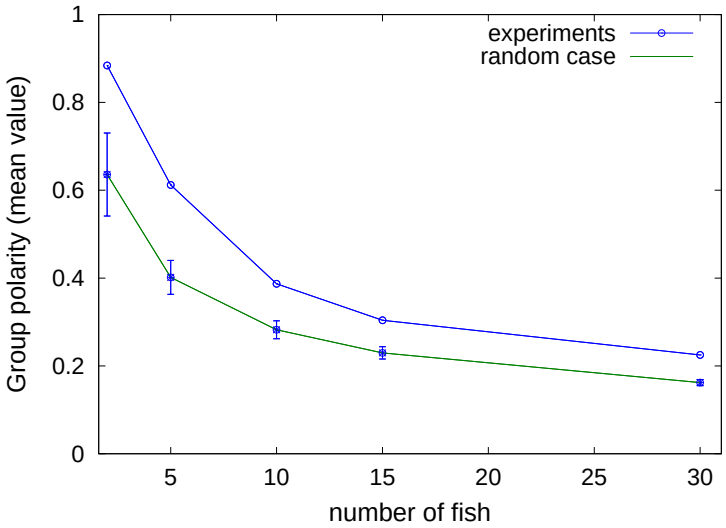

Figure 5.5: The mean value of the group polarity (φ) in the experiments and for a random distribution of velocity. The group polarity depends on the group size, the mean value decreases as the group size increases. We estimate the mean value of the group polarity with 10^5 replicates for each group size in the random case.

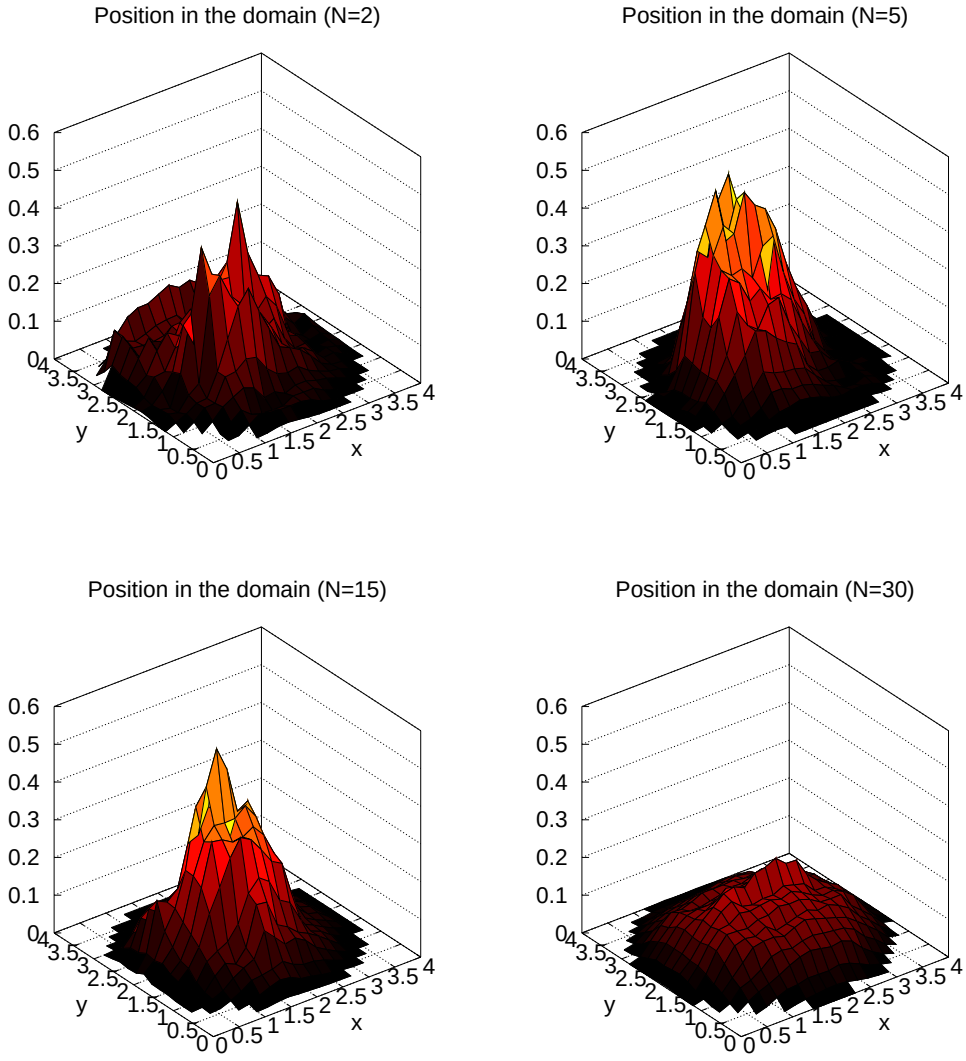

Figure 5.6: The distribution of fish in the basin for 4 group sizes (2, 5, 15 and 30 fish). We take a mean over all the experiments and time. The distribution are more concentrated in the center of the basin with 5 and 15.).

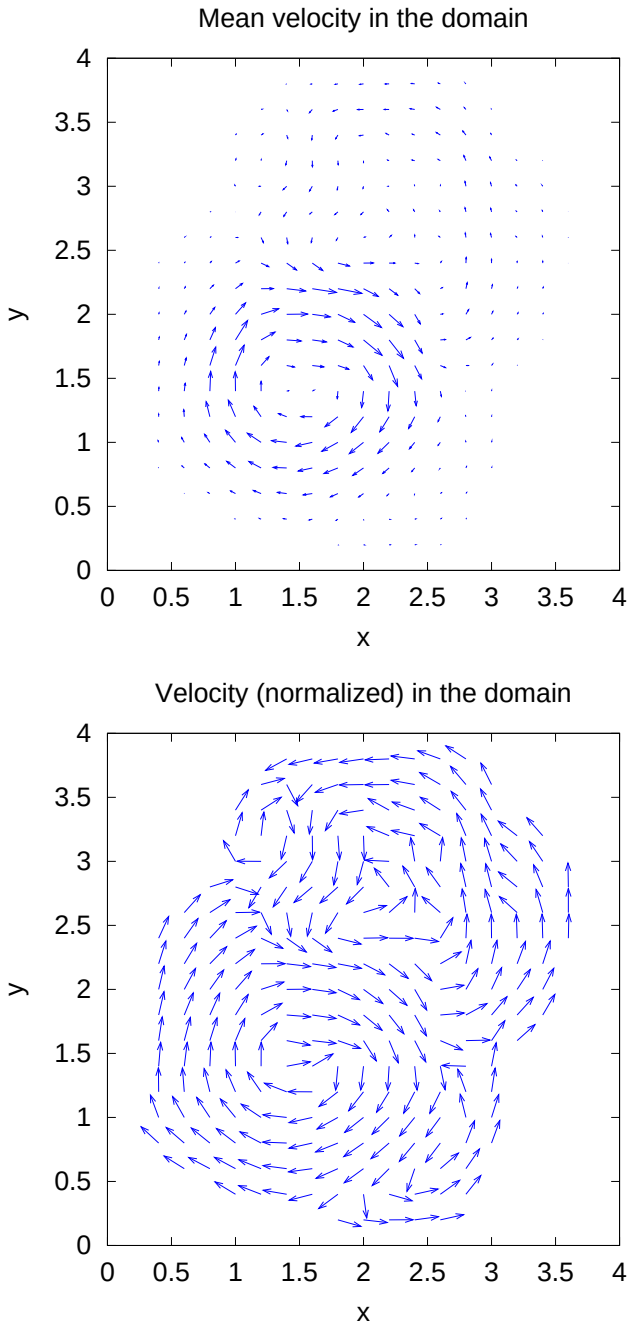

Figure 5.7: The flux $\bar{J}$ (eq. 3.3) ($\bar{J}$ is normalized at the lower figure) in the $6th$ experiment with 5 fish.

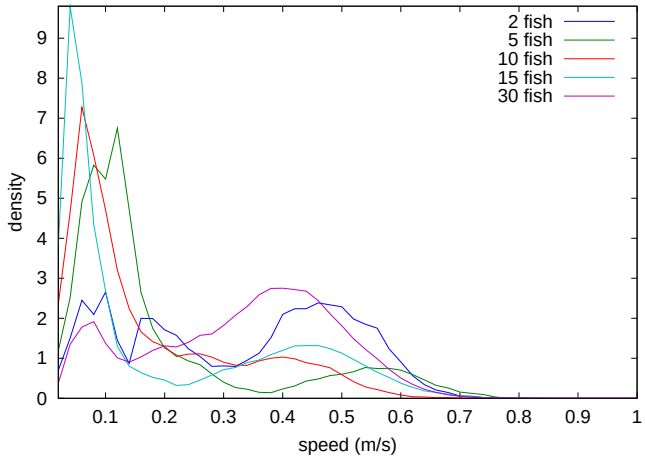

Figure 5.8: The norm of the velocity $|V|$ for different group sizes. There are two peaks in the distributions. This could indicate that fish have two main behaviors during the experiments, at rest or "active".

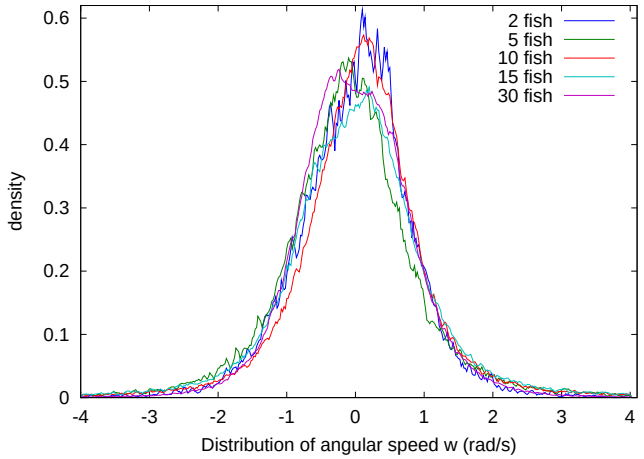

Figure 5.9: The distribution of the angular speed W for different group sizes. The distribution have Gaussian shape for each group sizes. The variance of the distribution is around .8 $(1/s^2)$.

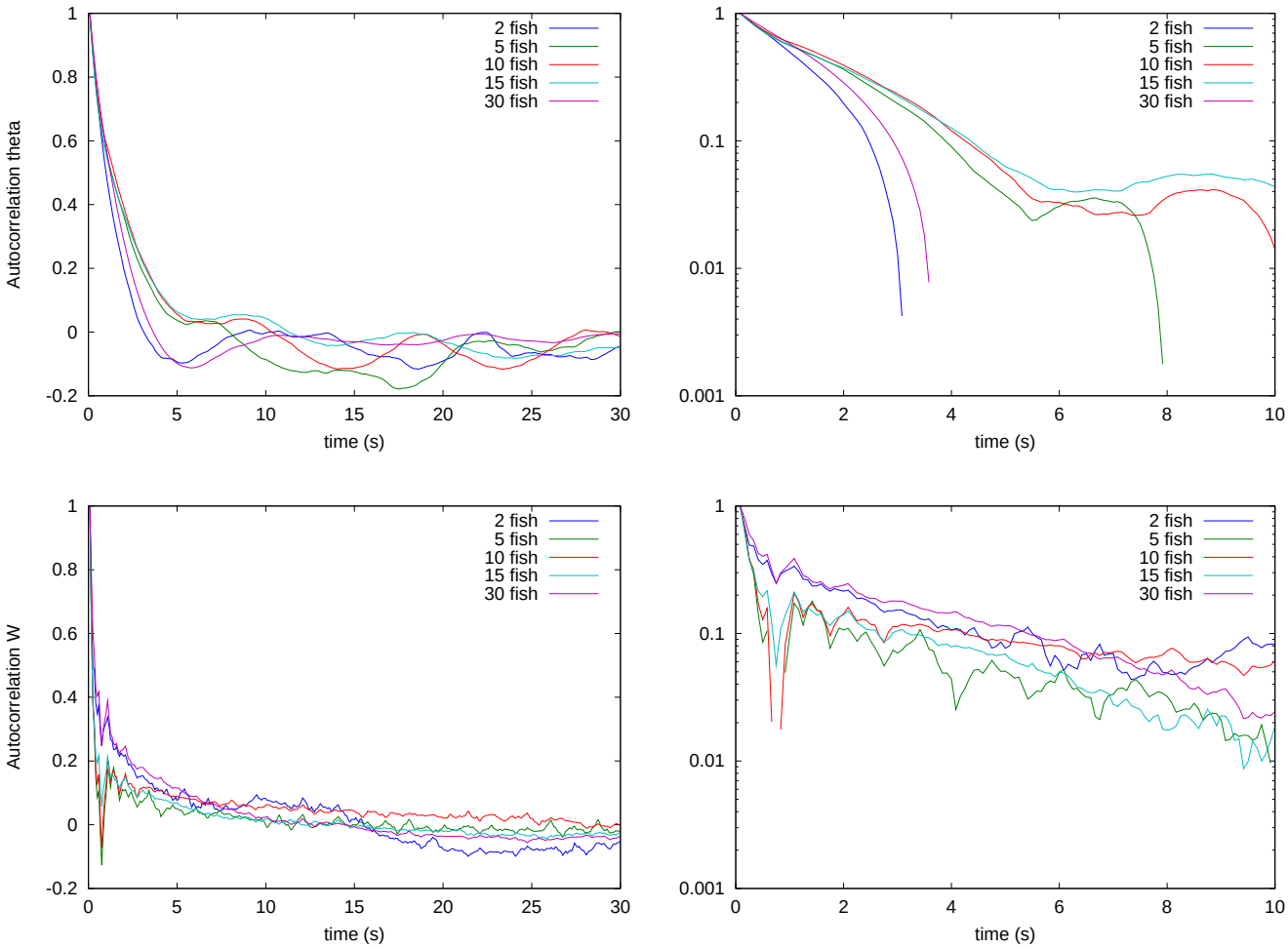

Figure 5.10: The autocorrelation of the direction θ (up) and angular speed W (down) in normal and semi-log plot. As for the mean square displacement, we can observe oscillation for the direction velocity θ. We do not have an exponential decay of the autocorrelation in θ (right-up corner). The autocorrelation of W decreases faster at the beginning (0 to 1 second) and then slow down afterward.

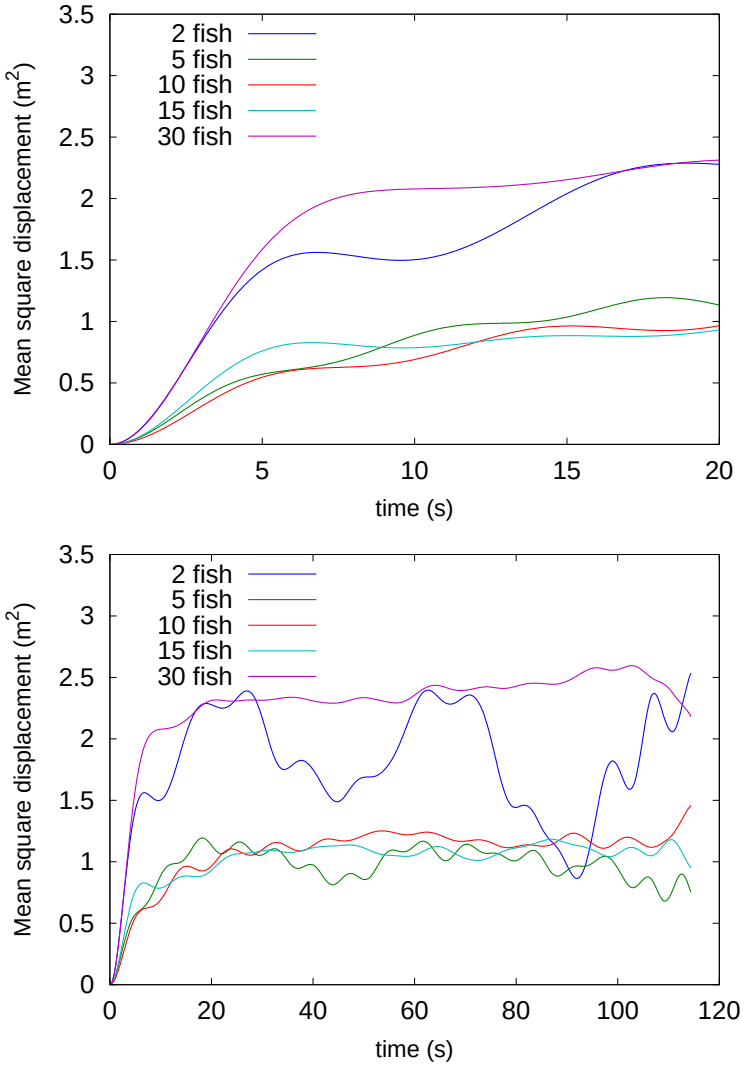

Figure 5.11: The mean square displacement (eq. 4.5) from 0 to 20 seconds (upper figure) and from 0 to 120 seconds (lower figure). We observe a linear growth of the curves between 1 and 5 seconds which allows to estimate the diffusion coefficient. The curves oscillate after that.

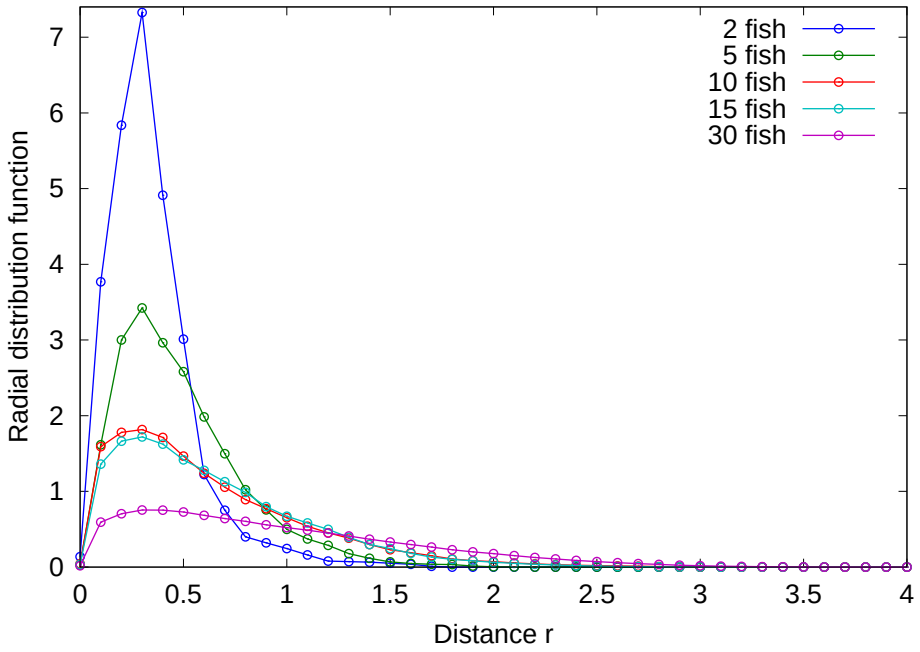

Figure 5.12: The radial distribution function presents a maximum around $r = 0.3m$ which is approximately one body length.

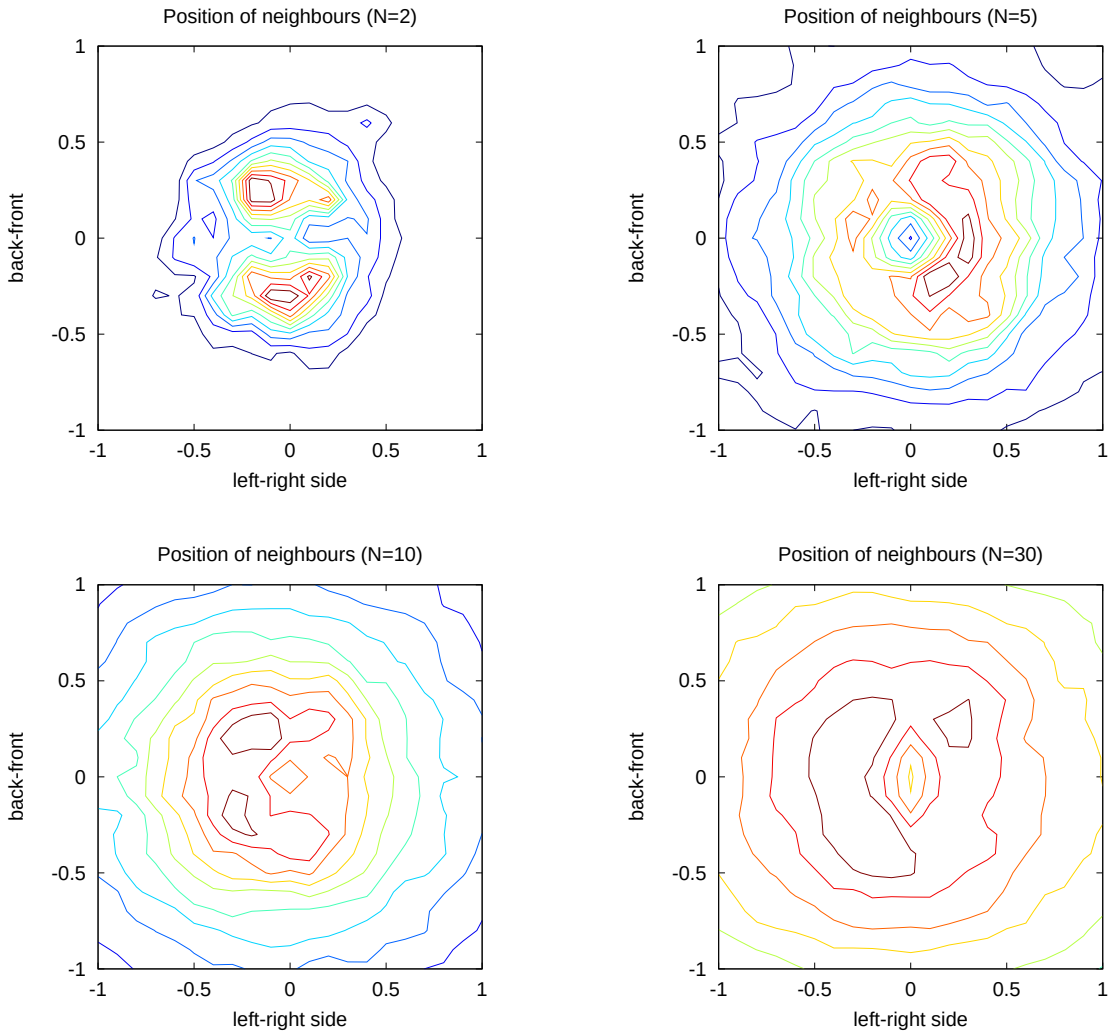

Figure 5.13: The relative position of neighbors in the frame of reference of a fish. There is a preferred position in the front and at the back for the experiments with 2 fish whereas the distribution becomes isotropic with higher density of fish.

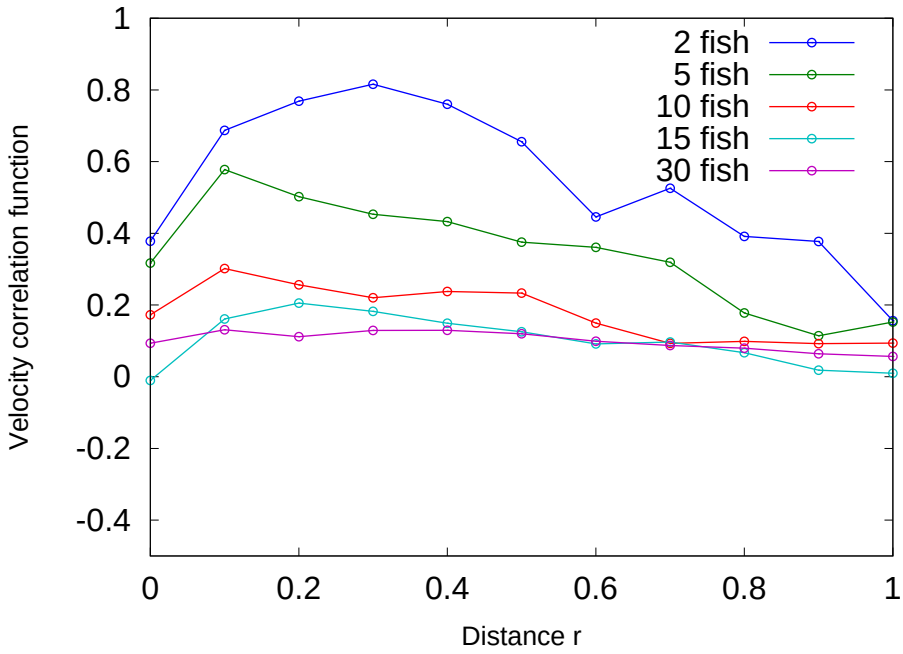

Figure 5.14: The velocity correlation function increases at short distance and decreases afterward.

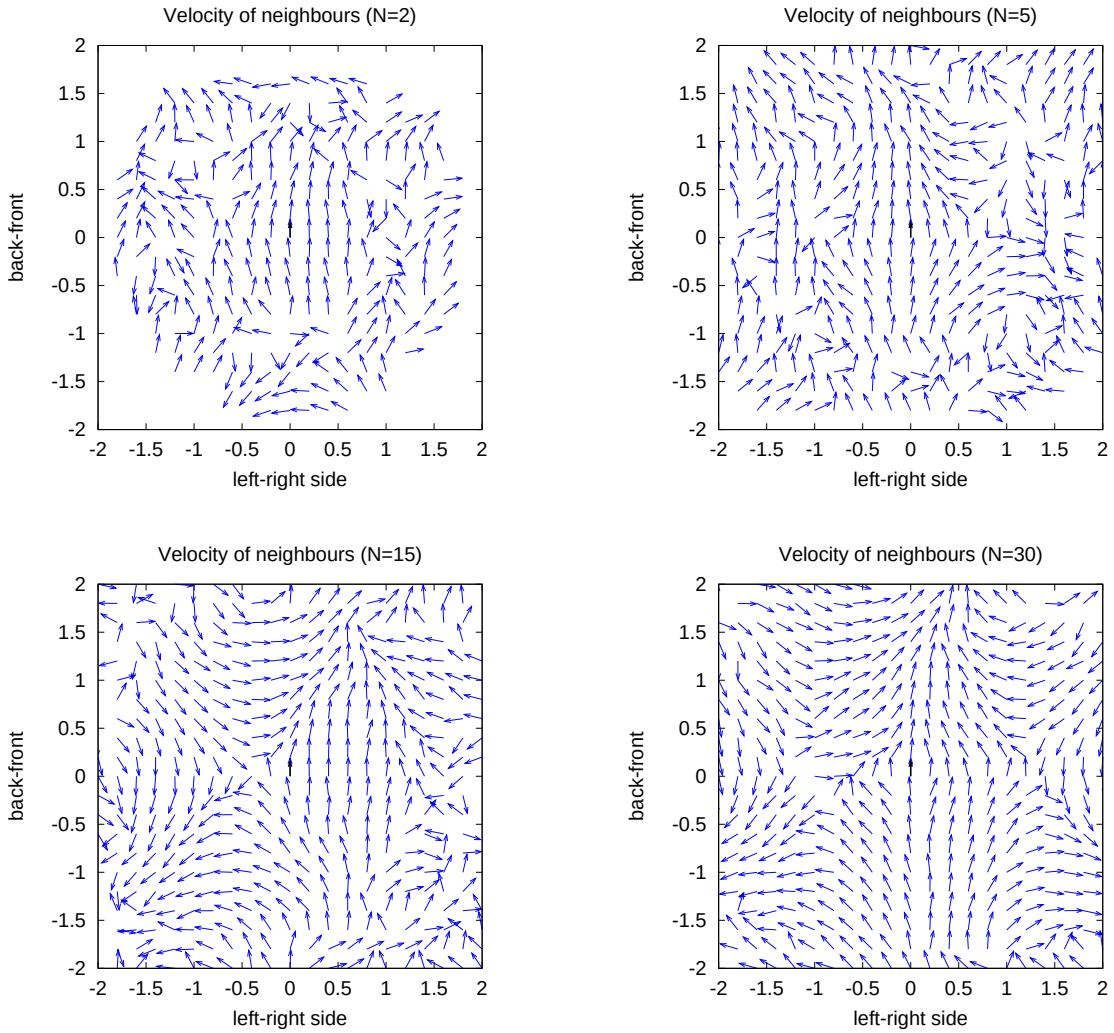

Figure 5.15: The mean velocity of the neighbors in the frame of reference of a fish. Vectors are normalized.

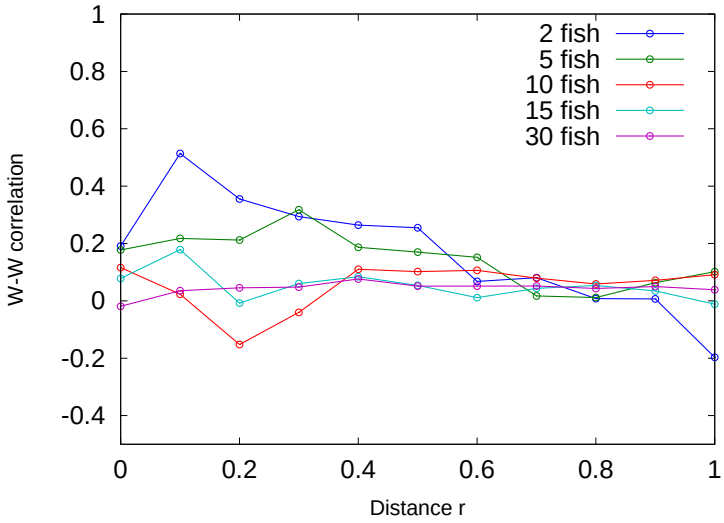

Figure 5.16: The angular speed correlation for different group sizes. We observe a positive correlation at short distance within the experiments with 2 fish.

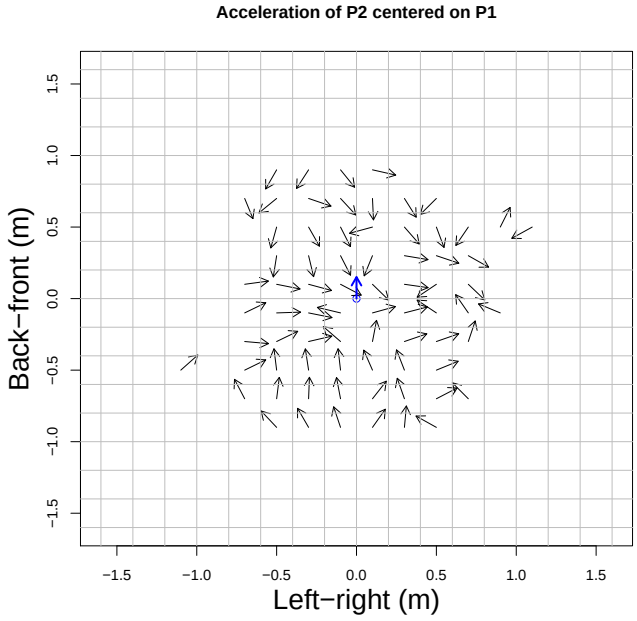

Figure 5.17: The (normalized) acceleration vector of one fish (P_2) in the frame of reference of the other one (P_1). We do not observe a clear pattern at short distance.

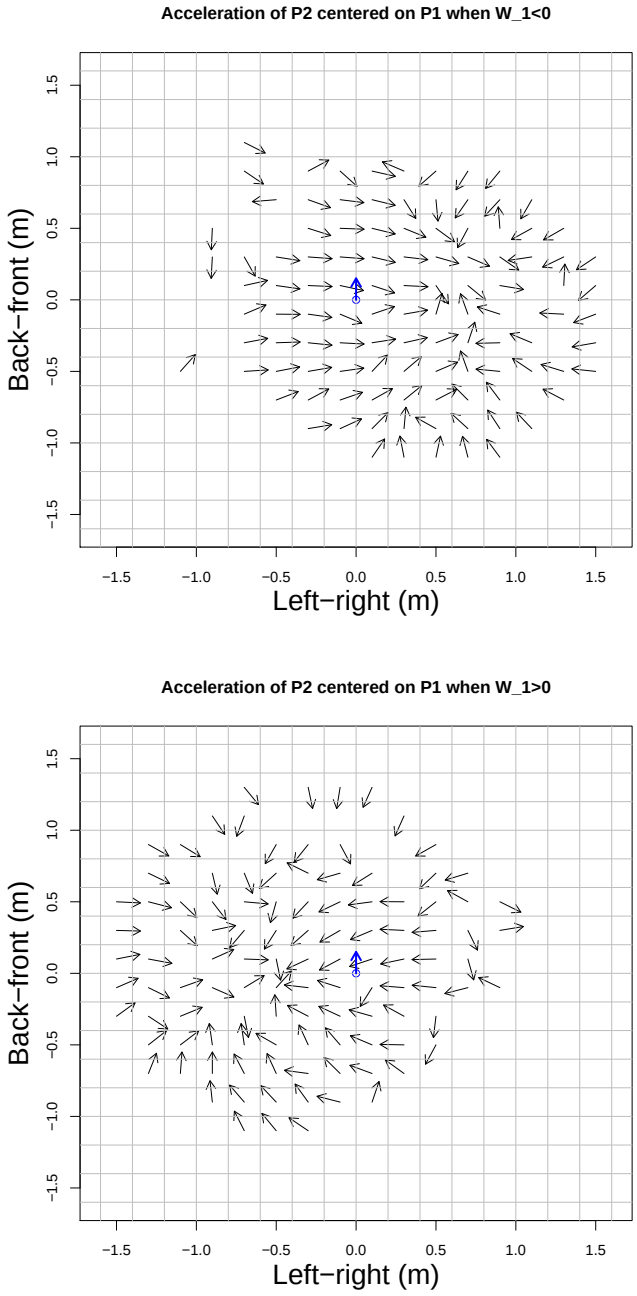

Figure 5.18: The (normalized) acceleration vector of one fish (P_2) in the frame of reference of the other one (P_1). Figure on top: acceleration of P_2 when P_1 turns to the left. Figure above: acceleration of P_2 when P_1 turns to the right. These graphics confirm that the accelerations of fish are correlated at short distance (figure 5.16).

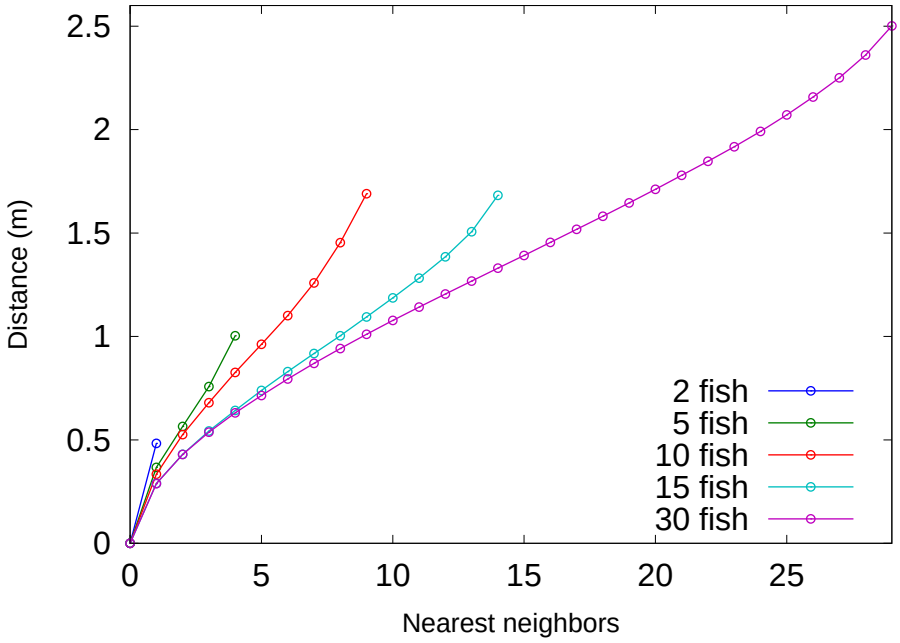

Figure 5.19: The mean distance of the nearest neighbors for different group sizes.

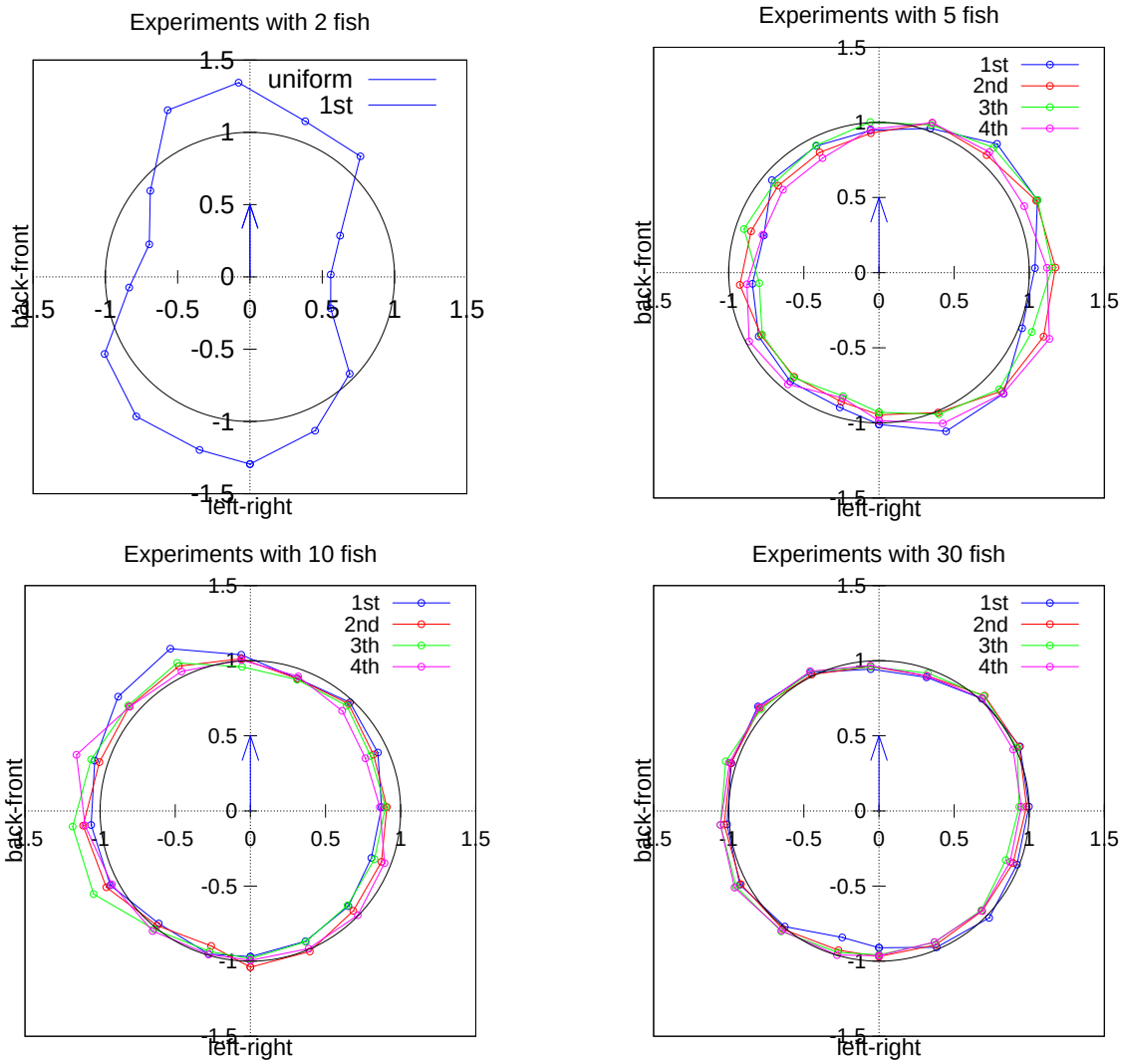

Figure 5.20: Angular density of nearest neighbors for different group sizes. Except in the experiments with 2 fish, the distributions are isotropic (uniformly distributed on the circle)

.

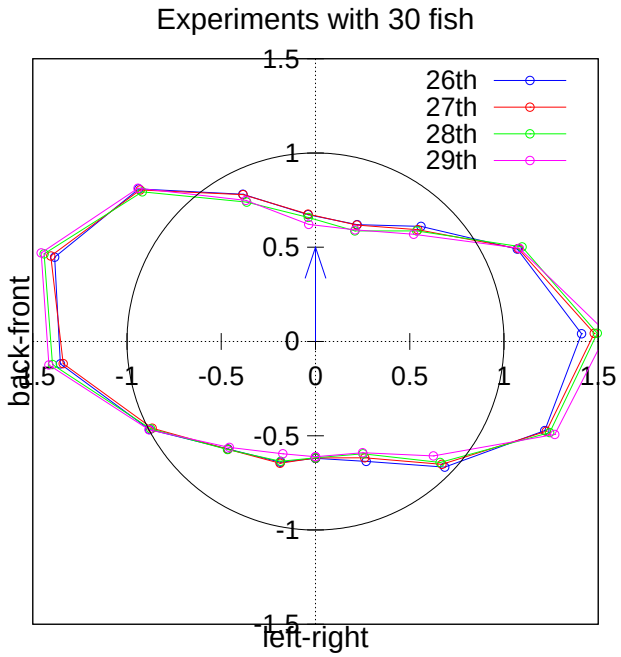

Figure 5.21: Angular density of the last nearest neighbors in the experiments with 30 fish. There is a higher probability to find the farthest neighbors laterally.

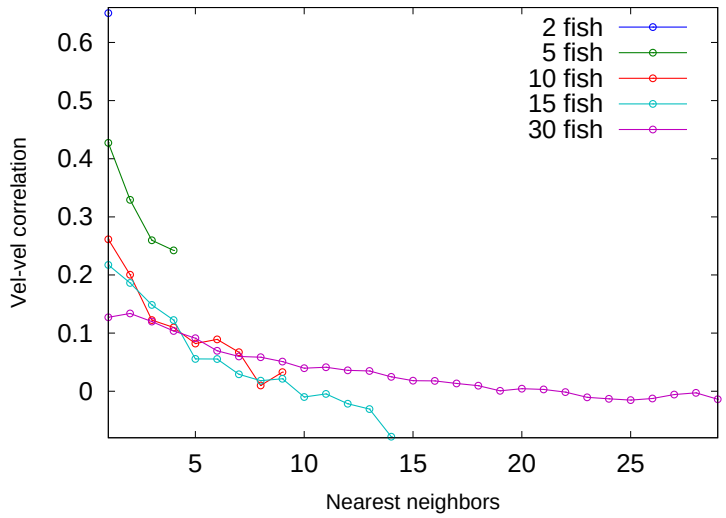

Figure 5.22: The alignment between a fish and its nearest neighbors for different group sizes. We compute the mean of the scalar product between normalized vector speed. The alignment decreases as we take into account farther neighbors.

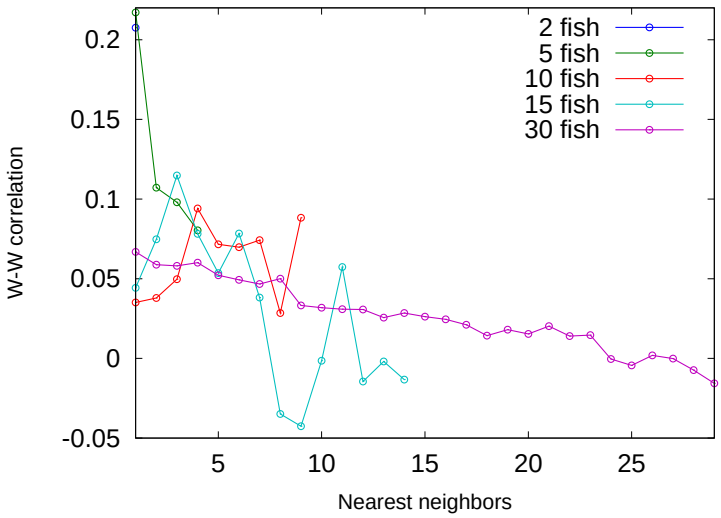

Figure 5.23: The product of angular speed between a fish and its nearest neighbors for different group sizes.

Bibliography

[1] B. Adamcsek, G. Palla, I.J. Farkas, I. Derenyi, and T. Vicsek. CFinder: locating cliques and overlapping modules in biological networks, 2006.

[2] M. Ballerini, N. Cabibbo, R. Candelier, A. Cavagna, E. Cisbani, I. Giardina, V. Lecomte, A. Orlandi, G. Parisi, A. Procaccini, et al. Interaction ruling animal collective behavior depends on topological rather than metric distance: Evidence from a field study. *Proceedings of the National Academy of Sciences*, 105(4):1232, 2008.

[3] E. Casellas, J. Gautrais, R. Fournier, S. Blanco, M. Combe, V. Fourcassie, G. Theraulaz, and C. Jost. From individual to collective displacements in heterogeneous environments. *Journal of Theoretical Biology*, 250(3):424–434, 2008.

[4] A. Cavagna, I. Giardina, A. Orlandi, G. Parisi, and A. Procaccini. The starflag handbook on collective animal behaviour: 2. three-dimensional analysis. *Arxiv preprint arXiv:0802.1674*, 2008.

[5] H. Chaté, F. Ginelli, G. Grégoire, and F. Raynaud. Collective motion of self-propelled particles interacting without cohesion. *Physical Review E*, 77(4):46113, 2008.

[6] Y. Chuang, M.R. D'Orsogna, D. Marthaler, A.L. Bertozzi, and L.S. Chayes. State transitions and the continuum limit for a 2d interacting, self-propelled particle system. *Physica D: Nonlinear Phenomena*, 232(1):33–47, 2007.

[7] I.D. Couzin, J. Krause, R. James, G.D. Ruxton, and N.R. Franks. Collective memory and spatial sorting in animal groups. *Journal of Theoretical Biology*, 218(1):1–11, 2002.

[8] P. Degond and S. Motsch. Large scale dynamics of the persistent turning walker model of fish behavior. *Journal of Statistical Physics*, 131(6):989–1021, 2008.

[9] MR D'Orsogna, YL Chuang, AL Bertozzi, and LS Chayes. Self-propelled particles with soft-core interactions: Patterns, stability, and collapse. *Physical Review Letters*, 96(10):104302, 2006.

[10] H. Fehske, R. Schneider, and A. Weisse. *Computational Many-Particle Physics*. Springer Verlag, 2007.

[11] J. Gautrais, C. Jost, M. Soria, A. Campo, S. Motsch, R. Fournier, S. Blanco, and G. Theraulaz. Analyzing fish movement as a persistent turning walker. *Journal of Mathematical Biology*, 58(3):429–445, 2009.

[12] G. Grégoire, H. Chaté, and Y. Tu. Moving and staying together without a leader. *Physica D: Nonlinear Phenomena*, 181(3-4):157–170, 2003.

[13] R.W. Hockney and J.W. Eastwood. *Computer Simulation Using Particles*. Institute of Physics Publishing, 1988.

[14] J. Hoshen and R. Kopelman. Percolation and cluster distribution. I. Cluster multiple labeling technique and critical concentration algorithm. *Physical Review B*, 14(8):3438–3445, 1976.

[15] R. Jeanson, S. Blanco, R. Fournier, J.L. Deneubourg, V. Fourcassié, and G. Theraulaz. A model of animal movements in a bounded space. *Journal of Theoretical Biology*, 225(4):443–451, 2003.

[16] J.K. Parrish and S.V. Viscido. Traffic rules of fish schools: a review of agent-based approaches. *Self-organisation and Evolution of Social Systems*, 2005.

[17] J.K. Parrish, S.V. Viscido, and D. Grunbaum. Self-organized fish schools: an examination of emergent properties. *Biological Bulletin, Marine Biological Laboratory, Woods Hole*, 202(3):296–305, 2002.

[18] M. Soria, P. Freon, and P. Chabanet. Schooling properties of an obligate and a facultative fish species. *Journal of Fish Biology*, 71:1257–1269, 2007.

[19] H. Spohn. *Large Scale Dynamics of Interacting Particles*. Springer-Verlag New York, 1991.

[20] T. Vicsek, A. Czirók, E. Ben-Jacob, I. Cohen, and O. Shochet. Novel type of phase transition in a system of self-driven particles. *Physical Review Letters*, 75(6):1226–1229, 1995.

[21] VA Vladimirov, MSC Wu, TJ Pedley, PV Denissenko, and SG Zakhidova. Measurement of cell velocity distributions in populations of motile algae. *Journal of Experimental Biology*, 207(7):1203–1216, 2004.

Part II
Derivation of a macroscopic equation for the Vicsek model

Chapter 6

Continuum limit of self-driven particles with orientation interaction

This chapter has given an article written in collaboration with P. Degond and published in the journal Mathematical Models and Methods in Applied Sciences: *Continuum limit of self-driven particles with orientation interaction*, M3AS, **18** (2008), no. 1, 1193–1215, and a note written in collaboration with P. Degond and published in the Comptes Rendus de l'Académie des Sciences: *Macroscopic limit of self-driven particles with orientation interaction*, C. R. Math. Acad. Sci. Paris **345** (2007), no. 10, 555–560.

Abstract. We consider the discrete Couzin-Vicsek algorithm (CVA) [1, 9, 19, 36], which describes the interactions of individuals among animal societies such as fish schools. In this article, we propose a kinetic (mean-field) version of the CVA model and provide its formal macroscopic limit. The final macroscopic model involves a conservation equation for the density of the individuals and a non conservative equation for the director of the mean velocity and is proved to be hyperbolic. The derivation is based on the introduction of a non-conventional concept of a collisional invariant of a collision operator.

Keywords. Individual based model, Fish behavior, Couzin-Vicsek algorithm, Asymptotic analysis, Orientation interaction, Hydrodynamic limit, Collision invariants.

1 Introduction

The discrete Couzin-Vicsek algorithm (CVA) [1, 9, 19, 36] has been proposed as a model for the interactions of individuals among animal societies such as fish schools. The individuals move with a velocity of constant magnitude. The CVA model describes in a discrete way the time evolution of the positions of the individuals and of their velocity angles measured from a reference direction. At each time step, the angle is updated to a new value given by the director of the average velocity of the neighbouring particles, with addition of noise. The positions are updated by adding the distance travelled during the time step by the fish in the direction specified by its velocity angle.

For the modeling of large fish schools which can reach up to several million individuals, it may be more efficient to look for continuum like models, which describe the fish society by macroscopic variables (e.g. mean density, mean velocity and so on). Several such phenomenological models exist (see e.g. [25, 34, 35]). Several attempts to derive continuum models from the CVA model are also reported in the literature [23, 29, 30], but the derivation and the mathematical 'qualities' of the resulting models have not been fully analyzed yet. One can also refer to [16, 26] for related models. An alternate model, the Persistent Turning Walker model, has been proposed in [18] on the basis of experimental measurements. Its large-scale dynamics is studied in [12]. Additional references on swarm aggregation and fish schooling can be found in [7]. Among other types of animal societies, ants have been the subject of numerous studies and the reader can refer (among other references) to [21, 33], and references therein.

In this work, we propose a derivation of a continuum model from a kinetic version of the CVA algorithm. For that purpose, we first rephrase the CVA model as a time continuous dynamical system (see section 2). Then, we pass to a mean-field version of this dynamical system (section 3). This mean field model consists of a kinetic equation of Fokker-Planck type with a force term resulting from the alignment interactions between the particles. More precisely, the mean-field model is written:

$$\varepsilon(\partial_t f^\varepsilon + \omega \cdot \nabla_x f^\varepsilon) = -\nabla_\omega \cdot (F_0^\varepsilon f^\varepsilon) + d\Delta_\omega f^\varepsilon + O(\varepsilon^2), \tag{1.1}$$

$$F_0^\varepsilon(x,\omega,t) = \nu\ (\mathrm{Id} - \omega \otimes \omega)\Omega^\varepsilon(x,t), \tag{1.2}$$

$$\Omega^\varepsilon(x,t) = \frac{j^\varepsilon(x,t)}{|j^\varepsilon(x,t)|}, \quad \text{and} \quad j^\varepsilon(x,t) = \int_{\upsilon\in\mathbb{S}^2} \upsilon\, f^\varepsilon(x,\upsilon,t)\, d\upsilon\,. \tag{1.3}$$

Here $f^\varepsilon(x,\omega,t)$ is the particle distribution function depending on the space variable $x \in \mathbb{R}^3$, the velocity direction $\omega \in \mathbb{S}^2$ and the time t. d is a scaled diffusion constant and $F_0^\varepsilon(x,\omega,t)$ is the mean-field interaction force between the particles which depends on an interaction frequency ν. This force tends to align the particles to the direction Ω^ε which is the director of the particle flux j^ε. the operators $\nabla_\omega\cdot$ and Δ_ω are respectively the gradient and the Laplace-Beltrami operators on the sphere. The matrix $(\mathrm{Id} - \omega \otimes \omega)$ is the projection matrix onto the normal plane to ω. $\varepsilon \ll 1$ is a small parameter measuring the ratio of the microscopic length scale (the distance travelled between two interactions) to the size of the observation domain. Here, the relevant scaling is a hydrodynamic scaling, which means that ε also equals the ratio of the microscopic time scale (the mean time between interactions) to the macroscopic observation time.

The 'hydrodynamic limit' $\varepsilon \to 0$ provides the large-scale dynamics of the CVA model (in its mean-field version (1.1)-(1.3)). The goal of this chapter is to (formally) investigate this limit. More precisely, the main result of this paper is the following theorem, which is proved in section 4:

Theorem 1.1 *(formal) The limit $\varepsilon \to 0$ of f^ε is given by $f^0 = \rho M_\Omega$ where $\rho = \rho(x,t) \geq 0$ is the total mass of f^0 and $\Omega = \Omega(x,t) \in \mathbb{S}^2$ is the director of its flux:*

$$\rho(x,t) = \int_{\omega \in \mathbb{S}^2} f^0(x,\omega,t)\, d\omega, \tag{1.4}$$

$$\Omega = \frac{j}{|j|}, \quad j(x,t) = \int_{\omega \in \mathbb{S}^2} f^0(x,\omega,t)\, \omega\, d\omega, \tag{1.5}$$

and M_Ω is a given function of $\omega \cdot \Omega$ only depending on ν and d which will be specified later on (see (4.16)). Furthermore, $\rho(x,t)$ and $\Omega(x,t)$ satisfy the following system of first order partial differential equations:

$$\partial_t \rho + \nabla_x \cdot (c_1 \rho \Omega) = 0, \tag{1.6}$$

$$\rho\, (\partial_t \Omega + c_2 (\Omega \cdot \nabla)\Omega) + \lambda\, (Id - \Omega \otimes \Omega) \nabla_x \rho = 0, \tag{1.7}$$

where the convection speeds c_1, c_2 and the interaction constant λ will be specified in the course of the chapter (see (4.41) and (4.63)).

Hydrodynamic limits have first been developed in the framework of the Boltzmann theory of rarefied gases. The reader can refer to [8, 11, 31] for recent viewpoints as well as to [6, 15, 37] for major landmarks in its mathematical theory. Hydrodynamic limits have been recently investigated in traffic flow modeling [4, 20] as well as in supply chain research [3, 14].

From the viewpoint of hydrodynamic limits, the originality of theorem 1.1 lies in the fact that the collision operator (i.e. the right-hand side of (1.1)) has a three dimensional manifold of equilibria (parametrized by the density ρ and the velocity director Ω) but has only a one-dimensional set of collisional invariants (corresponding to mass conservation). Indeed, the interaction does not conserve momentum and one should not expect any collisional invariant related to that conservation. The problem is solved by introducing a broader class of collisional invariants, such that their integral (with respect to ω) against the collision operator cancels only when the collision operator is applied to a subclass of functions. Here, a generalized class of collision invariants is associated with each direction Ω on the sphere and the corresponding subclass of functions have their flux in the direction of Ω. We show that such generalized collision invariants exist and that they lead to (1.7). In section 4.4, we show that this system is hyperbolic. The detailed qualitative study of the system as well as numerical simulations will be the subject of future work. A summary of this work can be found in [13].

An important consequence of this result is that the large-scale dynamics of the CVA model does not present any phase transition, in contrast with the observations of [36]. Indeed, the equilibrium is unique (for given density and velocity director).

Therefore, the model cannot exhibit any bi-stable behavior where shifts between two competing equilibria would trigger abrupt phase transitions, like in rod-like polymers (see e.g. [24] and references therein). Instead, the equilibrium gradually shifts from a collective one where all particles point in the same direction to an isotropic one as the diffusion constant d increases from 0 to infinity. Additionally, the hyperbolicity of the model does not allow lines of faults across unstable elliptic regions, like in the case of multi-phase mixtures or phase transitions in fluids or solids (see e.g. the review in [22] and references therein).

With these considerations in mind, a phenomenon qualitatively resembling a phase transition could occur if the coefficients c_1, c_2 and λ have sharp variations in some small range of values of the diffusion coefficient d. In this case, the model could undergo a rapid change of its qualitative features which would be reminiscent of a phase transition. One of our future goals is to verify or discard this possibility by numerically computing these constants.

There are many questions which are left open. For instance, one question is about the possible influence of a limited range of vision in the backwards direction. In this case, the asymmetry of the observation will bring more terms in the limit model. Similarly, one could argue that the angular diffusion should produce some spatial dissipation. Indeed, such dissipation phenomena are likely to occur if we retain the first order correction in the series expansion in terms of the small parameter ε (the so-called Hilbert or Chapman-Enskog expansions, see e.g. [11]). A deeper analysis is needed in order to determine the precise form of these diffusion terms. Another question concerns the possibility of retaining some of the non-local effects in the macroscopic model. It is likely that the absence of phase transition in the present model is related to the fact that the large-scale limit cancels most of the non-local effects (at least at leading order). The question whether retaining some non-locality effects in the macroscopic limit would allow the appearance of phase transitions at large scales would indeed reconcile the analytical result with the numerical observations. A result in this direction obtained with methods from matrix recursions can be found in [10]. Finally, the alignment interaction is only one of the aspects of the Couzin model, which also involves repulsion at short scales and attraction at large scales. The incorporation of these effects would allow to build a complete continuum model which would account for all the important features of this kind of social interaction.

2 A time continuous version of the discrete Couzin-Vicsek algorithm

The Couzin-Vicsek algorithm considers N point particles in $\mathbb{R}^3$ labeled by $k \in \{1, \dots N\}$ with positions X_k^n at the discrete times $t^n = n\Delta t$. The magnitude of the velocity is the same for all particles and is constant in time denoted by $c > 0$. The velocity vector is written $c\,\omega_k^n$ where ω_k^n belongs to the unit sphere $\mathbb{S}^2 = \{\omega \quad \text{s.t. } |\omega|^2 = 1\}$ of $\mathbb{R}^3$.

The Couzin-Vicsek algorithm is a time-discrete algorithm that updates the velocities and positions of the particles at every time step Δt according to the following

rules.

(i) The particle position of the k-th particle at time n is evolved according to:

$$X_k^{n+1} = X_k^n + c\,\omega_k^n \Delta t. \tag{2.1}$$

(ii) The velocity director of the k-th particle, ω_k^n, is changed to the director $\bar{\omega}_k^n$ of the average velocity of the neighboring particles with addition of noise. This algorithm tries to mimic the behaviour of some animal species like fish, which tend to align with their neighbors. Noise accounts for the inaccuracies of the animal perception and cognitive systems. The neighborhood of the k-th particle is the ball centered at X_k^n with radius $R > 0$ and $\bar{\omega}_k^n$ is given by:

$$\bar{\omega}_k^n = \frac{J_k^n}{|J_k^n|}, \quad J_k^n = \sum_{j,\,|X_j^n - X_k^n| \le R} \omega_j^n. \tag{2.2}$$

In the Couzin-Vicsek algorithm, the space is 2-dimensional and the orientations are vectors belonging to the unit sphere $\mathbb{S}^1$ in $\mathbb{R}^2$. One can write $\omega_k^n = e^{i\theta_k^n}$ with θ_k^n defined modulo 2π, and similarly $\bar{\omega}_k^n = e^{i\bar{\theta}_k^n}$. In the original version of the algorithm, a uniform noise in a small interval of angles $[-\alpha, \alpha]$ is added, where α is a measure of the intensity of the noise. This leads to the following update for the phases:

$$\theta_k^{n+1} = \bar{\theta}_k^n + \hat{\theta}_k^n, \tag{2.3}$$

where $\hat{\theta}_k^n$ are independent identically distributed random variables with uniform distribution in $[-\alpha, \alpha]$. Then, $\omega_k^{n+1} = e^{i\theta_k^{n+1}}$. In [36], Vicsek et al analyze the dynamics of this algorithm and experimentally demonstrate the existence of a threshold value α^*. For $\alpha < \alpha^*$, a coherent dynamics appears after some time where all the particles are nearly aligned. On the other hand, if $\alpha > \alpha^*$, disorder prevails at all times.

Here, we consider a three dimensional version of the Couzin-Vicsek algorithm, of which the two-dimensional original version is a particular case. Of course, formula (2.2) for the average remains the same in any dimension. For simplicity, we also consider a Gaussian noise rather than a uniformly distributed noise as in the original version of the algorithm. Therefore, our algorithm updates the velocity directors according to:

$$\omega_k^{n+1} = \hat{\omega}_k^n, \tag{2.4}$$

where $\hat{\omega}_k^n$ are random variables on the sphere centered at $\bar{\omega}_k^n$ with Gaussian distributions of variance $\sqrt{2D\Delta t}$ where D is a supposed given coefficient. If the Gaussian noise is discarded, the evolution of the orientations is given by

$$\omega_k^{n+1} = \bar{\omega}_k^n, \tag{2.5}$$

where $\bar{\omega}_k^n$ is the average defined at (2.2).

Now, we would like to take the limit $\Delta t \to 0$ and find a time-continuous dynamics. To do so, we first consider the deterministic algorithm (2.1), (2.5) and following [29], make some elementary remarks. First, because $|\omega_k^n| = |\omega_k^{n+1}|$, we have

$(\omega_k^{n+1} - \omega_k^n)(\omega_k^{n+1} + \omega_k^n) = 0$. Therefore, defining $\omega_k^{n+1/2} = (\omega_k^{n+1} + \omega_k^n)/2$ and using (2.5), we have the obvious relation:

$$\frac{\omega_k^{n+1} - \omega_k^n}{\Delta t} = \frac{1}{\Delta t}(\mathrm{Id} - \omega_k^{n+1/2} \otimes \omega_k^{n+1/2})(\bar{\omega}_k^n - \omega_k^n), \tag{2.6}$$

where Id denotes the Identity matrix and the symbol $\otimes$ denotes the tensor product of vectors. The matrix $\mathrm{Id} - \omega_k^{n+1/2} \otimes \omega_k^{n+1/2}$ is the orthogonal projector onto the plane orthogonal to $\omega_k^{n+1/2}$. Relation (2.6) simply expresses that the vector $\omega_k^{n+1} - \omega_k^n$ belongs to that plane.

Now, we let $\Delta t \to 0$. Then, the positions $X_k(t)$ and the orientations $\omega_k(t)$ become continuous functions of time. If we let $\Delta t \to 0$ in (2.6), the left-hand side obviously tends to $\partial\omega_k/\partial t$. The right hand side, however, does not seem to have an obvious limit. This is due to an improper choice of time scale. Indeed, if we run the clock twice as fast, the particles will interact twice as frequently. In the limit $\Delta t \to 0$, the number of interactions per unit of time is infinite and we should not expect to find anything interesting if we do not rescale the time. In order to have the proper time-scale for the model, we need to replace the tick of the clock Δt by a typical interaction frequency ν of the particles under consideration. For instance, in the case of fish, ν^{-1} is the typical time-interval between two successive changes in the fish trajectory to accommodate the presence of other fish in the neighbourhood. Therefore, we start from a discrete algorithm defined by

$$\frac{\omega_k^{n+1} - \omega_k^n}{\Delta t} = \nu\,(\mathrm{Id} - \omega_k^{n+1/2} \otimes \omega_k^{n+1/2})(\bar{\omega}_k^n - \omega_k^n), \tag{2.7}$$

together with (2.1) and in the limit $\Delta t \to 0$, we find the following continuous dynamical system:

$$\frac{dX_k}{dt} = c\,\omega_k, \tag{2.8}$$

$$\frac{d\omega_k}{dt} = \nu\,(\mathrm{Id} - \omega_k \otimes \omega_k)\bar{\omega}_k, \tag{2.9}$$

where we have used that $(\mathrm{Id} - \omega_k \otimes \omega_k)\omega_k = 0$. If the Gaussian noise is retained, then, the limit $\Delta t \to 0$ of the discrete algorithm is the following Stochastic Differential Equation:

$$\frac{dX_k}{dt} = c\,\omega_k, \tag{2.10}$$

$$d\omega_k = (\mathrm{Id} - \omega_k \otimes \omega_k)(\nu\,\bar{\omega}_k\,dt + \sqrt{2D}\,dB_t), \tag{2.11}$$

where dB_t is a Brownian motion with intensity $\sqrt{2D}$. Of course, this $\Delta t \to 0$ limit is formal but the convergence proof is outside the scope of the present chapter.

We slightly generalize this model by assuming that ν may depend on the angle between ω_k and $\bar{\omega}_k$, namely $\nu = \nu(\cos\theta_k)$, with $\cos\theta_k = \omega_k \cdot \bar{\omega}_k$. Indeed, it is legitimate to think that the ability to turn is dependent on the target direction. If we are considering fish, the ability to turn a large angle is likely to be reduced compared to small angles. We will assume that $\nu(\cos\theta)$ is a smooth and bounded function of $\cos\theta$.

3 Mean-field model of the discrete Couzin-Vicsek algorithm

We now consider the limit of a large number of particles $N \to \infty$. We first consider the case without Gaussian noise. For this derivation, we proceed e.g. like in [32]. We introduce the so-called empirical distribution $f^N(x, \omega, t)$ defined by:

$$f^N(x, \omega, t) = \frac{1}{N} \sum_{k=1}^{N} \delta(x - X_k(t))\, \delta(\omega, \omega_k(t)). \tag{3.1}$$

Here, the distribution $\omega \in \mathbb{S}^2 \to \delta(\omega, \omega')$ is defined by duality against a smooth function φ by the relation:

$$\langle \delta(\omega, \omega'), \varphi(\omega) \rangle = \varphi(\omega').$$

We note that $\delta(\omega, \omega') \neq \delta(\omega - \omega')$ because the sphere $\mathbb{S}^2$ is not left invariant by the subtraction operation. However, we have similar properties of δ such as $\delta(\omega, \omega') = \delta(\omega', \omega)$ where this relation is interpreted as concerning a distribution on the product $\mathbb{S}^2 \times \mathbb{S}^2$.

Then, it is an easy matter to see that f^N satisfies the following kinetic equation

$$\partial_t f^N + c\omega \cdot \nabla_x f^N + \nabla_\omega \cdot (F^N f^N) = 0, \tag{3.2}$$

where $F^N(x, \omega, t)$ is an interaction force defined by:

$$F^N(x, \omega, t) = \nu(\cos\theta^N)\, (\mathrm{Id} - \omega \otimes \omega) \bar{\omega}^N, \tag{3.3}$$

with $\cos\theta^N = \omega \cdot \bar{\omega}^N$ and $\bar{\omega}^N(x, \omega, t)$ is the average orientation around x, given by:

$$\bar{\omega}^N(x, \omega, t) = \frac{J^N(x, t)}{|J^N(x, t)|}, \quad J^N(x, t) = \sum_{j, |X_j^n - x| \leq R} \omega_j^n \,. \tag{3.4}$$

If, by any chance, J^N is equal to zero, we decide to assign to $\bar{\omega}^N(x, \omega, t)$ the value ω (which is the only way by which $\bar{\omega}^N(x, \omega, t)$ can depend on ω). In the sequel, this convention will not be recalled but will be marked by showing the dependence of $\bar{\omega}$ upon ω.

We recall the expressions of the gradient and divergence operator on the sphere. Let $x = (x_1, x_2, x_3)$ be a Cartesian coordinate system associated with an orthonormal basis (e_1, e_2, e_3) and let (θ, ϕ) be a spherical coordinate system associated with this basis, i.e. $x_1 = \sin\theta\cos\phi$, $x_2 = \sin\theta\sin\phi$, $x_3 = \cos\theta$. Let also (e_θ, e_ϕ) be the local basis associated with the spherical coordinate system ; the vectors e_θ and e_ϕ have the following coordinates in the Cartesian basis: $e_\theta = (\cos\theta\cos\phi, \cos\theta\sin\phi, -\sin\theta)$, $e_\phi = (-\sin\phi, \cos\phi, 0)$. Let $f(\omega)$ be a scalar function and $A = A_\theta e_\theta + A_\phi e_\phi$ be a tangent vector field. Then:

$$\nabla_\omega f = \partial_\theta f\, e_\theta + \frac{1}{\sin\theta}\, \partial_\phi f\, e_\phi, \quad \nabla_\omega \cdot A = \frac{1}{\sin\theta} \partial_\theta (A_\theta \sin\theta) + \frac{1}{\sin\theta} \partial_\phi A_\phi.$$

If the Cartesian coordinate system is such that $e_3 = \bar{\omega}^N$, then

$$F^N = -\nu(\cos\theta)\,\sin\theta\; e_\theta. \tag{3.5}$$

Back to system (3.2)-(3.4), we note that relation (3.4) can be written

$$\bar{\omega}^N(x,\omega,t) = \frac{J^N(x,t)}{|J^N(x,t)|}, \quad J^N(x,t) = \int_{|y-x|\le R,\, \upsilon\in\mathbb{S}^2} \upsilon f^N(y,\upsilon,t)\,dy\,d\upsilon\,. \tag{3.6}$$

We will slightly generalize this formula and consider $\bar{\omega}^N(x,\omega,t)$ defined by the following relation:

$$\bar{\omega}^N(x,\omega,t) = \frac{J^N(x,t)}{|J^N(x,t)|}, \quad J^N(x,t) = \int_{y\in\mathbb{R}^3,\, \upsilon\in\mathbb{S}^2} K(|x-y|)\,\upsilon\, f^N(y,\upsilon,t)\,dy\,d\upsilon\,, \tag{3.7}$$

where $K(|x|)$ is the 'observation kernel' around each particle. Typically, in formula (3.6), $K(|x|)$ is the indicator function of the ball centered at the origin and of radius R but we can imagine more general kernels modeling the fact that the influence of the particles fades away with distance. We will assume that this function is smooth, bounded and tends to zero at infinity.

Clearly, the formal mean-field limit of the particle system modeled by the kinetic system (3.2), (3.3), (3.7) is given by the following system:

$$\partial_t f + c\omega\cdot\nabla_x f + \nabla_\omega\cdot(Ff) = 0, \tag{3.8}$$

$$F(x,\omega,t) = \nu(\cos\bar{\theta})\,(\mathrm{Id} - \omega\otimes\omega)\bar{\omega}(x,\omega,t), \tag{3.9}$$

$$\bar{\omega}(x,\omega,t) = \frac{J(x,t)}{|J(x,t)|}, \quad J(x,t) = \int_{y\in\mathbb{R}^3,\, \upsilon\in\mathbb{S}^2} K(|x-y|)\,\upsilon\, f(y,\upsilon,t)\,dy\,d\upsilon\,, \tag{3.10}$$

with $\cos\bar{\theta} = \omega\cdot\bar{\omega}$. It is an open problem to rigorously show that this convergence holds. For interacting particle system, a typical result is as follows (see e.g. [32]). Suppose that the empirical measure at time $t = 0$ converges in the weak star topology of bounded measures towards a smooth function $f_I(x,\omega)$. Then, $f^N(x,\omega,t)$ converges to the solution f of (3.8)-(3.10) with initial datum f_I, in the topology of continuous functions of time on $[0,T]$ (for arbitrary $T > 0$) with values in the space of bounded measures endowed with the weak star topology. We will admit that such a result is true (may be with some modified functional setting) and leave a rigorous convergence proof to future work.

We will also admit that the mean-field limit of the stochastic particle system (2.10), (2.11) consists of the following Kolmogorov-Fokker-Planck equation

$$\partial_t f + c\omega\cdot\nabla_x f + \nabla_\omega\cdot(Ff) = D\Delta_\omega f, \tag{3.11}$$

again coupled with (3.9), (3.10) for the definition of F and $\bar{\omega}$, and where Δ_ω denotes the Laplace-Belltrami operator on the sphere:

$$\Delta_\omega f = \nabla_\omega\cdot\nabla_\omega f = \frac{1}{\sin\theta}\partial_\theta(\sin\theta\partial_\theta f) + \frac{1}{\sin^2\theta}\partial_{\phi\phi} f.$$

4 Hydrodynamic limit of the Mean-field Couzin-Vicsek model

4.1 Scaling

We are interested in the large time and space dynamics of the mean-field Fokker-Planck equation (3.11), coupled with (3.9), (3.10).

So far, the various quantities appearing in the system have physical dimensions. We first introduce the characteristic physical units associated with the problem and scale the system to dimensionless variables. Let ν_0 the typical interaction frequency scale. This means that $\nu(\cos\theta) = \nu_0\nu'(\cos\theta)$ with $\nu'(\cos\theta) = O(1)$ in most of the range of $\cos\theta$. We now introduce related time and space scales t_0 and x_0 as follows: $t_0 = \nu_0^{-1}$ and $x_0 = ct_0 = c/\nu_0$. This choice means that the time unit is the mean time between interactions and the space unit is the mean distance traveled by the particles between interactions. We introduce the dimensionless diffusion coefficient $d = D/\nu_0$. Note that D has also the dimension of a frequency so that d is actually dimensionless. We also introduce a scaled observation kernel K' such that $K(x_0|x'|) = K'(|x'|)$. Typically, if K is the indicator function of the ball of radius R, K' is the indicator of the ball of radius $R' = R/x_0$. The assumption that the interaction is non local means that $R' = O(1)$. In other words, the observation radius is of the same order as the mean distance travelled by the particles between two interactions. This appears consistent with the behaviour of a fish, but would probably require more justifications. In the present work, we shall take this fact for granted.

Let now $t' = t/t_0$, $x' = x/x_0$ the associated dimensionless time and space variables. Then, system (3.11), coupled with (3.9), (3.10) is written in this new system of units (after dropping the primes for the sake of clarity):

$$\partial_t f + \omega\cdot\nabla_x f + \nabla_\omega\cdot(Ff) = d\Delta_\omega f, \tag{4.1}$$

$$F(x,\omega,t) = \nu(\cos\bar\theta)\,(\mathrm{Id}-\omega\otimes\omega)\bar\omega(x,\omega,t), \quad \text{with} \quad \cos\bar\theta = \omega\cdot\bar\omega, \tag{4.2}$$

$$\bar\omega(x,\omega,t) = \frac{J(x,t)}{|J(x,t)|}, \quad J(x,t) = \int_{y\in\mathbb{R}^3,\,\upsilon\in\mathbb{S}^2} K(|x-y|)\,\upsilon\,f(y,\upsilon,t)\,dy\,d\upsilon\,. \tag{4.3}$$

The system now depends on only one dimensionless parameter d and two dimensionless functions which describe the behaviour of the fish: $\nu(\cos\bar\theta)$ and $K(x)$, which are all supposed to be of order 1.

Up to now, the system has been written at the microscopic level, i.e. at time and length scales which are characteristic of the dynamics of the individual particles. Our goal is now to investigate the dynamics of the system at large time and length scales compared with the scales of the individuals. For this purpose, we adopt new time and space units $\tilde t_0 = t_0/\varepsilon$, $\tilde x_0 = x_0/\varepsilon$ with $\varepsilon \ll 1$. Then, a set of new dimensionless variables is introduced $\tilde x = \varepsilon x$, $\tilde t = \varepsilon t$. In this new set of variables, the system is written (again,

dropping the tildes for clarity):

$$\varepsilon(\partial_t f^\varepsilon + \omega\cdot\nabla_x f^\varepsilon) = -\nabla_\omega\cdot(F^\varepsilon f^\varepsilon) + d\Delta_\omega f^\varepsilon, \tag{4.4}$$

$$F^\varepsilon(x,\omega,t) = \nu(\omega\cdot\bar\omega^\varepsilon)\ (\mathrm{Id}-\omega\otimes\omega)\bar\omega^\varepsilon(x,\omega,t), \tag{4.5}$$

$$\bar\omega^\varepsilon(x,\omega,t) = \frac{J^\varepsilon(x,t)}{|J^\varepsilon(x,t)|}, \quad J^\varepsilon(x,t) = \int_{y\in\mathbb{R}^3,\,\upsilon\in\mathbb{S}^2} K\left(\left|\frac{x-y}{\varepsilon}\right|\right)\,\upsilon\, f^\varepsilon(y,\upsilon,t)\,dy\,d\upsilon\,. \tag{4.6}$$

Our goal in this chapter is to investigate the formal limit $\varepsilon\to 0$ of this problem.

Our first task, performed in the following lemma, is to provide an expansion of $\bar\omega^\varepsilon$ in terms of ε.

Lemma 4.1 *We have the expansion:*

$$\bar\omega^\varepsilon(x,\omega,t) = \Omega^\varepsilon(x,t) + O(\varepsilon^2)\,, \tag{4.7}$$

where

$$\Omega^\varepsilon(x,t) = \frac{j^\varepsilon(x,t)}{|j^\varepsilon(x,t)|}, \quad \textit{and} \quad j^\varepsilon(x,t) = \int_{\upsilon\in\mathbb{S}^2}\upsilon\, f^\varepsilon(x,\upsilon,t)\,d\upsilon\,. \tag{4.8}$$

The proof of this lemma is elementary, and is omitted. That the remainder in (4.7) is of order ε^2 is linked with the fact that the observation kernel is isotropic. If an anisotropic kernel had been chosen, such as one favouring observations in the forward direction, then a term of order ε would have been obtained. This additional term would substantially change the dynamics. We leave this point to future work.

The quantity $j^\varepsilon(x,t)$ is the particle flux. We will also use the density, which is defined as a moment of f as well:

$$\rho^\varepsilon(x,t) = \int_{\upsilon\in\mathbb{S}^2} f^\varepsilon(x,\upsilon,t)\,d\upsilon\,. \tag{4.9}$$

Thanks to lemma 4.1, system (4.4)-(4.6) is written

$$\varepsilon(\partial_t f^\varepsilon + \omega\cdot\nabla_x f^\varepsilon) = -\nabla_\omega\cdot(F_0^\varepsilon f^\varepsilon) + d\Delta_\omega f^\varepsilon + O(\varepsilon^2), \tag{4.10}$$

$$F_0^\varepsilon(x,\omega,t) = \nu(\omega\cdot\Omega^\varepsilon)\ (\mathrm{Id}-\omega\otimes\omega)\Omega^\varepsilon(x,t), \tag{4.11}$$

$$\Omega^\varepsilon(x,t) = \frac{j^\varepsilon(x,t)}{|j^\varepsilon(x,t)|}, \quad \text{and} \quad j^\varepsilon(x,t) = \int_{\upsilon\in\mathbb{S}^2}\upsilon\, f^\varepsilon(x,\upsilon,t)\,d\upsilon\,. \tag{4.12}$$

We note that observing the system at large scales makes the interaction local and that this interaction tends to align the particle velocity to the direction of the local particle flux. This interaction term is balanced at leading order by the diffusion term which tends to spread the particles isotropically on the sphere. Obviously, an equilibrium distribution results from the balance of these two antagonist phenomena.

In the remainder of the chapter, we write $F[f^\varepsilon]$ for F_0^ε. We introduce the operator

$$Q(f) = -\nabla_\omega\cdot(F[f]f) + d\Delta_\omega f, \tag{4.13}$$

$$F[f] = \nu\ (\mathrm{Id}-\omega\otimes\omega)\Omega[f], \tag{4.14}$$

$$\Omega[f] = \frac{j[f]}{|\ j[f]\ |}, \quad \text{and} \quad j[f] = \int_{\omega\in\mathbb{S}^2}\omega\, f\,d\omega\,. \tag{4.15}$$

We note that $\Omega[f]$ is a non linear operator of f, and so are $F[f]$ and $Q(f)$. In the remainder, we will always suppose that f is as smooth and integrable as necessary. We leave the question of finding the appropriate functional framework to forthcoming work.

The operator Q acts on the angle variable ω only and leaves the other variables x and t as parameters. Therefore, it is legitimate to study the properties of Q as an operator acting on functions of ω only. This is the task performed in the following section.

4.2 Properties of Q

We begin by looking for the equilibrium solutions, i.e. the functions f which cancel Q. Let $\mu = \cos\theta$. We denote by $\sigma(\mu)$ an antiderivative of $\nu(\mu)$, i.e. $(d\sigma/d\mu)(\mu) = \nu(\mu)$. We define

$$M_\Omega(\omega) = C \exp(\frac{\sigma(\omega\cdot\Omega)}{d}), \quad \int M_\Omega(\omega)\, d\omega = 1\,. \tag{4.16}$$

The constant C is set by the normalization condition (second equality of (4.16)) ; it depends only on d and on the function σ but not on Ω.

We have the following:

Lemma 4.2 *(i) The operator Q can be written as*

$$Q(f) = d\ \nabla_\omega \cdot \left[M_{\Omega[f]} \nabla_\omega \left(\frac{f}{M_{\Omega[f]}} \right) \right], \tag{4.17}$$

and we have

$$H(f) := \int_{\omega\in\mathbb{S}^2} Q(f) \frac{f}{M_{\Omega[f]}}\, d\omega = -d \int_{\omega\in\mathbb{S}^2} M_{\Omega[f]} \left| \nabla_\omega \left(\frac{f}{M_{\Omega[f]}} \right) \right|^2 d\omega \le 0. \tag{4.18}$$

(ii) The equilibria, i.e. the functions $f(\omega)$ such that $Q(f) = 0$ form a three-dimensional manifold $\mathcal{E}$ given by

$$\mathcal{E} = \{\rho M_\Omega(\omega) \quad | \quad \rho \in \mathbb{R}_+, \quad \Omega \in \mathbb{S}^2\}\,, \tag{4.19}$$

and ρ is the total mass while Ω is the director of the flux of $\rho M_\Omega(\omega)$, i.e.

$$\int_{\omega\in\mathbb{S}^2} \rho\, M_\Omega(\omega)\, d\omega = \rho, \tag{4.20}$$

$$\Omega = \frac{j[\rho M_\Omega]}{|\, j[\rho M_\Omega]\,|}\,, \quad j[\rho M_\Omega] = \int_{\omega\in\mathbb{S}^2} \rho M_\Omega(\omega)\, \omega\, d\omega. \tag{4.21}$$

Furthermore, $H(f) = 0$ if and only if $f = \rho M_\Omega$ for arbitrary $\rho \in \mathbb{R}_+$ and $\Omega \in \mathbb{S}^2$.

The function σ being an increasing function of μ (since $\nu > 0$), M_Ω is maximal for $\omega\cdot\Omega = 1$, i.e. for ω pointing in the direction of Ω. Therefore, Ω plays the same

role as the average velocity of the classical Maxwellian of gas dynamics. The role of the temperature is played by the normalized diffusion constant d : it measures the 'spreading' of the equilibrium about the average direction Ω. Here the temperature is fixed by the value of the diffusion constant, in contrast with classical gas dynamics where the temperature is a thermodynamical variable whose evolution is determined by the energy balance equation.

An elementary computation shows that the flux can be written

$$j[\rho M_\Omega] = \langle \cos\theta \rangle_M \, \rho\Omega, \tag{4.22}$$

where for any function $g(\cos\theta)$, the symbol $\langle g(\cos\theta)\rangle_M$ denotes the average of g over the probability distribution M_Ω, i.e.

$$\langle g(\cos\theta)\rangle_M = \int M_\Omega(\omega) g(\omega\cdot\Omega)\, d\omega = \frac{\int_0^\pi g(\cos\theta) \exp(\frac{\sigma(\cos\theta)}{d}) \, \sin\theta \, d\theta}{\int_0^\pi \exp(\frac{\sigma(\cos\theta)}{d}) \, \sin\theta \, d\theta}. \tag{4.23}$$

We note that $\langle g(\cos\theta)\rangle_M$ does not depend on Ω but depends on d. In particular, $\langle g(\cos\theta)\rangle_M \to g(1)$ when $d \to 0$ while $\langle g(\cos\theta)\rangle_M \to \bar{g}$, the arithmetic average of g over the sphere, when $d \to \infty$ (with $\bar{g} = \int g(\omega\cdot\Omega)\, d\omega = \frac{1}{2}\int_0^\pi g(\cos\theta)\, \sin\theta \, d\theta$). Therefore, $\langle \cos\theta\rangle_M \to 1$ when $d \to 0$ and $\langle \cos\theta\rangle_M \to 0$ when $d \to \infty$. For a large diffusion, the equilibrium is almost isotropic and the magnitude of the velocity tends to zero while for a small diffusion, the distribution is strongly peaked in the forward direction and the magnitude of the velocity tends to 1, which is the velocity of the individual particles.

Proof of lemma 4.2. To prove (i), we introduce a reference frame such that $e_3 = \Omega[f]$. In spherical coordinates, we have

$$M_{\Omega[f]}(\omega(\theta,\phi)) = C\exp(d^{-1}\sigma(\cos\theta)). \tag{4.24}$$

Therefore,

$$\begin{aligned} \nabla_\omega(\ln M_{\Omega[f]}) &= \nabla_\omega[\,\ln\{\, C\exp(d^{-1}\sigma(\cos\theta))\,\}\,] \\ &= d^{-1}\nabla_\omega(\sigma(\cos\theta)) \\ &= -d^{-1}\nu(\cos\theta)\sin\theta\, e_\theta \\ &= d^{-1}F[f]\,, \end{aligned} \tag{4.25}$$

where ln denotes the logarithm and the last equality results from (3.5). Then, we deduce that

$$\begin{aligned} d\ \nabla_\omega\cdot\left[M_{\Omega[f]}\nabla_\omega\left(\frac{f}{M_{\Omega[f]}}\right)\right] &= d\ \nabla_\omega\cdot\left[\nabla_\omega f - f\nabla_\omega(\ln M_{\Omega[f]})\right] \\ &= d\Delta_\omega f - \nabla_\omega\cdot(F[f]f) = Q(f). \end{aligned} \tag{4.26}$$

(4.18) follows directly from (4.17) and Stokes theorem.

(ii) follows directly from (i). If $Q(f) = 0$, then $H(f) = 0$. But $H(f)$ is the integral of a non-negative quantity and can be zero only if this quantity is identically zero,

which means $f = \rho M_{\Omega[f]}$ for a conveniently chosen ρ. Since $\Omega[f]$ can be arbitrary, the result follows. The remaining statements are obvious. ∎

Our task now is to determine the collision invariants of Q, i.e. the functions $\psi(\omega)$ such that

$$\int_{\omega\in\mathbb{S}^2} Q(f)\,\psi\,d\omega = 0, \quad \forall f. \tag{4.27}$$

Using (4.17), this equation can be rewritten as

$$\int_{\omega\in\mathbb{S}^2} \frac{f}{M_{\Omega[f]}}\nabla_\omega\cdot(M_{\Omega[f]}\nabla_\omega\psi)\,d\omega = 0, \quad \forall f. \tag{4.28}$$

Clearly, if $\psi =$ Constant, ψ is a collisional invariant. On the other hand, there is no other obvious conservation relation, since momentum is not conserved by the interaction operator. The constants span a one-dimensional function space, while the set of equilibria is a three-dimensional manifold. So, we need to find some substitute to the notion of collisional invariant, otherwise, in the limit $\varepsilon \to 0$, the problem will be under-determined, and in particular, we will lack an equation for Ω (appearing in the expression of the equilibrium).

To solve the problem, we slightly change the viewpoint. We fix $\Omega \in \mathbb{S}^2$ arbitrarily, and we ask the problem of finding all ψ's which are collisional invariants of $Q(f)$ for all f with director $\Omega[f] = \Omega$. Such a function ψ is not a collisional invariant in the strict sense, because (4.27) is valid for all f but only for a subclass of f. But this weaker concept of a collisional invariant is going to suffice for our purpose. So, for fixed Ω, we want to find all ψ's such that

$$\int_{\omega\in\mathbb{S}^2} \frac{f}{M_\Omega}\nabla_\omega\cdot(M_\Omega\nabla_\omega\psi)\,d\omega = 0, \quad \forall f \text{ such that } \Omega[f] = \Omega. \tag{4.29}$$

Now, saying that $\Omega[f] = \Omega$ is equivalent to saying that $j[f]$ is aligned with $\Omega[f]$, or again to

$$0 = \Omega \times j[f] = \int_{\omega\in\mathbb{S}^2} f\,(\Omega\times\omega)\,d\omega. \tag{4.30}$$

This last formula can be viewed as a linear constraint and, introducing the Lagrange multiplier β of this constraint, β being a vector normal to Ω, we can restate the problem of finding the 'generalized' collisional invariants (4.29) as follows: Given $\Omega \in \mathbb{S}^2$, find all ψ's such that there exist $\beta \in \mathbb{R}^3$ with $\Omega\cdot\beta = 0$, and

$$\int_{\omega\in\mathbb{S}^2} \frac{f}{M_\Omega}\left\{\nabla_\omega\cdot(M_\Omega\nabla_\omega\psi) - \beta\cdot(\Omega\times\omega)M_\Omega\right\}\,d\omega = 0, \quad \forall f. \tag{4.31}$$

Now, (4.31) holds for all f without constraint and immediately leads to the following problem for ψ:

$$\nabla_\omega\cdot(M_\Omega\nabla_\omega\psi) = \beta\cdot(\Omega\times\omega)M_\Omega. \tag{4.32}$$

The problem defining ψ is obviously linear, so that the set $\mathcal{C}_\Omega$ of generalized collisional invariants associated with the vector Ω is a vector space. It is convenient to introduce a Cartesian basis (e_1, e_2, Ω) and the associated spherical coordinates (θ, ϕ). Then $\beta = (\beta_1, \beta_2, 0)$ and $\beta \cdot (\Omega \times \omega) = (-\beta_1 \sin\phi + \beta_2 \cos\phi) \sin\theta$. Therefore, we can successively solve for ψ_1 and ψ_2, the solutions of (4.32) with right-hand sides respectively equal to $-\sin\phi \sin\theta M_\Omega$ and $\cos\phi \sin\theta M_\Omega$.

We are naturally looking for solutions in an $L^2(\mathbb{S}^2)$ framework, since ψ is aimed at constructing macroscopic quantities by integration against f with respect to ω. Therefore, one possible framework is to look for both f and ψ in $L^2(\mathbb{S}^2)$ to give a meaning to these macroscopic quantities. We state the following lemma:

Lemma 4.3 *Let $\chi \in L^2(\mathbb{S}^2)$ such that $\int \chi \, d\omega = 0$. The problem*

$$\nabla_\omega \cdot (M_\Omega \nabla_\omega \psi) = \chi, \tag{4.33}$$

has a unique weak solution in the space $\overset{\circ}{H}{}^1(\mathbb{S}^2)$, the quotient of the space $H^1(\mathbb{S}^2)$ by the space spanned by the constant functions, endowed with the quotient norm.

Proof. We apply the Lax-Milgram theorem to the following variational formulation of (4.33):

$$\int_{\omega \in \mathbb{S}^2} M_\Omega \nabla_\omega \psi \cdot \nabla_\omega \varphi \, d\omega = \int_{\omega \in \mathbb{S}^2} \chi \varphi \, d\omega, \tag{4.34}$$

for all $\varphi \in \overset{\circ}{H}{}^1(\mathbb{S}^2)$. The function M_Ω is bounded from above and below on $\mathbb{S}^2$, so the bilinear form at the left-hand side is continuous on $\overset{\circ}{H}{}^1(\mathbb{S}^2)$. The fact that the average of χ over $\mathbb{S}^2$ is zero ensures that the right-hand side is a continuous linear form on $\overset{\circ}{H}{}^1(\mathbb{S}^2)$. The coercivity of the bilinear form is a consequence of the Poincare inequality: $\exists C > 0$ such that $\forall \psi \in \overset{\circ}{H}{}^1(\mathbb{S}^2)$:

$$|\psi|_{H^1} \geq C ||\psi||_{\overset{\circ}{L}{}^2} := C \min_{K \in \mathbb{R}} ||\psi + K||_{L^2}, \tag{4.35}$$

where $|\psi|_{H^1}$ is the H^1 semi-norm. We note that the Poincare inequality would not hold without taking the quotient. ∎

So, to each of the right-hand sides $\chi = -\sin\phi \sin\theta M_\Omega$ or $\chi = \cos\phi \sin\theta M_\Omega$ which have zero average on the sphere, there exist solutions ψ_1 and ψ_2 respectively (unique up to constants) of problem (4.33). We single out unique solutions by requesting that ψ_1 and ψ_2 have zero average on the sphere: $\int \psi_k \, d\omega = 0$, $k = 1, 2$. We can state the following corollary to lemma 4.3:

Proposition 4.4 *The set $\mathcal{C}_\Omega$ of generalized collisional invariants associated with the vector Ω which belong to $H^1(\mathbb{S}^2)$ is a three dimensional vector space $\mathcal{C}_\Omega = Span\{1, \psi_1, \psi_2\}$.*

More explicit forms for ψ_1 and ψ_2 can be found. By expanding in Fourier series with respect to ϕ, we easily see that

$$\psi_1 = -g(\cos\theta)\sin\phi, \quad \psi_2 = g(\cos\theta)\cos\phi, \tag{4.36}$$

where $g(\mu)$ is the unique solution of the elliptic problem on $[-1,1]$:

$$-(1-\mu^2)\partial_\mu(e^{\sigma(\mu)/d}(1-\mu^2)\partial_\mu g) + e^{\sigma(\mu)/d} g = -(1-\mu^2)^{3/2} e^{\sigma(\mu)/d}. \tag{4.37}$$

We note that no boundary condition is needed to specify g uniquely since the operator at the left-hand side of (4.37) is degenerate at the boundaries $\mu = \pm 1$. Indeed, it is an easy matter, using again Lax-Milgram theorem, to prove that problem (4.37) has a unique solution in the weighted H^1 space V defined by

$$V = \{g \,|\, (1-\mu^2)^{-1/2} g \in L^2(-1,1), \quad (1-\mu^2)^{1/2}\partial_\mu g \in L^2(-1,1)\}.$$

Furthermore, the Maximum Principle shows that g is non-positive.

For convenience, we introduce $h(\mu) = (1-\mu^2)^{-1/2} g \in L^2(-1,1)$ or equivalently $h(\cos\theta) = g(\cos\theta)/\sin\theta$. We then define

$$\vec{\psi}(\omega) = (\Omega \times \omega)\, h(\Omega \cdot \omega) = \psi_1 e_1 + \psi_2 e_2\,. \tag{4.38}$$

$\vec{\psi}$ is the vector generalized collisional invariant associated with the direction Ω.

4.3 Limit $\varepsilon \to 0$

The goal of this section is to prove theorem 1.1.

Again, we suppose that all functions are as regular as needed and that all convergences are as strong as needed. The rigorous proof of this convergence result is outside the scope of this article.

We start with eq. (4.10) which can be written

$$\varepsilon(\partial_t f^\varepsilon + \omega \cdot \nabla_x f^\varepsilon) = Q(f^\varepsilon) + O(\varepsilon^2). \tag{4.39}$$

We suppose that $f^\varepsilon \to f$ when $\varepsilon \to 0$. Then, from the previous equation, $Q(f^\varepsilon) = O(\varepsilon)$ and we deduce that $Q(f) = 0$. By lemma 4.2, $f = \rho M_\Omega$, with $\rho \geq 0$ and $\Omega \in \mathbb{S}^2$. Now, since Q operates on the variable ω only, this limit does not specify the dependence of f on (x,t), and consequently, ρ and Ω are functions of (x,t).

To find this dependence, we use the generalized collisional invariants. First, we consider the constant collisional invariants, which merely means that we integrate (4.39) with respect to ω. We find the continuity equation

$$\partial_t \rho^\varepsilon + \nabla_x \cdot j^\varepsilon = 0, \tag{4.40}$$

where ρ^ε and j^ε are the density and flux as defined above. It is an easy matter to realize that the right-hand side is exactly zero (and not $O(\varepsilon^2)$). In the limit $\varepsilon \to 0$, $\rho^\varepsilon \to \rho$ and $j^\varepsilon \to j = c_1 \rho \Omega$ with

$$c_1 = \langle \cos\theta \rangle_M, \tag{4.41}$$

and we get

$$\partial_t \rho + \nabla_x \cdot (c_1 \rho \Omega) = 0. \tag{4.42}$$

Now, we multiply (4.39) by $\vec{\psi}^\varepsilon = h(\omega \cdot \Omega[f^\varepsilon])\,(\Omega[f^\varepsilon] \times \omega)$, integrate with respect to ω and take the limit $\varepsilon \to 0$. We note that $\Omega[f^\varepsilon] \to \Omega$ and that $\vec{\psi}^\epsilon$ is smooth enough (given the functional spaces used for the existence theory), and consequently, $\vec{\psi}^\varepsilon \to \vec{\psi} = h(\omega \cdot \Omega)\,(\Omega \times \omega)$. Therefore, in the limit $\varepsilon \to 0$, we get:

$$\Omega \times X = 0\,, \quad X := \int_{\omega \in \mathbb{S}^2} (\partial_t(\rho M_\Omega) + \omega \cdot \nabla_x(\rho M_\Omega))\, h(\omega \cdot \Omega)\, \omega\, d\omega. \tag{4.43}$$

Saying that $\Omega \times X = 0$ is equivalent to saying that the projection of X onto the plane normal to Ω vanishes or in other words, that

$$(\mathrm{Id} - \Omega \otimes \Omega) X = 0\,. \tag{4.44}$$

This is the equation that we need to make explicit in order to find the evolution equation for Ω.

Elementary differential geometry gives the derivative of M_Ω with respect to Ω acting on a tangent vector $d\Omega$ to the sphere as follows:

$$\frac{\partial M_\Omega}{\partial \Omega}(d\Omega) = d^{-1} \nu(\omega \cdot \Omega)\,(\omega \cdot d\Omega)\, M_\Omega. \tag{4.45}$$

We deduce that

$$\partial_t(\rho M_\Omega) = M_\Omega\,(\partial_t \rho + d^{-1} \nu\, \rho\,(\omega \cdot \partial_t \Omega)), \tag{4.46}$$

$$(\omega \cdot \nabla_x)(\rho M_\Omega) = M_\Omega\,((\omega \cdot \nabla_x)\rho + d^{-1} \nu\, \rho\, \omega \cdot ((\omega \cdot \nabla_x)\Omega)). \tag{4.47}$$

Combining these two identities, we get:

$$\begin{aligned} \partial_t(\rho M_\Omega) + \omega \cdot \nabla_x(\rho M_\Omega) = \\ = M_\Omega \left[\partial_t \rho + \omega \cdot \nabla_x \rho + d^{-1} \nu \rho (\,\omega \cdot \partial_t \Omega + (\omega \otimes \omega) : \nabla_x \Omega\,)\right], \end{aligned} \tag{4.48}$$

where the symbol ':' denotes the contracted product of two tensors (if $A = (A_{ij})_{i,j=1,\dots,3}$ and $B = (B_{ij})_{i,j=1,\dots,3}$ are two tensors, then $A : B = \sum_{i,j=1,\dots,3} A_{ij} B_{ij}$) and $\nabla_x \Omega$ is the gradient tensor of the vector Ω: $(\nabla_x \Omega)_{ij} = \partial_{x_i} \Omega_j$. Therefore, the vector X, is given by:

$$X = \int_{\omega \in \mathbb{S}^2} \left[\partial_t \rho + \omega \cdot \nabla_x \rho + d^{-1} \nu \rho (\,\omega \cdot \partial_t \Omega + (\omega \otimes \omega) : \nabla_x \Omega\,)\right] \omega\, h\, M_\Omega\, d\omega. \tag{4.49}$$

The four terms in this formula, denoted by X_1 to X_4, are computed successively using spherical coordinates (θ, ϕ) associated with a Cartesian basis (e_1, e_2, Ω) where e_1 and e_2 are two vectors normal to Ω. In the integral (4.49), the functions $h = h(\cos\theta)$, $\nu = \nu(\cos\theta)$ and $M_\Omega = C \exp(\frac{\sigma(\cos\theta)}{d})$ only depend on θ. Therefore, the integrals with respect to ϕ only concern the repeated tensor products of ω.

We first have that $\int_0^{2\pi} \omega \, d\phi = 2\pi \, \cos\theta \, \Omega$, so that

$$X_1 = \int_{\omega \in \mathbb{S}^2} \partial_t \rho \, \omega \, h \, M_\Omega \, d\omega = 2\pi \, \partial_t \rho \int_0^\pi \cos\theta \, h(\cos\theta) \, M_\Omega(\cos\theta) \, \sin\theta \, d\theta \, \Omega, \tag{4.50}$$

and $(\mathrm{Id} - \Omega \otimes \Omega) X_1 = 0$.

Now, an easy computation shows that

$$\int_0^{2\pi} \omega \otimes \omega \, d\phi = \pi \sin^2\theta \, (\mathrm{Id} - \Omega \otimes \Omega) + 2\pi \cos^2\theta \, \Omega \otimes \Omega. \tag{4.51}$$

We deduce that

$$\begin{aligned} X_2 &= \int_{\omega \in \mathbb{S}^2} ((\omega \otimes \omega) \nabla_x \rho) \, h \, M_\Omega \, d\omega \\ &= \pi \int_0^\pi \sin^2\theta \, h \, M_\Omega \, \sin\theta \, d\theta \, (\mathrm{Id} - \Omega \otimes \Omega) \nabla_x \rho + \\ &\quad + 2\pi \int_0^\pi \cos^2\theta \, h \, M_\Omega \, \sin\theta \, d\theta \, (\Omega \cdot \nabla_x \rho) \, \Omega, \end{aligned} \tag{4.52}$$

which leads to:

$$(\mathrm{Id} - \Omega \otimes \Omega) X_2 = \pi \int_0^\pi \sin^2\theta \, h \, M_\Omega \, \sin\theta \, d\theta \, (\mathrm{Id} - \Omega \otimes \Omega) \nabla_x \rho. \tag{4.53}$$

Using (4.51) again, we find:

$$\begin{aligned} X_3 &= d^{-1} \rho \int_{\omega \in \mathbb{S}^2} ((\omega \otimes \omega) \partial_t \Omega) \, \nu \, h \, M_\Omega \, d\omega \\ &= \pi d^{-1} \rho \int_0^\pi \sin^2\theta \, \nu \, h \, M_\Omega \, \sin\theta \, d\theta \, (\mathrm{Id} - \Omega \otimes \Omega) \partial_t \Omega \\ &\quad + 2\pi d^{-1} \rho \int_0^\pi \cos^2\theta \, \nu \, h \, M_\Omega \, \sin\theta \, d\theta \, (\Omega \cdot \partial_t \Omega) \, \Omega. \end{aligned} \tag{4.54}$$

The second term at the r.h.s. of (4.54) vanishes since $\partial_t \Omega$ is normal to Ω (Ω being a unit vector). For the same reason, $(\mathrm{Id} - \Omega \otimes \Omega) \partial_t \Omega = \partial_t \Omega$ and we are left with:

$$(\mathrm{Id} - \Omega \otimes \Omega) X_3 = \pi d^{-1} \rho \int_0^\pi \sin^2\theta \, \nu \, h \, M_\Omega \, \sin\theta \, d\theta \, \partial_t \Omega. \tag{4.55}$$

We now need to compute the integral with respect to ϕ of the third tensor power of ω. After some computations, we are left with

$$\begin{aligned} \int_0^{2\pi} \omega \otimes \omega \otimes \omega \, d\phi &= \pi \sin^2\theta \cos\theta \, ((\mathrm{Id} - \Omega \otimes \Omega) \otimes \Omega + \Omega \otimes (\mathrm{Id} - \Omega \otimes \Omega) \\ &\qquad + [(\mathrm{Id} - \Omega \otimes \Omega) \otimes \Omega \otimes (\mathrm{Id} - \Omega \otimes \Omega)]_{:24}) \\ &\quad + 2\pi \cos^3\theta \; \Omega \otimes \Omega \otimes \Omega, \end{aligned} \tag{4.56}$$

where the index ': 24' indicates contraction of the indices 2 and 4. In other words, the tensor element $(\int_0^{2\pi} \omega \otimes \omega \otimes \omega \, d\phi)_{ijk}$ equals $\pi \sin^2\theta \cos\theta$ when (i, j, k) equals any of the triples $(1, 1, 3)$, $(2, 2, 3)$, $(3, 1, 1)$, $(3, 2, 2)$, $(1, 3, 1)$, $(2, 3, 2)$, equals $2\pi \cos^3\theta$ when

$(i,j,k) = (3,3,3)$ and is equal to 0 otherwise. Using Einstein's summation convention, the following formula follows:

$$\begin{aligned}(\int_0^{2\pi} \omega\otimes\omega\otimes\omega\, d\phi)\nabla_x\Omega &= \left(\int_0^{2\pi} \omega\otimes\omega\otimes\omega\, d\phi\right)_{ijk} \partial_{x_j}\Omega_k \\ &= \pi\sin^2\theta\cos\theta\,((\mathrm{Id}-\Omega\otimes\Omega)_{ij}\Omega_k\partial_{x_j}\Omega_k + \Omega_i(\mathrm{Id}-\Omega\otimes\Omega)_{jk}\partial_{x_j}\Omega_k + \\ &\qquad +(\mathrm{Id}-\Omega\otimes\Omega)_{ik}\Omega_j\partial_{x_j}\Omega_k) \\ &\quad +2\pi\cos^3\theta\ \Omega_i\Omega_j\Omega_k\partial_{x_j}\Omega_k. \end{aligned} \tag{4.57}$$

But since Ω is a unit vector, $\Omega_k\partial_{x_j}\Omega_k = \frac{1}{2}\partial_{x_j}(|\Omega|^2) = 0$ and the first and fourth terms in the sum vanish. The expression simplifies into:

$$\begin{aligned}(\int_0^{2\pi} \omega\otimes\omega\otimes\omega\, d\phi)\nabla_x\Omega &= \pi\sin^2\theta\cos\theta\,((\mathrm{Id}-\Omega\otimes\Omega):(\nabla_x\Omega))\,\Omega + \\ &\quad +\pi\sin^2\theta\cos\theta\,(\mathrm{Id}-\Omega\otimes\Omega)((\Omega\cdot\nabla)\Omega). \end{aligned} \tag{4.58}$$

The first term is parallel to Ω. Besides, since Ω is a unit vector, $(\Omega\cdot\nabla)\Omega$ is normal to Ω. So, we finally get

$$(\mathrm{Id}-\Omega\otimes\Omega)((\int_0^{2\pi} \omega\otimes\omega\otimes\omega\, d\phi)\nabla_x\Omega) = \pi\sin^2\theta\cos\theta\,(\Omega\cdot\nabla)\Omega. \tag{4.59}$$

This leads to the following formula for X_4:

$$\begin{aligned}(\mathrm{Id}-\Omega\otimes\Omega)X_4 &= d^{-1}\rho\,(\mathrm{Id}-\Omega\otimes\Omega)\left(\int_{\omega\in\mathbb{S}^2}(\omega\otimes\omega\otimes\omega)(\nabla_x\Omega)\,\nu\,h\,M_\Omega\,d\omega\right) \\ &= \pi d^{-1}\rho\int_0^\pi \sin^2\theta\cos\theta\,\nu\,h\,M_\Omega\,\sin\theta\,d\theta\ (\Omega\cdot\nabla)\Omega. \end{aligned} \tag{4.60}$$

Now, we insert the expressions of X_1 to X_4 into (4.44). Using notation (4.23), we finally find the evolution equation for Ω:

$$\begin{aligned}d^{-1}\rho\,\langle\sin^2\theta\,\nu\,h\rangle_M\ \partial_t\Omega + d^{-1}\rho\langle\sin^2\theta\cos\theta\,\nu\,h\rangle_M\,(\Omega\cdot\nabla)\Omega + \\ +\langle\sin^2\theta\,h\rangle_M\,(\mathrm{Id}-\Omega\otimes\Omega)\nabla_x\rho = 0. \end{aligned} \tag{4.61}$$

By the maximum principle, the function h is non-positive. Therefore, we can define similar averages as (4.23), substituting M_Ω with $\sin^2\theta\,\nu\,h\,M_\Omega$ and we denote such averages as $\langle g\rangle_{(\sin^2\theta)\nu h M}$. With such a notation, (4.61) becomes:

$$\rho\ (\partial_t\Omega + c_2(\Omega\cdot\nabla)\Omega) + \lambda\,(\mathrm{Id}-\Omega\otimes\Omega)\nabla_x\rho = 0, \tag{4.62}$$

with

$$c_2 = \langle\cos\theta\rangle_{(\sin^2\theta)\nu h M}\,, \quad \lambda = d\left\langle\frac{1}{\nu}\right\rangle_{(\sin^2\theta)\nu h M} \tag{4.63}$$

Collecting the mass and momentum eqs (4.42) and (4.62), we find the final macroscopic model of the Couzin-Vicsek algorithm:

$$\partial_t\rho + \nabla_x\cdot(c_1\rho\Omega) = 0, \tag{4.64}$$

$$\rho\ (\partial_t\Omega + c_2(\Omega\cdot\nabla)\Omega) + \lambda\,(\mathrm{Id}-\Omega\otimes\Omega)\nabla_x\rho = 0, \tag{4.65}$$

with the coefficients c_1, c_2 and λ given by (4.41) and (4.63). This ends the proof of theorem 1.1.

4.4 Hyperbolicity

The detailed study (both theoretical and numerical) of the properties of the continuum model (1.4), (1.5), will be the subject of future work. As a preliminary step, we look at the hyperbolicity of the model.

First, thanks to a temporal rescaling, $t = t'/c_1$, we can replace c_1 by 1, c_2 by $c := c_2/c_1$ and λ by $\lambda' = \lambda/c_1$. We will omit the primes for simplicity. Then, the system reads:

$$\partial_t \rho + \nabla_x \cdot (\rho \Omega) = 0, \tag{4.66}$$

$$\rho \, (\partial_t \Omega + c(\Omega \cdot \nabla)\Omega) + \lambda \, (\mathrm{Id} - \Omega \otimes \Omega)\nabla_x \rho = 0. \tag{4.67}$$

This rescaling amounts to saying that the magnitude of the velocity of the individual particles is equal to $1/c_1$ in the chosen system of units.

We choose an arbitrary fixed Cartesian coordinate system $(\Omega_1, \Omega_2, \Omega_3)$ and use spherical coordinates (θ, ϕ) in this system (see section 3). Then, $\Omega = (\sin\theta\cos\phi, \sin\theta\sin\phi, \cos\theta)$. A simple algebra shows that (ρ, θ, ϕ) satisfy the system

$$\partial_t \rho + \partial_x(\rho \sin\theta\cos\phi) + \partial_y(\rho\sin\theta\sin\phi) + \partial_z(\rho\cos\theta) = 0, \tag{4.68}$$

$$\begin{aligned}\partial_t \theta + c(&\sin\theta\cos\phi\,\partial_x\theta + \sin\theta\sin\phi\,\partial_y\theta + \cos\theta\partial_z\theta) + \\ &+\lambda\,(\cos\theta\cos\phi\,\partial_x \ln\rho + \cos\theta\sin\phi\,\partial_y\ln\rho - \sin\theta\,\partial_z\ln\rho) = 0,\end{aligned} \tag{4.69}$$

$$\begin{aligned}\partial_t \phi + c(&\sin\theta\cos\phi\,\partial_x\phi + \sin\theta\sin\phi\,\partial_y\phi + \cos\theta\partial_z\phi) + \\ &+\lambda\,(-\sin\theta\sin\phi\,\partial_x\ln\rho + \sin\theta\cos\phi\,\partial_y\ln\rho) = 0.\end{aligned} \tag{4.70}$$

Supposing that ρ, θ, ϕ are independent of x and y amounts to looking at waves which propagate in the z direction at a solid angle (θ, ϕ) with the velocity director Ω. In this geometry, the system reads:

$$\partial_t \rho + \cos\theta\,\partial_z\rho - \rho\sin\theta\,\partial_z\theta = 0, \tag{4.71}$$

$$\partial_t\theta + c\cos\theta\,\partial_z\theta - \lambda\,\sin\theta\,\partial_z\ln\rho = 0, \tag{4.72}$$

$$\partial_t\phi + c\cos\theta\,\partial_z\phi = 0. \tag{4.73}$$

This is a first order system of the form

$$\begin{pmatrix} \partial_t\rho \\ \partial_t\theta \\ \partial_t\phi \end{pmatrix} + A(\rho,\theta,\phi)\begin{pmatrix} \partial_z\rho \\ \partial_z\theta \\ \partial_z\phi \end{pmatrix} = 0, \tag{4.74}$$

with

$$A(\rho,\theta,\phi) = \begin{pmatrix} \cos\theta & -\rho\sin\theta & 0 \\ -\frac{\lambda\sin\theta}{\rho} & c\cos\theta & 0 \\ 0 & 0 & c\cos\theta \end{pmatrix}. \tag{4.75}$$

The eigenvalues $\gamma_\pm$ and γ_0 of the matrix $A(\rho,\theta,\phi)$ are readily computed and are given by

$$\gamma_0 = c\cos\theta, \quad \gamma_\pm = \frac{1}{2}\left[(c+1)\cos\theta \pm \left((c-1)^2\cos^2\theta + 4\lambda\sin^2\theta\right)^{1/2}\right]. \tag{4.76}$$

Two special cases are noteworthy. The case $\theta = 0$ (modulo π) corresponds to waves which propagate parallel to the velocity director. In this case, two eigenvalues are equal: $\gamma_0 = \gamma_+ = c$ and $\gamma_- = 1$. The eigenvectors corresponding to these three eigenvalues are respectively the density ρ, and the angles θ and ϕ. So far, the relative magnitude of c and 1 are not known. But, whatever the situation (c bigger or smaller or even equal to 1), the matrix is diagonalizable and therefore the system is hyperbolic.

The case $\theta = \pi/2$ (modulo π) corresponds to waves propagating normally to the velocity director. In this case, $\gamma_\pm = \pm 2\sqrt{\lambda}$ are opposite and $\gamma_0 = 0$. The system for (ρ,θ) reduces to a special form of the nonlinear wave equation. The sound speed which propagates in the medium due to the interactions between the particles has magnitude equal to $2\sqrt{\lambda}$.

If θ has an arbitrary value, then, a combination of these two phenomena occurs. For the two waves associated with $\gamma_\pm$, there is a net drift at velocity $(c+1)\cos\theta$ and two sound waves with velocities $\left((c-1)^2\cos^2\theta + 4\lambda\sin^2\theta\right)^{1/2}$. However, the speed of the wave associated with γ_0, is not equal to the drift of the two sound waves. A disymmetry appears which is not present in the usual gas dynamics equations. The resolution of the Riemann problem is left to future work.

5 Conclusion

In this chapter, we have studied the large-scale dynamics of the Couzin-Vicsek algorithm. For that purpose, we have rephrased the dynamics as a time-continuous one and have formulated it in terms of a kinetic Fokker-Planck equation. Then, a hydrodynamic scaling of this kinetic equation is introduced with small parameter ε and the limit when $\varepsilon \to 0$ is considered. We show that the macroscopic dynamics takes place on a three dimensional manifold consisting of the density and director of the mean-velocity. Using a new concept of generalized collision invariant, we are able to derive formally the set of equations satisfied by the parameters and we prove that the resulting system is hyperbolic.

Possible future directions involve the investigation of a limited range of vision in the backwards direction, the computation of the order ε diffusive corrections, the incorporation of more non-locality effects in the asymptotics and finally, the accounting of the other types of interactions, being of repulsive or attractive type.

Bibliography

[1] M. Aldana and C. Huepe, *Phase transitions in self-driven many-particle systems and related non-equilibrium models: a network approach*, J. Stat. Phys., 112, no 1/2 (2003), pp. 135–153.

[2] I. Aoki, *A simulation study on the schooling mechanism in fish*, Bulletin of the Japan Society of Scientific Fisheries, 48 (1982), pp. 1081–1088.

[3] D. Armbruster, P. Degond and C. Ringhofer, *A model for the dynamics of large queuing networks and supply chains*, SIAM J. Appl. Math., 66 (2006), pp. 896–920.

[4] A. Aw, A. Klar, M. Rascle and T. Materne, *Derivation of continuum traffic flow models from microscopic follow-the-leader models*, SIAM J. Appl. Math., 63 (2002), pp. 259–278.

[5] D. R. Brillinger, H. K. Preisler, A. A. Ager, J. G. Kie and B. S. Stewart, *Employing stochastic differential equations to model wildlife motion*, Bull Braz Math Soc, 33 (2002), pp. 385–408.

[6] R. E. Caflisch, *The fluid dynamic limit of the nonlinear Boltzmann equation*, Comm. Pure Appl. Math., 33 (1980), pp. 651-666.

[7] S. Camazine, J-L. Deneubourg, N. R. Franks, J. Sneyd, G. Theraulaz and E. Bonabeau, Self-Organization in Biological Systems, Princeton University Press, 2002.

[8] C. Cercignani, R. Illner, M. Pulvirenti, The mathematical theory of dilute gases, Springer-Verlag, New-York, 1991.

[9] I. D. Couzin, J. Krause, R. James, G. D. Ruxton and N. R. Franks, *Collective Memory and Spatial Sorting in Animal Groups*, J. theor. Biol., 218 (2002), pp. 1–11.

[10] F. Cucker, S. Smale, *Emergent Behavior in Flocks*, IEEE Transactions on Automatic Control, 52 (2007), pp. 852–862.

[11] P. Degond, *Macroscopic limits of the Boltzmann equation: a review*, in Modeling and computational methods for kinetic equations, P. Degond, L. Pareschi, G. Russo (eds), Modeling and Simulation in Science, Engineering and Technology Series, Birkhauser, 2003, pp. 3–57.

[12] P. Degond and S. Motsch. *Large scale dynamics of the Persistent Turning Walker Model of fish behavior*, J. Stat. Phy., 131(6):989–1021, 2008.

[13] P. Degond and S. Motsch, *Macroscopic limit of self-driven particles with orientation interaction*, note, to be published.

[14] P. Degond, C. Ringhofer, *Stochastic dynamics of long supply chains with random breakdowns*, à paraître dans SIAM J. Appl. Math.

[15] R. J. DiPerna, P. L. Lions, *On the Cauchy Problem for Boltzmann Equations: Global Existence and Weak Stability*, The Annals of Mathematics, 130, (1989), pp. 321-366.

[16] M. R. D'Orsogna, Y. L. Chuang, A. L. Bertozzi and L. Chayes, *Self-propelled particles with soft-core interactions: patterns, stability and collapse*, Phys. Rev. Lett., 2006.

[17] L. Edelstein-Keshet, *Mathematical models of swarming and social aggregation*, invited lecture, The 2001 International Symposium on Nonlinear Theory and its Applications, (NOLTA 2001) Miyagi, Japan (Oct 28-Nov 1, 2001).

[18] J. Gautrais, S. Motsch, C. Jost, M. Soria, A. Campo, R. Fournier, S. Bianco and G. Théraulaz, *Analyzing fish movement as a persistent turning walker*, in preparation.

[19] G. Grégoire, and H. Chaté, *Onset of collective and cohesive motion*, Phys. Rev. Lett., 92 (2004) 025702.

[20] D. Helbing, *Traffic and related self-driven many-particle systems*, Reviews of modern physics, 73 (2001), pp. 1067–1141.

[21] C. Jost et al., *From individual to collective ant displacements in heterogenous environments*, preprint, 2007.

[22] B. L. Keyfitz, *A geometric theory of conservation laws which change type*, Zeitschrift fur Angewandte Mathematik und Mechanik, 75, (1995), 571-581.

[23] V. L. Kulinskii, V. I. Ratushnaya, A. V. Zvelindovsky, D. Bedeaux, *Hydrodynamic model for a system of self-propelling particles with conservative kinematic constraints*, Europhys. Lett., 71 (2005), pp. 207–213.

[24] H. Liu, H. Zhang and P.W. Zhang *Axial Symmetry and Classification of Stationary Solutions of Doi-Onsager Equation on the Sphere with Maier-Saupe Potential*, Comm. Math. Sci. 3 (2), (2005), 201-218.

[25] A. Mogilner and L. Edelstein-Keshet, *A non-local model for a swarm*, J. Math. Biol., 38 (1999), pp. 534–570.

[26] A. Mogilner, L. Edelstein-Keshet, L. Bent and A. Spiros, *Mutual interactions, potentials, and individual distance in a social aggregation*, J. Math. Biol., 47 (2003), pp. 353–389.

[27] J. K. Parrish and S. V. Viscido, *Traffic rules of fish schools: a review of agent-based approaches*, in 'Self-Organization and Complexity', CK Hemelrijk (ed.), Cambridge University Press, 2003.

[28] J. K. Parrish, S. V. Viscido and D. Grünbaum, *Self-organized fish schools: an examination of emergent properties*, The biological bulletin, 202 (2002), pp. 296–305.

[29] V. I. Ratushnaya, D. Bedeaux, V. L. Kulinskii and A. V. Zvelindovsky, *Collective behaviour of self propelling particles with kinematic constraints ; the relations between the discrete and the continuous description*, Physica A, to appear.

[30] V. I. Ratushnaya, V. L. Kulinskii, A. V. Zvelindovsky, D. Bedeaux, *Hydrodynamic model for the system of self propelling particles with conservative kinematic constraints; two dimensional stationary solutions* Physica A, 366, (2006), pp. 107–114.

[31] Y. Sone, Kinetic Theory and Fluid Dynamics, Birkhauser, 2002.

[32] H. Spohn, Large scale dynamics of interacting particles, Springer, Berlin, 1991.

[33] Theraulaz et al., *Spatial patterns in ant colonies*, Proceedings of the National Academy of Sciences, 99 (2002), pp. 9645–9649.

[34] C. M. Topaz and A. L. Bertozzi, *Swarming patterns in a two-dimensional kinematic model for biological groups*, SIAM J. Appl. Math, 65 (2004), pp. 152–174.

[35] C. M. Topaz, A. L. Bertozzi, M. A. Lewis, *A nonlocal continuum model for biological aggregation*, Bull. Math. Biol., 68 (2006), pp. 1601–1623.

[36] T. Vicsek, A. Czirók, E. Ben-Jacob, I. Cohen and O. Shochet, *Novel type of phase transition in a system of self-driven particles*, Phys. Rev. Lett., 75 (1995), pp. 1226–1229.

[37] S-H. Yu, *Hydrodynamic limits with shock waves of the Boltzmann equation*, Comm. Pure Appl. Math., 58 (2004), pp. 409–443.

Chapter 7

Numerical simulations of a non-conservative hyperbolic system with geometric constraints describing swarming behaviour

This chapter is a work in progress in collaboration with Laurent Navoret.

Abstract. The Vicsek model is a very popular individual based model which describes collective behaviour among animal societies. A macroscopic version of the Vicsek model has been derived from a large scale limit of this individual based model 6. In this work, we want to numerically validate this Macroscopic Vicsek model (MV). To this aim, we compare simulations of the macroscopic and microscopic models one with each other. The MV model is a non-conservative hyperbolic equation with a geometric constraint. Due to the lack of theory for this kind of equation, we derive several equivalent for this system leading to specific numerical schemes. The numerical simulations reveals that the microscopic and macroscopic models are in good agreement provided that we choose one of the proposed formulations based on a relaxation of the geometric constraint. This confirms the relevance of the macroscopic equation but it also calls for a better theoretical understanding of this type of equations.

Keywords. Individual based model, Hyperbolic systems, Non-conservative equation, Geometric constraint, Relaxation, Splitting scheme

1 Introduction

This paper is devoted to the numerical study of a macroscopic version of the Vicsek model which describes swarming behaviour. This macroscopic model has been derived in [13] from the microscopic Vicsek model [28]. The goal of this work is to provide a numerical validation of the macroscopic model by comparing it with simulations of the microscopic model.

The Vicsek model [28] is widely used to describe swarming behaviour such as flock of birds [3], schools of fish [2, 25, 19, 9] (in this case the model is combined with an attractive-repulsive force) or recently the motion of locusts [5]. In this model, individuals have a constant velocity and they tend to align with theirs neighbours. Despite the simplicity of the model, a lot of questions remain open about it. A first field of research concerns phase transitions within the model depending on the level of noise in the model [28, 16, 24, 6]. Another question arises from the long time dynamics of the model [10, 11, 17]: is there convergence to a stationary state of the system? From another perspective, since collective displacements in natural environment can concern up to several million individuals, it is natural to look for a macroscopic version of the Vicsek model. On the one hand, macroscopic models constitute powerful analytical tools to study the dynamics at large scales [23, 8, 12]. On the other hand, the related numerical schemes are computationally much more efficient compared with particle simulations of a large number of interacting agents. In [13], a Macroscopic Vicsek model (MV) has been derived from a large scale limit of the "microscopic" Vicsek model. The macroscopic model is obtained from a rigorous perturbation theory of the original Vicsek model. Another macroscopic model is obtained in [4] based on more phenomenological closure assumptions.

The MV model presents several specificities which make the model interesting. First, it is a non-conservative hyperbolic system and secondly it involves a geometric constraint. These are the consequences at the macroscopic level of two specificities of the microscopic model: the total momentum is not conserved by the particle dynamics and the speed of the particles is constant. The first property is an intrinsic property of self-propelled particles and the second property is an usual assumption in the models of collective displacements [28, 9, 15]. Up to our knowledge the theory of such systems is almost empty. Non-conservative systems have been studied in the literature [**?**, 20, 7] but none of them involve geometric constraints.

In this work, since a theoretical framework for such systems is not available, we adopt several approaches. First, we introduce a conservative formulation for 1D problems, which is equivalent to the initial one for smooth solutions only. With this conservative formulation, we can use standard hyperbolic theory to build Riemann problem solution and shock capturing schemes [21]. The numerical scheme based on the conservative formulation is called *conservative method*. But since the equivalence with the original formulation is only valid for smooth solutions [22], there is no guarantee that the conservative formulation gives the right answer at shocks. For this reason, we introduce another formulation of the MV model where the constraint is treated through the relaxation limit of a unconstrained conservative system. This formulation leads to a natural numerical scheme based on a splitting between the conservative part of the

equation and the relaxation. This scheme will be refered to as the *splitting method*. For comparison purposes, two other numerical schemes are also used, an *upwind scheme* and a *semi-conservative* one (where only the mass conservation equation is treated in a conservative way).

The numerical simulations of the MV model reveal that the numerical schemes all agree on rarefaction waves but disagree on shock waves. To determine the correct solution, we use the microscopic model in the regime where its solution is close to that of the macroscopic model. In practice, this corresponds to regimes where the number of particles per domain of interaction is high. The splitting method turns out to be in good agreement with particle simulations of the microscopic model, by contrast with the other schemes. In particular, for an initial condition with a contact discontinuity, the solution given by the conservative form is simply a convection of the initial condition whereas the splitting method and the particle simulations agree on a different and more complex solution.

These results show first that the MV model well describes the microscopic model in the dense regime. Secondly, that the correct formulation of the MV model is given by the limit of a conservative equation with a stiff relaxation term.

The theoretical and numerical studies of the MV model highlight the specificity of non-conservative hyperbolic models with geometric constraints. More theoretical work is necessary in order to understand why the splitting method matches the microscopic model whereas the other methods do not. In particular, an extension of the theory developed in [7] to non-conservative relaxed models would be highly desirable.

The outline of the paper is as follows: first, we present the Vicsek and MV models in section 2. Then, we analyze the MV model and give two different formulations of the model in section 3. We develop different numerical schemes based on these formulations and we use them to numerically solve different Riemann problems in section 4. Finally, we compare simulations of the microscopic model with those of the macroscopic system in the same situations in section 5. Finally, we draw a conclusion.

2 Presentation of the Vicsek and Macroscopic Vicsek models

At the particle level, the Vicsek model describes the motion of particles which tend to align with theirs neighbours. We denote by x_k the position vector of the k^{th} particle and by ω_k its velocity with a constant speed ($|\omega_k| = 1$). To simplify, we suppose that the particles moves in a plane. Therefore $x_k \in \mathbb{R}^2$ and $\omega_k \in S^1$. The Vicsek model at the microscopic level is given by the following equations (in dimensionless variables):

$$\frac{dx_k}{dt} = \omega_k, \tag{2.1}$$

$$d\omega_k = (\mathrm{Id} - \omega_k \otimes \omega_k)(\bar{\omega}_k\, dt + \sqrt{2d}\, dB_t), \tag{2.2}$$

where Id is the identity matrix and the symbol $\otimes$ denotes the tensor product of vectors. d is the intensity of noise, B_t is the Brownian motion and $\bar{\omega}_k$ is the direction of mean

velocity around the k$^{\text{th}}$ particle defined by:

$$\bar{\omega}_k = \frac{J_k}{|J_k|}\,, \qquad J_k = \sum_{j,\,|x_j - x_k| \le R} \omega_j, \tag{2.3}$$

where R defines the radius of the interaction region. Equation (2.2) expresses the tendency of particles to move in the same direction as their neighbours. The operator $(\mathrm{Id} - \omega_k \otimes \omega_k)$ is the orthogonal projector onto the plane perpendicular to ω_k. It ensures that the velocity of particles remains constant. This model is already a modification of the original Vicsek model [28], which is a time-discrete algorithm.

The Macroscopic Vicsek model (MV) describes the evolution of two macroscopic quantities: the density of particles ρ and the direction of the flow Ω. The evolution of ρ and Ω is governed by the following equations:

$$\partial_t \rho + \nabla_x \cdot (c_1 \rho \Omega) = 0, \tag{2.4}$$

$$\rho\,(\partial_t \Omega + c_2(\Omega \cdot \nabla_x)\Omega) + \lambda\,(\mathrm{Id} - \Omega \otimes \Omega)\nabla_x \rho = 0, \tag{2.5}$$

$$|\Omega| = 1, \tag{2.6}$$

where c_1, c_2 and λ are some constants depending on the noise level d. The expressions of c_1, c_2 and λ are given in appendix 6. By contrast with the standard Euler system, the two convection coefficients c_1 and c_2 are different. The other specificity of this model is the constraint $|\Omega| = 1$. The operator $(\mathrm{Id} - \Omega \otimes \Omega)$ ensures that this constraint is propagated provided that it is true at the initial time. The passage from (2.1)-(2.2) to (2.4)-(2.5)-(2.6) is detailed in [13]. We note that vortex configurations are special stationary solutions of this model in two dimensions (see appendix 6). Up to our knowledge, this is the first swarming model which have such analytical solutions.

3 The Macroscopic Vicsek model

3.1 Theoretical analysis of the macroscopic model

To study model (2.4)-(2.5)-(2.6), we first use the rescaling $x' = x/c_1$. Then equations (2.4)-(2.5)-(2.6) are written:

$$\partial_t \rho + \nabla_{x'} \cdot (\rho \Omega) = 0, \tag{3.1}$$

$$\rho\,(\partial_t \Omega + c'(\Omega \cdot \nabla_{x'})\Omega) + \lambda'\,(\mathrm{Id} - \Omega \otimes \Omega)\nabla_{x'} \rho = 0, \tag{3.2}$$

$$|\Omega| = 1, \tag{3.3}$$

with $c' = c_2/c_1$ and $\lambda' = \lambda/c_1$. In the sequel, we drop the primes for clarity. We refer to the appendix 6 for the computation of c and λ. We have (see figure 7.18):

$$\frac{1}{2} < c < 1 \quad \text{and} \quad \lambda > 0, \quad \text{for all } d > 0. \tag{3.4}$$

In two dimensions, we use a parametrization of Ω in polar coordinates: $\Omega = (\cos\theta, \sin\theta)^T$. Therefore, equations (3.1)-(3.2) can be rewritten as:

$$\partial_t \rho + \partial_x (\rho \cos\theta) + \partial_y (\rho \sin\theta) = 0, \tag{3.5}$$

$$\partial_t \theta + c\cos\theta \partial_x \theta + c \sin\theta \partial_y \theta + \lambda \left(-\frac{\sin\theta}{\rho} \partial_x \rho + \frac{\cos\theta}{\rho} \partial_y \rho \right) = 0. \tag{3.6}$$

In this section, we suppose that ρ and θ are independent of y meaning that we are looking at waves which propagate in the x-direction. Under this assumption, the system reads:

$$\partial_t \begin{pmatrix} \rho \\ \theta \end{pmatrix} + A(\rho, \theta)\, \partial_x \begin{pmatrix} \rho \\ \theta \end{pmatrix} = 0, \tag{3.7}$$

with

$$A(\rho, \theta) = \begin{bmatrix} \cos\theta & -\rho \sin\theta \\ -\frac{\lambda \sin\theta}{\rho} & c\cos\theta \end{bmatrix}. \tag{3.8}$$

The characteristic velocities of this system are given by

$$\gamma_{1,2} = \frac{1}{2} \left[(c+1)\cos\theta \pm \sqrt{(c-1)^2 \cos^2\theta + 4\lambda \sin^2\theta} \right] \tag{3.9}$$

with $\gamma_1 < \gamma_2$. Therefore, the system is strictly *hyperbolic*. A possible choice of right eigenvectors is

$$\vec{r_1} = \begin{pmatrix} \rho \sin\theta \\ \cos\theta - \gamma_1 \end{pmatrix} \quad , \quad \vec{r_2} = \begin{pmatrix} c\cos\theta - \gamma_2 \\ \frac{\lambda \sin\theta}{\rho} \end{pmatrix}. \tag{3.10}$$

The two fields are genuinely nonlinear except at $\theta = 0$, $\theta = \pi$ and at the extrema values of γ_p which satisfy:

$$\tan^2\theta = \frac{1}{4\lambda} \left[\frac{((c-1)^2 - 4\lambda)^2}{(c+1)^2} - (c-1)^2 \right].$$

The Riemann invariant of the system (3.7) are given by:

$$I_1(\rho, \theta) = \log\rho - \int_{\theta_0}^{\theta} \frac{\sin s}{\cos s - \gamma_1(s)}\, ds \tag{3.11}$$

$$I_2(\rho, \theta) = \log\rho - \int_{\theta_0}^{\theta} \frac{c\cos s - \gamma_2(s)}{\lambda \sin s}\, ds. \tag{3.12}$$

The integral curve w_1 and w_2 starting from (ρ_l, θ_l) are given by:

$$\rho_1(\theta) = \rho_l \exp\left(\int_{\theta_0}^{\xi} \frac{\sin s}{\cos s - \gamma_1(s)}\, ds \right) \tag{3.13}$$

$$\rho_2(\theta) = \rho_l \exp\left(\int_{\theta_0}^{\xi} \frac{c\cos s - \gamma_2(s)}{\lambda \sin s}\, ds \right). \tag{3.14}$$

These are the rarefaction curves. To select the physically admissible rarefaction curve, we remark that γ_p must grow from the left to right states. The proofs of these elementary facts are omitted. The quantities $\gamma_{1,2}$ as functions of θ are depicted in figure 7.1.

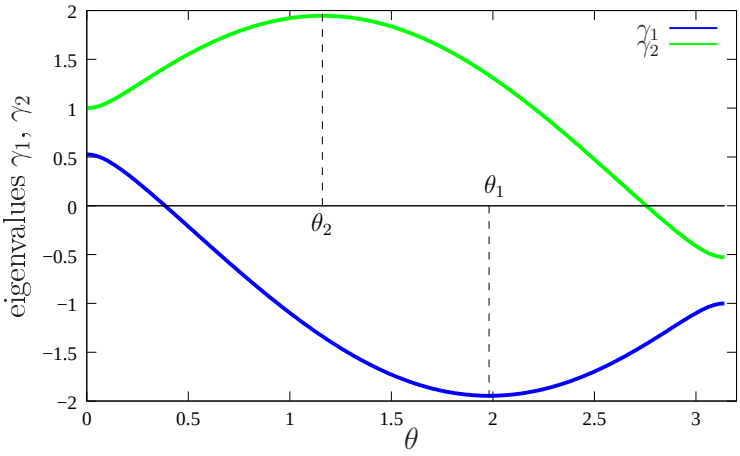

Figure 7.1: The two eigenvalues γ_1 and γ_2 depending on θ ($d = 1$ in this graph). For each curve, there exists a unique extremum (θ_1 and θ_2) which corresponds to a degeneracy of the system.

3.2 A conservative form of the MV model in dimension 1

For non-conservative systems, shock waves are not uniquely defined [22, 20]. However, in the present case, a conservative formulation of the system can be found in dimension 1. Indeed, it is an easy matter to see that, if $\sin\theta \neq 0$, system (3.7) can be rewritten in conservative form:

$$\partial_t \begin{pmatrix} \rho \\ f_1(\theta) \end{pmatrix} + \partial_x \begin{pmatrix} \rho\cos\theta \\ cf_2(\theta) - \lambda\log(\rho) \end{pmatrix} = 0, \tag{3.15}$$

with:

$$f_1(\theta) = \log\left|\tan\frac{\theta}{2}\right| = \log\left|\frac{\sin\theta}{\cos\theta+1}\right|, \tag{3.16}$$

$$f_2(\theta) = \log|\sin\theta|\,. \tag{3.17}$$

However, the functions f_1 and f_2 are singular when $\sin\theta = 0$ which means that the conservative form is only valid as long as θ stays away from $\theta = 0$.

The conservative form (3.15) leads to the following Rankine-Hugoniot conditions for shock waves: two states (ρ_l, θ_l) and (ρ_r, θ_r) are connected by a shock wave traveling at a constant speed s if

$$s\begin{pmatrix} \rho_r - \rho_l \\ f_1(\theta_r) - f_1(\theta_l) \end{pmatrix} = \begin{pmatrix} \rho_r\cos\theta_r - \rho_l\cos\theta_l \\ cf_2(\theta_r) - cf_2(\theta_l) - \lambda\log\rho_r + \lambda\log\rho_l \end{pmatrix}. \tag{3.18}$$

We can combine the two equations of the system (3.18) to eliminate the constant s, we are led to the expression of the shock curve:

$$\begin{aligned}(\rho_r - \rho_l)(cf_2(\theta_r) - cf_2(\theta_l) - \lambda\log\rho_r + \lambda\log\rho_l) \\ = (\rho_r\cos\theta_r - \rho_l\cos\theta_l)(f_1(\theta_r) - f_1(\theta_l)).\end{aligned} \tag{3.19}$$

This equation must be numerically solved. The entropic part of the shock curve is determined by the requirement that γ_p must satisfy the Lax entropy condition. In figure 7.2, we give an example of a solution of a Riemann problem obtained by computing the intersection of the shock and rarefaction curves.

3.3 The MV model as the relaxation limit of a conservative system

We are going to prove that the MV model (3.1)-(3.2)-(3.3) can be seen as the relaxation limit of a conservative hyperbolic model with a relaxation term. This link will be used later to build a new numerical scheme. More precisely, we introduce the relaxation model:

$$\partial_t \rho^\varepsilon + \nabla_x \cdot (\rho^\varepsilon \Omega^\varepsilon) = 0, \tag{3.20}$$

$$\partial_t \left(\rho^\varepsilon \Omega^\varepsilon\right) + c\nabla_x \cdot (\rho^\varepsilon \Omega^\varepsilon \otimes \Omega^\varepsilon) + \lambda \, \nabla_x \rho^\varepsilon = \frac{\rho^\varepsilon}{\varepsilon}(1 - |\Omega^\varepsilon|^2)\Omega^\varepsilon. \tag{3.21}$$

In this model, the constraint $|\Omega| = 1$ is replaced by a relaxation operator. Formally, in the limit $\varepsilon \to 0$, we recover the constraint $|\Omega| = 1$. More precisely, we have:

Proposition 3.1 *The relaxation model (3.20)-(3.20) converges to the MV model (3.1)-(3.2)-(3.3) as ε goes to zero.*

Proof. *(Formal)* We define $R^\varepsilon = \rho^\varepsilon(1 - |\Omega^\varepsilon|^2)\Omega^\varepsilon$. Suppose that as ε goes to zero:

$$\rho^\varepsilon \overset{\varepsilon\to 0}{\longrightarrow} \rho^0 \quad , \quad \Omega^\varepsilon \overset{\varepsilon\to 0}{\longrightarrow} \Omega^0. \tag{3.22}$$

Then $R^\varepsilon \overset{\varepsilon\to 0}{\longrightarrow} 0$, which generically implies that $|\Omega^0|^2 = 1$ (except where $\rho^0\Omega^0 = 1$ which one assume to be a negligible set). Therefore, we have:

$$\partial_t \Omega^0 \cdot \Omega^0 = 0 \quad , \quad (\Omega^0 \cdot \nabla_x)\Omega^0 \cdot \Omega^0 = 0. \tag{3.23}$$

Then since $R^\varepsilon \times \Omega^\varepsilon = 0$, we have:

$$\left(\partial_t \left(\rho^\varepsilon \Omega^\varepsilon\right) + c\nabla_x \cdot (\rho^\varepsilon \Omega^\varepsilon \otimes \Omega^\varepsilon) + \lambda \, \nabla_x \rho^\varepsilon\right) \times \Omega^\varepsilon = 0.$$

and consequently, when $\varepsilon \to 0$:

$$\partial_t \left(\rho^0 \Omega^0\right) + c\nabla_x \cdot \left(\rho^0 \Omega^0 \otimes \Omega^0\right) + \lambda \, \nabla_x \rho^0 = \alpha \Omega^0, \tag{3.24}$$

for a real number α to be determined. Taking the scalar product of (3.24) with Ω^0 and using (3.23), we find:

$$\alpha = \partial_t \rho^0 + c\nabla_x \cdot (\rho^0 \Omega^0) + \lambda \nabla_x \rho^0 \cdot \Omega^0.$$

Using the conservation of mass ($\partial_t \rho^0 = -\nabla_x \cdot (\rho^0 \Omega^0)$), we finally have:

$$\alpha = (c-1)\nabla_x \cdot (\rho^0 \Omega^0) + \lambda \nabla_x \rho^0 \cdot \Omega^0.$$

Therefore, the relaxation term satisfies:

$$\frac{1}{\varepsilon}R^{\varepsilon} = [(c-1)\nabla_x \cdot (\rho^0\Omega^0) + \lambda\nabla_x\rho^0 \cdot \Omega^0]\Omega^0 + 0(\varepsilon).$$

Inserting in (3.20)-(3.21) and taking the limit $\varepsilon \to 0$, we recover the MV model (3.1)-(3.2) at the first order in ε.

□

Remark 3.1 As for the MV model, we can also analyze the hyperbolicity of the left hand side of (3.20)-(3.21). The eigenvalues are given by:

$$\gamma_1 = cu - \sqrt{\Delta} \quad , \quad \gamma_2 = cu \quad , \quad \gamma_3 = cu + \sqrt{\Delta},$$

where u denotes the x-coordinate of Ω and $\Delta = \lambda - (c-c^2)u^2$. The system is hyperbolic if and only if $|u| < \sqrt{\frac{\lambda}{c-c^2}}$. As we can see in figure 7.3, for $u^2 = 1$, Δ is positive for any value of d. In particular, this implies that the relaxation model is hyperbolic for every $|u| \leq 1$.

4 Numerical simulations of the MV model

4.1 Numerical schemes

We propose four different numerical schemes, the first two schemes originate from the discussions of the previous section. The two other one based on the non-conservative form of the MV model.
We use the following notations: we fix a uniform stencil $(x_i)_i$ (with $|x_{i+1} - x_i| = \Delta x$) and a time step Δt. We denote by $U_i^n = (\rho_i^n, \theta_i^n)$ the value of the mass and speed angle at the position x_i and at time $n\Delta t$.

4.1.1 The conservative scheme

Here we use the conservative form of the MV model (3.15):

$$\partial_t V + \partial_x F(V) = 0, \tag{4.25}$$

with $V = (\rho, f_1(\theta))^T$ and $F(V) = (\rho\cos\theta,\, cf_2(\theta) - \lambda\log(\rho))^T$.
Using this formulation, we use a Roe method:

$$\frac{V_i^{n+1} - V_i^n}{\Delta t} + \frac{\widehat{F}_{i+} - \widehat{F}_{i-}}{\Delta x} = 0, \tag{4.26}$$

where the intermediate flux $\widehat{F}_{i+}$ is given by:

$$\widehat{F}_{i+} = \frac{F(V_i) + F(V_{i+1})}{2} - \left|\mathcal{A}(\overline{V}_{i+})\right| \frac{V_{i+1} - V_i}{2}, \tag{4.27}$$

and $\mathcal{A}$ is the Jacobian of the flux F:

$$\mathcal{A}(V) = DF(V) = \begin{bmatrix} \cos\theta & -\rho\sin^2\theta \\ -\frac{\lambda}{\rho} & c\cos\theta \end{bmatrix} \tag{4.28}$$

calculated at the mean value $\overline{V}_{i+} = \frac{V_i+V_{i+1}}{2}$.

As mentioned earlier, the conservative form is only valid when θ does not cross a singularity $\theta = 0$ or $\theta = \pi$ (i.e. $\sin\theta = 0$).
Nevertheless, numerically we can still use the formulation (4.26) when θ changes sign. Moreover, since f_1 is an even function, this only gives $|\theta^{n+1}|$. To determine the sign of θ^{n+1}, we use an auxiliary value $\widehat{\theta}$ which we update with the upwind scheme (4.33). The sign of θ is then determined using the sign of $\widehat{\theta}$.

4.1.2 The splitting method

The next scheme uses the relaxation model (3.20)-(3.20). The idea is to split the relaxation model in two parts, first the conservative part:

$$\begin{aligned} &\partial_t\rho + \nabla_x\cdot(\rho\Omega) = 0, \\ &\partial_t(\rho\Omega) + c\nabla_x\cdot(\rho\Omega\otimes\Omega) + \lambda\nabla_x\rho = 0. \end{aligned} \tag{4.29}$$

and then the relaxation part:

$$\begin{aligned} \partial_t\rho &= 0, \\ \partial_t(\rho\Omega) &= \frac{\rho}{\varepsilon}(1-|\Omega|^2)\Omega. \end{aligned} \tag{4.30}$$

We can reduce this last equation since $\partial_t\rho = 0$ to:

$$\partial_t\Omega = \frac{1}{\varepsilon}(1-|\Omega|^2)\Omega.$$

Since this equation only changes the vector field Ω in norm (i.e. $\partial_t\Omega\cdot\Omega^\perp = 0$), we can once again reduce this equation to:

$$\frac{1}{2}\partial_t|\Omega|^2 = \frac{1}{\varepsilon}(1-|\Omega|^2)|\Omega|^2. \tag{4.31}$$

Equation (4.31) can be explicitly solved:

$$|\Omega|^2 = \frac{1}{1+C_0\,\mathrm{e}^{-2/\varepsilon\,t}}, \tag{4.32}$$

with $C_0 = \frac{1}{|\Omega_0|^2} - 1$. We indeed take the limit $\varepsilon \to 0$ of this expression and replace the relation term by a mere normalization: $\Omega \to \Omega/|\Omega|$.

The conservative part is solved by a Roe method with a Roe matrix computed following [22] page 156.

4.1.3 Non-conservative schemes

We present two other numerical schemes based on the non-conservative formulation of the MV model.

(i) Upwind scheme

The method consists to update the value of U_i^n with the formula:

$$\frac{U_i^{n+1} - U_i^n}{\Delta t} + A^+ \left(\frac{U_i^n - U_{i-1}^n}{\Delta t} \right) + A^- \left(\frac{U_{i+1}^n - U_i^n}{\Delta t} \right) = 0, \tag{4.33}$$

where A^+ and A^- are (respectively) the positive and negative part of A, defined such that $A = A^+ - A^-$ and $|A| = A^+ + A^-$ and A^+, A^- are computed using an explicit diagonalization of A.

(ii) Semi-conservative scheme

One of the problem with the upwind scheme is that it does not conserve the total mass ($\int_x \rho(x)\, dx$). In order to keep this quantity constant in time, we use the equation of conservation of mass (3.1) in a conservative form:

$$\partial_t \rho + \partial_x H(\rho, \theta) = 0, \tag{4.34}$$

with $H(\rho, \theta) = \rho \cos\theta$. Therefore, a conservative numerical scheme associated with this equation would be:

$$\frac{\rho_i^{n+1} - \rho_i^n}{\Delta t} + \frac{\widehat{H}_{i+1/2} - \widehat{H}_{i-1/2}}{\Delta x} = 0, \tag{4.35}$$

where $\widehat{H}_{i+}$ is the numerical estimation of the flux H at the interface between x_i and x_{i+1}. To estimate numerically this flux, we use the following formula with $U_i = (\rho_i, \theta_i)$:

$$\widehat{H}_{i+1/2} = H(U_{i+1/2}) - |A|_\rho \left(\frac{U_{i+1}^n - U_i^n}{2} \right), \tag{4.36}$$

where the intermediate value is given by $U_{i+1/2} = \frac{U_i^n + U_{i+1}^n}{2}$ and $|A|_\rho$ is the first line of the absolute value of A.

For the estimation of the angle θ, we keep the same scheme as for the upwind scheme.

This numerical scheme uses one conservative equation (for the mass ρ) and a non-conservative equation (for the angle θ). It is thus referred to as the *semi-conservative* scheme.

4.2 Numerical simulations

To compare the various numerical schemes, we use a Riemann problem as initial condition. We choose solutions which consist of a rarefaction wave (figure 7.4) or a single shock wave (figure 7.5-7.6).

We take the following parameters: $d = 1$, the length of the domain is 10 units and the discontinuity for the Riemann problem is at $x = 5$ (the middle of the domain). The simulation is run during two time units with a time step $\Delta t = 2.10^{-2}$ and a space step $\Delta x = 5.10^{-2}$. For these values, the Courant number (C_n) is: 0.778. We use homogeneous Neumann conditions.

For the rarefaction wave, we take:

$$(\rho_l, \theta_l) = (2, 1.7) \quad , \quad (\rho_r, \theta_r) = (1.12, 0.60). \tag{4.37}$$

All the numerical schemes capture well the theoretical solution (see figure 7.4).

For the shock wave, we choose:

$$(\rho_l, \theta_l) = (1, 1.05) \quad , \quad (\rho_r, \theta_r) = (1.432\,,\, 1.7). \tag{4.38}$$

and the shock speed is: $s = -1.585$. The results of the numerical simulations using the four schemes are given in figure 7.5. The numerical solutions are in accordance with the theoretical solution given by the conservative formulation for all the numerical schemes. Nevertheless, the conservative scheme is in better accordance with this solution. For the other schemes, the shock speed differs slightly.

A second example of a shock wave is computed using the following initial condition:

$$(\rho_l, \theta_l) = (1, 0.314) \quad , \quad (\rho_r, \theta_r) = (2, 1.54) \tag{4.39}$$

The solutions given by the 4 numerical schemes are very different. Only the conservative method is in agreement with the solution given by the conservative formulation. But the conservative formulation is not necessary the right one. Indeed, in the next section, particle simulations show that the right solution is not given by the conservative formulation but rather by the splitting method.

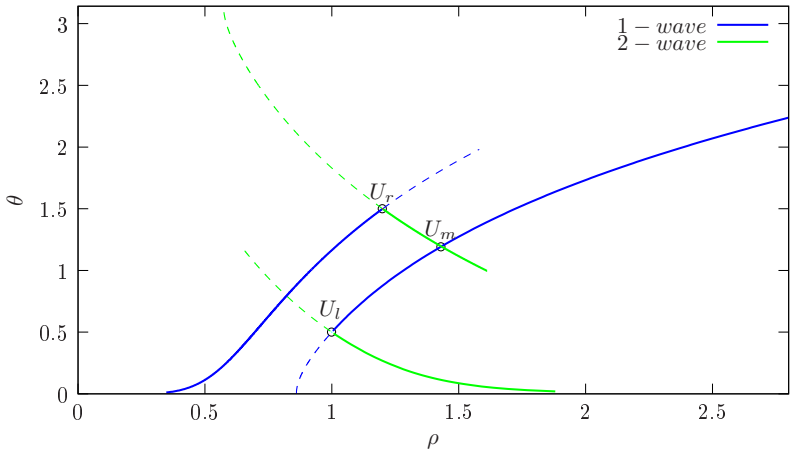

Figure 7.2: A solution of the Riemann problem with left and right states U_l and U_r (solid line for shock waves and dotted line for rarefaction waves). In this example, the solution is given by two shock waves.

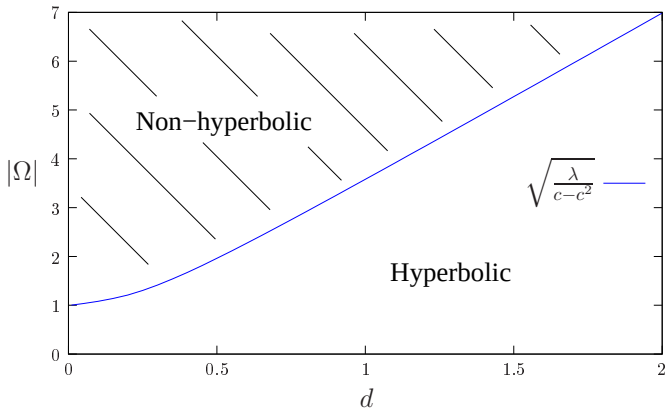

Figure 7.3: The quantity $\sqrt{\lambda/(c-c^2)}$ depending on d. The relaxation model is hyperbolic when the speed $|\Omega|$ is below the curve. At the limit $\varepsilon \to 0$, $|\Omega^\varepsilon| \to 1$ and therefore the model is hyperbolic for any d in this limit.

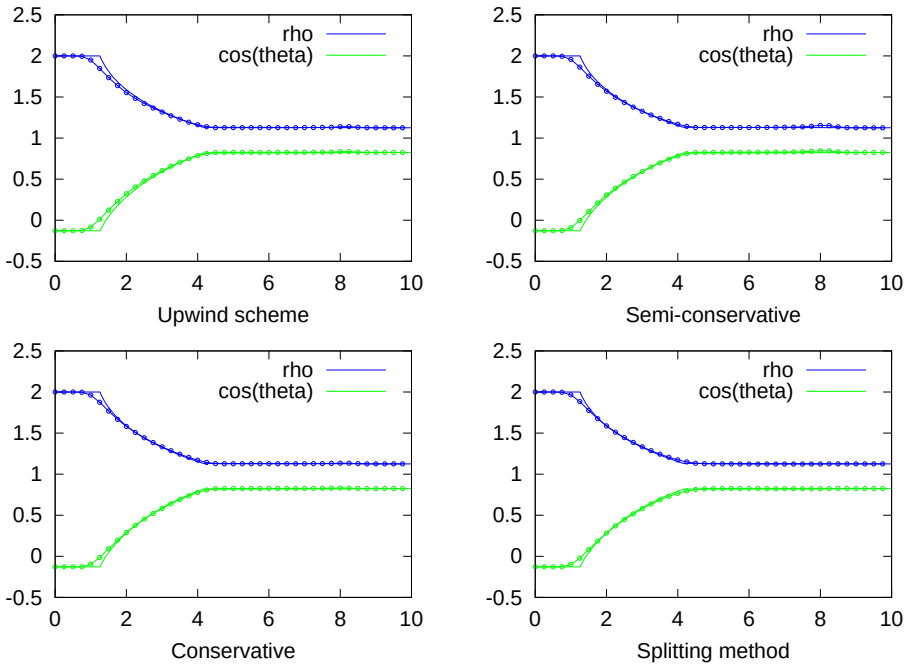

Figure 7.4: The theoretical solution of a Riemann problem (4.37) given by a rarefaction curve (solid line) and the numerical solutions (points), ρ (blue) and $\cos\theta$ (green) as functions of space. The simulations are run during 2 time units, with a time step $\Delta t = 2.10^{-2}$ and a space step $\Delta x = 5.10^{-2}$ (CFL=.778).

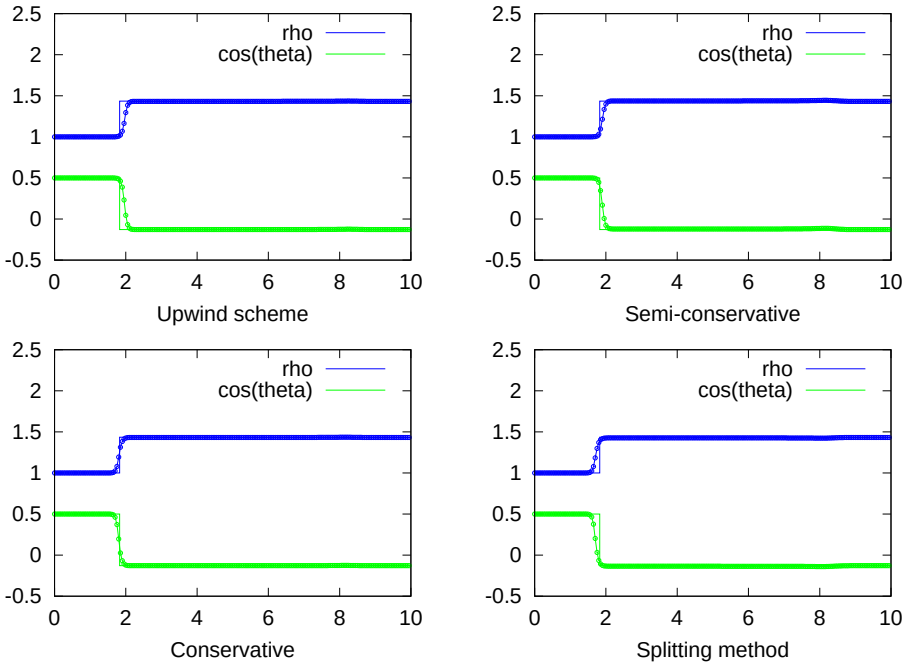

Figure 7.5: The theoretical solution of a Riemann problem (4.38) given by a shock wave (solid line) and the numerical solutions (points). Abscissa represents the space domain and ordinate represents the value of the mass (blue) and the angle of the speed θ (green). The simulations are run during 2 time unit, with time step $\Delta t = 2.10^{-2}$ and space step $\Delta x = 5.10^{-2}$ (CFL = .778).

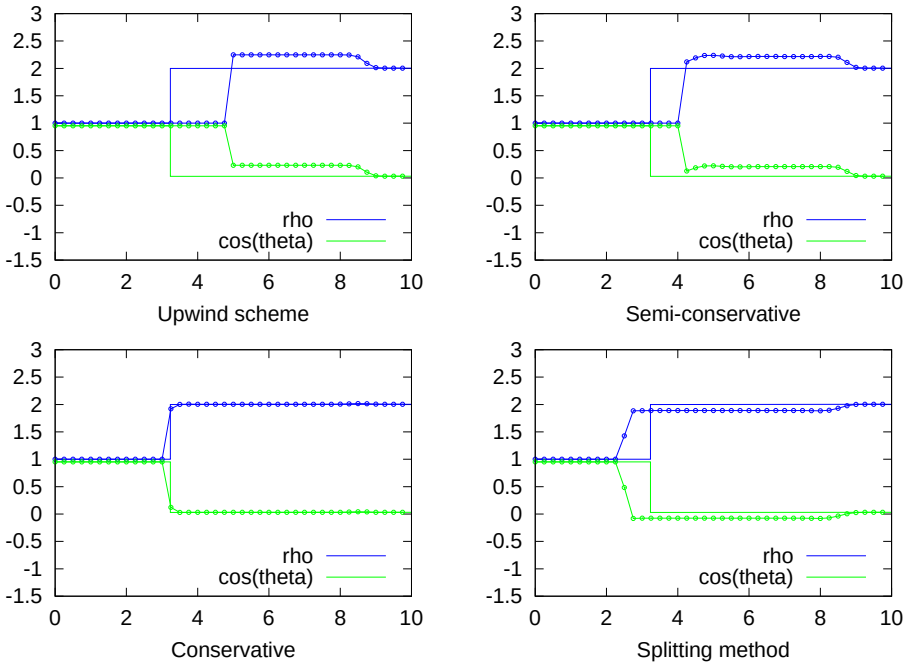

Figure 7.6: The theoretical solution of a Riemann problem (4.39) given by a shock wave (solid line) and the numerical solutions (points). Abscissa represents the space domain and ordinate represents the value of the mass (blue) and the angle of the speed θ (green). The simulations are run during 2 time unit, with time step $\Delta t = 2.10^{-2}$ and space step $\Delta x = 5.10^{-2}$ (CFL = .778).

5 The microscopic versus macroscopic Vicsek models

5.1 Local equilibrium

In this part, we would like to validate the macroscopic Vicsek model by the simulation of the microscopic Vicsek. The model relies on the fact that the particle distribution function is at local equilibrium given by a Von Mises distribution M_Ω (see [13]):

$$M_\Omega(\omega) = C \exp\left(\frac{\omega \cdot \Omega}{d}\right) \tag{5.1}$$

where C is set by the normalization condition[1]. The goal of this section is to numerically show that the particle distribution of a microscopic Vicsek formulation is close in certain regimes to a Von Mises distribution.

To this aim, in appendix 6 we propose a numerical scheme to solve system (2.2). The setting for our particle simulations is as follows: we consider a square box with periodic boundary conditions. As initial condition for the position x_i, we choose a uniform random distribution in space. The velocity is initially distributed according to a uniform distribution on the unit circle.

During the simulation, we compute the empirical distribution of the speed angle θ and the average direction Ω of the particles. We then compare this empirical distribution with its theoretical distribution $M_\Omega(\theta)$ given by (5.1).

In figure 7.7, we give an example of a comparison between the distribution of speed angle θ and the theoretical distribution M_Ω predicted by the theory.

Since the distribution of speed angle converges, we have a theoretical value of the mean velocity. We denote by φ_N the mean velocity of particles and φ the theoretical value given by the stationary distribution:

$$\varphi_N = \frac{1}{N}\left|\sum_{k=1}^{N} \omega_k\right| \quad , \quad \varphi = \left|\int_\omega \omega\, M_\Omega(\omega)\, d\omega\right|. \tag{5.2}$$

At least locally in x, we have that $\varphi_N \xrightarrow{\epsilon \to 0} \varphi$. In figure 7.8, we compare the two distributions for different values of the noise d and we can see that the two distributions are in good agreement. We also observe a smooth transition from order ($\varphi \approx 1$) to disorder ($\varphi << 1$) as it has been measured in the original Vicsek model [28].

The situation is different when we look at a larger system. We still have convergence of the particle distribution to a local equilibrium $\rho(x)\, M_{\Omega(x)}(\omega)$, but the mean direction $\Omega(x)$ now depends on x. Therefore the average velocity of the particles in all the domain differs from the expected theoretical value (5.1)-(5.2). We illustrate this phenomena in figure 7.9: we fix the density of particles and we increase the size of the box. As we can observe, the mean velocity φ_N (5.2) has a smaller value when the size of the box increases. This phenomena has been previously observed in [6]. The average velocity φ_N can also differ from the expected theoretical value φ (5.1)-(5.2) when the density of particles is low. In figure 7.10, we fix the size of the box ($L = 10$) and we increase

[1] explicitly given by $C^{-1} = 2\pi\, I_0(d^{-1})$ where I_0 is the modified Bessel function of order 0

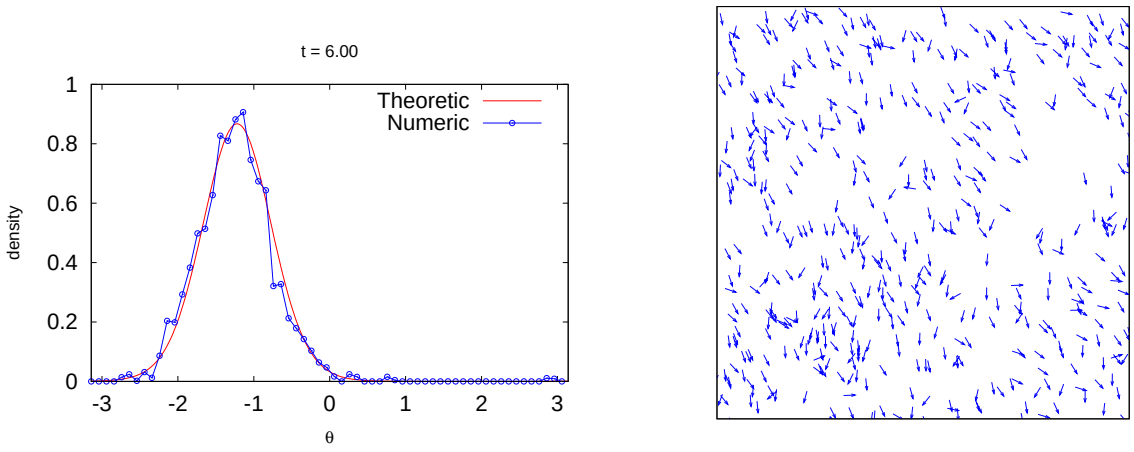

Figure 7.7: Left figure: the distribution of velocities (with $\omega = (\cos\theta, \sin\theta)$) compared with its theoretical distribution after 6 time units of simulation. Right figure: the corresponding particle simulation. Parameters of the simulation: $Lx = 1$, $Ly = 1$ (domain size), number of particles $N = 500$, $\varepsilon = 1/4$, $R = .5$, $d = .2$, $\Delta t = 2.10^{-3}$.

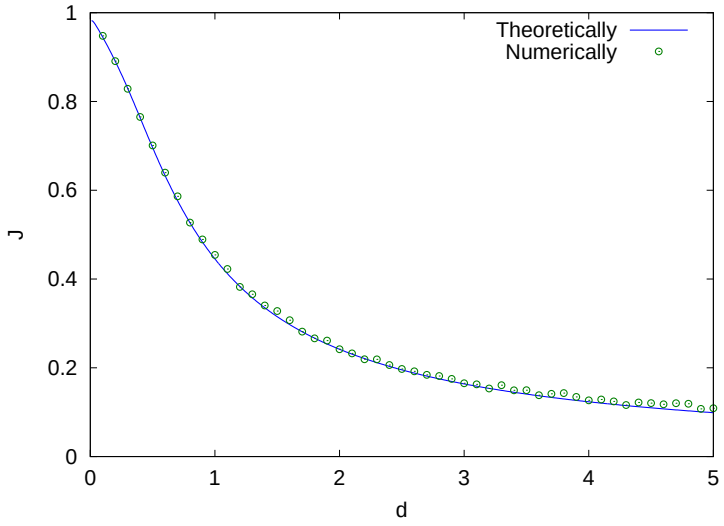

Figure 7.8: The mean velocity φ (5.2) for different values of d. Parameters of the simulation: $Lx = 1$, $Ly = 1$ (domain size), number of particles $N = 200$, radius of interaction $R = .5$, duration of the simulation 180 unit time, $\Delta t = .02$ unit time.

the density of particles (the density is given by the number of particles inside the circle of interaction). At low density, the mean velocity φ_N is much more smaller than the theoretical prediction φ. But as the density of particles increases, the mean velocity φ_N grows (see also [28]) and moreover φ_N converges to φ. Because of that, a dense regime of particles has to be used in the following in order to numerically compare the microscopic model with the MV model.

5.2 Microscopic versus Macroscopic dynamics

We now compare the evolution of the two macroscopic quantities ρ and Ω for the two models. We have seen that the different schemes applied to the macroscopic equation could give different solutions (see figure 7.6). Therefore, we expect that particle simulations will indicate what is physically relevant solution of the macroscopic equation.

We first briefly discuss particle simulations of a Riemann problem (see also appendix 6). First, we have to choose a left state (ρ_l, θ_l), a right state (ρ_r, θ_r) and the noise level d. Then we distribute a proportion $\frac{\rho_l}{\rho_l+\rho_r}$ of the particles uniformly in the interval $[0, 5]$ and the remaining particles uniformly in the interval $[5, 10]$. Then, we generate speed angle θ for the particles according to the distribution M_Ω (5.1) with $\Omega_l = (\cos\theta_l, \sin\theta_l)^T$ on the left side and $\Omega_r = (\cos\theta_r, \sin\theta_r)^T$ on the right side. We use the numerical scheme given in appendix 6 to generate particle trajectories. To make the computation simpler, we choose periodic boundary conditions. Therefore the number of particles is conserved. As a consequence, there are two Riemann problems corresponding to discontinuities at $x = 5$ and at $x = 0$ or 10 (which is the same by periodicity). We use a particle-in-cell method [14, 18] to estimate the two macroscopic quantities: the density ρ and the direction of the flux Ω (which gives θ). In order to reduce the noise due to the finite number of particles, we take a mean over several simulations to estimate the density ρ and θ (10 simulations in our examples).

In figure 7.11, we show a numerical solution for the following Riemann problem:

$$(\rho_l,\, \theta_l) = (1,\, 1.5) \quad , \quad (\rho_r,\, \theta_r) = (2,\, 1.83) \quad , \quad d = 0.2 \tag{5.3}$$

using particle simulations and the macroscopic equation. We represent the solutions in a 2D representation. Since the initial condition is such that the density ρ and the direction θ are independent of the y-direction, we only represent ρ and θ along the x-axis in the following figures.

In figure 7.12, we represent the two solutions (the particle and the macroscopic one) with only a dependence in the x-direction. Three quantities are represented: the density (blue), the speed angle θ (green) and the variance of the angle distribution (red). The macroscopic model supposes that the variance of θ should be constant everywhere. Nevertheless, we can see that the variance is larger in regions where the density is lower. For ρ and θ, we see clearly the propagation of a shock in the middle of the domain and a rarefaction at the boundary. The CPU time for one numerical solution at the particle level is about 140 seconds with the parameters given in figure 7.12. For the macroscopic equation, the CPU time is about 0.1 second which represent

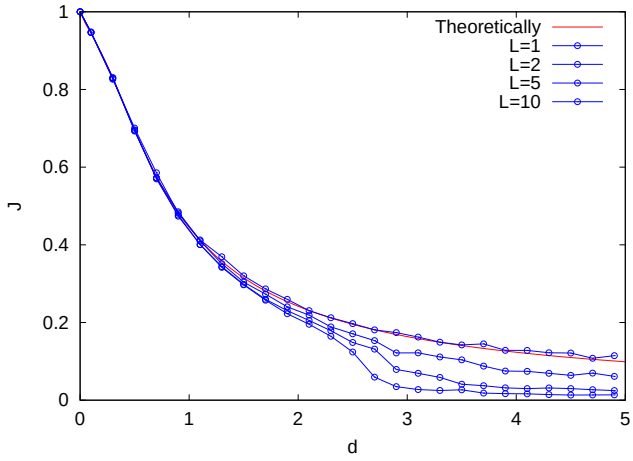

Figure 7.9: The mean velocity φ (5.2) for different values of d. We use different domain sizes and we keep the same density of particles. As the domain size increases, the total flux φ decreases which means that particles are less aligned globally. Parameters of the simulations: $L = 1, 2, 5, 10$ (domain size), number of particles $N = 200, 800, 5000, 20000$, radius of interaction $R = .5$, duration of the simulation 180 time units, $\Delta t = .02$ time units.

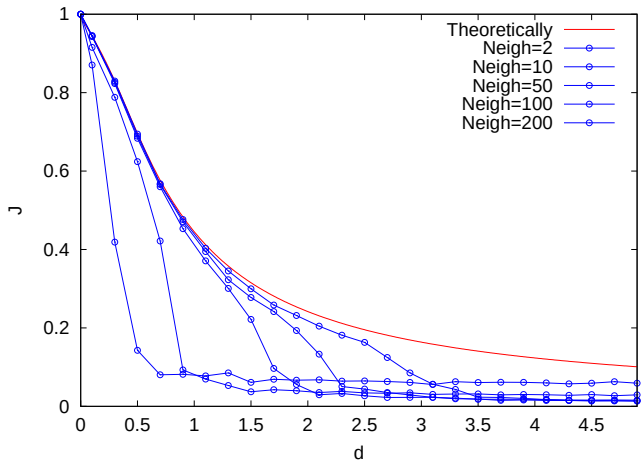

Figure 7.10: The mean velocity φ (5.2) for different values of d. We change the density of particles (given by the mean number of neighbours in unit of radius of interaction). When we increase the mean number of neighbours, particles are more aligned. Parameters of the simulations: $L = 10$ (domain size), number of particles $N = 254, 1273, 6366, 12732$, and 25464, radius of interaction $R = .5$, duration of the simulation 180 time units, $\Delta t = .02$ time unit.

a cost reduction of four orders of magnitude compared with the particle simulations. Since we have to take an average over many particle simulations, the cost reduction is even larger.

In figure 7.13, we use the same Riemann problem to set the initial position as in figure 7.6 both with $d = 1$ (4.39). We use a larger domain in x ($L = 20$ space units) in order to avoid the effect of the periodic boundary condition. The upwind scheme and the semi-conservative method are clearly not in accordance with the particle simulations. Moreover, the splitting method is in in better agreement with the particle simulation since the shock speed is closer to the values given by the particle simulations than that predicted by the conservative scheme.

Finally, our last simulations concerns a contact discontinuity. We simply initialize with:

$$(\rho_l, \theta_l) = (1, 1) \quad , \quad (\rho_r, \theta_r) = (1, -1) \quad , \quad d = 0.2\,. \tag{5.4}$$

i.e. we reflect the angle with respect to the x-axis across the middle point $x = 5$. A natural solution for this problem is the contact discontinuity propagating at speed $c\,cos(1)$:

$$\rho(t, x) = 1 \quad , \quad \theta(t, x) = \theta_0(x - c\cos(1)t), \tag{5.5}$$

with $\theta_0(x) = -1$ when $x < 5$ and $\theta_0(x) = 1$ when $x > 5$. This is the solution provided by the conservative scheme (figure 7.14). But surprisingly, the splitting method and the particle simulation agree on a different solution. Indeed, the solutions given by the particles and the splitting method are in fairly good agreement with each other, which seems to indicate that the "physical solution" to the contact problem (5.4) is not given by the conservative formulation (5.5) but by a much more complex profile. The constraint of unit speed drastically changes the profile of the solution compared with what would be found for a standard system of conservative laws.

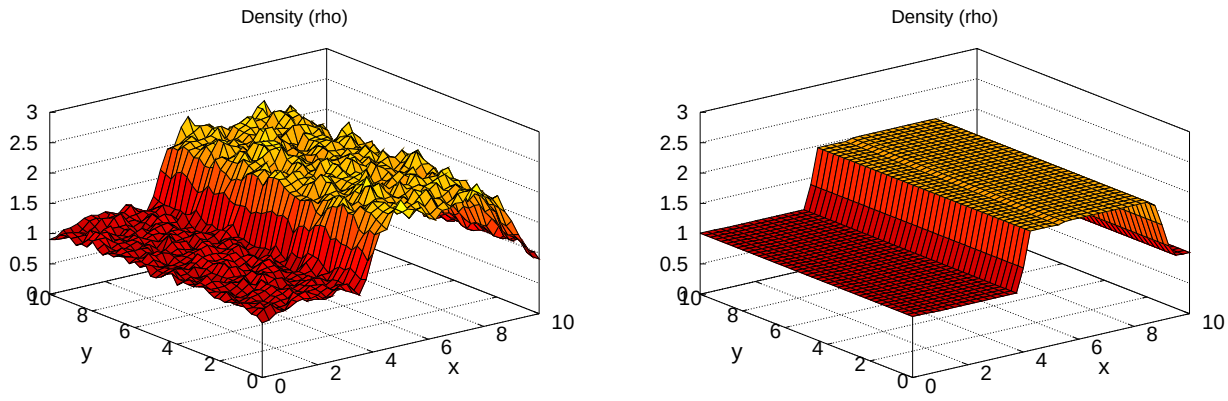

Figure 7.11: The particle density in space ρ computed with particle simulations (left) and the macroscopic equations (right). We initialize with a Riemann problem (5.3). Numerical parameters for the particle simulations: $N = 2.10^6$ particles, $\Delta t = .01$, $\varepsilon = 1/10$, $R = .5$, $Lx = Ly = 10$, we take a mean over 10 computations. Numerical parameters for the macroscopic model: $\Delta t = .01$, $\Delta x = .025$ (CFL=0.416). We use the splitting method. The simulations are run during 2 time units.

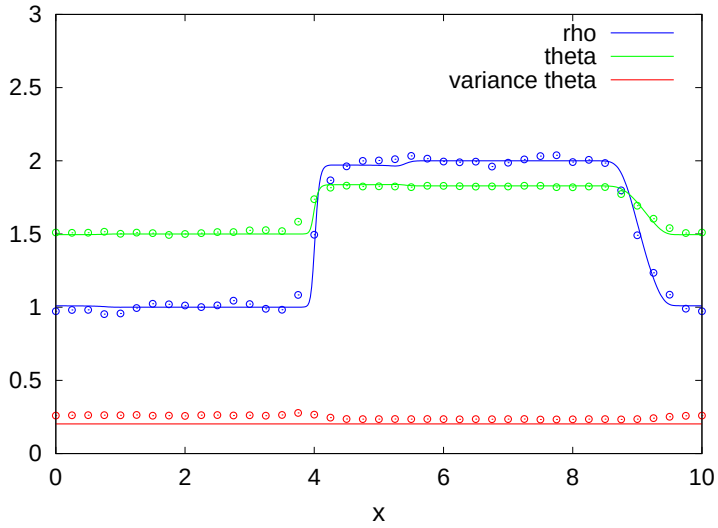

Figure 7.12: The solution of a Riemann problem (5.3) with $d = .2$ computed with the splitting method (solid line) and with particle simulations (dots). In blue, we represent the density ρ, in green the speed angle θ and in red the variance of the speed angle distribution. The parameters are the same as in figure 7.11. We only change the representation of the solution (1D-representation). The simulation is run during 2 time units as in figure 7.11.

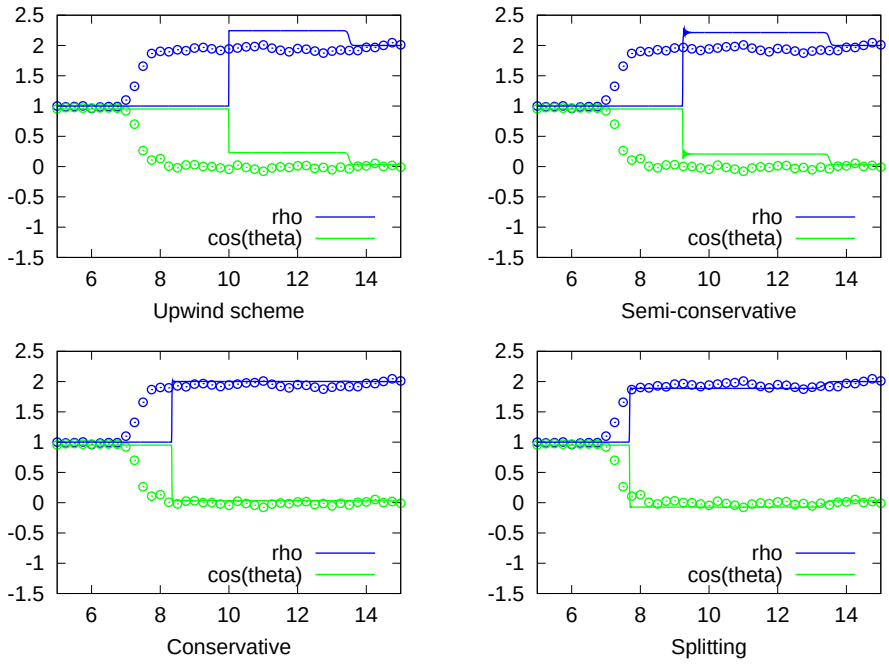

Figure 7.13: The solution of a Riemann problem (4.39) with $d = 1$ computed using the macroscopic model and particle simulations of the microscopic model (see figure 7.12). Numerical parameters for the macroscopic model: $\Delta t = .01$, $\Delta x = .025$ (CFL=0.778). Numerical parameters for the particle simulation: $N = 2.10^6$ particles, $\Delta t = .02$, $\varepsilon = .1$, $R = .5$, $Lx = 20$ and $Ly = 1$. We take a mean over 50 simulations. The simulations are run during 6 time units. Since $d = 1$, fluctuations are higher (see figure 7.9), we have to increase the density of particles to reduce this effect.

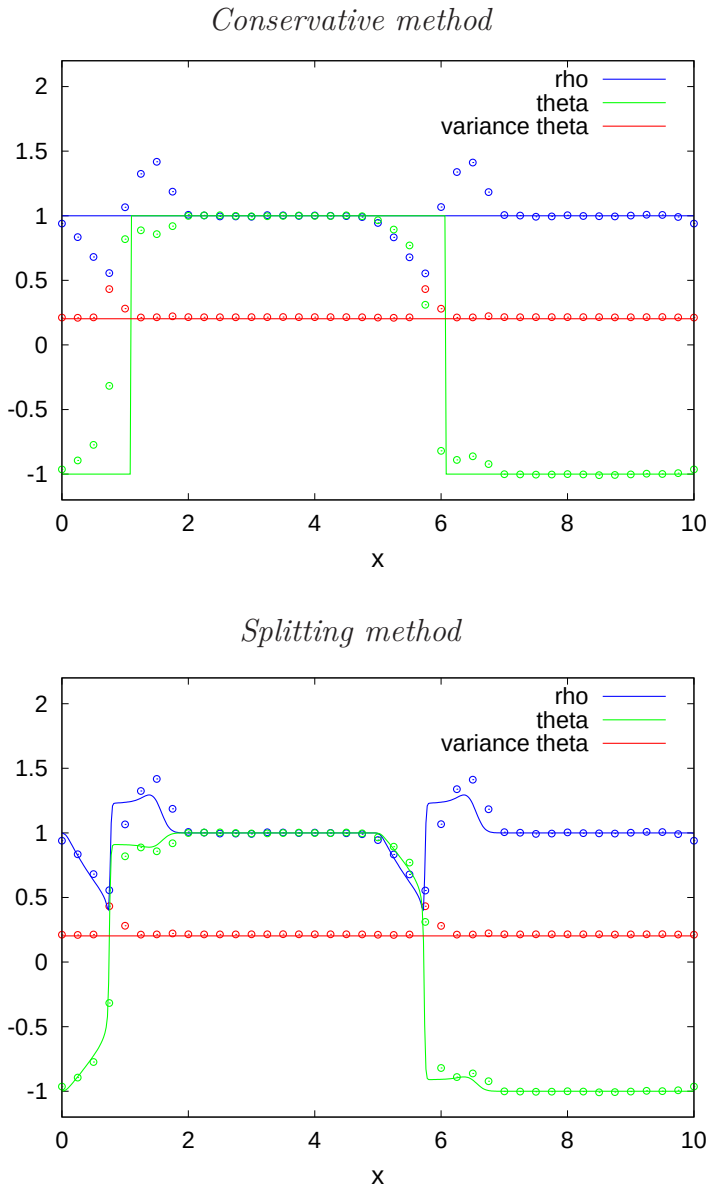

Figure 7.14: The solution of the Riemann problem (5.4) computed with the conservative method (top), the splitting method (down) and with particle simulations (dots). Numerical parameters for the macroscopic model: $\Delta t = .01$, $\Delta x = .025$ (CFL=0.416). Numerical parameters for the particle simulations: $N = 10^6$ particles, $\Delta t = .01$, $\varepsilon = 1/10$, $R = .5$, $Lx = 10$, $Ly = 1$. We take a mean over 100 simulations. The simulations are run during 2 time units.

6 Conclusion

In this work, we have numerically studied both the microscopic Vicsek model and its macroscopic version [13]. Due to the geometric constraint that the velocity should be of norm one, the standard theory of hyperbolic systems is not applicable. Therefore, we have proposed several numerical schemes to solve it. By comparing the numerical simulations of the microscopic and macroscopic equations, it appears that the scheme based on a relaxation formulation of the model, used in conjunction with a splitting method is in good agreement with particle simulations. The other schemes do not show a similar good agreement. In particular, with an initial condition given by a contact discontinuity, the splitting method and the microscopic model provide a similar solution which turn to be much more complex than could be expected.

These results confirm the relevance of the macroscopic Vicsek model. Since the CPU time is much lower with the macroscopic equation, the macroscopic Vicsek model is an effective tool to simulate the Vicsek dynamics in a dense regime of particles.

Many problems are still open concerning the macroscopic Vicsek model. We have seen that the splitting method gives results which are in accordance with particle simulations. But, we have to understand why this particular scheme captures well the particle dynamics better than the other schemes. Since the macroscopic equation has original characteristics, this question is challenging. Another point concerns the particle simulations. We have seen that the particles density has a strong effect on the variance of the velocity distribution. When the density is low, the variance is larger. The macroscopic equation does not capture this effect since the variance of the distribution is constant. Works in progress aims at taking into account this density effect.

Appendix A : The coefficients c_1, c_2 and λ

The analytical expression of the coefficient c_1 involved the distribution of the local equilibrium M_Ω (5.1). The two others coefficients (c_2 and λ) involve also the solution g of the following elliptic equation:

$$-(1-x^2)\,\partial_x[\mathrm{e}^{x/d}(1-x^2)\partial_x g] + \mathrm{e}^{x/d} g = -(1-x^2)^{3/2}\mathrm{e}^{x/d}, \tag{6.1}$$

on the interval $x \in [-1,1]$,

If we define the function $h = \frac{g}{\sqrt{1-x^2}}$ and $M(x) = \exp(\frac{x}{d})$, these macroscopic coefficients can be written as:

$$c_1 = <\cos\theta>|_M = \frac{\int_0^\pi \cos\theta\, M(\cos\theta)\sin\theta\, d\theta}{\int_0^\pi M(\cos\theta)\sin\theta\, d\theta}, \tag{6.2}$$

$$c_2 = <\cos\theta>|_{\sin^2\theta\, hM} = \frac{\int_0^\pi \cos\theta\, \sin^2\theta\, h(\cos\theta) M(\cos\theta)\sin\theta\, d\theta}{\int_0^\pi \sin^2\theta\, h(\cos\theta) M(\cos\theta)\sin\theta\, d\theta}, \tag{6.3}$$

$$\lambda = d. \tag{6.4}$$

In the above expressions, we can see that $0 \le c_1, c_2 \le 1$.

Now we are going to explore two asymptotics of g when the parameter d is small or large.

Lemma 6.1 *Let g be the solution of equation (6.1). We have the asymptotics:*

$$g \overset{d\to 0}{\sim} d\left[asin(x) - \frac{\pi}{2}\right] + o(d), \tag{6.5}$$

$$g \overset{d\to\infty}{\sim} -\frac{1}{2}\sqrt{1-x^2} + \frac{1}{12\,d} x\sqrt{1-x^2} + o\left(\frac{1}{d}\right). \tag{6.6}$$

Proof. Introducing the Hilbert space:

$$V = \{g \,|\, (1-\mu^2)^{-1/2} g \in L^2(-1,1), \quad (1-\mu^2)^{1/2}\partial_\mu g \in L^2(-1,1)\}$$

we have already seen in [13] that there exists a unique solution g of (6.1). Moreover this solution is negative.

To derive the asymptotic behaviour of g depending on d, we first develop (6.1):

$$\partial_x[(1-x^2)\partial_x g] + (1-x^2)\,\frac{1}{d}\partial_x g - \frac{g}{1-x^2} = (1-x^2)^{1/2}. \tag{6.7}$$

When $d \to 0$, we have:

$$\partial_x g = 0$$

on the interval $[-1+\varepsilon, 1-\varepsilon]$ for all $\varepsilon > 0$. Since g belongs to V, we also have the boundary condition $g(-1) = g(1) = 0$, so g converge to 0 when $d \to 0$.
To derive the next order of convergence in the limit $d \to 0$, we normalize g with $g = d\widetilde{g}$, which gives:

$$d\,\partial_x[(1-x^2)\partial_x \widetilde{g}] + (1-x^2)\partial_x \widetilde{g} - d\,\frac{\widetilde{g}}{1-x^2} = (1-x^2)^{1/2}. \tag{6.8}$$

In the limit $d \to 0$, we deduce that:

$$(1-x^2)\partial_x \widetilde{g} = (1-x^2)^{1/2}, \tag{6.9}$$

which has an explicit solution: $\widetilde{g} = \text{asin}(x) + c$. Since $\widetilde{g} \leq 0$, we have $c \leq -\frac{\pi}{2}$. Numerically, we in fact find that $c = -\frac{\pi}{2}$ but the proof is still open.
This formally proves (6.5).

When $d \to +\infty$, (6.7) gives:

$$\partial_x[(1-x^2)\partial_x g_0] - \frac{g_0}{1-x^2} = (1-x^2)^{1/2}. \tag{6.10}$$

A simple calculation shows that $g_0 = -\frac{1}{2}\sqrt{1-x^2}$ is a solution of (6.10).
To derive the next order of convergence, we look at the difference $v = d(g - g_0)$, which satisfies (see (6.7) and (6.10)):

$$\partial_x[(1-x^2)\partial_x v] + (1-x^2)\,\frac{1}{d}\partial_x v - \frac{v}{1-x^2} = -(1-x^2)\,\partial_x g_0.$$

In the limit $d \to +\infty$, v satisfies:

$$\partial_x[(1-x^2)\partial_x v] - \frac{v}{1-x^2} = -\frac{1}{2}x\sqrt{1-x^2}. \tag{6.11}$$

A simple calculation shows that $v = \frac{1}{12}x\sqrt{1-x^2}$ is solution of (6.11).
Therefore we formally have the expression (6.6) in the proposition. □

In figure 7.15, we numerically compute the function g (6.1). We use a finite element method with a space step $\Delta x = 10^{-3}$. The two asymptotics of g when $d \to 0$ and $d \to +\infty$ are computed in figure 7.16.

Proposition 6.2 *The two coefficients c_1 and c_2 defined (resp.) by the equations (6.2) and (6.3) satisfy the following asymptotics:*

$$c_1 \overset{d\to 0}{\sim} 1 - d + O(d^2) \tag{6.12}$$

$$c_1 \overset{d\to +\infty}{\sim} \frac{1}{3d} + O\left(\frac{1}{d^2}\right) \tag{6.13}$$

$$c_2 \overset{d\to \infty}{\sim} \frac{1}{6d} + o\left(\frac{1}{d}\right). \tag{6.14}$$

Proof. We have an explicit expression for the coefficient c_1 using the change of unknowns $x = \cos(\theta)$:

$$c_1 = \coth\left(\frac{1}{d}\right) - d, \tag{6.15}$$

where $\coth(s) = \frac{e^s + e^{-s}}{e^s - e^{-s}}$. The expressions of (6.12) and (6.13) are simply deduced by a Taylor expansion of the last expression.

For the coefficient c_2, we insert the development of g (6.6) in expression (6.3). □

Remark 6.1 The behaviour of c_2 when $d \to 0$ is more difficult to analyze. The density probability $\sin\theta\, h\, M$ used in formula (6.3) becomes singular in this limit. Nevertheless, due to the expression of M_Ω, the density converges to a Dirac delta at 0 which explains why $c_2 \overset{d\to 0}{\sim} 1$. To capture the next order of convergence, we need to find the second order correction of g in the limit $d \to 0$ which is not available. However, numerically we find that:

$$c_2 \overset{d\to 0}{\sim} 1 - 2d + o(d).$$

In figure 7.17 and 7.18, we numerically compute the coefficients c_1, c_2, c_2/c_1, λ/c_1 and theirs asymptotics.

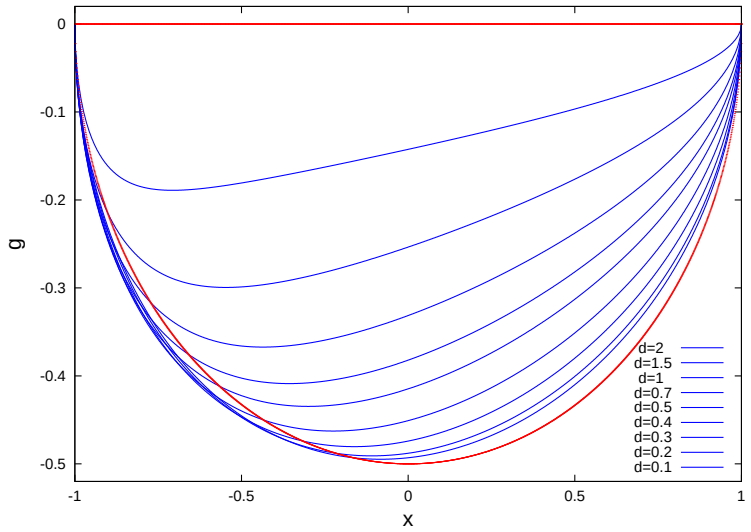

Figure 7.15: The numerical solution g (6.1) for different values of the parameter d. We have the following asymptotic (see lemma 6.1): $g \overset{d\to 0}{\longrightarrow} 0$ and $g \overset{d\to\infty}{\longrightarrow} -\frac{1}{2}\sqrt{1-x^2}$.

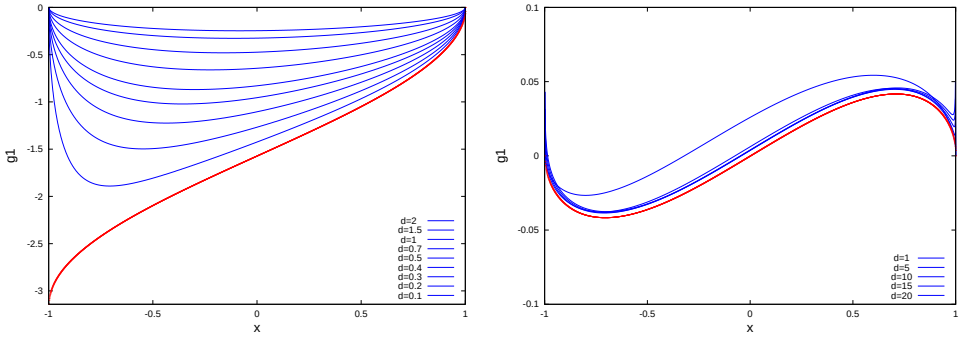

Figure 7.16: Left figure: the first correction g_1 of g when $d \to 0$. The red curve is the theoretical asymptotic limit: $g_1 = g/d \xrightarrow{d\to 0} \text{asin}(x) - \frac{\pi}{2}$ (see lemma 6.1). Right figure: the first correction g_1 of g when $d \to +\infty$. The red curve is the theoretical asymptotic: $g_1 = d(g + \frac{1}{2}\sqrt{1-x^2}) \xrightarrow{d\to 0} \frac{1}{12} x\sqrt{1-x^2}$ (see lemma 6.1).

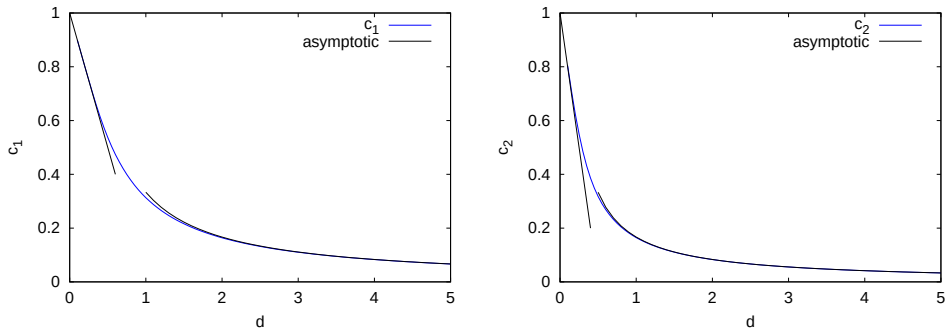

Figure 7.17: The coefficients c_1 and c_2 and their two asymptotics (black lines) (see proposition 6.2) computed with $\Delta x = 10^{-3}$.

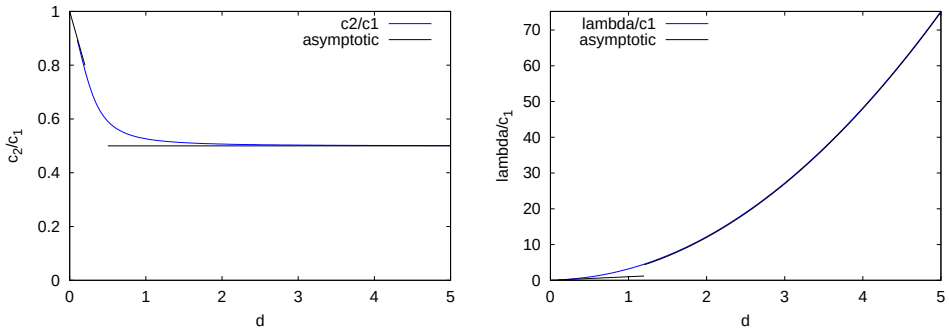

Figure 7.18: The ratio c_2/c_1 and λ/c_1 and their two asymptotics (black lines) (see proposition 6.2) computed with $\Delta x = 10^{-3}$.

Appendix B : Special solution of the MV model

In this appendix, a vortex configuration is exhibited as a stationary solution of the MV model (2.4)-(2.5)-(2.6) in dimension 2. A stationary state of the MV model has to satisfy:

$$\begin{aligned} &\nabla_x \cdot (\rho\Omega) = 0, \\ &c(\Omega \cdot \nabla_x)\Omega + \lambda\,(\mathrm{Id} - \Omega \otimes \Omega)\tfrac{\nabla_x \rho}{\rho} = 0. \end{aligned} \tag{6.16}$$

Introducing the polar coordinates, $\rho(r,\theta)$, $\Omega(r,\theta) = f_r(r,\theta)\vec{e}_r + f_\theta(r,\theta)\vec{e}_\theta$, where $\vec{e}_r = (\cos\theta, \sin\theta)^T$ and $\vec{e}_\theta = (-\sin\theta, \cos\theta)^T$, we are able to formulate the proposition:

Proposition 6.3 *The following initial condition is a stationary state of the MV model (6.16):*

$$\rho(r) = C\, r^{c/\lambda} \qquad , \qquad \Omega = \vec{e}_\theta, \tag{6.17}$$

where C is a constant.

Proof. With the expression of ρ and Ω given by (6.17), the divergence of the mass is zero and the gradient of ρ is orthogonal to Ω, therefore the system (6.16) reduces to:

$$c(\Omega \cdot \nabla_x)\Omega + \lambda \frac{\nabla_x \rho}{\rho} = 0, \tag{6.18}$$

or in polar coordinates:

$$c\frac{1}{r}\partial_\theta\, \vec{e}_\theta \;+\; \lambda \frac{\rho(r)}{\rho(r)}\vec{e}_r = 0.$$

Since $\partial_\theta \vec{e}_\theta = -\vec{e}_r$, we can easily check that the solution of this equation is given by: $\rho(r) = C\, r^{c/\lambda}$. □

Appendix C : Numerical schemes for particle simulations

In the limit $\varepsilon \to 0$, an explicit Euler method for the differential system (2.1)-(2.2) impose a restriction time step condition of $\frac{1}{\varepsilon}\Delta t < 1$. Therefore, we develop an implicit scheme for this system. The idea is to go back to the original Vicsek model (see [13]). We use the formulation:

$$\frac{\omega^{n+1} - \omega^n}{\Delta t} = (\mathrm{Id} - \omega^{n+1/2} \otimes \omega^{n+1/2})(\bar{\omega}^n - \omega^n) \tag{6.19}$$

where $\omega^{n+1/2} = \frac{\omega^n + \omega^{n+1}}{|\omega^n + \omega^{n+1}|}$. When $\Delta t = 1$, we recover exactly the original Vicsek model [28]. (6.19) can in fact be solved explicitly. First, we have to see that ω^{n+1} belongs to the unit circle (i.e. $|\omega^{n+1}| = 1$). Then, since $\omega^{n+1} - \omega^n$ is an orthogonal projection of $\widetilde{\omega}^n = \Delta t(\bar{\omega}^n - \omega^n)$, ω^{n+1} and ω_n are on the circle $\mathcal{C}$ with center $B = \omega_n + \frac{\widetilde{\omega}^n}{2}$ and radius $\left|\frac{\widetilde{\omega}^n}{2}\right|$. This fully defines ω^{n+1} since ω^n and ω^{n+1} are the two intersection points

of the unit circle and the circle $\mathcal{C}$. Denoting θ the angle of the unit vector ω, we easily check that we have in terms of angles:

$$\theta^{n+1} = \theta^n + 2(\widehat{\omega^n, B}).$$

To take into account the effect of the noise, we simply add a random variable:

$$\theta^{n+1} = \theta^n + 2(\widehat{\omega^n, B}) + \sqrt{2d\,\Delta t}\,\epsilon_n$$

where ϵ_n is a standard normal distribution independent of θ^n.

Algorithm used to solve a Riemann problem with particles.

We summarize below the different steps to numerically solve a Riemann problem, that is a discontinuity between two equilibrium states:

1. Choose a Riemann problem $(\rho_l,\, \theta_l)$ and $(\rho_r,\, \theta_r)$.
2. Initiate the particles $(x_k, \omega_k)_{i=1..N}$ according to the distributions $\rho_l M_{\Omega_l}$ and $\rho_r M_{\Omega_r}$.
3. Let evolve the particles in time using the time-discretization (6) of equation (2.2).
4. Compute the mass ρ and the direction of the flux Ω using Particle-In-Cell method [18] in order to compare the simulation with the one of the MV model.

Bibliography

[1] M. Aldana and C. Huepe. Phase Transitions in Self-Driven Many-Particle Systems and Related Non-Equilibrium Models: A Network Approach. *Journal of Statistical Physics*, 112(1):135–153, 2003.

[2] I. Aoki. A simulation study on the schooling mechanism in fish. *Bulletin of the Japanese Society of Scientific Fisheries (Japan)*, 1982.

[3] M. Ballerini, N. Cabibbo, R. Candelier, A. Cavagna, E. Cisbani, I. Giardina, V. Lecomte, A. Orlandi, G. Parisi, A. Procaccini, et al. Interaction ruling animal collective behavior depends on topological rather than metric distance: Evidence from a field study. *Proceedings of the National Academy of Sciences*, 105(4):1232, 2008.

[4] E. Bertin, M. Droz, and G. Gregoire. Boltzmann and hydrodynamic description for self-propelled particles (4 pages). *PHYSICAL REVIEW-SERIES E-*, 74(2):22101, 2006.

[5] J. Buhl, DJT Sumpter, ID Couzin, JJ Hale, E. Despland, ER Miller, and SJ Simpson. From disorder to order in marching locusts, 2006.

[6] H. Chaté, F. Ginelli, G. Grégoire, and F. Raynaud. Collective motion of self-propelled particles interacting without cohesion. *Physical Review E*, 77(4):46113, 2008.

[7] GQ Chen, CD Levermore, and TP Liu. Hyperbolic conservation laws with sti relaxation and entropy. *Comm. Pure Appl. Math*, 47:787, 1994.

[8] Y. Chuang, M.R. D'Orsogna, D. Marthaler, A.L. Bertozzi, and L.S. Chayes. State transitions and the continuum limit for a 2d interacting, self-propelled particle system. *Physica D: Nonlinear Phenomena*, 232(1):33–47, 2007.

[9] I.D. Couzin, J. Krause, R. James, G.D. Ruxton, and N.R. Franks. Collective memory and spatial sorting in animal groups. *Journal of Theoretical Biology*, 218(1):1–11, 2002.

[10] F. Cucker and S. Smale. Emergent behavior in flocks. *IEEE TRANSACTIONS ON AUTOMATIC CONTROL*, 52(5):852, 2007.

[11] F. Cucker and E. Mordecki. Flocking in noisy environments. *Journal de mathématiques pures et appliquées*, 2007.

[12] P. Degond and S. Motsch. Large scale dynamics of the persistent turning walker model of fish behavior. *Journal of Statistical Physics*, 131(6):989–1021, 2008.

[13] P. Degond and S. Motsch. Macroscopic limit of self-driven particles with orientation interaction. *Comptes rendus-Mathématique*, 345(10):555–560, 2007.

[14] H. Fehske, R. Schneider, and A. Weisse. *Computational Many-Particle Physics*. Springer Verlag, 2007.

[15] J. Gautrais, C. Jost, M. Soria, A. Campo, S. Motsch, R. Fournier, S. Blanco, and G. Theraulaz. Analyzing fish movement as a persistent turning walker. *Journal of Mathematical Biology*, 58(3):429–445, 2009.

[16] G. Grégoire and H. Chaté. Onset of collective and cohesive motion. *Physical Review Letters*, 92(2):25702, 2004.

[17] S.Y. Ha and E. Tadmor. From particle to kinetic and hydrodynamic descriptions of flocking. *Arxiv preprint arXiv:0806.2182*, 2008.

[18] R.W. Hockney and J.W. Eastwood. *Computer Simulation Using Particles*. Institute of Physics Publishing, 1988.

[19] A. HUTH and C. WISSEL. The simulation of the movement of fish schools. *Journal of theoretical biology*, 156(3):365–385, 1992.

[20] P.L. LeFloch. Entropy weak solutions to nonlinear hyperbolic systems under nonconservative form. *Communications in Partial Differential Equations*, 13(6):669–727, 1988.

[21] R.J. LeVeque. *Numerical Methods for Conservation Laws*. Birkhäuser, 1992.

[22] R.J. LeVeque and MyiLibrary. *Finite volume methods for hyperbolic problems*. Cambridge University Press, 2002.

[23] A. Mogilner and L. Edelstein-Keshet. A non-local model for a swarm. *Journal of Mathematical Biology*, 38(6):534–570, 1999.

[24] M. Nagy, I. Daruka, and T. Vicsek. New aspects of the continuous phase transition in the scalar noise model (SNM) of collective motion. *Physica A: Statistical Mechanics and its Applications*, 373:445–454, 2007.

[25] C.W. Reynolds. Flocks, herds and schools: A distributed behavioral model. pages 25–34, 1987.

[26] AS Sznitman. Topics in propagation of chaos. Ecole d'été de probabilités de Saint-Flour XIX-1989. *Lecture Notes in Math*, 1464:165–251, 1989.

[27] E.F. Toro. *Riemann solvers and numerical methods for fluid dynamics*. Springer New York, 1997.

[28] T. Vicsek, A. Czirók, E. Ben-Jacob, I. Cohen, and O. Shochet. Novel type of phase transition in a system of self-driven particles. *Physical Review Letters*, 75(6):1226–1229, 1995.

Part III
Homogenization theory

Chapter 8

Random integrals and correctors in homogenization

This chapter has given an article written in collaboration with G. Bal, J. Garnier and V. Perrier, and published in the journal Asymptotic Analysis: *Random integrals and correctors in homogenization*, Asymptot. Anal., **59** (2008), no. 1, 1–26.

Abstract. This chapter concerns the homogenization of a one-dimensional elliptic equation with oscillatory random coefficients. It is well-known that the random solution to the elliptic equation converges to the solution of an effective medium elliptic equation in the limit of a vanishing correlation length in the random medium. It is also well-known that the corrector to homogenization, i.e. the difference between the random solution and the homogenized solution, converges in distribution to a Gaussian process when the correlations in the random medium are sufficiently short-range. Moreover, the limiting process may be written as a stochastic integral with respect to standard Brownian motion. We generalize the result to a large class of processes with long-range correlations. In this setting, the corrector also converges to a Gaussian random process, which has an interpretation as a stochastic integral with respect to fractional Brownian motion. Moreover, we show that the longer the range of the correlations, the larger is the amplitude of the corrector. Derivations are based on a careful analysis of random oscillatory integrals of processes with long-range correlations. We also make use of the explicit expressions for the solutions to the one-dimensional elliptic equation.

Keywords. Homogenization, Partial Differential Equations with random coefficients, Long-range memory effects, Central limit, Gaussian processes

1 Introduction

Homogenization theory for second-order elliptic equations with highly oscillatory coefficients is well developed, both for periodic and random coefficients; see e.g. [2, 6]. The analysis of correctors, which measure the difference between the heterogeneous solution and the homogenized solution, is more limited.

In the periodic setting, the solution of so-called cell problems allow us to obtain explicit expressions for the correctors. Denoting by ε the size of the cell of periodicity of the oscillatory coefficients, the amplitude of the corrector for a second-order equation is typically of order ε [2, 6].

In the random setting, the situation is complicated by the fact that the local problems are no longer defined on compact cells. And as it turns out, the amplitude of the correctors is no longer of size ε in general, where ε now measures the correlation length of the random heterogeneities. Relatively few general estimates are available in the literature on the size of the correctors; see [13]. For the one-dimensional second-order elliptic equation (see (2.1) below), much more is known because of the availability of explicit expressions for the solutions (see (2.3) below). The analysis of correctors was taken up in [4], where it is shown that the correctors' amplitude is of order $\sqrt{\varepsilon}$ provided that the random coefficients have sufficiently short-range correlations so that, among other properties, their correlation function is integrable. Moreover, the corrector may be shown to converge in distribution in the space of continuous paths to a Gaussian process, which may be written as a stochastic integral with respect to Brownian motion. This result is recalled in Theorem 2.5 below. The work [4] also proposes error estimates for the corrector in the case of longer-range correlations, when the correlation function of the random coefficients is no longer integrable. The limiting behavior of the corrector is however not characterized.

This paper reconsiders the analysis of correctors for the one-dimensional equation when the correlation function of the random coefficients is no longer integrable, and more precisely takes the form $R(\tau) \sim \tau^{-\alpha}$ as $\tau \to \infty$ for some $0 < \alpha < 1$. Longer-range correlations are modeled by smaller values of α. A prototypical example of a continuous, stationary process with long-range correlation is a normalized Gaussian process g_x with a correlation function $R_g(\tau) = \mathbb{E}\{g_x g_{x+\tau}\}$ that decays as $\tau^{-\alpha}$. The random coefficients for the elliptic equation we consider in this paper are mean zero stationary processes that can be written as $\varphi(x) = \Phi(g_x)$, where Φ is a bounded function. Under appropriate assumptions on Φ, the correlation function of φ also decays as $\tau^{-\alpha}$ as $\tau \to \infty$.

For the random coefficients described above, we show that the corrector to homogenization has an amplitude of order ε^{α} and converges in distribution to a Gaussian process that may be represented as a stochastic integral with respect to a fractional Brownian motion W_t^H with Hurst index $H = 1 - \frac{\alpha}{2}$. The limit $\alpha \to 1$ thus converges to the case of integrable correlation function. Note however that in the limit of very long-range correlations as $\alpha \to 0$, the influence of the corrector becomes more and more important. The main tool in our derivation is a careful convergence analysis in distribution of oscillatory integrals of the form $\int_0^1 K(x,t)\varepsilon^{-\frac{\alpha}{2}}\varphi(\frac{t}{\varepsilon})dt$ to a stochastic integral with respect to fractional Brownian motion, where $K(x,t)$ is a known kernel

and $\varphi(t)$ is a random process with long-range correlations. This analysis extends weak convergence results obtained for sums of random variables or for integrals of random processes with long-range correlations in [12, 9].

The paper is structured as follows. Section 2 presents the heterogeneous and homogeneous one-dimensional elliptic equations and describes our hypotheses on the random coefficients. The section concludes by a statement of Theorem 2.4, which is our main result. The analysis of random oscillatory integrals of the form $\int_0^1 F(t)\varepsilon^{-\frac{\alpha}{2}}\varphi(\frac{t}{\varepsilon})dt$ is carried out in section 3. Theorem 3.1 shows their convergence to stochastic integrals with respect to fractional Brownian motion W_t^H. Section 4 shows how the results of section 3 extend to the analysis of the processes of the form $\int_0^1 K(x,t)\varepsilon^{-\frac{\alpha}{2}}\varphi(\frac{t}{\varepsilon})dt$ that arise in the analysis of the correctors to homogenization. The convergence in distribution in the space of continuous paths of such processes to a Gaussian processes is summarized in theorem 4.1. The theoretical results are backed up by numerical simulations in section 5. After a detailed description of the construction of random processes with given long-range correlations, we demonstrate the convergence of random oscillatory integrals and of homogenization correctors to their appropriate limits as stochastic integrals with respect to fractional Brownian motion. Some concluding remarks are given in section 7.

2 One-dimensional homogenization

2.1 Homogenization problem

We are interested in the solution to the following elliptic equation with random coefficients

$$\begin{aligned} &-\frac{d}{dx}\Big(a\Big(\frac{x}{\varepsilon},\omega\Big)\frac{d}{dx}u^\varepsilon\Big) = f(x), \qquad 0\le x\le 1, \quad \omega\in\Omega,\\ &u^\varepsilon(0,\omega)=0, \qquad u^\varepsilon(1,\omega)=q. \end{aligned} \tag{2.1}$$

Here $a(x,\omega)$ is a stationary ergodic random process such that $0<a_0\le a(x,\omega)\le a_0^{-1}$ a.e. for $(x,\omega)\in(0,1)\times\Omega$, where $(\Omega,\mathcal{F},\mathbb{P})$ is an abstract probability space. The source term $f\in W^{-1,\infty}(0,1)$ and $q\in\mathbb{R}$. Classical theories for elliptic equations then show the existence of a unique solution $u(\cdot,\omega)\in H^1(0,1)$ $\mathbb{P}-$a.s.

As the scale of the micro-structure ε converges to 0, the solution $u^\varepsilon(x,\omega)$ converges $\mathbb{P}$-a.s. weakly in $H^1(0,1)$ to the deterministic solution $\bar{u}$ of the homogenized equation

$$\begin{aligned} &-\frac{d}{dx}\Big(a^*\frac{d}{dx}\bar{u}\Big) = f(x), \qquad 0\le x\le 1,\\ &\bar{u}(0)=0, \qquad \bar{u}(1)=q. \end{aligned} \tag{2.2}$$

The effective diffusion coefficient is given by $a^*=\Big(\mathbb{E}\{a^{-1}(0,\cdot)\}\Big)^{-1}$, where $\mathbb{E}$ is mathematical expectation with respect to $\mathbb{P}$. See e.g. [6, 7, 10].

The above one-dimensional boundary value problems admit explicit solutions. In-

troducing $a^\varepsilon(x) = a(\frac{x}{\varepsilon})$ and $F(x) = \int_0^x f(y)dy$, we have:

$$u^\varepsilon(x,\omega) = c^\varepsilon(\omega)\int_0^x \frac{1}{a^\varepsilon(y,\omega)}dy - \int_0^x \frac{F(y)}{a^\varepsilon(y,\omega)}dy, \qquad c^\varepsilon(\omega) = \frac{q + \displaystyle\int_0^1 \frac{F(y)}{a^\varepsilon(y,\omega)}dy}{\displaystyle\int_0^1 \frac{1}{a^\varepsilon(y,\omega)}dy} \tag{2.3}$$

$$\bar{u}(x) = c^*\frac{x}{a^*} - \int_0^x \frac{F(y)}{a^*}dy, \qquad c^* = a^*q + \int_0^1 F(y)dy. \tag{2.4}$$

Our aim is to characterize the behavior of $u^\varepsilon - \bar{u}$ as $\varepsilon \to 0$.

2.2 Hypothesis on the random process a

In order to characterize the behavior of the corrector $u^\varepsilon - \bar{u}$ as $\varepsilon \to 0$, we need additional assumptions on the random process $a(x,\omega)$. Let us define the mean zero stationary random process

$$\varphi(x,\omega) = \frac{1}{a(x,\omega)} - \frac{1}{a^*}. \tag{2.5}$$

Hypothesis [H] *We assume that φ is of the form*

$$\varphi(x) = \Phi(g_x), \tag{2.6}$$

where Φ is a bounded function such that

$$\int \Phi(g)e^{-\frac{g^2}{2}}dg = 0, \tag{2.7}$$

and g_x is a stationary Gaussian process with mean zero and variance one. The autocorrelation function of g:

$$R_g(\tau) = \mathbb{E}\Big\{g_x g_{x+\tau}\Big\},$$

is assumed to have a heavy tail of the form

$$R_g(\tau) \sim \kappa_g \tau^{-\alpha} \text{ as } \tau \to \infty, \tag{2.8}$$

where $\kappa_g > 0$ and $\alpha \in (0,1)$.

Remark 2.1 This hypothesis is satisfied by a large class of random coefficients. For instance, if we take $\Phi = \text{sgn}$, then φ models a two-component medium. If we take $\Phi = \tanh$ or $\arctan$, then φ models a continuous medium with bounded variations.

The autocorrelation function of the random process a has a heavy tail, as stated in the following proposition.

Proposition 2.1 *The process φ defined by* (2.6) *is a stationary random process with mean zero and variance V_2. Its autocorrelation function*

$$R(\tau) = \mathbb{E}\{\varphi(x)\varphi(x+\tau)\} \tag{2.9}$$

has a heavy tail of the form

$$R(\tau) \sim \kappa \tau^{-\alpha} \text{ as } \tau \to \infty, \tag{2.10}$$

where $\kappa = \kappa_g V_1^2$,

$$V_1 = \mathbb{E}\Big\{g_0 \Phi(g_0)\Big\} = \frac{1}{\sqrt{2\pi}} \int g \Phi(g) e^{-\frac{g^2}{2}} dg\,, \tag{2.11}$$

$$V_2 = \mathbb{E}\Big\{\Phi^2(g_0)\Big\} = \frac{1}{\sqrt{2\pi}} \int \Phi^2(g) e^{-\frac{g^2}{2}} dg\,. \tag{2.12}$$

Proof The fact that φ is a stationary random process with mean zero and variance V_2 is straightforward in view of the definition of φ. In particular, Eq. (2.7) implies that φ has mean zero.
For any x, τ, the vector $(g_x, g_{x+\tau})^T$ is a Gaussian random vector with mean $(0,0)^T$ and 2×2 covariance matrix:

$$C = \begin{pmatrix} 1 & R_g(\tau) \\ R_g(\tau) & 1 \end{pmatrix}.$$

Therefore the autocorrelation function of the process φ is

$$\begin{aligned} R(\tau) &= \mathbb{E}\Big\{\Phi(g_x)\Phi(g_{x+\tau})\Big\} = \frac{1}{2\pi\sqrt{\det C}} \iint \Phi(g_1)\Phi(g_2) \exp\Big(-\frac{g^T C^{-1} g}{2}\Big) d^2 g \\ &= \frac{1}{2\pi\sqrt{1-R_g^2(\tau)}} \iint \Phi(g_1)\Phi(g_2) \exp\Big(-\frac{g_1^2 + g_2^2 - 2R_g(\tau) g_1 g_2}{2(1-R_g^2(\tau))}\Big) dg_1 dg_2\,. \end{aligned}$$

For large τ, the coefficient $R_g(\tau)$ is small and we can expand the value of the double integral in powers of $R_g(\tau)$, which gives the autocorrelation function of φ. ∎

To simplify notation, we no longer write the ω-dependence explicitly and we define $\varphi^\varepsilon(x) = \varphi(\frac{x}{\varepsilon})$.

2.3 Analysis of the corrector

The purpose of this section is to show that the error term $u^\varepsilon - \bar{u}$ has two different contributions: integrals of random processes with long term memory effects and lower-order terms. The analysis of integrals of the random processes with long term memory effects is carried out in the next sections. The following lemma, whose proof can be found in Section 4.2, provides an estimate for the magnitude of these integrals.

Lemma 2.2 *Let $\varphi(x)$ be a mean zero stationary random process of the form (2.6). There exists $K > 0$ such that, for any $F \in L^\infty(0,1)$, we have*

$$\sup_{x \in [0,1]} \mathbb{E}\Big\{\Big| \int_0^x \varphi^\varepsilon(t) F(t) dt \Big|^2\Big\} \le K \|F\|_\infty^2 \varepsilon^\alpha\,. \tag{2.13}$$

As a corollary, we obtain the following:

Corollary 2.3 *Let $\varphi(x)$ be a mean zero stationary random process of the form (2.6) and let $f \in W^{-1,\infty}(0,1)$. The solutions u^ε of (2.3) and $\bar{u}$ of (2.4) verify that:*

$$u^\varepsilon(x) - \bar{u}(x) = -\int_0^x \varphi^\varepsilon(y)F(y)dy + (c^\varepsilon - c^*)\frac{x}{a^*} + c^*\int_0^x \varphi^\varepsilon(y)dy + r^\varepsilon(x), \qquad (2.14)$$

where

$$\sup_{x\in[0,1]} \mathbb{E}\{|r^\varepsilon(x)|\} \leq K\varepsilon^\alpha\,, \qquad (2.15)$$

for some $K > 0$. Similarly, we have that

$$c^\varepsilon - c^* = a^*\int_0^1 \Big(F(y) - \int_0^1 F(z)dz - a^*q\Big)\varphi^\varepsilon(y)dy + \rho^\varepsilon, \qquad (2.16)$$

where

$$\mathbb{E}\{|\rho^\varepsilon|\} \leq K\varepsilon^\alpha\,, \qquad (2.17)$$

for some $K > 0$.

Proof We first establish the estimate for $c^\varepsilon - c$. We write

$$c^\varepsilon - c^* = \frac{\int_0^1 F(y)\Big(\frac{1}{a^\varepsilon(y)} - \frac{1}{a^*}\Big)dy}{\int_0^1 \frac{1}{a^\varepsilon(y)}dy} + \Big(q + \frac{1}{a^*}\int_0^1 F(y)dy\Big)\Big(\frac{1}{\int_0^1 \frac{1}{a^\varepsilon(y)}dy} - \frac{1}{\frac{1}{a^*}}\Big),$$

which gives (2.16) with

$$\rho^\varepsilon = \frac{a^*}{\int_0^1 \frac{1}{a^\varepsilon(y)}dy}\left[(a^*q + \int_0^1 F(y)dy)\left(\int_0^1 \varphi^\varepsilon(y)dy\right)^2 - \int_0^1 F(y)\varphi^\varepsilon(y)dy\int_0^1 \varphi^\varepsilon(y)dy\right].$$

Since $\int_0^1 \frac{1}{a^\varepsilon(y)}dy$ is bounded from below a.e. by a positive constant a_0, we deduce from Lemma 2.2 and the Cauchy-Schwarz estimate that $\mathbb{E}\{|\rho^\varepsilon|\} \leq K\varepsilon^\alpha$. The analysis of $u^\varepsilon - \bar{u}$ follows along the same lines. We write

$$u^\varepsilon(x) - \bar{u}(x) = c^\varepsilon\int_0^x \frac{1}{a^\varepsilon(y)}dy - \int_0^x \frac{F(y)}{a^\varepsilon(y)}dy - c^*\frac{x}{a^*} + \int_0^x \frac{F(y)}{a^*}dy,$$

which gives (2.14) with

$$r^\varepsilon(x) = (c^\varepsilon - c^*)\int_0^x \varphi^\varepsilon(y)dy = r_1^\varepsilon(x) + r_2^\varepsilon(x),$$

where we have defined

$$\begin{aligned} r_1^\varepsilon(x) &= \left[a^*\int_0^1 \Big(F(y) - \int_0^1 F(z)dz - a^*q\Big)\varphi^\varepsilon(y)dy\right]\left[\int_0^x \varphi^\varepsilon(y)dy\right], \\ r_2^\varepsilon(x) &= \rho^\varepsilon\left[\int_0^x \varphi^\varepsilon(y)dy\right]. \end{aligned}$$

The Cauchy-Schwarz estimate and Lemma 2.2 give that $\mathbb{E}\{|r_1^\varepsilon(x)|\} \leq K\varepsilon^\alpha$. Besides, φ^ε is bounded by $\|\Phi\|_\infty$, so $|r_2^\varepsilon(x)| \leq \|\Phi\|_\infty|\rho^\varepsilon|$. The estimate on ρ^ε then shows that $\mathbb{E}\{|r_2^\varepsilon(x)|\} \leq K\varepsilon^\alpha$. ∎

The previous corollary shows that the error term $u^\varepsilon(x) - \bar{u}(x)$ involves integrals of random coefficients of order $\varepsilon^{\alpha/2}$ up to lower-order terms of order ε^α.

2.4 Homogenization theorem

The results we obtain in the following sections allow for the following characterization of the correctors.

Theorem 2.4 *Let u^ε and $\bar{u}$ be the solutions in (2.3) and (2.4), respectively, and let $\varphi(x)$ be a mean zero stationary random process of the form (2.6). Then $u^\varepsilon - \bar{u}$ is a random process in $\mathcal{C}(0,1)$, the space of continuous functions on $[0,1]$. We have the following convergence in distribution in the space of continuous functions $\mathcal{C}(0,1)$:*

$$\frac{u^\varepsilon(x) - \bar{u}(x)}{\varepsilon^{\frac{\alpha}{2}}} \xrightarrow{\text{distribution}} \sqrt{\frac{\kappa}{H(2H-1)}}\mathcal{U}^H(x), \tag{2.18}$$

where

$$\mathcal{U}^H(x) = \int_{\mathbb{R}} K(x,t)dW_t^H, \tag{2.19}$$

$$K(x,t) = \mathbf{1}_{[0,x]}(t)\Big(c^* - F(t)\Big) + x\Big(F(t) - \int_0^1 F(z)dz - a^*q\Big)\mathbf{1}_{[0,1]}(t). \tag{2.20}$$

Here $\mathbf{1}_{[0,x]}$ is the characteristic function of the set $[0,x]$ and W_t^H is a fractional Brownian motion with Hurst index $H = 1 - \frac{\alpha}{2}$.

The proof of this theorem is postponed to Section 4.3. For the convenience of the reader, we present a rapid overview of the integration theory with respect to a fractional Brownian motion. The fractional Brownian motion W_t^H is a mean zero Gaussian process with autocorrelation function

$$\mathbb{E}\{W_t^H W_s^H\} = \frac{1}{2}\Big(|t|^{2H} + |s|^{2H} - |s-t|^{2H}\Big). \tag{2.21}$$

In particular, the variance of W_t^H is $\mathbb{E}\{|W_t^H|^2\} = |t|^{2H}$. The increments of W_t^H are stationary but not independent for $H \neq \frac{1}{2}$. Moreover, W_t^H admits the following spectral representation

$$W_t^H = \frac{1}{2\pi C(H)} \int_{\mathbb{R}} \frac{e^{i\xi t} - 1}{i\xi|\xi|^{H-\frac{1}{2}}} d\hat{W}(\xi), \quad t \in \mathbb{R}, \tag{2.22}$$

where

$$C(H) = \left(\frac{1}{2H\sin(\pi H)\Gamma(2H)}\right)^{1/2}, \tag{2.23}$$

and $\hat{W}$ is the Fourier transform of a standard Brownian motion W, that is, a complex Gaussian measure such that:

$$\mathbb{E}\Big\{d\hat{W}(\xi)\overline{d\hat{W}(\xi')}\Big\} = 2\pi\delta(\xi - \xi')d\xi d\xi'\,.$$

Note that the constant $C(H)$ is defined such that $\mathbb{E}\{(W_1^H)^2\} = 1$ because we have that

$$C^2(H) = \frac{1}{2\pi}\int_{\mathbb{R}} \frac{|e^{i\xi} - 1|^2}{|\xi|^{2H+1}} d\xi\,.$$

The integral with respect to the fractional Brownian motion is defined for a large class of deterministic functions F (see [11] for an extensive review). Functions in $L^1(\mathbb{R}) \cap L^2(\mathbb{R})$ are in the class of integrable functions when $H \in (\frac{1}{2}, 1)$, which is the range of values of H considered in Theorem 2.4. Using the representation (2.22), we have, in distribution, for any $F \in L^1(\mathbb{R}) \cap L^2(\mathbb{R})$,

$$\int_{\mathbb{R}} F(t) dW_t^H = \frac{1}{2\pi C(H)} \int_{\mathbb{R}} \frac{\hat{F}(\xi)}{|\xi|^{H-\frac{1}{2}}} d\hat{W}(\xi)\,,$$

where the Fourier transform $\hat{F}(\xi)$ of a function $F(t)$ is defined by

$$\hat{F}(\xi) = \int_{\mathbb{R}} e^{it\xi} F(t) dt\,. \tag{2.24}$$

When $F, G \in L^1(\mathbb{R}) \cap L^2(\mathbb{R})$, the random vector $(\int_{\mathbb{R}} F(t) dW_t^H, \int_{\mathbb{R}} G(t) dW_t^H)$ is a mean zero Gaussian vector with covariance

$$\mathbb{E}\left\{ \int_{\mathbb{R}} F(t) dW_t^H \int_{\mathbb{R}} G(t) dW_t^H \right\} = \frac{1}{2\pi C(H)^2} \int_{\mathbb{R}} \frac{\hat{F}(\xi)\overline{\hat{G}(\xi)}}{|\xi|^{2H-1}} d\xi\,.$$

As a consequence, in Theorem 2.4, the limit process $\mathcal{U}^H(x)$ is a mean zero Gaussian process with autocorrelation function given by

$$\mathbb{E}\big\{\mathcal{U}^H(x)\mathcal{U}^H(y)\big\} = \frac{1}{2\pi C(H)^2} \int_{\mathbb{R}} \frac{\hat{K}(x,\xi)\overline{\hat{K}(y,\xi)}}{|\xi|^{2H-1}} d\xi\,, \tag{2.25}$$

where $\hat{K}(x,\xi)$ is the Fourier transform with respect to t of $K(x,t)$. Finally, using the notation

$$\int_0^x F(s) dW_t^H = \int_{\mathbb{R}} \mathbf{1}_{[0,x]}(s) F(s) dW_t^H\,,$$

the limit process $\mathcal{U}^H(x)$ defined by (2.19) can also be written as

$$\mathcal{U}^H(x) = c^* W_x^H - \int_0^x F(t) dW_t^H + x \int_0^1 F(t) dW_t^H - x \left(\int_0^1 F(z) dz - a^* q \right) W_1^H\,.$$

The result of Theorem 2.4 should be contrasted with the convergence result for processes with short term memory:

Theorem 2.5 *Let u^ε and $\bar{u}$ be as in Theorem 2.4 and let $\varphi(x)$ be a mean zero stationary random process of the form (2.6). If the correlation function R_g of g is integrable (instead of being equivalent to $\tau^{-\alpha}$ at infinity), then R is also integrable. The corrector $u^\varepsilon - \bar{u}$ is a random process in $\mathcal{C}[0,1]$ and we have the following convergence in $\mathcal{C}(0,1)$*

$$\frac{u^\varepsilon(x) - \bar{u}(x)}{\sqrt{\varepsilon}} \xrightarrow{\text{distribution}} \left(2 \int_0^\infty R(\tau) d\tau \right)^{1/2} \mathcal{U}(x), \tag{2.26}$$

where

$$\mathcal{U}(x) = \int_{\mathbb{R}} K(x,t) dW_t, \tag{2.27}$$

$K(x,t)$ is given by (2.20)*, and W_t is standard Brownian motion.*

The limit process $\mathcal{U}(x)$ can also be written in the form

$$\mathcal{U}(x) = c^* W_x - \int_0^x F(t) dW_t + x \int_0^1 F(t) dW_t - x \left(\int_0^1 F(z) dz - a^* q \right) W_1 \,.$$

Such a result is based on standard techniques of approximation of oscillatory integrals [8] and was first derived in [4]. In the next sections, we focus our attention to the analysis of random variables or random processes defined in terms of integrals of random processes with long-term memory.

3 Convergence of random integrals

In this section, we aim at proving the following theorem.

Theorem 3.1 *Let φ be of the form (2.6) and let $F \in L^1(\mathbb{R}) \cap L^\infty(\mathbb{R})$. We define the mean zero random variable M_F^ε by*

$$M_F^\varepsilon = \varepsilon^{-\frac{\alpha}{2}} \int_{\mathbb{R}} \varphi^\varepsilon(t) F(t) dt \,. \tag{3.28}$$

Then the random variable M_F^ε converges in distribution as $\varepsilon \to 0$ to the mean zero Gaussian random variable M_F^0 defined by

$$M_F^0 = \sqrt{\frac{\kappa}{H(2H-1)}} \int_{\mathbb{R}} F(t) dW_t^H \,, \tag{3.29}$$

where W_t^H is a fractional Brownian motion with Hurst index $H = 1 - \frac{\alpha}{2}$.

The limit random variable M_F^0 is a Gaussian random variable with mean zero and variance

$$\mathbb{E}\{|M_F^0|^2\} = \frac{\kappa}{H(2H-1)} \times \frac{1}{2\pi C(H)^2} \int_{\mathbb{R}} \frac{|\hat{F}(\xi)|^2}{|\xi|^{2H-1}} d\xi \,. \tag{3.30}$$

In order to prove Theorem 3.1, we show in Subsection 3.1 that the variance of M_F^ε converges to the variance of M_F^0 as $\varepsilon \to 0$. In Subsection 3.2, we prove convergence in distribution by using the Gaussian property of the underlying process g_x.

3.1 Convergence of the variances

We begin with a key technical lemma.

Lemma 3.2 *1. There exist $T, K > 0$ such that the autocorrelation function $R(\tau)$ of the process φ satisfies*

$$|R(\tau) - V_1^2 R_g(\tau)| \leq K R_g(\tau)^2, \qquad \text{for all} \quad |\tau| \geq T.$$

2. There exist T, K such that

$$|\mathbb{E}\{g_x \Phi(g_{x+\tau})\} - V_1 R_g(\tau)| \leq K R_g^2(\tau) \qquad \text{for all} \quad |\tau| \geq T.$$

Proof The first point is a refinement of what we proved in Proposition 2.1: we found that the autocorrelation function of the process φ is

$$R(\tau) \;=\; \frac{1}{2\pi\sqrt{1-R_g^2(\tau)}}\iint \Phi(g_1)\Phi(g_2)\exp\Big(-\frac{g_1^2+g_2^2-2R_g(\tau)g_1g_2}{2(1-R_g^2(\tau))}\Big)dg_1dg_2\,.$$

For large τ, the coefficient $R_g(\tau)$ is small and we can expand the value of the double integral in powers of $R_g(\tau)$, which gives the result of the first item. The proof of the second item follows along the same lines. We first write

$$\mathbb{E}\Big\{g_x\Phi(g_{x+\tau})\Big\} = \frac{1}{2\pi\sqrt{1-R_g^2(\tau)}}\iint g_1\Phi(g_2)\exp\Big(-\frac{g_1^2+g_2^2-2R_g(\tau)g_1g_2}{2(1-R_g^2(\tau))}\Big)dg_1dg_2\,,$$

and we expand the value of the double integral in powers of $R_g(\tau)$. ∎

For $F\in L^1(\mathbb{R})\cap L^\infty(\mathbb{R})$, we define the mean zero random variable $M_F^{\varepsilon,g}$ by

$$M_F^{\varepsilon,g} = \varepsilon^{-\frac{\alpha}{2}}\int_{\mathbb{R}} g_{\frac{t}{\varepsilon}}F(t)dt\,. \tag{3.31}$$

The purpose of this subsection is to determine the limits of the variances of the variables M_F^{ε} and $M_F^{\varepsilon,g}$.

Lemma 3.3 *Let $F\in L^1(\mathbb{R})\cap L^\infty(\mathbb{R})$ and let g_x be the Gaussian random process described in Hypothesis [H]. Then*

$$\lim_{\varepsilon\to 0}\mathbb{E}\Big\{\Big|M_F^{\varepsilon,g}\Big|^2\Big\} = \frac{\kappa_g 2^{-\alpha}\Gamma(\frac{1-\alpha}{2})}{\sqrt{\pi}\Gamma(\frac{\alpha}{2})}\int_{\mathbb{R}}\frac{|\hat F(\xi)|^2}{|\xi|^{1-\alpha}}d\xi\,. \tag{3.32}$$

Proof We write the square of the integral as a double integral, which gives

$$\mathbb{E}\Big\{\Big|\int_{\mathbb{R}}F(y)g_{\frac{y}{\varepsilon}}dy\Big|^2\Big\} = \int_{\mathbb{R}^2}R_g\Big(\frac{y-z}{\varepsilon}\Big)F(y)F(z)dydz\,.$$

This implies the estimate

$$\begin{aligned}\Big|\mathbb{E}\Big\{\Big|M_F^{\varepsilon,g}\Big|^2\Big\} - \int_{\mathbb{R}^2}\frac{\kappa_g}{|y-z|^\alpha}F(y)F(z)dydz\Big| \\ \le \int_{\mathbb{R}^2}\Big|\varepsilon^{-\alpha}R_g\Big(\frac{y-z}{\varepsilon}\Big) - \frac{\kappa_g}{|y-z|^\alpha}\Big||F(y)||F(z)|dydz\,.\end{aligned}$$

By (2.8), for any $\delta>0$, there exists T_δ such that, for all $|\tau|\ge T_\delta$,

$$\Big|R_g(\tau)-\kappa_g\tau^{-\alpha}\Big|\le\delta\tau^{-\alpha}\,.$$

We decompose the integration domain into three subdomains D_1, D_2, and D_3:

$$\begin{aligned}D_1 &= \Big\{(y,z)\in\mathbb{R}^2\,,\,|y-z|\le T_\delta\varepsilon\Big\}\,,\\ D_2 &= \Big\{(y,z)\in\mathbb{R}^2\,,\,T_\delta\varepsilon<|y-z|\le 1\Big\}\,,\\ D_3 &= \Big\{(y,z)\in\mathbb{R}^2\,,\,1<|y-z|\Big\}\,.\end{aligned}$$

First,

$$\begin{aligned}
&\int_{D_1}\left|\varepsilon^{-\alpha}R_g\Big(\frac{y-z}{\varepsilon}\Big)-\frac{\kappa_g}{|y-z|^\alpha}\right||F(y)||F(z)|dydz\\
&\quad\le\int_{D_1}\left|\varepsilon^{-\alpha}R_g\Big(\frac{y-z}{\varepsilon}\Big)\right||F(y)||F(z)|dydz+\int_{D_1}\kappa_g|y-z|^{-\alpha}|F(y)||F(z)|dydz\\
&\quad\le 2\varepsilon^{-\alpha}\|R_g\|_\infty\int_{\mathbb{R}}\int_0^{T_\delta\varepsilon}|F(y+z)|dy|F(z)|dz+2\kappa_g\int_{\mathbb{R}}\int_0^{T_\delta\varepsilon}y^{-\alpha}|F(y+z)|dy|F(z)|dz\\
&\quad\le 2\varepsilon^{-\alpha}\|R_g\|_\infty\|F\|_\infty\|F\|_1\int_0^{T_\delta\varepsilon}dy+2\kappa_g\|F\|_\infty\|F\|_1\int_0^{T_\delta\varepsilon}y^{-\alpha}dy\\
&\quad\le\|F\|_\infty\|F\|_1\left(2T_\delta R_g(0)+\frac{2\kappa_g T_\delta^{1-\alpha}}{1-\alpha}\right)\varepsilon^{1-\alpha}\,,
\end{aligned}$$

where we have used the fact that $R_g(\tau)$ is maximal at $\tau=0$, and the value of the maximum is equal to the variance of g. Second,

$$\begin{aligned}
\int_{D_2}\left|\varepsilon^{-\alpha}R_g\Big(\frac{y-z}{\varepsilon}\Big)-\frac{\kappa_g}{|y-z|^\alpha}\right||F(y)||F(z)|dydz &\le \delta\int_{D_2}|y-z|^{-\alpha}|F(y)||F(z)|dydz\\
&\le 2\delta\|F\|_\infty\|F\|_1\int_{T_\delta\varepsilon}^1 y^{-\alpha}dy\\
&\le \frac{2\delta\|F\|_\infty\|F\|_1}{1-\alpha}\,,
\end{aligned}$$

and finally

$$\begin{aligned}
\int_{D_3}\left|\varepsilon^{-\alpha}R_g\Big(\frac{y-z}{\varepsilon}\Big)-\frac{\kappa_g}{|y-z|^\alpha}\right||F(y)||F(z)|dydz &\le \delta\int_{D_3}|y-z|^{-\alpha}|F(y)||F(z)|dydz\\
&\le \delta\int_{D_3}|F(y)||F(z)|dydz\\
&\le \delta\|F\|_1^2\,.
\end{aligned}$$

Therefore, there exists $K>0$ such that

$$\limsup_{\varepsilon\to0}\left|\mathbb{E}\Big\{\Big|M_F^{\varepsilon,g}\Big|^2\Big\}-\int_{\mathbb{R}^2}\frac{\kappa_g}{|y-z|^\alpha}F(y)F(z)dydz\right|\le K\left(\|F\|_\infty^2+\|F\|_1^2\right)\delta\,.$$

Since this holds true for any $\delta>0$, we get

$$\lim_{\varepsilon\to0}\left|\mathbb{E}\Big\{\Big|M_F^{\varepsilon,g}\Big|^2\Big\}-\int_{\mathbb{R}^2}\frac{\kappa_g}{|y-z|^\alpha}F(y)F(z)dydz\right|=0\,.$$

We recall that the Fourier transform of the function $|x|^{-\alpha}$ is

$$\widehat{|x|^{-\alpha}}(\xi)=c_\alpha|\xi|^{\alpha-1}\,,\qquad c_\alpha=\int_{\mathbb{R}}\frac{e^{it}}{|t|^\alpha}dt=\frac{\sqrt{\pi}2^{1-\alpha}\Gamma(\frac{1-\alpha}{2})}{\Gamma(\frac{\alpha}{2})}\,.\tag{3.33}$$

Using the Parseval equality, we find that

$$\int_{\mathbb{R}^2}\frac{1}{|y-z|^\alpha}F(y)F(z)dydz=\frac{c_\alpha}{2\pi}\int_{\mathbb{R}}\frac{|\hat F(\xi)|^2}{|\xi|^{1-\alpha}}d\xi\,.$$

The right-hand side is finite, because (i) $F \in L^1(\mathbb{R})$ so that $\hat{F}(\xi) \in L^\infty(\mathbb{R})$, (ii) $F \in L^1(\mathbb{R}) \cap L^\infty(\mathbb{R})$ so $F \in L^2(\mathbb{R})$ and $\hat{F} \in L^2(\mathbb{R})$, and (iii) $\alpha \in (0,1)$. ∎

Lemma 3.4 *Let $F \in L^1(\mathbb{R}) \cap L^\infty(\mathbb{R})$ and let the process $\varphi(x)$ be of the form (2.6). Then we have:*

$$\lim_{\varepsilon \to 0} \mathbb{E}\Big\{ (M_F^\varepsilon - V_1 M_F^{\varepsilon,g})^2 \Big\} = 0\,.$$

Proof. We write the square of the integral as a double integral:

$$\mathbb{E}\Big\{ (M_F^\varepsilon - V_1 M_F^{\varepsilon,g})^2 \Big\} = \varepsilon^{-\alpha} \int_{\mathbb{R}^2} F(y)F(z)Q(\frac{y}{\varepsilon},\frac{z}{\varepsilon})dydz\,,$$

where

$$Q(y,z) = \mathbb{E}\Big\{ \Phi(g_y)\Phi(g_z) - V_1\Phi(g_y)g_z - V_1 g_y \Phi(g_z) + V_1^2 g_y g_z \Big\}\,.$$

By Lemma 3.2 and (2.8), there exist K, T such that $|Q(y,z)| \le K|y-z|^{-2\alpha}$ for all $|x-y| \ge T$. Besides, Φ is bounded and g_x is square-integrable, so there exists K such that, for all $y, z \in \mathbb{R}$, $|Q(y,z)| \le K$. We decompose the integration domain $\mathbb{R}^2$ into three subdomains D_1, D_2, and D_3:

$$\begin{aligned} D_1 &= \Big\{ (y,z) \in \mathbb{R}^2\,,\, |y-z| \le T\varepsilon \Big\}\,, \\ D_2 &= \Big\{ (y,z) \in \mathbb{R}^2\,,\, T\varepsilon < |y-z| \le 1 \Big\}\,, \\ D_3 &= \Big\{ (y,z) \in \mathbb{R}^2\,,\, 1 < |y-z| \Big\}\,. \end{aligned}$$

We get the estimates

$$\begin{aligned} \Big| \int_{D_1} F(y)F(z)Q(\frac{y}{\varepsilon},\frac{z}{\varepsilon})dydz \Big| &\le K \int_{D_1} |F(y)||F(z)|dydz \\ &\le 2K \int_{\mathbb{R}} \int_0^{T\varepsilon} |F(y+z)|dy|F(z)|dz \\ &\le 2K\|F\|_\infty \|F\|_1 T\varepsilon\,, \end{aligned}$$

$$\begin{aligned} \Big| \int_{D_2} F(y)F(z)Q(\frac{y}{\varepsilon},\frac{z}{\varepsilon})dydz \Big| &\le K \int_{D_2} \Big|\frac{y}{\varepsilon} - \frac{z}{\varepsilon}\Big|^{-2\alpha} |F(y)||F(z)dydz \\ &\le 2K\varepsilon^{2\alpha} \int_{\mathbb{R}} \int_{T\varepsilon}^1 y^{-2\alpha}|F(y+z)|dy|F(z)|dz \\ &\le 2K\|F\|_1\|F\|_\infty \varepsilon^{2\alpha} \int_{T\varepsilon}^1 y^{-2\alpha}dy \\ &\le 2K\|F\|_1\|F\|_\infty \begin{cases} \dfrac{1}{1-2\alpha}\varepsilon^{2\alpha} \text{ if } \alpha < \dfrac{1}{2} \\ |\ln(T\varepsilon)|\varepsilon \text{ if } \alpha = \dfrac{1}{2} \\ \dfrac{T^{1-2\alpha}}{2\alpha-1}\varepsilon \text{ if } \alpha > \dfrac{1}{2} \end{cases} \end{aligned}$$

$$\begin{aligned}\left|\int_{D_3} F(y)F(z)Q(\frac{y}{\varepsilon},\frac{z}{\varepsilon})dydz\right| &\leq K\int_{D_3}\left|\frac{y}{\varepsilon}-\frac{z}{\varepsilon}\right|^{-2\alpha}|F(y)||F(z)dydz\\ &\leq 2K\varepsilon^{2\alpha}\int_{\mathbb{R}}\int_1^\infty y^{-2\alpha}|F(y+z)|dy|F(z)|dz\\ &\leq 2K\varepsilon^{2\alpha}\int_{\mathbb{R}}\int_1^\infty |F(y+z)|dy|F(z)|dz\\ &\leq 2K\|F\|_1^2\varepsilon^{2\alpha}\,,\end{aligned}$$

which gives the desired result:

$$\lim_{\varepsilon\to 0}\varepsilon^{-\alpha}\left|\int_{\mathbb{R}^2} F(y)F(z)Q(\frac{y}{\varepsilon},\frac{z}{\varepsilon})dydz\right| = 0\,.$$

■

The following proposition is now a straightforward corollary of Lemmas 3.3 and 3.4 and the fact that $\kappa = \kappa_g V_1^2$.

Proposition 3.5 *Let $F \in L^1(\mathbb{R}) \cap L^\infty(\mathbb{R})$ and let the process $\varphi(x)$ be of the form (2.6). Then we find that:*

$$\lim_{\varepsilon\to 0}\mathbb{E}\Big\{\Big|M_F^\varepsilon\Big|^2\Big\} = \frac{\kappa 2^{-\alpha}\Gamma(\frac{1-\alpha}{2})}{\sqrt{\pi}\Gamma(\frac{\alpha}{2})}\int_{\mathbb{R}}\frac{|\hat F(\xi)|^2}{|\xi|^{1-\alpha}}d\xi\,. \tag{3.34}$$

Remark 3.1 The limit of the variance of M_F^ε is (3.34) and the variance of M^0 is (3.30). These two expressions are reconciled by using the identity $1-\alpha = 2H-1$ and standard properties of the Γ function, namely $\Gamma(H)\Gamma(H+\frac12) = 2^{1-2H}\sqrt{\pi}\Gamma(2H)$ and $\Gamma(1-H)\Gamma(H) = \pi(\sin(\pi H))^{-1}$. We get

$$\frac{2^{-\alpha}\Gamma(\frac{1-\alpha}{2})}{\sqrt{\pi}\Gamma(\frac{\alpha}{2})} = \frac{2^{-2+2H}\Gamma(H-\frac12)}{\sqrt{\pi}\Gamma(1-H)} = \frac{2^{-2+2H}\Gamma(H+\frac12)}{\sqrt{\pi}(H-\frac12)\Gamma(1-H)} = \frac{\Gamma(2H)\sin(\pi H)}{\pi(2H-1)}\,.$$

By (2.23) this shows that

$$\frac{2^{-\alpha}\Gamma(\frac{1-\alpha}{2})}{\sqrt{\pi}\Gamma(\frac{\alpha}{2})}2\pi = \frac{1}{H(2H-1)C(H)^2}\,,$$

and this implies that the variance (3.30) of M_F^0 is exactly the limit (3.34) of the variance of M_F^ε:

$$\lim_{\varepsilon\to 0}\mathbb{E}\Big\{\Big|M_F^\varepsilon\Big|^2\Big\} = \mathbb{E}\Big\{\Big|M_F^0\Big|^2\Big\}\,.$$

3.2 Convergence in distribution

We can now give the proof of Theorem 3.1.

Step 1. The sequence of random variables $M_F^{\varepsilon,g}$ defined by (3.31) converges in distribution as $\varepsilon\to 0$ to

$$M_F^{0,g} = \sqrt{\frac{\kappa_g}{H(2H-1)}}\int_{\mathbb{R}} F(t)dW_t^H\,.$$

Since the random variable $M_F^{\varepsilon,g}$ is a linear transform of a Gaussian process, it has Gaussian distribution. Moreover, its mean is zero. The same statements hold true for $M_F^{0,g}$. Therefore, the characteristic functions of $M_F^{\varepsilon,g}$ and $M_F^{0,g}$ are

$$\mathbb{E}\Big\{e^{i\lambda M_F^{\varepsilon,g}}\Big\} = \exp\left(-\frac{\lambda^2}{2}\mathbb{E}\Big\{(M_F^{\varepsilon,g})^2\Big\}\right), \quad \mathbb{E}\Big\{e^{i\lambda M_F^{0,g}}\Big\} = \exp\left(-\frac{\lambda^2}{2}\mathbb{E}\Big\{(M_F^{0,g})^2\Big\}\right),$$

where $\lambda \in \mathbb{R}$. Convergence of the characteristic functions implies that of the distributions [5]. Therefore, it is sufficient to show that the variance of $M_F^{\varepsilon,g}$ converges to the variance of $M_F^{0,g}$ as $\varepsilon \to 0$. This follows from Lemma 3.3.

Step 2: M_F^ε converges in distribution to M_F^0 as $\varepsilon \to 0$.

Let $\lambda \in \mathbb{R}$. Since $M_F^0 = V_1 M_F^{0,g}$, we have

$$\begin{aligned}\left|\mathbb{E}\Big\{e^{i\lambda M_F^\varepsilon}\Big\} - \mathbb{E}\Big\{e^{i\lambda M_F^0}\Big\}\right| \;\leq\; & \left|\mathbb{E}\Big\{e^{i\lambda M_F^\varepsilon}\Big\} - \mathbb{E}\Big\{e^{i\lambda V_1 M_F^{\varepsilon,g}}\Big\}\right| \\ & + \left|\mathbb{E}\Big\{e^{i\lambda V_1 M_F^{\varepsilon,g}}\Big\} - \mathbb{E}\Big\{e^{i\lambda V_1 M_F^{0,g}}\Big\}\right|. \qquad (3.35)\end{aligned}$$

Since $|e^{ix} - 1| \leq |x|$ we can write

$$\left|\mathbb{E}\Big\{e^{i\lambda M_F^\varepsilon}\Big\} - \mathbb{E}\Big\{e^{i\lambda V_1 M_F^{\varepsilon,g}}\Big\}\right| \leq |\lambda|\mathbb{E}\Big\{|M_F^\varepsilon - V_1 M_F^{\varepsilon,g}|\Big\} \leq |\lambda|\mathbb{E}\Big\{(M_F^\varepsilon - V_1 M_F^{\varepsilon,g})^2\Big\}^{1/2},$$

which goes to zero by the result of Lemma 3.4. This shows that the first term of the right-hand side of (3.35) converges to 0 as $\varepsilon \to 0$. The second term of the right-hand side of (3.35) also converges to zero by the result of Step 1. This completes the proof of Theorem 3.1.

4 Convergence of random processes

Let F_1, F_2 be two functions in $L^\infty(0,1)$. We consider the random process $M^\varepsilon(x)$ defined for any $x \in [0,1]$ by

$$M^\varepsilon(x) = \varepsilon^{-\frac{\alpha}{2}}\left(\int_0^x F_1(t)\varphi^\varepsilon(t)dt + x\int_0^1 F_2(t)\varphi^\varepsilon(t)dt\right). \qquad (4.36)$$

With the notation (3.28) of the previous section, we have

$$M^\varepsilon(x) = M_{F_x}^\varepsilon = \varepsilon^{-\frac{\alpha}{2}}\int_{\mathbb{R}} F_x(t)\varphi^\varepsilon(t)dt\,,$$

where

$$F_x(t) = F_1(t)\mathbf{1}_{[0,x]}(t) + xF_2(t)\mathbf{1}_{[0,1]}(t) \qquad (4.37)$$

is indeed a function in $L^1(\mathbb{R}) \cap L^\infty(\mathbb{R})$.

Theorem 4.1 *Let φ be a random process of the form (2.6) and let $F_1, F_2 \in L^\infty(0,1)$. Then the random process $M^\varepsilon(x)$ defined by (4.36) converges in distribution as $\varepsilon \to 0$ in the space of the continuous functions $\mathcal{C}(0,1)$ to the continuous Gaussian process*

$$M^0(x) = \sqrt{\frac{\kappa}{H(2H-1)}}\int_{\mathbb{R}} F_x(t)dW_t^H\,, \qquad (4.38)$$

where F_x is defined by (4.37) and W_t^H is a fractional Brownian motion with Hurst index $H = 1 - \frac{\alpha}{2}$.

The limit random process M^0 is a Gaussian process with mean zero and autocorrelation function given by

$$\mathbb{E}\Big\{M^0(x)M^0(y)\Big\} = \frac{\kappa}{H(2H-1)} \times \frac{1}{2\pi C(H)^2} \int_{\mathbb{R}} \frac{\hat{F}_x(\xi)\overline{\hat{F}_y(\xi)}}{|\xi|^{2H-1}} d\xi \,. \tag{4.39}$$

The proof of Theorem 4.1 is based on a classical result on the weak convergence of continuous random processes [3]:

Proposition 4.2 *Suppose $(M^\varepsilon)_{\varepsilon\in(0,1)}$ are random processes with values in the space of continuous functions $\mathcal{C}(0,1)$ with $M^\varepsilon(0) = 0$. Then M^ε converges in distribution to M^0 provided that:*

(i) for any $0 \le x_1 \le \ldots \le x_k \le 1$, the finite-dimensional distribution $(M^\varepsilon(x_1), \cdots, M^\varepsilon(x_k))$ converges to the distribution $(M^0(x_1), \ldots, M^0(x_k))$ as $\varepsilon \to 0$.

(ii) $(M^\varepsilon)_{\varepsilon\in(0,1)}$ is a tight sequence of random processes in $\mathcal{C}(0,1)$. A sufficient condition for tightness of $(M^\varepsilon)_{\varepsilon\in(0,1)}$ is the Kolmogorov criterion: $\exists \delta, \beta, C > 0$ such that

$$\mathbb{E}\Big\{\Big|M^\varepsilon(s) - M^\varepsilon(t)\Big|^\beta\Big\} \le C|t-s|^{1+\delta} \,, \tag{4.40}$$

uniformly in $\varepsilon, t, s \in (0,1)$.

We split the proof of Theorem 4.1 into two parts: in the next subsection, we prove the point (i), and next, we prove (ii).

4.1 Convergence of the finite-dimensional distributions

For the proof of convergence of the finite-dimensional distributions, we want to show that for each set of points $0 \le x_1 \le \cdots \le x_k \le 1$ and each $\Lambda = (\lambda_1, \ldots, \lambda_k) \in \mathbb{R}^k$, we have the following convergence result for the characteristic functions:

$$\mathbb{E}\Big\{ \exp\Big(i\sum_{j=1}^k \lambda_j M^\varepsilon(x_j)\Big)\Big\} \xrightarrow{\varepsilon\to 0} \mathbb{E}\Big\{ \exp\Big(i\sum_{j=1}^k \lambda_j M^0(x_j)\Big)\Big\} \,. \tag{4.41}$$

Convergence of the characteristic functions implies that of the joint distributions [5]. Now the above characteristic function may be recast as

$$\mathbb{E}\Big\{ \exp\Big(i\sum_{j=1}^k \lambda_j M^\varepsilon(x_j)\Big)\Big\} = \mathbb{E}\Big\{ \exp i\Big(\varepsilon^{-\frac{\alpha}{2}} \int_{\mathbb{R}} \varphi^\varepsilon(t) F_\Lambda(t) dt\Big)\Big\} \,, \tag{4.42}$$

where

$$F_\Lambda(t) = \Big(\sum_{j=1}^k \lambda_j \mathbf{1}_{[0,x_j]}(t)\Big) F_1(t) + \Big(\sum_{j=1}^k \lambda_j x_j\Big) \mathbf{1}_{[0,1]}(t) F_2(t) \,.$$

Since $F_\Lambda \in L^\infty(\mathbb{R}) \cap L^1(\mathbb{R})$ when $F_1, F_2 \in L^\infty(0,1)$, we can apply Theorem 3.1 to obtain that:

$$\mathbb{E}\Big\{ \exp\Big(i \sum_{j=1}^k \lambda_j M^\varepsilon(x_j) \Big) \Big\} \xrightarrow{\varepsilon \to 0} \mathbb{E}\Big\{ \exp i \Big(\sqrt{\frac{\kappa}{H(2H-1)}} \int_{\mathbb{R}} F_\Lambda(t) dW_t^H \Big) \Big\},$$

which in turn establishes (4.41).

4.2 Tightness

It is possible to control the increments of the process M^ε, as shown by the following proposition.

Proposition 4.3 *There exists K such that, for any $F_1, F_2 \in L^\infty(0,1)$ and for any $x, y \in [0,1]$,*

$$\sup_{\varepsilon \in (0,1)} \mathbb{E}\Big\{ \Big| M^\varepsilon(y) - M^\varepsilon(x) \Big|^2 \Big\} \leq K \Big(\|F_1\|_\infty^2 |y-x|^{2-\alpha} + \|F_2\|_\infty^2 |y-x|^2 \Big), \qquad (4.43)$$

where M^ε is defined by (4.36).

Proof. The proof is a refinement of the ones of Lemmas 3.3 and 3.4. We can split the random process M^ε into two components: $M^\varepsilon(x) = M^{\varepsilon,1}(x) + M^{\varepsilon,2}(x)$, with

$$M^{\varepsilon,1}(x) = \varepsilon^{-\frac{\alpha}{2}} \int_0^x F_1(t) \varphi^\varepsilon(t) dt\,, \qquad M^{\varepsilon,2}(x) = x \varepsilon^{-\frac{\alpha}{2}} \int_0^1 F_2(t) \varphi^\varepsilon(t) dt\,.$$

We have

$$\mathbb{E}\Big\{ \Big| M^\varepsilon(y) - M^\varepsilon(x) \Big|^2 \Big\} \leq 2\mathbb{E}\Big\{ \Big| M^{\varepsilon,1}(y) - M^{\varepsilon,1}(x) \Big|^2 \Big\} + 2\mathbb{E}\Big\{ \Big| M^{\varepsilon,2}(y) - M^{\varepsilon,2}(x) \Big|^2 \Big\}.$$

The second moment of the increment of $M^{\varepsilon,2}$ is given by

$$\mathbb{E}\Big\{ \Big| M^{\varepsilon,2}(y) - M^{\varepsilon,2}(x) \Big|^2 \Big\} = |x-y|^2 \varepsilon^{-\alpha} \int_{[0,1]^2} R\Big(\frac{z-t}{\varepsilon}\Big) F_2(z) F_2(t) dz dt\,.$$

Since there exists $K > 0$ such that $|R(\tau)| \leq K \tau^{-\alpha}$ for all τ, we have

$$\begin{aligned} \varepsilon^{-\alpha} \int_{[0,1]^2} R\Big(\frac{z-t}{\varepsilon}\Big) F_2(z) F_2(t) dz dt &\leq K \int_{[0,1]^2} |z-t|^{-\alpha} |F_2(z)| |F_2(t)| dz dt \\ &\leq K \|F_2\|_\infty^2 \int_{-1}^1 |z|^{-\alpha} dz = \frac{2K}{1-\alpha} \|F_2\|_\infty^2\,, \end{aligned}$$

which gives the following estimate

$$\mathbb{E}\Big\{ \Big| M^{\varepsilon,2}(y) - M^{\varepsilon,2}(x) \Big|^2 \Big\} \leq \frac{2K}{1-\alpha} \|F_2\|_\infty^2 |x-y|^2\,.$$

The second moment of the increment of $M^{\varepsilon,1}$ for $x < y$ is given by

$$\mathbb{E}\Big\{ \Big| M^{\varepsilon,1}(y) - M^{\varepsilon,1}(x) \Big|^2 \Big\} = \varepsilon^{-\alpha} \int_{[x,y]^2} R\Big(\frac{z-t}{\varepsilon}\Big) F_1(z) F_1(t) dz dt\,.$$

We distinguish the cases $|y-x| \le \varepsilon$ and $|y-x| \ge \varepsilon$.

First case. Let us assume that $|y-x| \le \varepsilon$. Since R is bounded by V_2, we have

$$\mathbb{E}\Big\{\Big|M^{\varepsilon,1}(y) - M^{\varepsilon,1}(x)\Big|^2\Big\} \le V_2 \|F_1\|_\infty^2 \varepsilon^{-\alpha} |y-x|^2 .$$

Since $|y-x| \le \varepsilon$, this implies

$$\mathbb{E}\Big\{\Big|M^{\varepsilon,1}(y) - M^{\varepsilon,1}(x)\Big|^2\Big\} \le V_2 \|F_1\|_\infty^2 |y-x|^{2-\alpha} .$$

Second case. Let us assume that $|y-x| \ge \varepsilon$. Since R can be bounded by a power-law function $|R(\tau)| \le K\tau^{-\alpha}$ we have

$$\begin{aligned}
\mathbb{E}\Big\{\Big|M^{\varepsilon,1}(y) - M^{\varepsilon,1}(x)\Big|^2\Big\} &\le K\|F_1\|_\infty^2 \int_{[x,y]^2} |z-t|^{-\alpha} dz dt \\
&\le 2K\|F_1\|_\infty^2 \int_x^y \int_0^{y-x} t^{-\alpha} dt dz \\
&\le \frac{2K}{1-\alpha} \|F_1\|_\infty^2 |y-x|^{2-\alpha} ,
\end{aligned}$$

which completes the proof. ∎

This Proposition allows us to get two results.

1) By applying Proposition 4.3 with $F_2 = 0$ and $y = 0$, we prove Lemma 2.2.

2) By applying Proposition 4.3, we obtain that the increments of the process M^ε satisfy the Kolmogorov criterion (4.40) with $\beta = 2$ and $\delta = 1-\alpha > 0$. This gives the tightness of the family of processes M^ε in the space $\mathcal{C}(0,1)$.

4.3 Proof of Theorem 2.4

We can now give the proof of Theorem 2.4. The error term can be written in the form

$$\varepsilon^{-\frac{\alpha}{2}} \left(u^\varepsilon(x) - \bar{u}(x)\right) = \varepsilon^{-\frac{\alpha}{2}} \left(\int_0^x F_1(t)\varphi^\varepsilon(t)dt + x \int_0^1 F_2(t)\varphi^\varepsilon(t)dt \right) + \widetilde{r}^\varepsilon(x) ,$$

where $F_1(t) = c^* - F(t)$, $F_2(t) = F(t) - \int_0^1 F(z)dz - a^*q$, and $\widetilde{r}^\varepsilon(x) = \varepsilon^{-\alpha/2}[r^\varepsilon(x) + \rho^\varepsilon a^{*-1} x]$. The first term of the right-hand side is of the form (4.36). Therefore, by applying Theorem 4.1, we get that this process converges in distribution in $\mathcal{C}(0,1)$ to the limit process (2.19). It remains to show that the random process $\widetilde{r}^\varepsilon(x)$ converges as $\varepsilon \to 0$ to zero in $\mathcal{C}(0,1)$ in probability.

We have

$$\mathbb{E}\{|\widetilde{r}^\varepsilon(x) - \widetilde{r}^\varepsilon(y)|^2\} \le 2\varepsilon^{-\alpha}\mathbb{E}\{|r^\varepsilon(x) - r^\varepsilon(y)|^2\} + 2a^{*-2}\varepsilon^{-\alpha}\mathbb{E}\{|\rho^\varepsilon|^2\}|x-y|^2 ,$$

From the expression (2.18) of r^ε, and the fact that c^ε can be bounded uniformly in ε by a constant c_0, we get

$$\varepsilon^{-\alpha}\mathbb{E}\{|r^\varepsilon(x) - r^\varepsilon(y)|^2\} \le 2\varepsilon^{-\alpha} c_0 \mathbb{E}\left\{ \left| \int_x^y \varphi^\varepsilon(t)dt \right|^2 \right\} .$$

Upon applying Proposition 4.3, we obtain that there exists $K > 0$ such that

$$\varepsilon^{-\alpha}\mathbb{E}\{|r^\varepsilon(x) - r^\varepsilon(y)|^2\} \leq K|x-y|^{2-\alpha}\,.$$

Besides, since ρ^ε can be bounded uniformly in ε by a constant ρ_0, we have $\mathbb{E}\{|\rho^\varepsilon|^2\} \leq \rho_0\mathbb{E}\{|\rho^\varepsilon|\} \leq K\varepsilon^\alpha$ for some $K > 0$. Therefore, we have established that there exists $K > 0$ such that

$$\mathbb{E}\{|\widetilde{r}^\varepsilon(x) - \widetilde{r}^\varepsilon(y)|^2\} \leq K|x-y|^{2-\alpha}\,,$$

uniformly in ε, x, y. This shows that $\widetilde{r}^\varepsilon(x)$ is a tight sequence in the space $\mathcal{C}(0,1)$ by the Kolmogorov criterion (4.40). Furthermore, the finite-dimensional distributions of $\widetilde{r}^\varepsilon(x)$ converges to zero because

$$\sup_{x\in[0,1]} \mathbb{E}\Big\{|\widetilde{r}_\varepsilon(x)|\Big\} \overset{\varepsilon\to 0}{\longrightarrow} 0$$

by (2.15) and (2.17). Proposition 4.2 then shows that $\widetilde{r}^\varepsilon(x)$ converges to zero in distribution in $\mathcal{C}(0,1)$. Since the limit is deterministic, the convergence actually holds true in probability.

5 Numerical results for Theorem 2.5

In this section, we numerically study the convergence of the error term in the case where $F = 0$, $q = 1$, and the driving process $\varphi(x)$ has an integrable autocorrelation function. The solutions of the random elliptic equation (2.1) and of the homogenized equation (2.2) are given by

$$u_\varepsilon(x) = \frac{1}{\int_0^1 \frac{1}{a_\varepsilon}\,dy}\int_0^x \frac{1}{a_\varepsilon}\,dy \quad ; \quad \bar{u}(x) = x\,.$$

Using the decomposition $\varphi_\varepsilon = \frac{1}{a_\varepsilon} - \frac{1}{a_*}$ and assuming that $a_* = 1$, we have

$$u_\varepsilon(x) = \frac{x + \int_0^x \varphi_\varepsilon\,dy}{1 + \int_0^1 \varphi_\varepsilon\,dy}\,.$$

We study the the convergence of the process at the point $x = \frac{1}{2}$, where we have

$$u_\varepsilon(\frac{1}{2}) = \frac{\frac{1}{2} + \int_0^{\frac{1}{2}} \varphi_\varepsilon\,dy}{1 + \int_0^1 \varphi_\varepsilon\,dy} \overset{\varepsilon\to 0}{\longrightarrow} \frac{1}{2} = \bar{u}(\frac{1}{2}).$$

5.1 Generation of the driving process

We carry out numerical simulations in the case where the random process $\varphi(x)$ is of the form $\Phi(g_x)$ with g_x a stationary Ornstein-Uhlenbeck process and $\Phi(x) = \frac{1}{2}\mathrm{sgn}(x)$ (see Figure 8.1). This is a simple model for a two-component random medium.

The Ornstein-Uhlenbeck process is the solution of the stochastic differential equation [5]

$$dg_x = -g_x dx + \sqrt{2}dW_x\,,$$

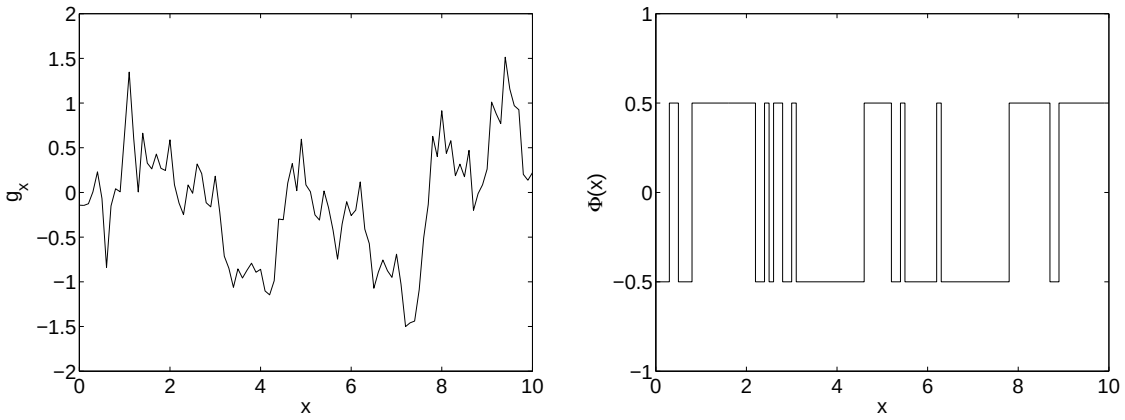

(a) **(b)**

Figure 8.1: Simulation of the Ornstein-Uhlenbeck process g_x (picture (a)) and the induced bounded process $\varphi(x) = \frac{1}{2}\mathrm{sgn}(g_x)$ (picture (b)).

where W_x is a standard Brownian motion. If we suppose that g_0 is a Gaussian random variable with mean 0 and variance 1 independent of the driving Brownian motion, then $(g_x)_{x\geq 0}$ is a stationary, mean zero, Gaussian process with the autocorrelation function $\mathbb{E}\{g_x g_{x+\tau}\} = \exp(-|\tau|)$. Moreover, it is a Markovian process, which makes it easy to simulate a realization of the Ornstein-Uhlenbeck process $(g_{k\Delta x})_{k\geq 0}$ sampled at times $(k\Delta x)_{k\geq 0}$ by the following recursive procedure:
- $g_0 = G_0$,
- $g_{(k+1)\Delta x} = e^{-\Delta x} g_{k\Delta x} + \sqrt{1 - \mathrm{e}^{-2\Delta x}} G_{k+1}$,
where $(G_k)_{k\geq 0}$ is a sequence of independent and identically distributed Gaussian random variables with mean 0 and variance 1. Note that the simulation is exact independently of the value of the grid step Δx.

Lemma 5.1 *If g_x is the stationary Ornstein-Uhlenbeck process and $\varphi(x) = \frac{1}{2}\mathrm{sgn}(g_x)$, then $\varphi(x)$ is a stationary, mean zero, random process with the autocorrelation function*

$$R(\tau) = \mathbb{E}\{\varphi(x+\tau)\varphi(x)\} = \frac{1}{4}\left(1 - \frac{2}{\pi}\arctan(\sqrt{\mathrm{e}^{2|\tau|} - 1})\right).$$

Proof. Since $g \mapsto \mathrm{sgn}(g)$ is an odd function, it is obvious that $\varphi(x)$ has mean zero. Denoting $a_\tau = e^{-|\tau|}$ and $b_\tau = \sqrt{1 - e^{-2|\tau|}}$, the autocorrelation function of $\varphi(x)$ can be

computed as follows:

$$\begin{aligned} R(\tau) &= \mathbb{E}\{\Phi(g_0)\Phi(g_\tau)\} = \frac{1}{4}\,\mathbb{E}\{\mathrm{sgn}(g_0)\mathrm{sgn}(g_\tau)\} \\ &= \frac{1}{4}\,\frac{1}{2\pi}\int_{\mathbb{R}^2} \mathrm{sgn}(x)\mathrm{sgn}(a_\tau x + b_\tau y)\,\mathrm{e}^{-\frac{x^2+y^2}{2}}\,dxdy \\ &= \frac{1}{4}\,\frac{2}{2\pi}\int_{\mathbb{R}^+\times\mathbb{R}} \mathrm{sgn}(x)\mathrm{sgn}(a_\tau x + b_\tau y)\,\mathrm{e}^{-\frac{x^2+y^2}{2}}\,dxdy \\ &= \frac{1}{4\pi}\int_0^\infty \int_{\theta=-\pi/2}^{-\pi/2+\theta_\tau} (-1)\,\rho\mathrm{e}^{-\frac{\rho^2}{2}}\,d\theta d\rho + \frac{1}{4\pi}\int_0^\infty \int_{\theta=\theta_\tau}^{\pi/2} 1\,\rho\mathrm{e}^{-\frac{\rho^2}{2}}\,d\theta d\rho \\ &= \frac{1}{4\pi}\,[-\theta_\tau + (\pi-\theta_\tau)] = \frac{1}{4}\left(1 - \frac{2}{\pi}\theta_\tau\right), \end{aligned}$$

with $\theta_\tau = \arctan(\frac{b_\tau}{a_\tau}) = \arctan(\sqrt{\mathrm{e}^{2|\tau|}-1})$. ∎

5.2 Convergence of the corrector

We now study the convergence of $u_\varepsilon(\frac{1}{2})$ to $\bar{u}(\frac{1}{2})$. The value of the integral $\int_0^1 F(s)\varphi_\varepsilon(s)\,ds$ is approximated by the standard quadrature formula

$$\int_0^1 F(s)\varphi_\varepsilon(s)\,ds = \int_0^1 F(s)\varphi\left(\frac{s}{\varepsilon}\right)\,ds = \varepsilon\int_0^{1/\varepsilon} F(\varepsilon y)\varphi(y)\,dy \approx \varepsilon\sum_{i=0}^{n} F(i\varepsilon\Delta x)\varphi(i\Delta x)\Delta x,$$

with $n = [1/(\varepsilon\Delta x)]$ and $\Delta x = 0.1$ in our simulations.

We first estimate the convergence order of the variance of $(u_\varepsilon - \bar{u})(\frac{1}{2})$ when $\varepsilon \to 0$. The following values are given to ε:

$$\varepsilon \in \{0.0001,\, 0.0002,\, 0.0005,\, 0.001,\, 0.002,\, 0.005,\, 0.01,\, 0.05,\, 0.1\}.$$

For each ε, we perform 10^4 simulations and compute the empirical variance. The results are shown in Figure 8.2a. The asymptotic theory predicts that the convergence is linear in ε:

$$\mathrm{Var}\Big\{u_\varepsilon(\frac{1}{2}) - \bar{u}(\frac{1}{2})\Big\} = \sigma^2\varepsilon + o(\varepsilon)\,, \qquad \sigma^2 = 2a_*\int_0^\infty R(\tau)\,d\tau \approx 0.0865.$$

The computation of a linear regression of the empirical variance with respect to ε, with the two, three, etc.. first points give 0.0865, 0.0875, 0.0870, which is different from the theoretical prediction by less than 1%.

We now check the convergence in law of $\frac{1}{\sqrt{\varepsilon}}\,(u_\varepsilon(\frac{1}{2}) - \bar{u}(\frac{1}{2}))$. Theorem 2.5 predicts that

$$\frac{1}{\sqrt{\varepsilon}}\,(u_\varepsilon(x) - \bar{u}(x)) \xrightarrow{law} \left(2\int_0^\infty R(\tau)\,d\tau\right)^{1/2}\mathcal{U}(x),$$

with $\mathcal{U}(x) = a_* W_x - a_* x W_1$, so that in our case

$$\frac{1}{\sqrt{\varepsilon}}\Big(u_\varepsilon(\frac{1}{2}) - \bar{u}(\frac{1}{2})\Big) \xrightarrow{law} G,$$

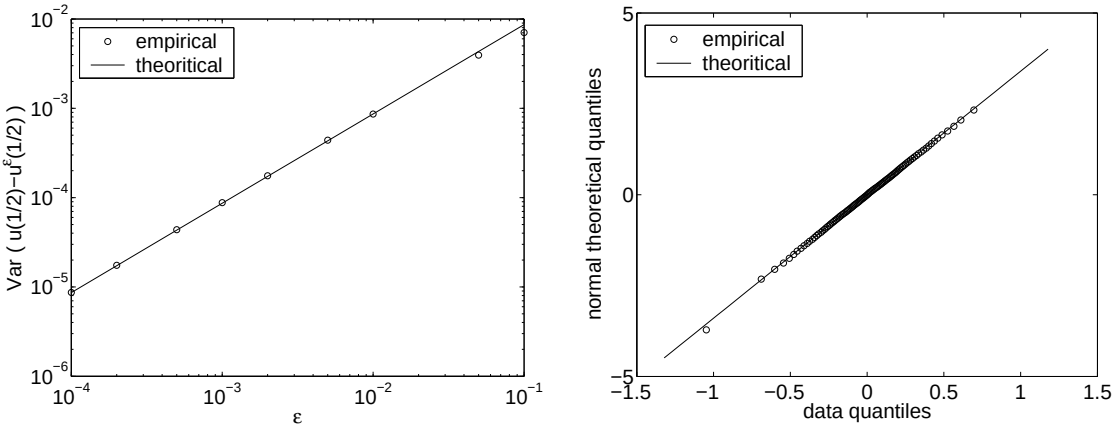

(a) **(b)**

Figure 8.2: Picture (a): Variance of $(u_\varepsilon - u)(\frac{1}{2})$ as a function of ε, in log-log scale. The convergence rate of the variance in log log scale has a slope equal to one, which proves that the convergence is proportional to ε. Picture (b): Normal QQ plot for the distribution of $\varepsilon^{-\frac{1}{2}}(u^\varepsilon - \bar{u})\left(\frac{1}{2}\right)$ with $\varepsilon = 0.0001$, which confirms the Gaussian behavior of the error.

where G is a Gaussian random variable with mean zero and variance

$$\sigma^2 = 2\int_0^\infty R(\tau)\,d\tau\,\mathrm{Var}\Big\{\mathcal{U}(\frac{1}{2})\Big\} = 2a_*\int_0^\infty R(\tau)\,d\tau \approx 0.0865$$

In Figure 8.2b, we compare the distribution of $\frac{1}{\sqrt{\varepsilon}}\,(u_\varepsilon(\frac{1}{2}) - \bar{u}(\frac{1}{2}))$ for $\varepsilon = 10^{-4}$ with the one of G by plotting the normal QQ plot which shows perfect agreement (a normal QQ plot is a scatter-plot with the quantiles of the sample on the horizontal axis and the expected normal quantiles on the vertical axis).

6 Numerical results for Theorem 2.4

6.1 Generation of the driving process

To test the result of Theorem 2.4, we need to generate a Gaussian process with a heavy tail. We choose to generate the increments of a fractional Brownian motion: $g_x = W^H_{x+1} - W^H_x$. Since fractional Brownian motion is not a Markovian process, it cannot be generated iteratively. Many different methods have been developed to simulate fractional Brownian motions based on integral representations in terms of standard Brownian motions, spectral representations, or wavelet decompositions (see the review [1]). In this paper we use the Choleski method because it is the simplest method to implement. It is based on the following facts:
1) the fractional Brownian motion W^H_x and the process g_x are Gaussian processes,
2) the autocorrelation function of the fractional Brownian motion is known (see (2.21)), so that it is possible to calculate the covariance matrix C of the Gaussian vector

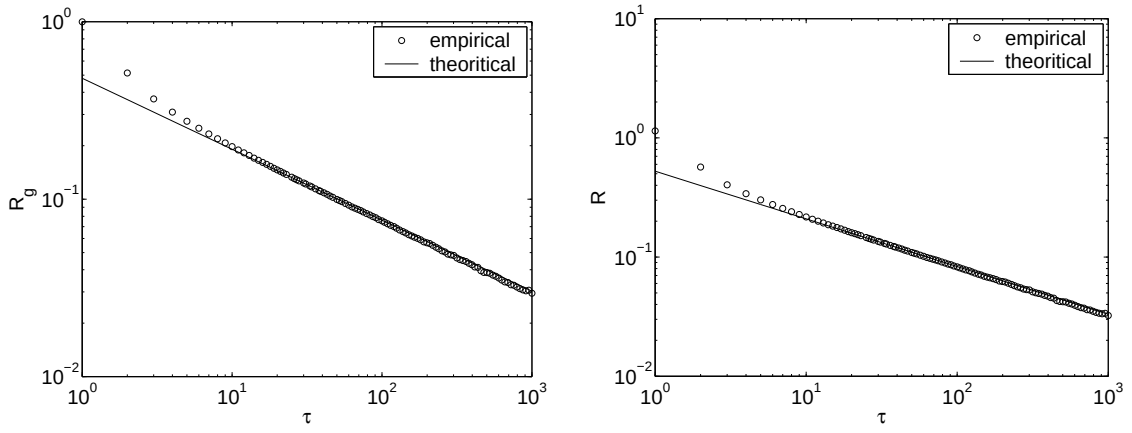

(a) **(b)**

Figure 8.3: A series of 10^5 numerical simulations of the vector $(g_{k\Delta x})_{k=0,\dots,N}$ is carried out in the case where $g_x = W^H_{x+1} - W^H_x$, $H = 0.8$, $N = 2000$, and $\Delta x = 1$. Picture (a): The empirical autocorrelation of g_x is compared with the theoretical asymptotic behavior $\tau \mapsto H(2H-1)\tau^{2H-2}$. Picture (b): The empirical autocorrelation of $\varphi(x)$ is compared with the theoretical asymptotic behavior $\tau \mapsto V_1^2 H(2H-1)\tau^{2H-2}$.

$(g_{k\Delta x})_{k=0,\dots,N}$,
3) if X is a vector of independent and identically distributed random variables with Gaussian distribution, mean 0, and variance 1, then MX is a mean zero Gaussian vector with covariance matrix MM^T.

The Choleski method consists in
1) computing a square root $\sqrt{C}$ of the covariance matrix C of the Gaussian vector $(g_{k\Delta x})_{k=0,\dots,N}$,
2) generating a vector X of $N+1$ independent and identically distributed Gaussian random variables with mean 0 and variance 1,
3) computing the vector $\sqrt{C}X$.

This method is exact, in the sense that the simulated vector $\sqrt{C}X$ has the distribution of $(g_{k\Delta x})_{k=0,\dots,N}$, whatever the grid step Δx may be. The method is, however, computationally expensive. In fact, only the computation of the square root of the matrix C is costly. Once this computation has been carried out, it is straightforward to generate a sequence of independent and identically distributed random vectors with the distribution of $(g_{k\Delta x})_{k=0,\dots,N}$.

We apply the Choleski method to generate 10^5 realizations of the vector $(g_{k\Delta x})_{k=0,\dots,N}$ with $\Delta x = 1$ and $N = 2000$. The Hurst parameter is equal to 0.8. The empirical autocorrelation function is shown in Figure 8.3 and compared with its theoretical asymptotic behavior $\tau \mapsto H(2H-1)\tau^{2H-2}$ $[\tau \to \infty]$. When τ becomes large, the fluctuations become large compared to $R(\tau)$ because $R(\tau) \to 0$. A linear regression made on the interval $[10, 100]$ gives the power law fit Kt^β, with $K = 0.4901$ and $\beta = 0.3964$, which is in agreement with the theoretical values $K = 0.48$ and $\beta = 0.4$.

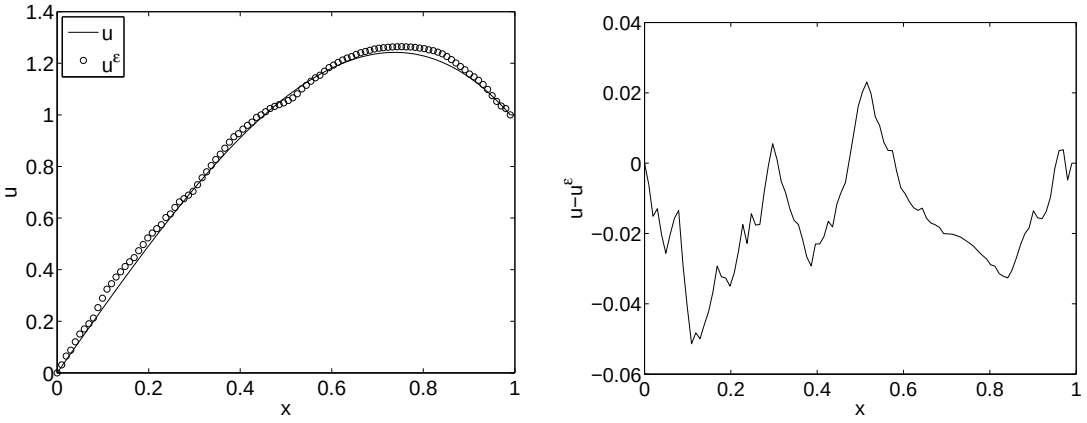

(a) **(b)**

Figure 8.4: Picture (a) compares the homogenized solution (solid line) with the solution of (2.1) obtained for $\varepsilon = 0.0033$ and for a particular realization of the random process φ (circles). Picture (b) plots the difference between u^ε and $\bar{u}$.

We suppose that the random medium is described by the stationary random process

$$\frac{1}{a(x)} = \frac{9}{2} + \frac{8}{\pi}\arctan(g_x). \tag{6.44}$$

The asymptotic behavior of its autocorrelation function is theoretically given by (2.11) with

$$V_1 = \frac{1}{\sqrt{2\pi}}\,\frac{8}{\pi}\int_{-\infty}^{+\infty} x\arctan(x)\mathrm{e}^{-\frac{x^2}{2}}\,dx \approx 1.6694.$$

The empirical autocorrelation function of the process determined by a series of 10^5 experiments is shown in Figure 8.3, where we observe that the theoretical and empirical curves agree very well.

6.2 Convergence of the corrector

We now study the convergence of the solution of the homogenization problem (2.1) as $\varepsilon \to 0$. We choose $F(x) = x^2$ and $q = 1$. For $a(x)$ given by (6.44), we find that $a^\star = \frac{2}{9}$. A solution obtained with a particular realization of the random process with $\varepsilon = 0.0033$ is shown in Figure 8.4 and compared with the theoretical solution of the homogenized problem.

We estimate the order of convergence of the variance of the corrector $(u_\varepsilon - u)(\frac{1}{2})$ when $\varepsilon \to 0$. The following values are given to ε:

$$\varepsilon \in \{0.0033,\ 0.0017,\ 0.0011,\ 0.00091,\ 0.00077,\ 0.00062,\ 0.0004\}. \tag{6.45}$$

For each value of ε, we run 10^4 numerical experiments, compute the empirical variance of the corrector, and compare with the asymptotic theoretical variance predicted by

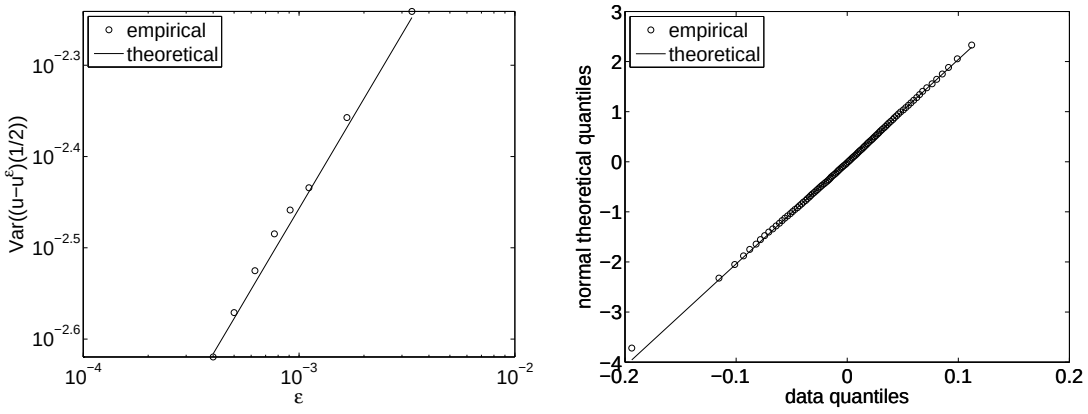

(a) (b)

Figure 8.5: Picture (a): Empirical variance of $(u_\varepsilon - \bar{u})(\frac{1}{2})$ as a function of ε, in log-log scale (circles), compared with the asymptotic theoretical variance (6.46) predicted by Theorem 2.4. Picture (b): Normal QQ plot for $(u^\varepsilon - \bar{u})\left(\frac{1}{2}\right)$ with $\varepsilon = 0.0004$, which confirms the Gaussian behavior of the corrector term.

Theorem 2.4:

$$\mathrm{Var}\Big\{u_\varepsilon(\frac{1}{2}) - \bar{u}(\frac{1}{2})\Big\} = \sigma_H^2 \varepsilon^{2-2H} + o(\varepsilon^{2-2H}) \tag{6.46}$$

with $2 - 2H = 0.4$ and

$$\sigma_H^2 = \mathrm{Var}\left(\sqrt{\frac{\kappa}{H(2H-1)}} \int_{\mathbb{R}} K\left(\frac{1}{2}, t\right) dW_t^H\right) \approx 0.0553.$$

The results are presented in Figure 8.5a and show good agreement. More quantitatively, a linear regression of the logarithm of the empirical variance of the error with respect to $\log \varepsilon$ gives:

$$\mathrm{Var}\Big\{u^\varepsilon(\frac{1}{2}) - \bar{u}(\frac{1}{2})\Big\} \approx 0.0581 \varepsilon^{0.4041} \tag{6.47}$$

which agrees very well with (6.46). Finally, we can check that the distribution of the limit process is Gaussian by observing that the normal QQ plot in Figure 8.5b is indeed a straight line.

7 Conclusions

We have shown that the corrector to homogenization, i.e., the difference between the random solution to an elliptic equation with random coefficients and the deterministic solution to the appropriately homogenized elliptic equation, strongly depends on the statistics of the random medium. When the correlation function of the random diffusion coefficient is integrable, such a corrector is of order $\sqrt{\varepsilon}$, where ε measures the correlation length of the random medium. When the correlation function behaves like $\tau^{-\alpha}$, which measures long-memory effects, then the difference becomes of order $\varepsilon^{\frac{\alpha}{2}}$ for $0 < \alpha < 1$.

The corrector to the homogenized solution may thus be arbitrarily large asymptotically for very small values of α, which corresponds to pronounced long-memory effects.

Moreover, up to smaller terms of order ε^α, the corrector to homogenization is a centered Gaussian process, which may conveniently and explicitly be written as a stochastic integral with respect to fractional Brownian motion. Such a random behavior of the corrector may provide an accurate quantitative model for the statistical instability (i.e., the dependency with respect to the specific realization of the random medium) of practical and experimental measurements. This central-limit-type behavior may be extremely difficult and costly to adequately capture by numerical simulations of the elliptic equation with random coefficients because of the very large number of random variables involved in the modeling of a random medium with a small correlation length ($\varepsilon \ll 1$).

The results presented in this paper are based on the explicit integral representation (2.3) of the solution to the one-dimensional elliptic equation (2.1). Such formulas are not available in higher space dimensions. Although we are tempted to believe that similar behaviors will remain valid in higher space dimensions, namely that long-memory effects will trigger large random corrections to homogenization, this remains a conjecture at present.

Bibliography

[1] J.-M. Bardet, G. Lang, G. Oppenheim, A. Philippe, and M. S. Taqqu, *Generators of the long-range dependence processes: a survey*, in Theory and applications of long-range dependence, P. Doukhan, G. Oppenheim, and M. S. Taqqu, editors, Birkhauser (2003), pp. 579-624.

[2] A. Bensoussan, J.-L. Lions, and G. C. Papanicolaou, *Boundary layers and homogenization of transport processes*, Res. Inst. Math. Sci., Kyoto Univ. **15** (1979), 53–157.

[3] P. Billingsley, *Convergence of Probability Measures*, Wiley, New York, 1999.

[4] A. Bourgeat and A. Piatnitski, *Estimates in probability of the residual between the random and the homogenized solutions of one-dimensional second-order operator*, Asympt. Anal. **21** (1999), 303–315.

[5] L. Breiman, *Probability*, Classics in Applied Mathematics, SIAM, Philadelphia, 1992.

[6] V. V. Jikov, S. M. Kozlov, and O. A. Oleinik, *Homogenization of differential operators and integral functionals*, Springer, New York, 1994.

[7] S. M. Kozlov, *The averaging of random operators*, Math. USSR Sb. **109** (1979), 188–202.

[8] H. J. Kushner, *Approximation and weak convergence method for random processes, with applications to stochastic systems theory*, MIT Press, Cambridge, 1984.

[9] R. Marty, *Asymptotic behavior of differential equations driven by periodic and random processes with slowly decaying correlations*, ESAIM: Probability and Statistics **9** (2005), 165–184.

[10] G. C. Papanicolaou and S. R. S. Varadhan, *Boundary value problems with rapidly oscillating random coefficients*, in Random fields, Vol. I, II (Esztergom, 1979), Colloq. Math. Soc. János Bolyai, 27, North Holland, New York, 1981, pp. 835–873.

[11] V. Pipiras and M. S. Taqqu, *Integration questions related to fractional Brownian motion*, Probab. Theor. Related Fields **118** (2000), 251–291.

[12] M. S. Taqqu, *Weak convergence to fractional Brownian motion and to the Rosenblatt process*, Z. Wahrscheinlichkeitstheorie verw. Geb. **31** (1975), 287–302; *Convergence of integrated processes of arbitrary Hermite rank*, Z. Wahrscheinlichkeitstheorie verw. Geb. **50** (1979), 53-83.

[13] V. V. Yurinskii, *Averaging of symmetric diffusion in a random medium*, Siberian Math. J. **4** (1986), 603–613. English translation of: Sibirsk. Mat. Zh. **27** (1986), 167–180 (Russian).

Conclusion (version française)

Dans cette thèse, nous avons étudié d'une manière théorique et numérique des modèles de déplacements en biologie et en particulier nous nous sommes intéressé à la dérivation de modèles macroscopiques à partir de modèles microscopiques, appelés modèles individus centrés en biologie.

Nous avons tout d'abord étudié un nouveau modèle de déplacement de poisson, le modèle "Persistent Turning Walker" (PTW) qui est basé sur des données expérimentales (chapitre 1). Nous avons dérivé un modèle macroscopique à partir de ce modèle de deux manières distinctes (chapitre 2-3). Ensuite, nous avons étudié un modèle d'interaction général appelé modèle de Vicsek. Dans un premier temps, nous avons dérivé un modèle macroscopique à partir de ce modèle microscopique (chapitre 6). À la suite de quoi, nous avons validé numériquement l'équation macroscopique obtenu en comparant les simulations numériques du modèle microscopique et du modèle macroscopique (chapitre 7).

La modélisation des déplacements collectifs est un sujet extrèment vaste qui nécessite des outils et des méthodes très variés. Il existe de nombreuses directions dans lesquelles nous pouvons prolonger les travaux effectués.

Parmi les développements à court terme qu'il nous reste à étudier, un premier point est de développer un modèle d'interaction entre poissons basé sur les données expérimentales. L'analyse des données expérimentales (chapitre 5) permettra alors d'aider à la construction du modèle et de le valider. Des travaux sont en cours pour introduire dans le modèle PTW un terme supplémentaire modélisant les interactions entre congénères.

Il serait aussi intéressant de généraliser la méthode utilisée pour dériver un modèle macroscopique à partir du modèle de Vicsek à d'autres modèles de déplacement en biologie comme par exemple le modèle proposé par Couzin. Nous pourrions ainsi observer et prédire à partir du modèle macroscopique la formation de différentes structures (formation alignée, vortex).

D'une manière plus générale, l'introduction des invariants collisionnels généralisés utilisée dans la dérivation du modèle macroscopique de Vicsek pourrait être appliqués à d'autres modèles en théorie cinétique pour lesquelles nous n'avons pas préservation du moment cinétique.

Nous avons commencé à étudier le modèle macroscopique dérivé à partir du modèle de Vicsek et nous avons mise en évidence que les solutions à ce modèle sont plus complexes qu'elles ne semblaient l'être. Néanmoins, il est nécessaire par la suite de développer un cadre théorique pour ce type d'équation (équation hyperbolique non

conservative avec contrainte géométrique). L'idéal serait de trouver un critère permettant de sélectionner les bonnes solutions faibles. Pour l'instant, nous nous sommes servis du modèle microscopique. Mais la méthode est peu précise et nécessite des temps de calculs très longs.

Enfin, il serait intéressant d'étudier les modèles de déplacement en biologie à partir des équations cinétiques. Ceci permettrait d'avoir une description intermédiaire entre modèles microscopiques et modèles macroscopiques. On pourrait ainsi développé des méthodes numériques multi-échelle comme cela se fait en dynamique des gaz.

Conclusion (English version)

In this thesis, we have studied theoretically and numerically models of animals displacement in biology. We took a particular interest in the derivation of macroscopic models from microscopic models, called also in biology individual based model.

We first have considered a new model for fish displacement, the "Persistent Turning Walker" model (PTW) which is based on experimental data (Chapter 1). We have derived a macroscopic model from this model using two different methods (Chapter 2-3). After that, we have studied a general models of interacting particles called Vicsek model. In a first step, we have derived a macroscopic model from this microscopic model (Chapter 6). Then we have validated the macroscopic equation obtained by comparing the numerical simulations of the microscopic and macroscopic equation (Chapter 7).

The mathematical modeling of collective displacements is a wide subject that requires extensive tools and various methods. There are many directions in which we can extend the work done.

Among the short-term developments, a first point is to develop a model of interaction between fish based on experimental data. The analysis of experimental data (Chapter 5) will help in the construction of the model. Works are underway to introduce in the PTW model an additional term to model the interactions between congeners.

It would also be interesting to generalize the method used to derive a macroscopic model from the Vicsek model to other models of displacement such as the model proposed by Couzin. We should observe and predict the formation of different structures (highly polarized group, vortex formation) from the macroscopic model.

More generally, the introduction of generalized collisional invariants opens new perspectives in kinetic theory. In particular, this method could be applied to other kinetic equation which do not preserve the kinetic moment.

We have began to study the macroscopic model derived from the model of Vicsek and we have shown that the solutions to this model are more complex than we expected. However, it is necessary to develop a theoretical framework for this type of equation (hyperbolic equation with non-conservative constraint geometric). Ideally, we would like to find a criterion to select the correct weak solution. At the moment, we only use the microscopic model to determine what is the relevant solution, but this method is imprecise and requires a lot of CPU time.

Finally, it would be interesting to study models of displacements in biology from kinetic equations. This would allow to have an intermediate description between mi-

croscopic and macroscopic models. Then we could develop multiscale methods in the numerical simulation of collective displacement as it has been develop in gas dynamics.

Résumé

La modélisation des déplacements d'animaux peut se faire à deux échelles différentes. On peut soit décrire les trajectoires de chaque individu séparément en utilisant des modèles dit individu centré (échelle "microscopique"), ou bien on peut décrire la dynamique collective du groupe d'individus au moyen de quantités "macroscopiques" (densité, flux...). Dans cette thèse, nous nous sommes intéressés à relier ces deux échelles de description, à savoir dériver des modèles macroscopiques à partir de modèles microscopiques. Cette approche permet de relier dynamique individuelle et dynamique collective.

Nous nous sommes tout d'abord intéressé à un nouveau modèle de déplacement de poisson appelé "Persistent Turning Walker" (PTW) introduit à partir de données expérimentales. Nous avons donnés deux méthodes pour dériver une équation de diffusion à partir de ce modèle, une méthode utilisant des outils d'analyse fonctionnelle et une deuxième méthode utilisant des outils probabilistes. L'originalité du modèle PTW réside principalement dans l'utilisation de la courbure pour décrire le déplacement individuel, cette nouveauté permet d'étendre d'autres types de modèles ainsi que l'analyse statistique de trajectoires expérimentales.

Dans un deuxième temps, nous avons étudié le modèle dit de Vicsek qui est un modèle individu centré très répandu dans la modélisation de déplacements d'animaux. Nous avons pour la première fois dérivé un modèle macroscopique à partir de ce modèle (un système hyperbolique non-conservatif avec une contrainte géométrique). Les simulations numériques du modèle macroscopique obtenu nous ont ensuite montré la pertinence du modèle macroscopique pour décrire la dynamique microscopique du modèle Vicsek à grandes échelles.

Mots clés : Mathématiques et Biologie, Modèle Individu Centré, Équations Différentielles Stochastiques, Équations Cinétiques, Analyse Asymptotique, Approximation Diffusion, Systèmes Hyperboliques.

Abstract

The modeling of animals displacements can occur at two different scales. One may either describes the trajectories of each individual using the so-called individual based models (at a "microscopic" scale), or we can describe the dynamics of the all group with "macroscopic" quantities (density, flux...). In this thesis, we want to connect these two descriptions, the microscopic and the macroscopic scale. Therefore, we can link individual and global dynamics.

In a first part, we have introduced a new model for fish displacement called "Persistent Turning Walker" (PTW) based on experimental data. We have given two methods to derive a diffusion equation from this model, a method using tools from functional analysis and a second method using probabilistic tools. The originality of the PTW model mainly relies in the use of curvature to describe individual displacement, this novelty has been used to extend other types of models and to analyse experimental trajectories.

In a second part, we have studied the so-called Vicsek model which is an individual based model widespread used in the modeling of animals displacements. We have derived for the first time a macroscopic model from this model (a non-conservative hyperbolic system with a geometric constraint). The numerical simulations of the macroscopic model obtained have shown the relevance of the macroscopic model to describe the microscopic dynamics of the Vicsek model at large scales.

Key words : Mathematical biology, Individual based model, Stochastic diffential equation, Kinetic equation, Asymptotic analysis, Diffusion approximation, Hyperbolic systems.